Development of methods for in vitro characterisation of antibody-drug conjugates

Chapman, Terry

Award date:
2019

Awarding institution:
University of Bath

Development of methods for in vitro characterisation of antibody-drug conjugates

Terry James Chapman

A thesis submitted for the degree of Doctor of Philosophy

University of Bath

Department of Pharmacy and Pharmacology

April 2019

This research has been carried out under the supervision of
Dr. Andrew G. Watts

And under the guidance of
Dr. Richard V. Parry

Signed …….. Date …….

Dedicated to all those who have encouraged or supported me.

“Do not go where the path may lead, go where there is no path and leave a trail.”

Ralph Waldo Emerson, 1803 – 1882

“The value of an idea lies in the using of it.”

Thomas A. Edison, 1847 – 1931

“Success consists of going from failure to failure without loss of enthusiasm.”

Winston Churchill, 1874 – 1965

Contents

Abstract

Chemotherapy has grown, from chemotherapeutic agents discovered in the 1940s still used today, such as vincristine, to antibody therapies developed in the 1990s such as trastuzumab. Antibody drug conjugates (ADCs) are a class of drug that have been theorized about since the turn of the 20th century, they are a potent cytotoxic drug and an antibody combined. Trastuzumab emtansine, licensed in 2013, has broken headlines, as it outperforms current gold standard therapies, but costs £90K per patient a year.

Stability studies performed on aseptically prepared biopharmaceuticals, conforming to the requirements set out in the NHS's 'A Standard Protocol for Deriving and Assessment of Stability. Part 2' allow the shelf life of products prepared under a Section 10 exemption or a Specials License to be extended beyond their summary of products characteristics shelf life (typically 24-48 hours). Shelf life extensions have many benefits e.g. reducing logistics issues for product storage and transportation, a safety net of time in case a product cannot be administered, batch production minimising drug wastage, which allows prices of medicines to be reduced.

The work herein details research dedicated to enabling a stability study to be performed on the ADC, trastuzumab emtansine. We identified and validated many techniques for characterisation of the biopharmaceutical infliximab and published an NHS compliant stability study. A 7-day shelf life can be applied to infliximab by all UK hospitals. These techniques were then evaluated by their ability to characterise trastuzumab emtansine and if they remained stability indicating, a minimum requirement for a stability study.
Where necessary, methods were optimised or developed anew, to enable full characterisation of the ADC trastuzumab emtansine. This involved validation of a new chromatography method, the design, construction and validation of an infrared spectroscopy method, and creative thinking to overcome low sensitivity of intact LC-MS. This allowed a stability study to be performed and a shelf life extension for trastuzumab emtansine was achieved. Furthermore, some preliminary work regarding ADC in use safety and the applicability of the developed methods regarding differently designed ADCs, such as brentuximab vedotin was carried out.

Acknowledgements

Firstly, I wish to give thanks to my supervisor Dr. Andrew Watts, without whom I may not have gotten my initial student placement at Bath ASU, setting me down the rewarding path of pharmaceutical stability studies. I am grateful he let me take the reins of my PhD and for his confidence that I could achieve things when others didn't.

Secondly, a lot of gratitude is due to Dr. Richard Parry, who helped me to learn more about the subtleties of cell culture and bioassays than I previously knew existed.

I would like to thank Dr. Charareh Pourzand and Dr. Olivier Reelfs for use of their laboratory and centrifugal equipment, and Dr. Daniel Pantos, for his help with circular dichroism analysis.

Dr. Chris Stapleton deserves a hearty handshake for helping me understand how I could build my own QDS, something I didn't even know existed until I met him.

I would like to thank, Dr. Benjamin Young, master of puns, for his assistance in and out of the laboratory, throughout my PhD.

Dr. Shaun Reeksting and Dr. Mervyn Lewis are also owed a big thank you for their assistance with mass spectrometry analysis.

I would like to thank Joshua Carter and Francesca Mason for their help, especially in the latter stages of my PhD.

Bath ASU receive much appreciation from me, for sponsoring my PhD, and for supporting me during this process.

Furthermore, multiple staff at the University of Bath have helped me with access to equipment or getting hold of reagents, it's all helped, I appreciate it all.

I would also like to thank my parents and Grandma, who have encouraged me to always try my best and work hard, ever since I can remember. They still haven't stopped.

A lot of gratitude is owed to my wonderful fiancée 'Jordan', who has supported, encouraged and loved me throughout my PhD, and has had to put up with many late nights without me, especially during the writing of this thesis.

Finally, Rosie kept me far happier than I should have been, when my life was getting turned upside down during 2018.

Abbreviations

2D	Two dimensional
3D	Three dimensional
4-OHT	4-hydroxy-tamoxifen
5-FU	5-fluorouracil
Ab	Antibody
ADC	Antibody drug conjugate
ADCC	Antibody dependent cellular cytotoxicity
ANOVA	One-way analysis of variance
API	Active pharmaceutical ingredient
ASU	Aseptic services unit
ATCC	American type culture collection
ATR	Attenuates total reflectance
BP	British pharmacopeia
BT-474	Breast tumour 474
C3DEM	Cryo three dimensional electron microscopy
CCAF	Chemical characterisation and analysis facility
CD	Circular dichroism
CDC	Complement dependent cytotoxicity
CDNN	Circular dichroism neural network
CDR	Complementary determining regions
CDS	Circular dichroism spectroscopy
C_H	Conserved heavy
CIM	Convective interaction media
C_L	Conserved light
Conc’	Concentration
Da	Dalton
DAD	Diode array detector
DAR	Drug antibody Ratio
DLS	Dynamic light scattering
DM-1	Derivative maytansinoid 1
DM-4	Derivative maytansinoid 4
DMEM	Dulbecco’s modified eagles serum
DMSO	Dimethyl sulfoxide
DNA	Deoxyribonucleic acid
EC50	Effective concentration of 50% maximal response
ELISA	Enzyme linked immuno-sorbent assay
EP	European pharmacopeia
Fab	Fragment antigen binding
Fc	Fragment Crystallisable
FC	Flow cell
FTIR	Fourier-transform infrared
g	Gram
GCT-27	Germ cell tumour - 27

GE	Gel electrophoresis
HaCaT	Human aneuploid immortal keratinocyte
HC	Heavy chain
HepG2	Hepatocyte cell line G2
HER2	human epidermal growth factor receptor 2
HgCdTe	Mercury-cadmium-telluride
HIC	Hydrophobic interaction chromatography
HPLC	High pressure liquid chromatography
HS1	HPLC system 1
HS2	HPLC system 2
HS3	HPLC system 3
ICH	International council for harmonization
IgG	Immunoglobulin G
IPA	Isopropyl alcohol
IR	Infrared
IRS	Infrared spectroscopy
LC	Light chain
LC-MS	Liquid chromatography mass spectrometry
LGC	Laboratory of the government chemist
LOD	Limit of detection
LOQ	Limit of quantification
M	Molar
mAb	Monoclonal antibody
MFI	Microflow imaging
MHRA	Medicines Health Regulatory Agency
min	Minute
µg	Microgram
µL	Microlitre
µM	Micromolar
µm	Micrometre
mg	Milligram
mL	Millilitre
mM	Millimolar
mm	Millimetre
MMAE	Monomethyl auristatin E
MMAF	Monomethyl auristatin F
mmc	Maleimidomethylcyclohexane-1-carboxylate
MOPP	Mechlorethamine, vincristine, procarbazine and prednisone
MS	Mass Spectrometry
MTS	3-(4,5-dimethylthiazol-2-yl)-5-(3-carboxymethoxyphenyl)-2-(4-sulfophenyl)-2H-tetrazolium
MTT	Dimethylthiazol-2-yl diphenyltetrazolium bromide
MW	Molecular weight
NaCl	Sodium chloride

NHS	National Health Service
nL	Nanolitre
nM	Nanomolar
nm	Nanometre
NMR	Nuclear magnetic resonance
NPR	Non-porous resin
ρg	Picogram
PAGE	Polyacrylamide gel electrophoresis
PDB	Protein Data Bank
PE	Polyethylene
PhD	Philosophiae doctor (Doctor of philosophy)
PNGase	Peptide N-glycosidase
PO	Polyolefin
PP	Polypropylene
PSPA	Primary sequence prediction algorithms
PVC	Polyvinyl chloride
QA	Quality assurance
QDS	Quantitative data set
QTOF	Quantitative time of flight
R&D	Research and development
RCSB	Research Collaboratory for Structural Bioinformatics
RMM	Resonant mass measurement
RMSECV	Root mean square error of the coefficient of variation
RNase	Ribonuclease
RPD	Residual prediction deviation
RP-HPLC	Reverse phase high pressure liquid chromatography
RPMI	Roswell Park Memorial Institute
RSD	Relative standard deviation
SD	Standard deviation
SDS	Sodium dodecyl sulphate
SEC	Size exclusion chromatography
SEM	Scanning electron microscopy
SMCC	Succinimidyl 4-(N-maleimidomethyl)cyclohexane-1-carboxylate
SPC	Summary of product characteristics
TAA	Tumour associated antigens
TCEP	Tris(2-carboxyethyl)phosphine
TE	Trastuzumab emtasine
THPP	Tris(hydroxypropyl)phosphine
TIC	Total ion count
TNF	Tumour necrosis factor
TSA	Tumour specific antigen
USP	Unites States Pharmacopeia
UV	Ultraviolet
VAMP	Vincristine, methotrexate, 6-mercaptopurine and prednisone
V_H	Variable heavy

V_L	Variable light
VWD	Variable wavelength detector
WEHI-164	Walter and Eliza Hall cell line 164
WST	Water soluble tetrazolium
XRC	X-ray crystallography
XTT	2,3-Bis-(2-methoxy-4-nitro-5-sulfophenyl)-2H-tetrazolium-5-carboxanilide

List of Figures

List of Tables

Chapter 1. Introduction

1.1 Cytotoxic Chemotherapy

1.1.1 The development of cytotoxic chemotherapy

During World War 2, an American ship secretly carrying bombs containing 100 tons of chlormethine (**1**) was destroyed while docked in Bari, Italy during a German air raid on the city. Chlormethine, is a nitrogen mustard and survivors of the attack exhibited unusual symptoms for a simple air strike. Dr Stewart Alexander was sent to aid their treatment and investigate the cause of their unusual symptoms. He found evidence of the mustard gas bombs in the wreckage of the American ship and noted that the people affected by the mustard gas had reduced white blood cell counts, suggesting nitrogen mustards were toxic to white blood cells.[1] Based on Dr Alexander's observations, Dr Alfred Gilman and Dr Louis Goodman hypothesised nitrogen mustards would also kill cancerous white blood cells. They performed a single patient experiment on a man with advanced lymphoma, a cancer of white blood cells. He agreed to an experimental treatment that involved having intravenous injections of a nitrogen mustard.[2] The patient responded to this therapy and his tumours decreased in size allowing him to swallow, eat and sleep. This trial is considered the first recorded use of cytotoxic chemotherapy.[2]

In 1948 Dr Sydney Farber published a paper documenting the first complete remission of leukaemia using the chemotherapeutic agent aminopterin (**2**).[3] This paved the way for Farber's subsequent work on chemotherapeutic agents, many of which are still used today. For example vincristine (**3**), which increased leukaemia remission rates above 80% [4] and methotrexate (**4**),[5] (**Figure 1.1**). Faber's work on methotrexate identified that the chemotherapy dosing regimen must be designed to limit the toxic side effects. He proposed shorter infusions with a more concentrated solution to be administered once every three weeks to lessen the side effects while retaining the

therapeutic activity.[5] The general public perceived chemotherapy as very dangerous, this is because many patients died while suffering from chemotherapy's extreme side effects and very few had sustained remission. Farber's work increased the survivability of patients receiving chemotherapy and improved its public perception.

Most early research was directed at blood cell cancers, as intravenous infusions allowed the drugs to readily reach their targets. Solid tumours, such as breast cancer and stomach carcinomas, are harder for drugs to reach and therefore harder to treat. Nonetheless, work undertaken by Roy Hertz demonstrated how methotrexate could affect choriocarcinomas (cancers of the uterus).[6] William Wilson demonstrated how 5-fluorouracil (5-FU, **5**) could be used to treat solid cancers as a monotherapy (**Figure 1.2**).[7] In addition, some people began experimenting with adjuvant therapy, administering 5-FU (**5**) following surgical removal of tumour tissue.[8] Adjuvant therapy drastically improved solid tumours remission rates and many tumours became more treatable than ever before.

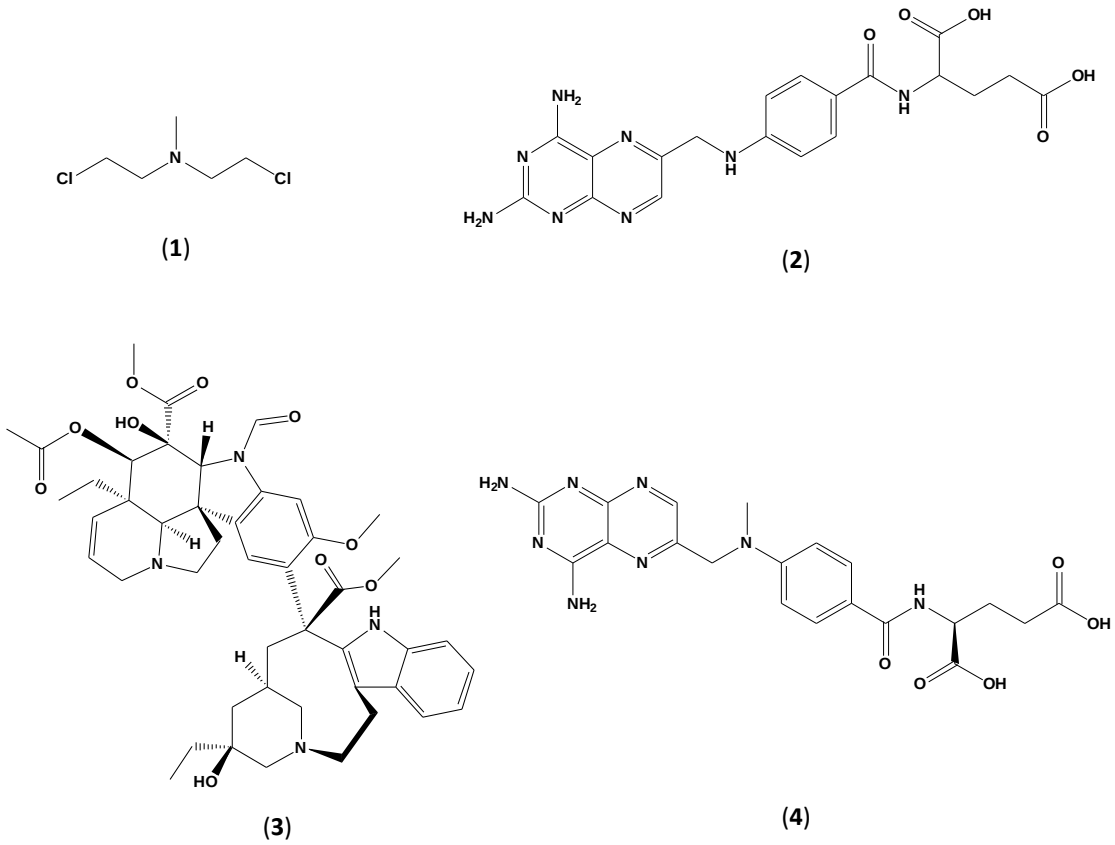

Figure 1.1. The chemical structures of the cytotoxic chemotherapy agents Chlormethine (**1**), Aminopterin (**2**), Vincristine (**3**) and Methotrexate (**4**).

While in 1957 Dr Ellison had been investigating combination therapy,[9] the co-administration of two or more chemotherapeutic agents, following a publication by Dr Law regarding the effectiveness of combination therapy on drug resistant cancers, [10] it was in the 1960's when combination therapy really took off, with the introduction of two particular chemotherapy regimens. The first regimen used vincristine (**3**), methotrexate (**4**), 6-mercaptopurine (6-MP, **6**), and prednisone (**7**) and was referred to as VAMP. [11,12] The second regimen used mechlorethamine (**1**), vincristine (**3**), prednisone (**7**) and procarbazine (**8**) and was referred to as MOPP. [13,14] The VAMP regime managed to achieve a remission rate over 50%,[15] while the MOPP regimen was reported to produce substantial durations of remission in patients compared to the standard treatments at the time.[14] Combination therapy is still used today, due to superior clinical outcomes over monotherapy. This is partly because combination therapy slows the development of drug resistance.[16] It was well known about bacterial cells developing drug resistance during the 1960's and this served as a good model for understanding how combination therapy prevented the development of drug resistance in cancer.[16]

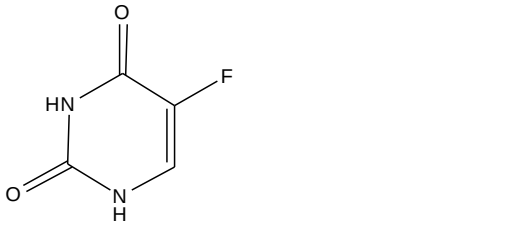

(**5**)

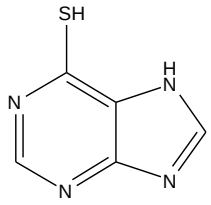

(**6**)

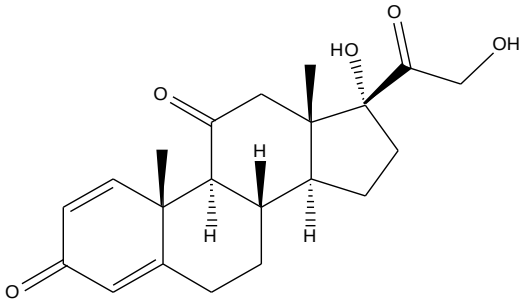

(**7**)

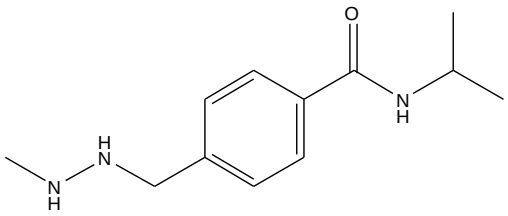

(**8**)

Figure 1.2. Chemical structures of the chemotherapy drugs 5-Fluorouracil (**5**), 6-Mercaptopurine (**6**), Prednisone (**7**) and Procarbazine (**8**).

Between 1960 and 1970, Dr Harold Skipper published many papers on chemotherapy and made some important advances. These included: the development of animal models of cancer which he used to study cancer treatment [17], based on that research he proposed a theory that drugs don't kill a specific number or mass of cancer cells but a specific percentage of cancer cells present. [18] Finally he applied the knowledge he had gained from his animal models to design chemotherapy regimens to kill the entire cancer cell population before it could grow back. [19]

Between the period of 1940 and 1970 the treatment of cancer evolved from simple surgery or radiation therapy, to adjuvant combination therapies with well-designed dosing regimens to spare the patient but kill the cancer. However, even with these advances, patient mortality remained almost unchanged.[20]

1.1.2 The drawbacks of cytotoxic chemotherapy

A major problem with traditional chemotherapy was that patients could not tolerate higher doses of these non-selective cytotoxic drugs, without suffering from potentially fatal side effects. [20] As small molecule cytotoxic chemotherapy lacks targeting, it is limited by the side effects of the drugs that act on all cells of a body not just cancerous cells. Especially as some cancers do not exhibit increased growth rates via evading growth suppressors or sustaining proliferative growth signals, instead satisfying other hallmarks of cancer, such as avoiding immune destruction, tumor-promoting inflammation, genome instability and mutation, resisting cell death. [244]

Cytotoxic drugs are still used to treat cancer, even though they have numerous awful side effects including: hair loss, nausea, damage to the mouth and pharynx, diarrhoea, damage to bone marrow as well as long term effects such as cardiac toxicity, lung damage and kidney failure. [245]

1.2 Non-cytotoxic Chemotherapy

1.2.1 Emergence of non-cytotoxic chemotherapy

Tamoxifen (**9**) is a drug that was initially developed as a contraceptive during the 1960's. It acts as a prodrug, having to be metabolised into a more active compound known as 4-hydroxy-tamoxifen (**10**), which binds to the oestrogen receptor as a partial agonist and this reduces cell growth and division (**Figure 1.3**). Tamoxifen was trialled in breast cancer which was known to be associated with the oestrogen receptors, and this study found that most patients responded. Furthermore, at higher doses the response rate increased while the side effects remained negligible. [21] Tamoxifen soon became a gold standard drug for treating breast cancer when used alongside cytotoxic chemotherapy drugs. [22]

Our understanding of growth factors and cellular signalling pathways was expanded in 1986 with the work of Goustin *et al.* [23] They demonstrated that cancerous cells can have different growth requirements, such as constituently active receptors and upregulated expression of growth receptors. They identified this was due to proto-oncogenes such as human epidermal growth factor receptor 2 (HER2, **Figure 1.4**) [24] [25] and the colony stimulating factor 1 receptor (**Figure 1.5**). [23] [26] They proposed proteins in these signalling pathways that would make good targets for anticancer drugs, as they could selectively affect aberrant cells, while having minimal effect on normal cells. Goustin's ideas were realized when imatinib (**11**), an inhibitor of a tumour specific antigen (TSA), was successfully tested.[27] Imatinib was able to inhibit the growth and proliferation of cancer cells that expressed the TSA even though it lacked cytotoxic activity. [27]

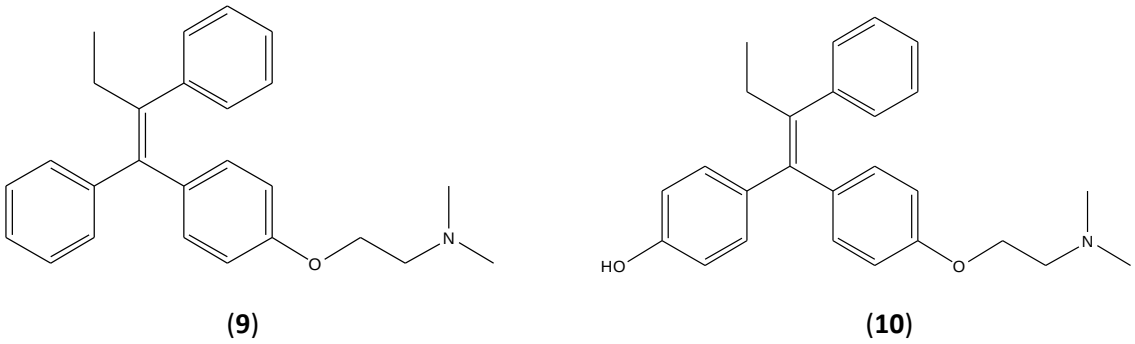

(**9**) (**10**)

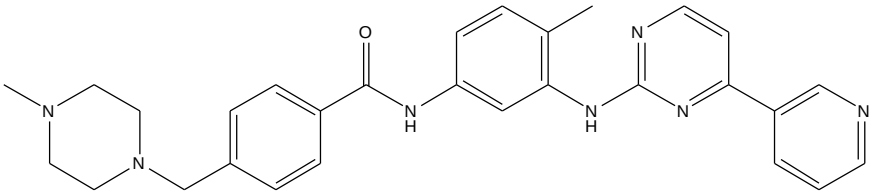

(**11**)

Figure 1.3. The chemical structure of Tamoxifen (**9**), 4-hydroxy-tamoxifen (**10**) and Imatinib (**11**).

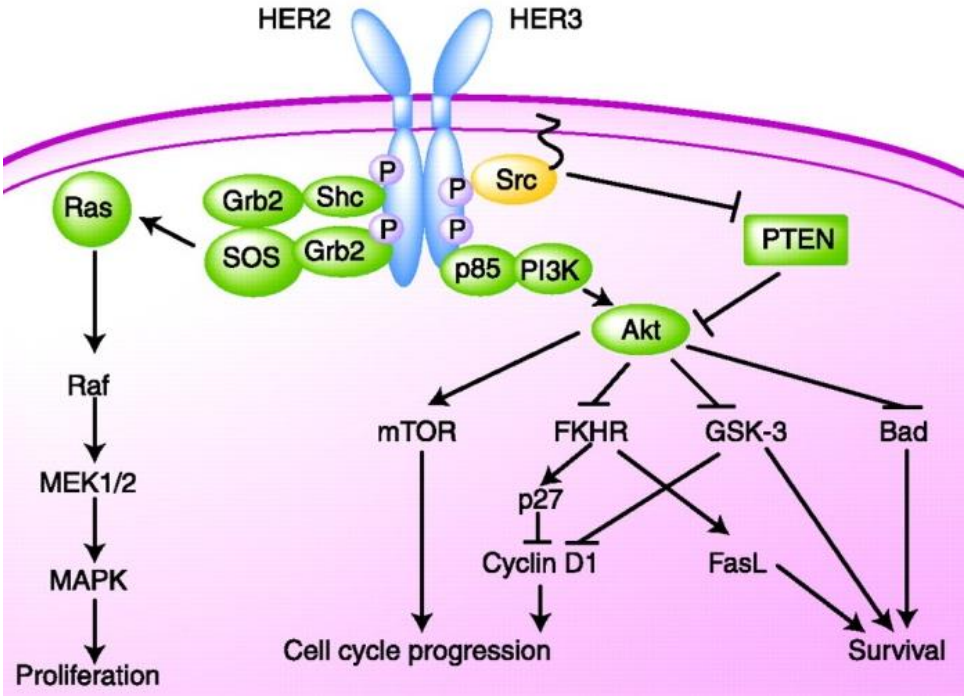

Figure 1.4. HER2 intracellular signalling pathways. Figure taken from Lin and Winner. [28]

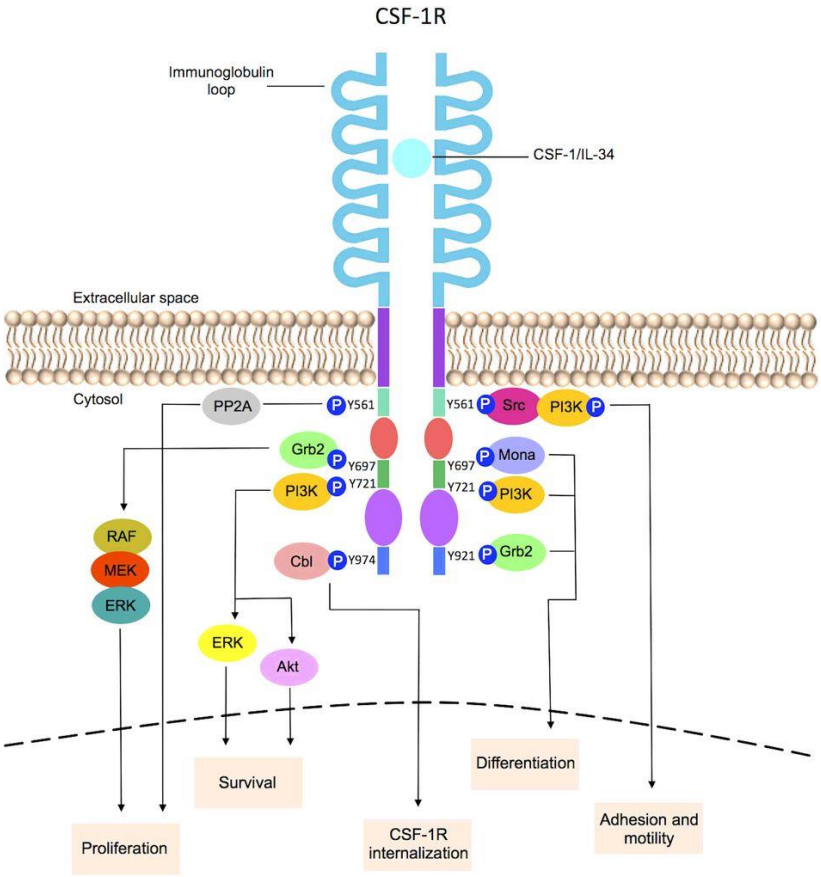

Figure 1.5. Colony stimulating factor receptor 1 intracellular signalling pathways. Figure taken from Achkova and Mahar [29]

Over time many small molecule drugs that targeted molecular pathways were discovered and tested, including inhibitors of many kinases involved in cancer as well as proteasome and VEGF inhibitors. [27, 246, 247, 248]

1.2.2 Drawbacks of non-cytotoxic chemotherapy

Non-cytotoxic drugs have much better side effect profiles than more traditional cytotoxic drugs. [27] However these molecular pathway inhibitors do not work indefinitely, with resistance often developing due to mutations. Resistance to imatinib developed in patients with advances chronic myeloid leukaemia due to mutations in the target kinase that made the kinase resistant to imatinib. [247] Mutations that cause resistance are diverse, using kinase inhibitors as an example, resistance can develop via over expression of the kinases, mutation of the kinase inhibitor binding site, kinase receptor mutations, drug transporter mutations and mutations to drug-metabolizing pathways.

[246] Furthermore, these non-cytotoxic drugs may have less aggressive side effects, but they do still have adverse effects for patients taking them, such as diarrhoea, skin toxicity and hypertension. [247] Clinical trials and pharmacoepidemiological reviews have revealed, that while molecular targeted therapies such as imatinib are important in cancer therapy there are numerous complications such as: an improved response rate and progression free survival improvements but no improvement to overall survival in clinical trials, issues of patient section due to the development of resistance or specific population groups that do not benefit from the drug due to genetic differences, as well as higher cost compared to traditional chemotherapeutic agents. [248] Additionally, these non-cytotoxic drugs are typically used alongside cytotoxic chemotherapy as cancerous cell death is a desired outcome of cancer therapy, as well as slowing their growth and metastasis, however in some indications co-therapy of a traditional-cytotoxic drug and a molecular targeted small molecule does not lead to an improvement in survival rates. [248] Fortunately, research on a class of biological molecules also able to interact with molecular targets, known as antibodies, had been taking place for almost 100 years and was about to revolutionize cancer therapy.

1.3 Antibodies as drugs

1.3.1 Foundational antibody research

At the turn of the 20th century, Dr Paul Ehrlich proposed the theory that cells interacted with nutrients and toxins through side chains that were specific for certain toxins and nutrients (**Figure 1.6**).[30] He later coined the term receptor to describe these side chains. He also hypothesised that the body would produce blood soluble receptors specific to toxins in response to an infection. He speculated this would prevent toxins from interacting with the receptors on cells. He described these hypothetical soluble receptors as 'antibodies'. Ehrlich was a visionary and unfortunately his theory was not readily accepted before he died in 1915. [31, 30] However, the receptor theory became a central concept in pharmacology from the 1950's onward.

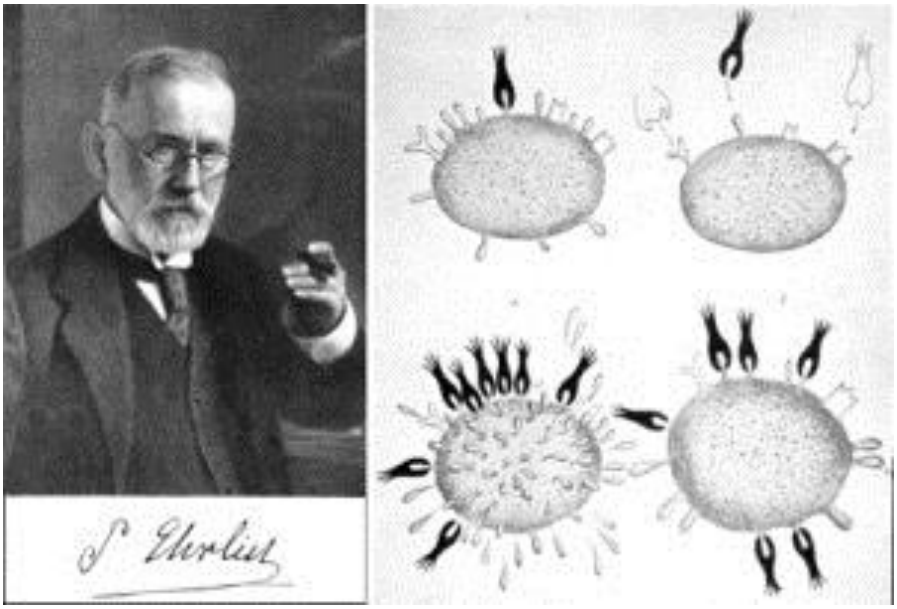

Figure 1.6. Dr Paul Ehrlich and diagrams of his receptor theory, including receptors and antibodies.[32]

The structure of antibodies, also known as immunoglobulins, was initially solved by Gerald Edelman and Rodney Porter. Both scientists experimented with antibodies by denaturing them with chemicals. Edelman managed to reduce an antibody into two pairs of protein fragments. [33] These were the heavy and light chains as we know them today (**Figure 1.7**).[34] At the same time, Rodney Porter had performed experiments on antibodies, using the enzyme papain, which created two fragments that retained their antigen binding properties and one fragment that crystallized at low temperatures. These became known as the fragment antigen binding (Fab) and fragment crystallisable (Fc) (**Figure 1.8**). [35] The Nobel Prize in Physiology or Medicine 1972 was awarded jointly to Gerald M. Edelman and Rodney R. Porter for “their discoveries concerning the chemical structure of antibodies."

Figure 1.7. Simple diagram of an antibody, with the heavy chains coloured grey and the light chains coloured blue. [36]

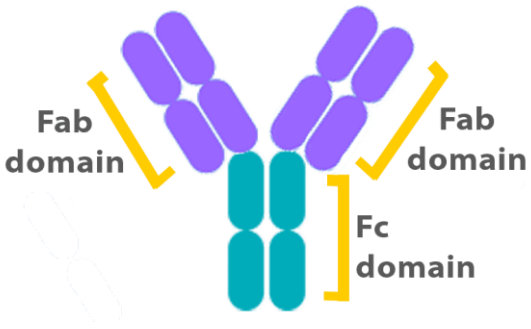

Figure 1.8. Simple diagram of an antibody, with both Fab regions colour purple and the Fc region coloured green. [37]

While we had an understanding of the structure and purpose of antibodies, we still did not know how they managed to be so specific while having such similar structures. In 1970 Dr Wu and Dr Kabat published their work on what they termed the "complementary determining regions" or CDRs.[38] These were short regions on the heavy and light chains of the Fab regions which controlled the antigen specificity through different amino acid sequences (**Figure 1.9**). [38]

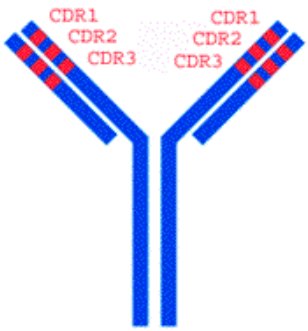

Figure 1.9. Simple diagram of an antibody, with the CDRs coloured red. [39]

Putting all of this information together we now understand an antibody is a protein that forms part of the mammalian adaptive immune system. Antibodies are proteins that have a quaternary structure, meaning they are constructed of more than one sequence of amino acids. More specifically, IgG antibodies are made of two pairs of amino acid sequences (four polypeptide chains in total). These four proteins are known as the heavy and light chains. Heavy chains have a molecular weight of about 50 kDa each, while the light chains are about 25 kDa each (**Figure 1.10**). The heavy and light chains are held together by disulphide bonds. Therapeutic antibodies typically contain

four inter-chain disulphide bonds, two between the heavy chains and one between each pair of heavy and light chains (**Figure 1.10**). This gives antibodies a flexible "Y" shaped quaternary structure. The structure is flexible as the heavy chains contain "hinge regions" (**Figure 1.10**).

The Fc domain is located on the tail or trunk of the antibody, close to where the two heavy chains are attached through disulphide bonds (**Figure 1.10**). This domain is constant between antibodies of the same isotype and controls the activation of the immune system. The 'arms' of the antibody where the light and heavy chains are attached are known as Fab domains. These Fab domains contain variable sections that confer the antibodies selectivity. The variable sections contain complementary determining regions or CDRs (**Figure 1.10**). The CDRs are responsible for the selective binding to the target antigen. The heavy and light chain CDRs form an antigen binding site, also known as a paratope, and the specific complementary sequence found on the antibody is known as the epitope. Some antibodies that bind to the same target antigen, such as trastuzumab and pertuzumab, bind to different epitopes on the same antigen.

There are 5 known classes of antibodies, also known as immunoglobulins: IgA, IgD, IgE, IgG and IgM. [249] Each class is differentiated and defined by their conserved heavy chain domains. IgA, IgD and IgG each have the conserved domains known as CH1, CH2 and CH3, while IgE and IgM have an additional region, CH4. [249] Furthermore, while IgD, IgE and IgG are monomeric (**Figure 1.7 - 1.9**), IgA is dimeric, and IgM is pentameric. [249] Antibodies expressed on the surface of B cells are IgD, while secreted antibodies tend to be IgG. [249] The other classes of antibodies won't be discussed in this thesis.

Figure 1.10 shows an IgG1 antibody with important features highlighted. The heavy chains are blue with the three conserved subunits in dark blue, labelled C_H1-3, while the variable subunit is a pale blue and labelled V_H. You can see the hinge regions located between C_H2 and C_H1 on each heavy chain. The light chains are coloured green, with the conserved light subunit in darker green, labelled C_L and the variable light subunit in paler green labelled V_L. The CDRs are represented as the tips of orange

antigen binding sites; these are labelled L1-3 and H1-3 depending on if they are from the light or heavy chain. The antigen binding region, also known as the paratope, is orange. Lastly the 12 disulphide bonds are shown in red. The V_L, C_L, V_H and C_H1 subunits all contain intra-chain disulphide bonds, these account for 8 of the disulphide bonds. There are 4 inter-chain disulphide bonds that hold the chains together, these are located between the C_L and C_H1 subunits and two disulphide bonds are between the heavy chain hinge regions.

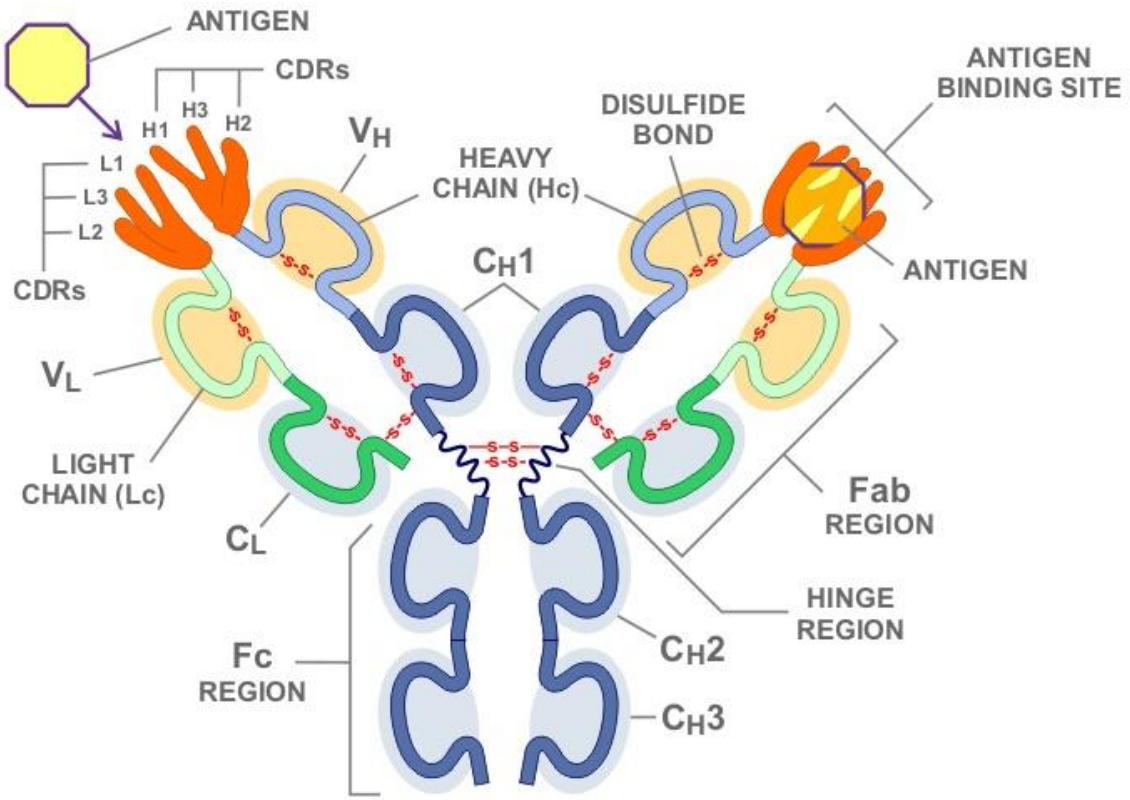

Figure 1.10. Highly detailed diagram of an IgG1 antibody.
Taken from Janeway, Travers, Walport and Schlomchik. [64]

The mammalian immune system contains cells known as B cells which through complex mechanism produce antibodies with specific CDR regions, conferring each antigen they produce with the same antigen specify. [250] These antigen specific antibodies are fixed to the plasma membrane of the B-cells which can then bind to antigens. B cells can then process the antigen and present it on major histocompatibility complex 2 molecules. [250] T helper cells can interact with the presented antigen via their

T cell receptors, which then activate the B-cells via an interaction of the CD40, expressed on B-cells and CD40 ligand expressed on T cells. [250] The B cell is now activated and will proliferate as an effector cell which will secrete the same antibodies that originally bound the antigen. [250] Effector B cells will progress to large plasma cells which can secrete 2000 antibodies a second, however large plasma cells sacrifice their ability to grow or divide, lasting only a matter of days, though some will persist in bone marrow for months. [250] Once secreted, antibodies typically circulate in the blood and lymph until they find and bind their target antigen. Once bound to an antigen, typically a foreign protein, the immune system can take further steps to remove the entity, most often a virus or bacteria. [250]

The Fc region of an antibody can activate various immune pathways including the complement system which can drive histamine release via C3a, phagocytosis via opsonin (C3b) coating of microorganisms, promotes chemotaxis and activates white blood cells via C5a and bacterial lysis via C5-9. [251] This is known as complement dependent cytotoxicity (CDC)

The Fc region can also promote phagocytosis of the antibody bound target via interactions with neutrophils and macrophages, this occurs without the need for opsonin from the complement cascade. Once ingested via phagocytosis the neutrophils and macrophages assault the antibody bound target with proteolytic enzymes and reactive oxygen species which damage the bacteria or virus. [251] This is known as antibody dependent cellular phagocytosis (ADCP)

Another mechanism mediated through the FC region is antibody dependent cellular cytotoxicity (ADCC). This is a mechanism through which the FC region of the antibodies interacts with specific effector cells, most commonly natural killer (NK) cells, which are white blood cells that express FC receptors. Once bound to an FC region of an antibody, the NK cells release granzyme and perforin, which create pores in plasma membranes, allowing the granzyme to enter the target cells, which then initiate apoptosis. [252]

IgG antibodies come in a variety of subclasses (**Figure 1.11**). [59] Although all IgG subclasses share over 90% of the same amino acid sequence, there are significant differences between IgG subclass effector functions. The structural difference between IgG subclasses is primarily at the CH2 and hinge domains. Both of these domains are involved with Fc receptor and complement protein interaction, which is what controls CDC, ADCP and ADCC. IgG1, IgG2, and IgG4 isotypes are used as therapeutic antibodies. IgG1 antibodies elicit stronger ADCC and CDC promotion than IgG2 and IgG4 isotypes. [60] IgG2 antibodies tend to have very little CDC activity and only promote ADCC at very high cell binding densities. [60] The IgG4 isotype has less ADCC activation but is able to promote CDC using the same glycan structures as IgG1 antibodies. [61]

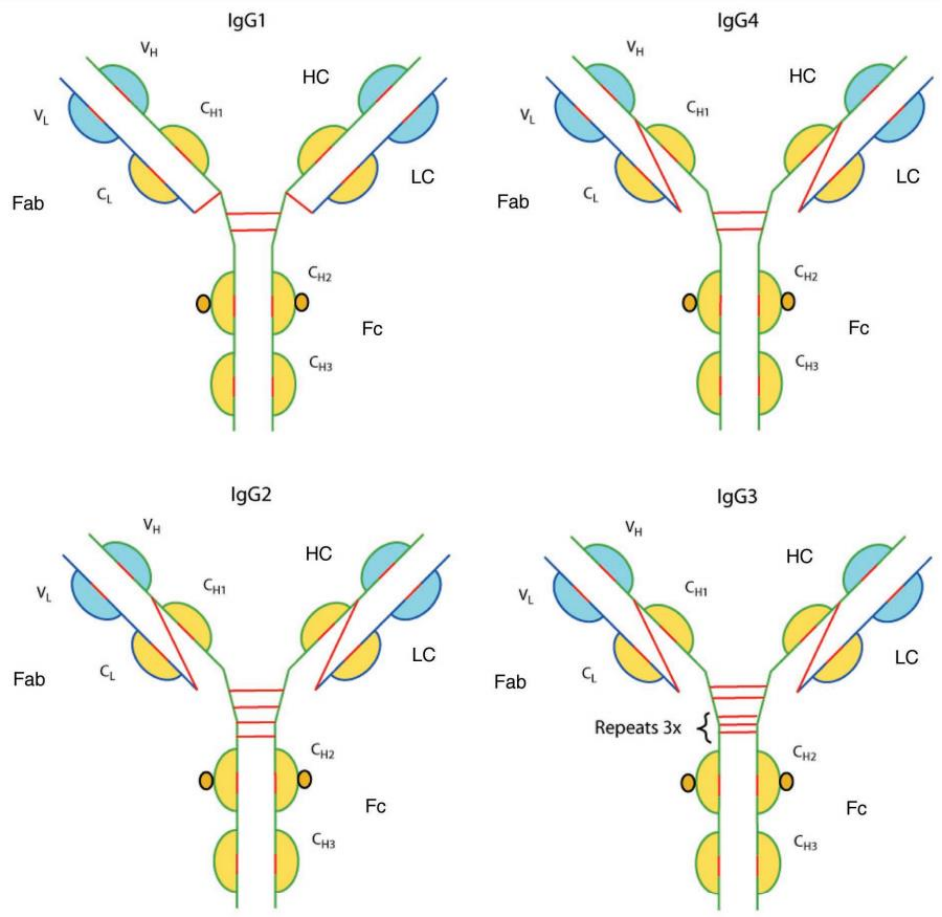

Figure 1.11. Diagrams of IgG isotypes. Disulphide bonds are shown in red. Taken from Correia. [62]

While the protein structure of antibodies is critical for their binding and affects effector function, so too does the glycosylation of the antibody. [57] Glycosylation is a post-translational modification of an antibody, through which glycans are attached to the antibody. These glycans are large monosaccharide chains, often containing: mannose, *N*-acetylglucosamine, *N*-glycolylneuraminic, galactose, sialic acid, xylose and/or fucose. [57] The glycosylation of antibodies is heterogenous, with at least 36 potential chain structures. [254] Some glycan modifications have been associated with adjustments in effector function, which are described below (**Figure 1.12)**.

Fucosylation, the attachment of fucose to glycans, can affect the binding of antibodies to types of Fc receptors. More specifically, core-afucosylation, the lack of a fucose on the molecules of the glycan chain, causes a tighter binding to a type of Fc receptor which increases ADCC and ADCP. [57, 254] Galactosylation, the attachment of galactose to glycans, is reported to confer anti-inflammatory activity to IgG antibodies. [57] Sialyation, the attachment of sialic acid, has been shown to decrease ADCC but only if the antibody was core-fucosylated, and had no effect on core-afucosylated antibodies. [254] Sialyation has also been shown to increase anti-inflammatory activity. [57]

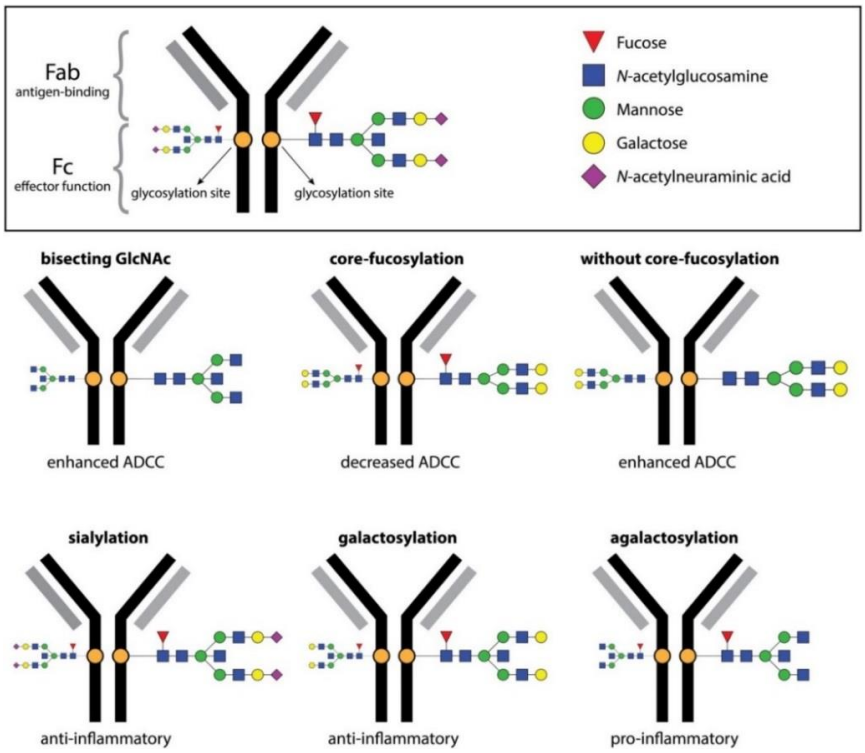

Figure 1.12. Examples of different Fc region glycosylation chains and the observed cellular effects. Taken from Lauc, Pezer, Rudan and Campbell. [57]

Antibodies that target upregulated proteins expressed on cancer cells, would direct the immune system to conduct CDC, ADCP and ADCC against the cancerous cells, as well as binding to and blocking receptors that may be involved in cancer related signal propagation, such as growth signalling. However, although we now had a clearer understanding of antibody structure, we could not make antibodies very well, with the key limitations being specificity and quantity. In 1975 César Milstein and Georges Köhler published a paper which explained how to use their hybridoma technique to make a cell capable of producing large quantities of antibodies that were specific towards a single target (**Figure 1.13**). [40] The Nobel Prize in Physiology or Medicine 1984 was awarded jointly to Niels K. Jerne, Georges J.F. Köhler and César Milstein "for theories concerning the specificity in development and control of the immune system and the discovery of the principle for production of monoclonal antibodies.".

Their method worked by harvesting splenocytes from mice already primed against a specific antigen via intravenous immunization. Some of the spleenocytes harvested should be B cells that have antigens expressed against the antigen used during the immunization. These cells are then fused with immortal b cell cancers cells that don't have the hypoxanthine-guanine phosphoribosyltransferase (HGPRT) gene, using either electrofusion or polyethylene glycol. This procedure should produce a mixture of cells that are immortal myelomas that lack HGPRT, harvested B cells that secrete the antibody and immortal fusion cells that secrete the antibody and have the HGPRT gene. This mixture of cells is grown on hypoxanthine-aminopterin-thymidine medium for up to two weeks. The unfused myeloma cells lack HGPRT and as the aminopterin blocks nucleotide synthesis they die. The unfused B cells die due to their short lifespan. The remaining cells must all be hybridoma cells, which will produce antibodies towards the same target, hence 'monoclonal' antibodies. [41] The hybridomas can be cultivated and the secreted antibody purified from the media they are grown in typically via affinity chromatography. Protein A or G coated resin can be used to bind the antibodies via their Fc regions, this binding will occur at neutral pHs (7.5). Once the resin is at capacity, the chromatographic conditions can be adjusted to lower the pH to around pH 2.5, which

washes the bound antibody off the resin. [41] This enables the isolation and purification of monoclonal antibodies from the supernatant taken from the hybridoma cell cultures.

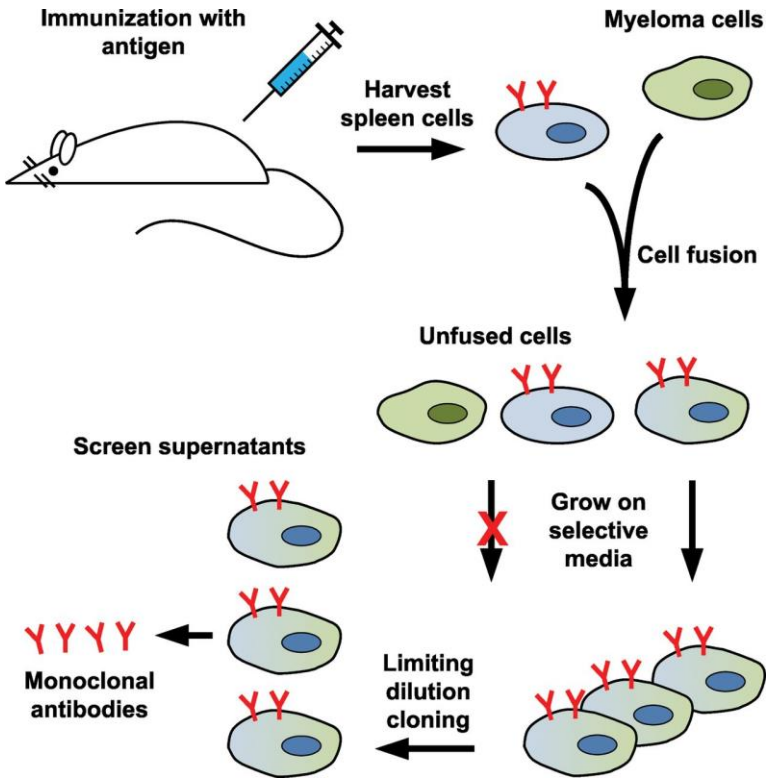

Figure 1.13. Diagram of method for production of a monoclonal antibody using hybridoma cells. Figure taken from Sgro [41]

Following Köhler and Milstein's methods, monoclonal antibodies (mAbs) could then be made against a specific target. This allowed mAbs to be made as drugs against extracellularly expressed disease associated proteins, something which is common in many cancers.

1.3.2 Early therapeutic antibodies

Ideally a therapeutic antibody would be targeted to a protein that is expressed exclusively on or over expressed on cancerous cells. This would enable the specific or selective activation of the immune system via CDC, ADCP and ADCC against cancerous cells. Antibodies can also bind to receptors antagonistically and prevent activation of cancer associated receptors, such as over-expressed growth receptors. However, with

antibodies being produced in murine hybridoma cells, immunogenicity soon became a problem. [40,41] Early clinical trials with murine antibodies such as Muromonab-CD3, failed mainly due to potentially fatal immune system activation and development of anti-mouse antibodies which reduced the effectiveness of the drug after repeated administrations. [43]

To overcome the issue of immunogenicity, scientists began working on minimising the murine content of the antibody (**Figure 1.14**). Chimeric antibodies were first developed by Vernon Oi who developed a method of combining the constant region of a human antibody with the variable antigen binding domain of a murine antibody.[44] These chimeric antibodies were approximately 66% human and demonstrated a more tolerable side effect profile than fully murine antibodies.[45] Taking this even further was Greg Winter who developed a method of producing "humanised" antibodies, which are human antibodies with only the CDRs transplanted in from murine antibodies.[46] Humanised antibodies are over 80% human and exhibit the least amount of immune activation and anti-drug antibody production upon administration.[45]

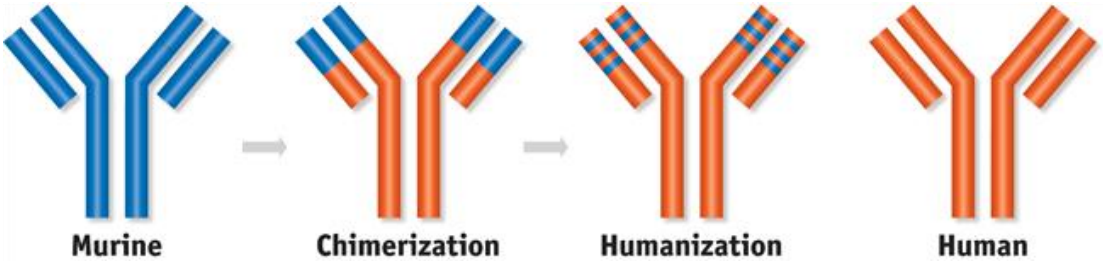

Figure 1.14. Simple diagram of antibodies, with murine protein in blue and human protein in orange. [47]

In 1997, a chimeric antibody called rituximab was the first monoclonal antibody approved for cancer treatment. Rituximab targets CD20, a protein expressed on B-cells. Once bound to CD20, rituximab promotes ADCC and CDC (**Figure 1.15**). Rituximab in combination with cytotoxic chemotherapy improved response rates and progression free survival. [48] CD20 has no known function and Rituximab's therapeutic effect is solely from ADCC and CDC.

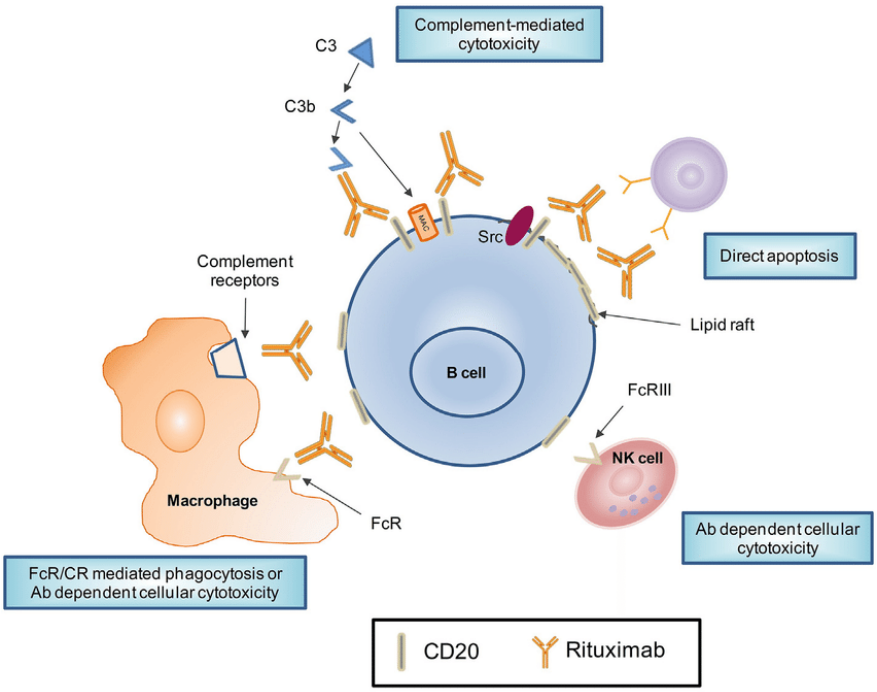

Figure 1.15. Rituximab's mechanisms of action, including CDC, direct apoptosis, antibody (Ab) dependent cellular cytotoxicity and ADCC. Figure taken from Falduto. [49]

In 1998, Trastuzumab was the first humanized antibody licensed for use to treat cancer. Trastuzumab targets the HER2 receptor, a protein overexpressed in about 20% of breast cancers. [24] Once bound to HER2, trastuzumab promotes ADCC, CDC and direct apoptosis much like rituximab does when bound to CD20 (**Figure 1.15**). However, as HER2 is a functional receptor, trastuzumab also downregulates HER2 signalling. HER2 activation promotes cell growth, which is why overexpression is typically associated with cancer (**Figure 1.4**). While trastuzumab initially inhibits HER2 signalling, it is found that within 1 year most cancers will have developed resistance. [51] As such, trastuzumab is often administered in combination with cytotoxic chemotherapy drugs which extends the duration of its use before drug resistance develops and improves the rate of remission and clinical outcomes. [52,53]

1.3.3 Current clinical use of antibodies in cancer therapy

Antibodies are used in a variety of ways to treat cancer. Many antibodies act as anticancer agents through ADCC and CDC and scientists have engineered antibodies to exhibit increased levels of ADCC and CDC promotion.[54,55] These second generation

antibodies demonstrate how we can modify Fc region glycosylation of antibody directed to the same targets as first generation antibodies, but now with greater efficacy and improved tolerability.[56] For example, ocrelizumab targets CD20 like rituximab, but is humanised and has been glycoengineered to increase effector function at the Fc region (**Figure 1.12**). This means ocrelizumab produces milder adverse effects and up to 5 times the level of ADCC.[56]

Alternatively, some antibodies do not treat cancer by targeting the cancer itself but target the immune system. So-called 'immune checkpoint blockers' inhibit signals that dampen down a human's immune system. For example, ipilimumab antagonizes the inhibitory receptor of CTLA-4, resulting in T-cells with increased activity. [255] Combined administration of ipilimumab with a cytotoxic drug called dacarbazine causes a significant improvement in survival compared to patients only administered with dacarbazine. [255] There are also antibodies that antagonise PD-1 and PD-L1 such as pembrolizumab and atezolizumab respectively. [255] PD-1, expressed on activated T and B cells, when bound with PD-L1 propagates an inhibitory signal to the immune cells. [255]

Monoclonal antibodies have proven to be a revolutionary tool in the treatment and management of cancer. A study in 2014, found addition of trastuzumab to HER2+ breast cancer therapy caused a 37 % improvement in overall survival. The 10-year disease free survival rate for HER2 positive breast cancer was over 73 % and overall survival was at 84 %. [52,53] When rituximab was added to combination chemotherapy treatments for B-cell lymphoma the duration of response increased from 14 months to 38 months, and the objective response rate increased from 75 % to 92 %. [49] Second-generation antibodies, such as obinituzumab have been shown to outperform their first-generation equivalents, for example progression free survival increased 9 % comparing rituximab with obinituzumab chemotherapy in the GALLIUM trial. [256] However, there are still many issues with antibody therapies in current clinical use, such as side effects, resistance and limited response rates, these are described more detail in the next section.

1.3.4 Problems with antibodies in cancer therapy

Paul Ehrlich is famous for having described “The Magic Bullet”.[30] He proposed antibodies were magic bullets, able to kill microbes in the body without harming the host. However he gave up on this concept when he discovered antibodies could not always kill microbes.[30] Since then numerous issues with antibodies have been identified, which are described below.

Most antibodies have unpleasant side effects such as nausea, vomiting, dizziness, headaches, fevers, and rigors as well as potential drug specific adverse events such as anti-CD-20 infusion reactions, anti-EGFR antibodies skin, lung, and gastro intestinal toxicity, anti-HER2 antibodies cardiotoxicity, anti-VEGF delayed wound healing, and immune -checkpoint blocker autoimmune effects. [255]

Compared to small molecule drugs, antibodies have a high cost, especially second-generation antibodies. According to the online British National Formulary, [257] the small molecule cytotoxic drug doxorubicin costs ~£20 per mL, rituximab costs ~£350 per mL, and ocrelizumab costs ~£4800 per mL. These high costs are especially problematic for the NHS, due to limited funding requiring resource allocation to maximise the cost effectiveness of care, while the main effect on private healthcare is rapidly rising costs of cancer treatment and a willingness to pay these costs if possible, thus resulting in an ever-widening health care gap between the richer and poorer of society. [259, 260]

Additionally, cancers are known to development resistance to antibody therapy via a number of mechanisms. [258] For example trastuzumab therapy of HER2 positive breast cancer often only works for 18 months before resistance emerges. [258] The resistant to trastuzumab can be due to: over expression of a membrane associated glycoprotein that sterically hinders binding of trastuzumab to HER2, increased signalling activity of insulin-like growth factor recptor-1, mutation of HER2 into a truncated form that does not have an extra-cellular domain for trastuzumab to bind to,

and mutation of signalling proteins downstream of HER2 that increased activity or reduce signalling inhibition, making inhibition of HER2 less effective. [258] While these are examples of resistance to trastuzumab, similar mechanisms of resistance affect other antibodies such as rituximab along with other such as down regulation of CD20. [258]

Lastly while co-administration of antibodies has been shown to improve patient outcome with better overall objective response, longer progression free survival and higher 10-year survival rates, [52, 53] some patients to not respond to therapy, resistance develops, cancer often eventually progresses, and patients die. [258] Ideally the therapies to treat cancer would have a 100 % response rate and indefinite progression free survival, but that is not the reality of modern cancer therapy. Furthermore, second-generation antibodies are not living up to their original promise, for example in some clinical trials ocrelizumab has failed to demonstrate any difference regarding disease progression compared with rituximab, although there were some statistically significant improvements in the number and severity of adverse events and side effects. [261]

Like Ehrlich before us, we must conclude that antibodies are not the magic bullets that he had envisioned and they are also not a perfect answer to cancer, even with all the advances we have, such as glycoengineered antibodies and co-administration with immune modulators and cytotoxic drugs, for example in the phase 2 trial GALEN, which combines atezolizumab, obinituzumab and lenalidomide to treat lymphomas metastasised into the central nervous system. [262] The GALEN trial had a 90 % response rate, but a mean response rate of only 9 months. [262] Clearly new tools are required for the ongoing treatment of cancer, which brings us to antibody drug conjugates.

1.4 Antibody drug conjugates

1.4.1 A brief history

The idea to link (or conjugate) potent cytotoxic small molecules to an antibody had been around for decades before it was technically possible, going as far back as Ehrlich himself. In 1993 a paper was published, demonstrating a conjugate of doxorubicin and a chimeric monoclonal antibody targeted to a tumour associated protein. This antibody drug conjugate was called BR96-Doxorubicin and it cured 94 % of rats with lung cancer.[66] Once bound to the target protein, the conjugate was internalized into the cell, where the doxorubicin, a topoisomerase II inhibitor, is cleaved from the antibody and can cause DNA cleavage (**Figure 1.16**).[66] Following this finding, there was a surge in the number of antibodies conjugated to different cytotoxic drugs that were investigated.[67] These new drugs fall under the wide drug class of immunoconjugates, which covers any antibody, fragment of antibody, or targeted protein, conjugated to cytotoxic drugs, bacterial toxins, radionuclides, cytokines, enzymes etc. More specifically, the type of immunoconjugate that will be discussed in this thesis is known as an antibody-drug conjugate (ADC).

Unfortunately, BR96-doxorubicin did not perform well in human clinical trials. [68] A major problem identified was the difference between targeting tumour associated antigens (TAA) and tumour specific antigens (TSA), as targeting TAA can lead to off target toxicity and reduced therapeutic capacity.[69] For example, BR96-doxorubicin was found to have severe gastric side effects due to the expression of the target antigen in gastric mucosal cells.[70] Another tragedy occurred when, an ADC in phase one clinical trials caused the death of one of its seven patients and caused major adverse skin reactions in other patients.[71] The ADC was immediately discontinued, with unexpected off target toxicity to blame for the fatality.

ADCs use extremely potent cytotoxic drugs or “warheads”. If the target antigen is not tumour specific it must be upregulated, by a significant degree, in the cancerous

cells. If the antigen is also upregulated in a non-target cell population, severe off target toxicity will be dose limiting and preclude therapeutic activity. [69] The issue of antigen distribution is confounded by xenograft cancer models where human tumours are cultivated in non-human hosts. This means the target antigen could only be expressed in the tumour and not elsewhere in the host, which does not help identify off target toxicity.[72] More modern genetically engineered tumour models have proven more predictive of human response.[72]

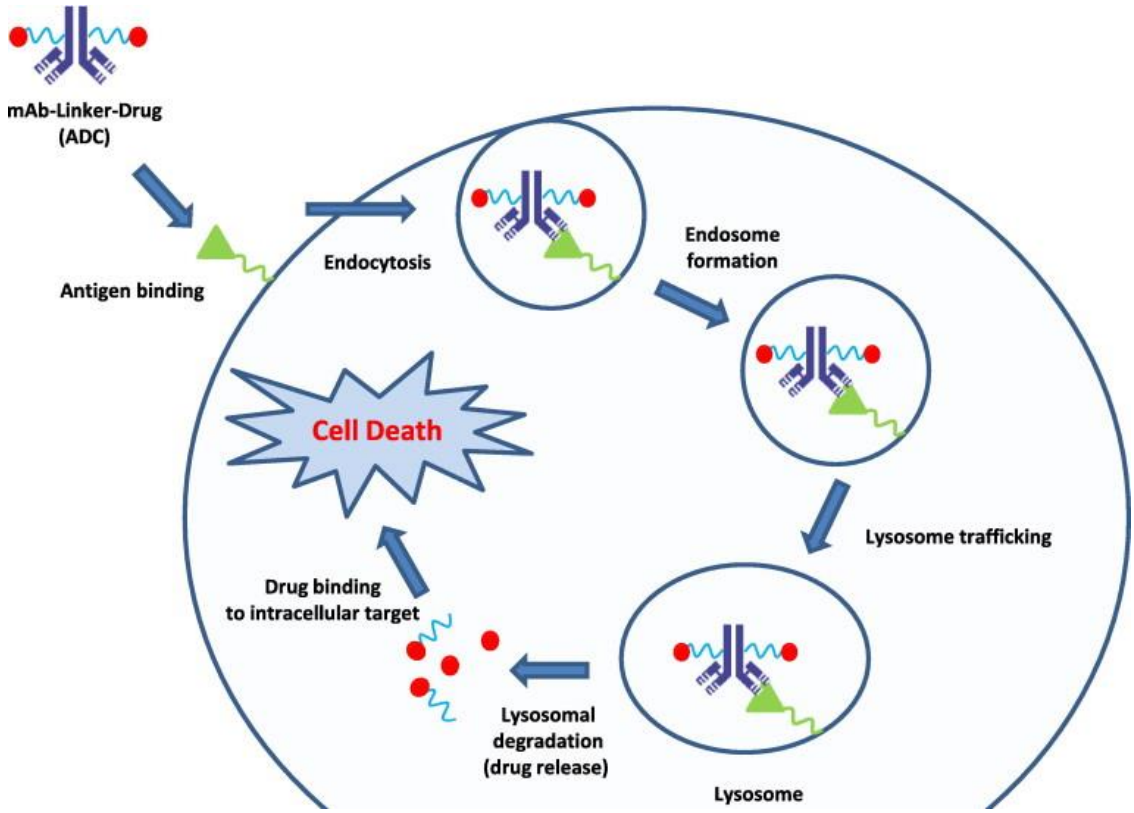

Figure 1.16. Mechanism of ADC internalisation and drug release.
Taken from Bouchard, Viskov and Garcia-Escheverria. [73]

In 2001, an ADC known as gemtuzumab ozagamicin was given accelerated approval to market. While it had overcome many hurdles that other ADCs could not, it was subsequently withdrawn from the market in 2010. An ongoing clinical trial had revealed that gemtuzumab ozagamicin actually increased the rate of mortality from 1.4% to 5.7% and had equivalent therapeutic outcomes compared to conventional therapies. [75] Gemtuzumab ozagamicin was reintroduced in 2017 at a third of its original dose (3mg/mL), in a revised dosing regimen (three administrations for the first induction

only, then one administration per consolidation course, as opposed to every 14 days) and a different patient group (Co-administration with daunorubicin or cytarabine) . [76] This was after it was demonstrated in another clinical trial that gemtuzumab ozagamicin could increase overall survival compared to conventional therapies. [76]

In 2011, brentuximab vedotin was the second ADC approved to market, closely followed by trastuzumab emtansine in 2013. In 2017, inotozumab ozagamicin became the fourth and most recently approved ADC.

1.4.2 The target protein

The target protein should ideally be a tumour specific, extracellularly expressed, internalising protein. But if the target antigen is only highly upregulated in the cancerous cells, a tumour associated target can work. All market approved ADCs currently target tumour associated proteins and not tumour specific ones. Gemtuzumab ozagamicin targets CD33 [77], a receptor often overexpressed in leukaemia (**Figure 1.17**)[78], while brentuximab vedotin targets CD30 [79], a receptor expressed in activated B and T cells that is associated with lymphoma (**Figure 1.18**).[80] Trastuzumab emtansine targets HER2,[81] a receptor overexpressed in 20% of breast cancers (**Figure 1.19**).[24]

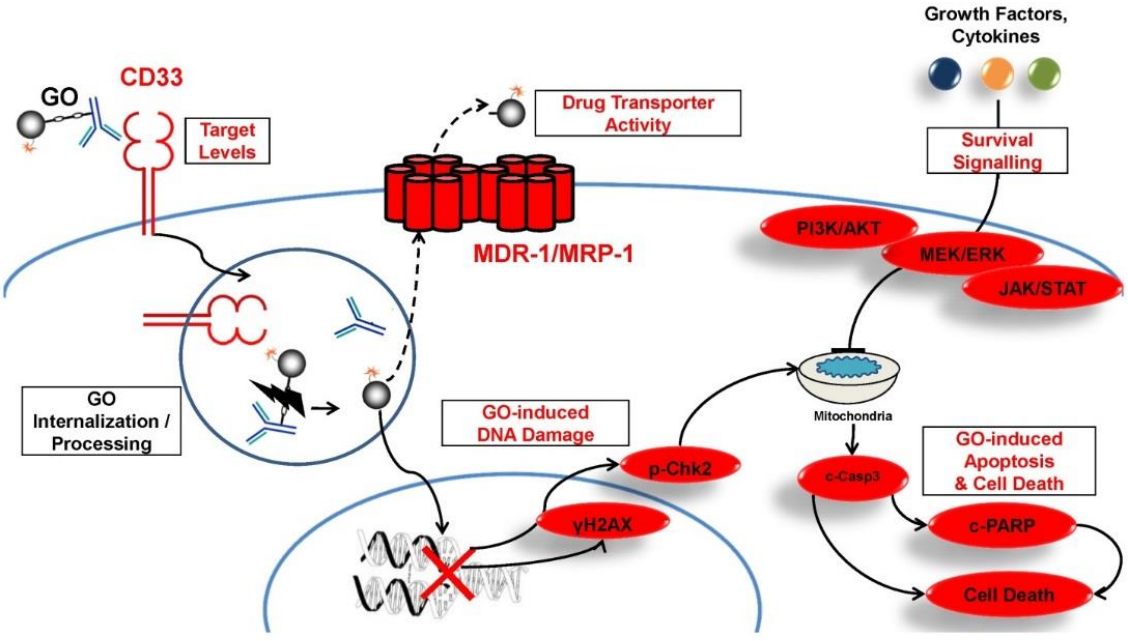

Figure 1.17. Gemtuzumab ozagamicin's mechanism of action. Taken from Rosen *et al.* [82]

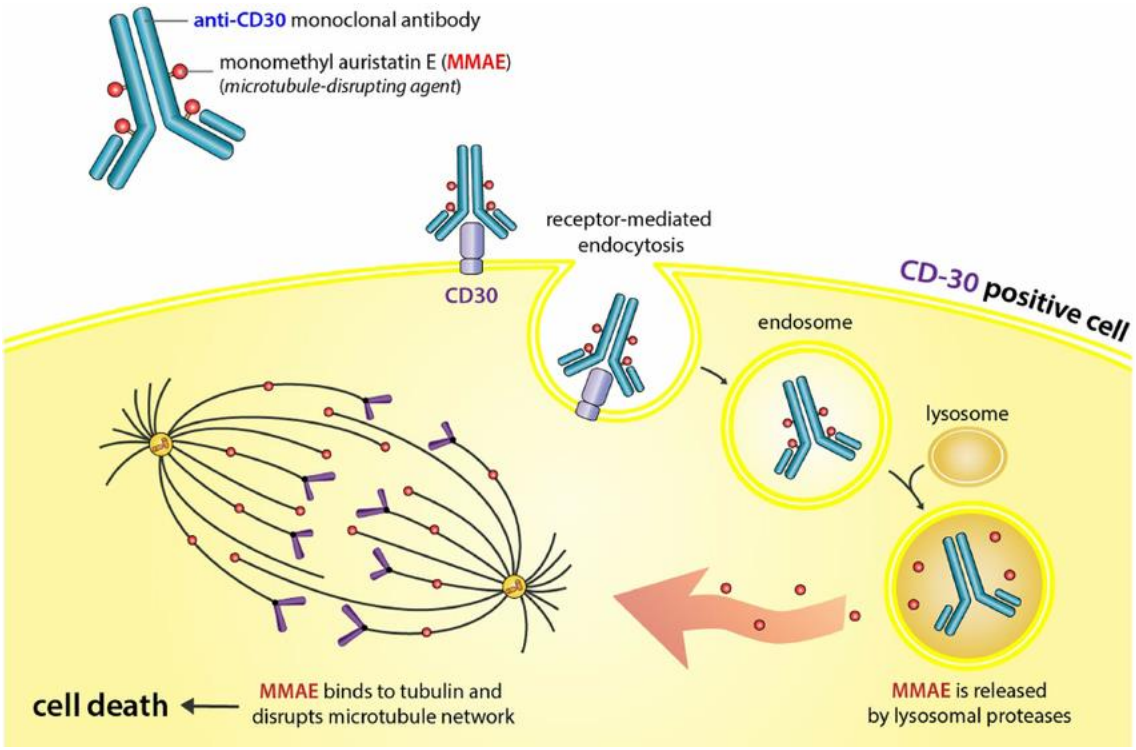

Figure 1.18. Brentuximab vedotin's mechanism of drug release and action. Taken from Eyre, Khan, Hall and Collins. [83]

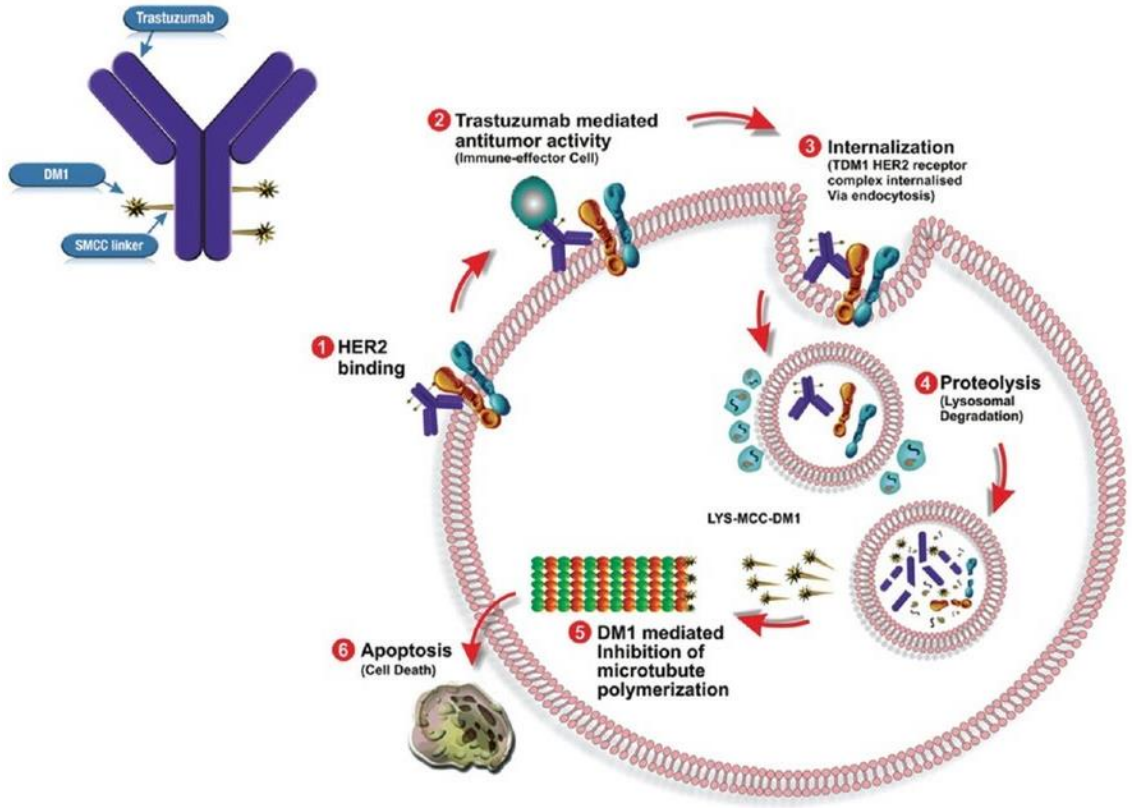

Figure 1.19. Trastuzumab emtansine's mechanism of drug release. Taken from Gogia *et al*. [84]

1.4.3 Antibody species

The antibody species is referring to whether it is murine, chimeric, humanized or even fully human (**Figure 1.14**). Ideally, fully human antibodies would be the starting point for any new ADC, however the technology to create fully human antibodies is expensive and so many new antibodies and ADCs are humanized, as they still work, and the final product is less costly and so more likely to be available. Over time, the technology to create fully human antibodies will become common place. Currently: gemtuzumab ozagamicin is humanized, brentuximab vedotin is chimeric, trastuzumab emtansine is humanized and inotozumab ozagamicin is humanized. Additionally, there are chimeric, humanized and fully human ADCs currently in development. [85]

1.4.4 Linker chemistry

The linkers in ADCs are responsible for holding the warhead and antibody together. This means the linker controls the site of attachment to the antibody and the conjugation chemistry to the warhead. The linker is an extremely important aspect of ADCs as it effects payload distribution, drug to antibody ratio (DAR), warhead release and warhead potency.

Linkers currently used in ADCs target either nitrogen or sulphur atoms on the surface of the antibody. These atoms are found in lysine and cysteine amino acid residues respectively (**Figure 1.20**). There are between 30 and 40 externally accessible lysine residues on an IgG1 antibody [85,86] and linker attachment to the lysine residues typically varies between 1 and 8 payload attachments per antibody. This allows a staggering 8.65 million potential regional-isomers across all the DARs. [87] Alternatively, there are only 8 externally accessible cysteine residues on an IgG1 antibody, which are the cysteine residues responsible for the inter-chain disulphide bonds (**Figure 1.10**). While the DAR for ADC's utilising cysteine reactive linkers can still vary from 1 to 8, the potential positional-isomers across all DARs is only 255. [87] Furthermore, the attachment

typically occurs at both cysteines that form a disulphide bond, leading to predominantly 2, 4 and 6 DARs being most abundant. This reduces the number of cysteine linked positional-isomers down to 126, resulting in a significant difference in overall ADC heterogeneity.

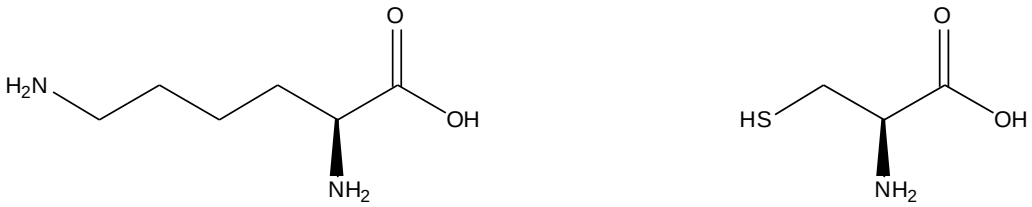

(**12**) (**13**)

Figure 1.20. The chemical structures of amino acids lysine (**12**) and cysteine (**13**).

Trastuzumab emtansine utilizes the linker succinimidyl 4-(N-maleimidomethyl) cyclohexane-1-carboxylate (SMCC, **14**). [274] The SMCC linker forms an amide bond to a lysine residue on the antibody via its amine reactive NHS-ester and a thioether bond to the DM-1 warhead via a sulphur reactive maleimide, (**Figure 1.21**). [274] The SMCC linker is described as non-cleavable, however the thioether bond is susceptible to retro-michael reactions, liberating the warhead. It is mainly inside a lysosome, where enzymes can digest the antibody, that the lysine-linker-DM1 conjugates are released and able to affect tubulin dimers (**Figure 1.19**).

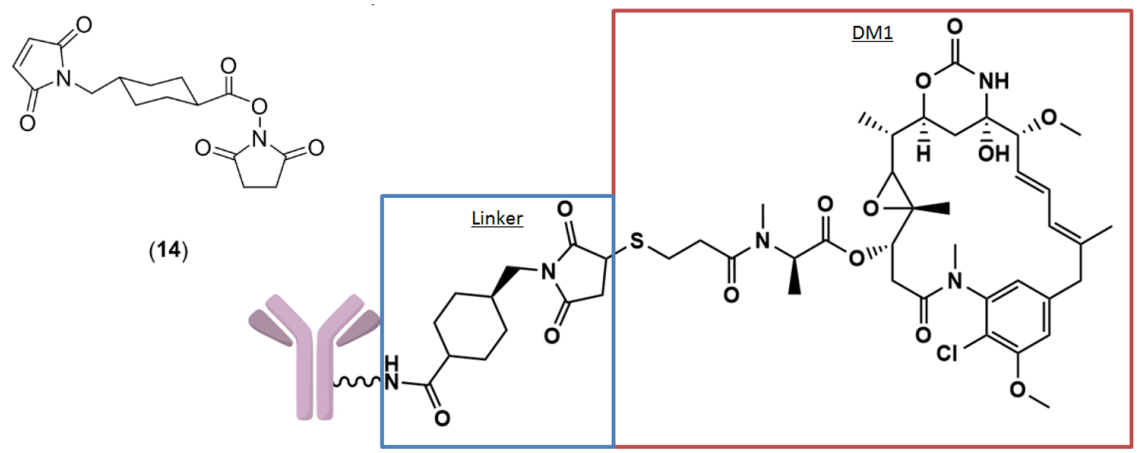

Figure 1.21. Chemical structure of the linker SMCC (**14**) and its incorporation within the ADC trastuzumab emtansine.

Gemtuzumab ozagamicin and inotozumab ozagamicin both use 4-(4-acetylphenoxy)-butanoic acid (**15**) as a linker, to form an amide bond with a lysine residue on the antibody (**Figure 1.22**). [274] Both gemtuzumab ozagamicin and inotozumab ozagamicin also use a calicheamicin molecule which is modified using 3-mercapto-3-methylbutyryl hydrazide (**16**) through a disulphide bond. [274] The 4-(4-acetylphenoxy)butanoic acid can then form a hydrazone bond with the 3-mercapto-3-methylbutyryl hydrazide to attach the warhead to the antibody (**Figure 1.22**). [274] While the disulphide bond is relatively stable in the body, the hydrazone is rapidly hydrolysed in acidic environments such as the lysosome. This liberates the cytotoxic calicheamicin, which is then able to attack DNA (**Figure 1.17**).

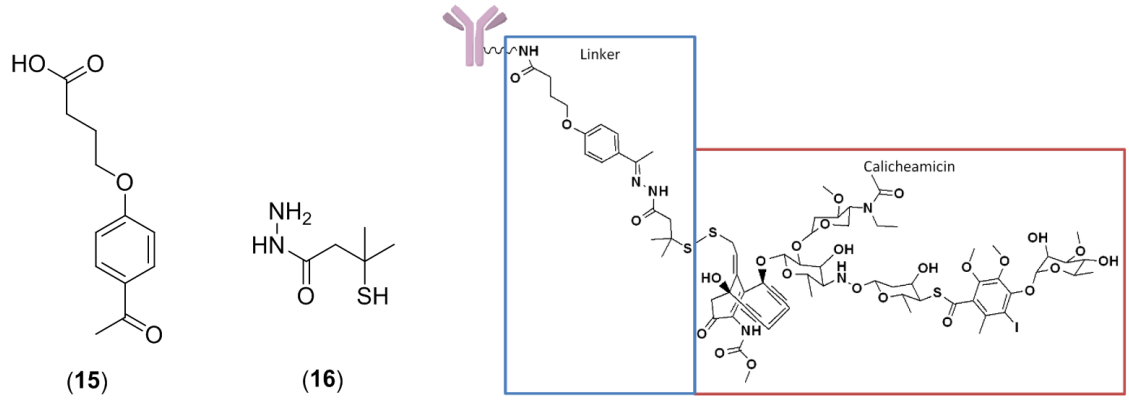

Figure 1.22. Chemical structures of linker components 4-(4-acetylphenoxy)-butanoic acid (**15**) and 3-mercapto-3-methylbutyryl hydrazide (**16**) and their incorporation within the ADC's gemtuzumab ozagamicin and inotozumab ozagamicin.

Brentuximab vedotin utilizes a more complex linker with multiple components (**Figure 1.23**). Connecting the antibody to the linker structure is 6-maleimidohexanoic acid (**17**) which forms a thioether with the sulphur atom of cysteine residues on the antibody. [274] Compound (**17**) is then connected to a valine-citrulline group composed of (**18**) and (**19**), which is in turn is connected to the 4-aminobenzyl carbamate (**20**) (**Figure 1.22**). The bonds between each component of this linker are stable amide bonds and the linker to antibody bond is a thioether (**Figure 1.25**). However, an enzyme known as

cathepsin B recognises the valine-citrulline amide bond and then selectively cleaves the amide bond between the citrulline group and 4-aminobenzyl carbamate. [274] This creates an MMAE-4-aminobenzyl carbamate conjugate that rapidly undergoes a spontaneous 1,6-elimination, resulting in the free MMAE cytotoxic.

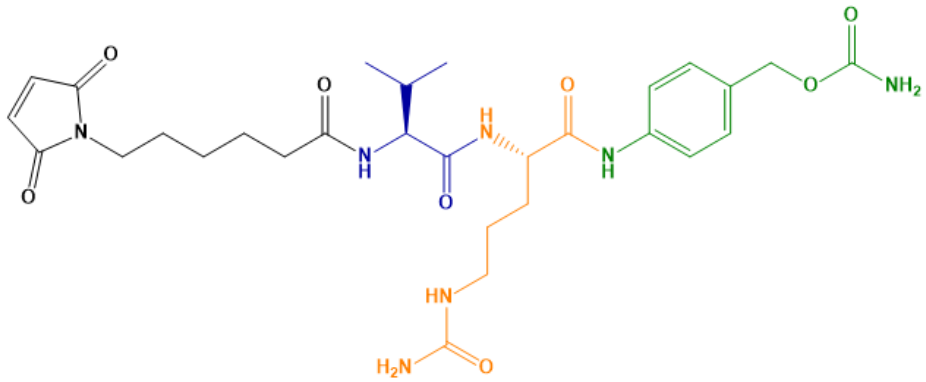

Figure 1.23. The chemical structure of the linker used in brentuximab vedotin.

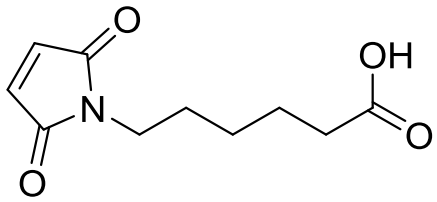

(**17**)

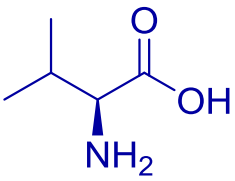

(**18**)

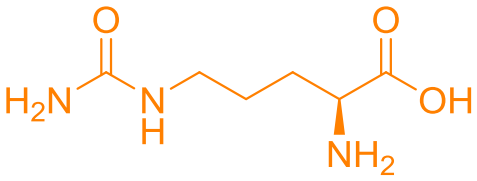

(**19**)

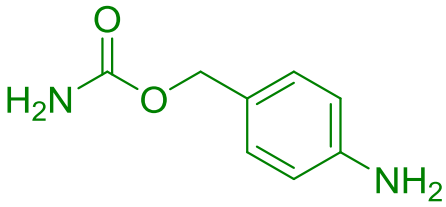

(**20**)

Figure 1.24. The chemical structures of 6-maleimidohexanoic acid (**17**), Valine (**18**), Citrulline (**19**) and 4-aminobenzyl carbamate (**20**).

When attaching the linker to the antibody the duration of reaction and ratio of reagents will control how many linkers become chemically attached to each antibody. However, the chemistry for cysteine and lysine attachment is not precise enough to yield only antibodies with the same number of linkers bound. The number of linkers bound

will be heterogeneous with a mean average being the best way of quantifying the number of drugs that will subsequently bind to the linkers. Gemtuzumab ozagamicin is reported to have an average drug to antibody ratio (DAR) of 3, but it is as mixture containing naked gemtuzumab and gemtuzumab ozagamicin with a DAR of up to 6. [88] Brentuximab vedotin is reported to have a mean DAR of 4 [89] but is predominantly present with DARs of 2, 4 and 6 due to its cysteine attachment. [89] Trastuzumab emtansine has a mean DAR of 3.5, but is present with DARs of 0 to 8. [89] ADCs with DARs below 3 have lower therapeutic activity than those with DAR 3 and above, assuming only the DAR is changed. [90] ADCs with DARs of 7 and 8 are cleared from the body much faster resulting in reduced therapeutic activity, assuming only the DAR is changed. [91] Ideally the mean DAR will be 4, with most of the drug present at DARs of 3-6, this should yield the best balance of therapeutic activity, rate of clearance, and chemical stability. [90,91]

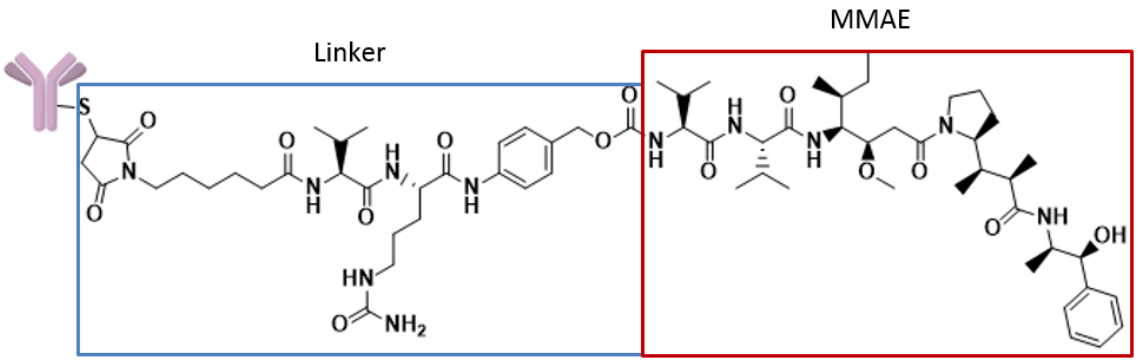

Figure 1.25. Chemical structure of brentuximab vedotin's linker and cytotoxic drug.

Linker chemistry between the linker and the drug is broadly classed as cleavable or non-cleavable. [90] Essentially, cleavable linkers allow the cytotoxic drug or "warhead" to be released without the linker or additional amino acids remaining attached. Typically cleavable linkers are acid labile such as the hydrazone linkers used in gemtuzumab ozagamicin and inotozumab ozagamicin (**Figure 1.22**), or are enzymatically cleavable such as the citrulline-valine linker that is cleaved by the protease 'cathepsin B' in brentuximab vedotin (**Figure 1.25**). [90] Trastuzumab emtansine uses a non-cleavable linker, so the warhead is not released on its own. Once trastuzumab emtansine has been internalised, the entire ADC is degraded inside a lysosome generating amino acid-drug conjugates, such as lysine-maleimidocaproyl-DM1 (**Figure 1.26**).[90]

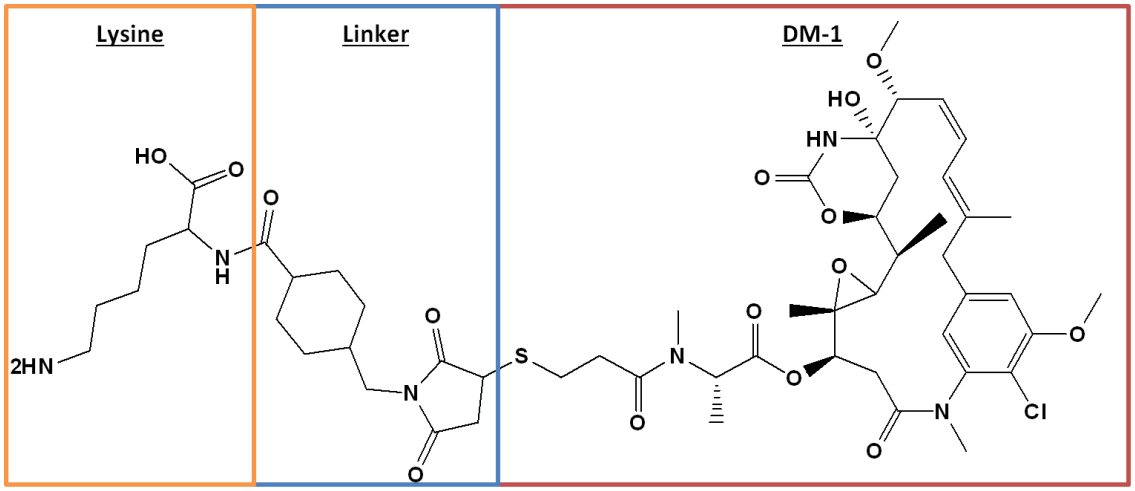

Figure 1.26. Chemical structure of the lysine-maleimidocaproyl-DM1 conjugate.

1.4.5 The warheads

In relation to ADC's, the term warhead refers to the cytotoxic drug attached to the antibody. ADCs typically use cytotoxic drugs that act via one of two mechanisms, DNA synthesis inhibitors or tubulin inhibitors. [91] The maytansinoid derivative DM-1 is used in trastuzumab emtansine while DM-4 is used in many other ADCs in clinical trials. [73] Maytansinoids are sourced from the bark of the *Mayentus ovatus* shrub. [92] These molecules bind to tubulin, a protein that composes the dynamic microtubules used in the cell cycle. By binding to the tubulin on microtubules Maytansinoids inhibit the tubulin depolymerisation and microtubule reorganisation. The cytoskeleton becomes static, stalling the cell cycle between the G2 phase and M phase, leading to apoptosis. [73] DM-1 is drawn and labelled in **Figure 1.26**.

The auristatins, MMAE and MMAF, are also tubulin inhibitors. MMAE is used in brentuximab vedotin while MMAF is used many other ADCs in clinical trials. Auristatins are derivatives of dolastatins originally found in the sea hare *Dolabella auricularia.* [73] Auristatins bind to free tubulin and prevent it from polymerizing. This means new microtubules can't form and the cytoskeleton fails to assemble, leading to apoptosis. [73] MMAE is drawn and labelled in **Figure 1.25**.

Calicheamicin is a DNA synthesis inhibitor used in gemtuzumab ozagamicon, inotozumab ozagamicin and other ADCs in clinical trials. It was originally found to be produced in the bacteria *Micromonospora echinospora ssp. Calichensis.*[73] Calicheamicin binds to DNA and generates a double free radical on the DNA. The diradical DNA is extremely unstable and rapidly reacts with oxygen in its immediate environments leading to double strand scission. This DNA disruption then initiates apoptosis. [73] Calicheamicin is drawn and labelled in **Figure 1.22**.

The warheads for ADCs are chosen on the basis of their extreme cytotoxic potency. To put this into perspective, Doxorubicin is a cytotoxic chemotherapeutic drug which was also used in early ADCs that failed in the clinic. Calicheamicin is 4000 times more potent than doxorubicin,[93] and cannot be used without attachment to a targeting motif. DM1 and MMAE are also significantly more toxic than licensed cytotoxic drugs that act via similar mechanisms. [81,94] The reason why warheads must be so potent is that only a small percentage of the ADC will reach the cancerous cells,[95] so the warheads must be potent enough to initiate apoptosis at very low intracellular concentrations.[95,96]

1.4.6 ADC summary

In summary, while an ADC is defined as an antibody linked to a cytotoxic drug, ADCs are more than just the sum of their parts. There are seven key choices to make when designing an effective ADC:

1) Antibody target
2) Antibody isotype
3) Antibody species
4) Antibody to linker conjugation chemistry
5) Drug to antibody ratio
6) Linker to drug conjugation chemistry
7) Cytotoxic ‘warhead’

Most of the original issues with ADCs have been overcome or identified, for example: the antibody host species raising an immune response, has been solved by using humanized or fully human antibodies, where human antibody content is over 80%. Drug heterogeneity with regards to DAR and positional-isomers has been improved by linking via cysteine residues, (and more recently engineered amino acid residues) which drastically reduces DAR and isomer variability.

ADCs are close to Paul Ehrlich's concept of a magic bullet and are in high demand by patients around the world. There are four licensed ADCs; brentuximab vedotin which treats Hodgkin's lymphoma, trastuzumab emtansine which treats HER2+ breast cancer, gemtuzumab ozagamicin which treats acute myeloid leukaemia and inotozumab ozagamicin which treats acute lymphoblastic leukaemia. While gemtuzumab ozagamicin had some issues regarding *in vivo* linker stability, all licensed ADCs have been demonstrated as better than the pre-existing gold standard therapies in at least one indication each. Furthermore, there are over 65 ADCs in clinical trials, with 10 of these in phase three trials. [97]

1.5 Biopharmaceuticals in clinical practice

Most drugs for infusion or injection, which includes all antibodies and ADCs, come as concentrated solutions or lyophilized (freeze dried) powders for reconstitution into concentrated solutions. These are stored in vials, which usually have a 1 to 3 year shelf-life. For administration to the patient, the concentrated solutions first need to be transferred into a delivery device, such as a syringe, infusion bag or ambulatory infusion pump. A volume of diluent such as water for injection, 0.9% w/v NaCl solution for injection, or 5% w/v glucose solution for injection, is usually added to the device to dilute the concentrated drug solution. The process of combining drug, diluent and/or devices is known as compounding.

Compounding is very important as it allows the use of concentrated drug solutions or if it is required, lyophilised powders. These have much greater stability than products at ready to use concentrations, where the concentrations of excipients such as buffering agents or detergents like polysorbate 80 would be limited. This makes concentrated drug vials more convenient for pharmaceutical companies to manufacture and sell and for healthcare providers to store and use, limiting the risk of purchased stock going out of date. Compounding also allows drugs to be used in a great variety of devices, such as different brands or sizes of infusion bag, or syringes. Furthermore, patient specific products can be made when standardized dosing is not applicable.

Compounding is performed in many places, such as hospital pharmacies, aseptic pharmacy units, or even on a hospital ward. For example, a nurse may withdraw and administer a drug as per a doctor's instructions via a syringe. A pharmacy technician may reconstitute a lyophilised drug powder, and then add a specific volume of the reconstituted drug to a saline infusion bag that had previously had a specific volume of saline withdrawn, thus creating a defined concentration of a drug in a defined volume, this is often done to create 'patient specific' products. Once the sterile drug solution or lyophilized powder has been compromised, typically the airtight rubber septum has been breached, the product must be discarded within 4-48 hours, as specified in each drugs summary of product characteristics (SPC).

Aseptic compounding is simply compounding but performed in an aseptic environment to prevent microbial contamination of the products. This is typically performed in a class 2 biological safety cabinet or laminar flow cabinet, which meet or exceed all grade A conditions for environmental sterility, as specified in the "Rules and Guidance for Pharmaceutical Manufacturers and Distributors 2017.[98] By preventing microbial contamination of the product, the inherent stability of the specific combination of container, drug and diluent can be used to determine the maximum shelf-life of the new product. In the UK, pharmacists supervising aseptic compounding can apply up to seven days of shelf life according to available stability data. This is known as the 'Medicines Act 1968 Section 10 Exemption' allowing pharmacists that are

following an official prescription to make products and apply up to short extensions. To extend beyond seven days requires a Medicines Health Regulatory Agency (MHRA) Specials license. 'Specials' are any unlicensed medicinal products, such as patient specific products, which require specific concentrations, volumes or administration devices or more broadly require special manufacturing for the individual patient. An extended shelf-life of at least seven days makes the logistics of compounding and then administering the products much easier.

Most large hospitals have an aseptic compounding unit. These units are costly to build and run. The number of products requiring aseptic compounding is increasing, indicated by an annual 4.8% increase in chemotherapy product production, furthermore the complexity of products has increased resulting in an even greater rate of increase in NHS aseptic service workload. [223] A compounding unit's production capacity limit can be increased by extending the operating hours of the unit or physically expanding the compounding unit. Otherwise more products will be prepared in non-aseptic environments, by less practiced staff and with no operator protection. It has been advised since 1976 by multiple advisory bodies that products for parenteral administration are manufactured and assembled under aseptic conditions. [99] Reports have shown increased risk to patients and staff when products are assembled in wards, theatres, clinics and in the patient's home compared to aseptic preparation areas. [100]

The Department of Health, National Patient Safety Agency and multiple independent researchers have been trying to get assembly of high risk products out of clinical areas and into aseptic manufacturing units for over three decades. Support for this idea has only grown stronger as more evidence is compiled explaining why this should happen. This is for the safety of the patients and as such should be a priority for all hospitals and staff. No identified risks should be accepted as part of patient treatment when there are alternatives like outsourcing for ready to use products. And with research showing that moving assembly of these products out of clinical areas will increase the workload on the in-house units by 50%, major changes will have to be made with regards to the supply and manufacture of high risk medicinal products. In 2003 the

UK Department of Health identified working with industry and creating commercial partnerships as a positive action and one of the 4 central pillars of modernising the NHS manufacturing service.

Aseptic compounding allows more effective allocation of staff skill sets, reducing the time a nurse or doctor spends compounding on a ward or theatre allowing them to focus on nursing or diagnosing patients. Rather than using a section 10 exemption, most commercial manufacturers have an MHRA specials license. A key difference is that with a specials license is that you can apply a shelf life over 7 days. The longer the shelf life extension the more likely costs can be saved by reducing wastage, capitalising on batch production and the easier it is logistically to manufacture, transport, store and then administer the product. Furthermore, commercial manufacturers typically have purpose built aseptic compounding units with an infrastructure built solely around them, this keeps overheads low and often allows expansion if close to the capacity limit of the unit. Hospital pharmacy units tend to be built inside pre-existing hospitals meaning space is usually not available for expansion into, and the infrastructure isn't designed around the compounding unit which leads to increased overheads, furthermore, an internal hospital unit will supply to a much smaller customer base (almost exclusively the hospital it is based in) than an external commercial unit, therefore downtime can also be an issue of unnecessary running costs. External commercial aseptic compounding units offer UK hospitals a way of sourcing 'Special' products at a better price than they could make for themselves and with a longer and more useful shelf life than they would normally be able to apply (some UK hospital compounding pharmacies do have specials licenses). The main benefits are only apparent when extended stability can be applied to products, and to this end the NHS has published guidance regarding the assessment of stability studies for small molecule and biotherapeutic medicines.

1.6 The stability and degradation of antibodies

1.6.1 Mechanisms of degradation

Antibodies can be degraded via a number of different mechanisms, including: elevated temperatures (thermal stress), physical agitation (mechanical stress), light (photolytic stress), exposure to air and O_2 (oxidative stress), changes in pH (acidic or basic stress), interface interaction / adhesion (air-liquid, air-solid, solid-liquid). [263]

Thermal stress can cause changes to an antibodies structure, resulting in unfolding of the higher order structure. [263] Increased temperature will also increase the kinetic energy of the antibodies, resulting in more frequent and more energetic protein-protein interaction and protein-interface interactions. [263, 264] Lastly, when unfolded hydrophobic amino acid residues that would usually be inaccessible, can be exposed. The exposed hydrophobic residues can react with each other, container surfaces, lubricant or dissolved oxygen. [263] Thus, thermal stress is highly damaging to antibodies, and will drive aggregation resulting in aggregates that can range from dimers to visible aggregates. [263, 264] Interestingly antibodies Fab and Fc regions will unfold at different temperatures, 63–71 °C and 73–82 °C respectively. [263]

Mechanical stress can be applied to antibodies during their manufacturing process, but more relevant to aseptic compounding is dilution/reconstitution, mixing, withdrawal into a syringe and addition to a device, such as an infusion bag, followed by transportation of the device. Reconstitution allows the antibodies to move around and interact with other antibodies, excipients, surfaces and air interfaces. This will be followed by a mixing step, typically in a swirling motion, to ensure all the drug is dissolved and the mixture is homogenous. Swirling however results in mechanical stress as well as exposure to a variety of interfaces at which adhesion may occur, leading to aggregation. [263, 264] Once the concentrate is satisfactorily mixed, it will be drawn up into a syringe using a metal needle. The needles have narrow internal diameters and the rate at which the drug is withdrawn

can cause shear stress to affect the antibodies, which has been associated with antibody aggregation. [264] The antibody may then be injected into another device such as an infusion bag or ambulatory pump, containing a diluent such as 5 % w/v glucose or 0.9 % w/v NaCl. This addition to a large volume of diluent dramatically dilutes the excipients that the antibody was originally stored in, as well as altering the pH and is followed by another mixing step, during which mechanical stress, exposure to air-liquid and air-solid interfaces can cause further aggregation and unfolding. [263, 264] Finally, bags will need to be transported, it is understood devices should contain as little headspace as possible to limit mechanical stress, limit the dissolving of oxygen into the drug solution and limit the air-surface and air-liquid interaction. [263]

Many drugs are stored in amber vials or wrapped in light proof bags. This is to protect the drugs from UV rays, which can cause photolytic degradation. [263, 264] UV light can provide the energy required to cross-link sulphides, tyrosine residues and induce non-covalent aggregation. [263, 264] Furthermore, UV radiation can drive oxidation of methionine and histidine residues. [263] Photolytic degradation is often associated with discolouration of antibody solutions as well as loss of functional activity. [263]

Oxidation of histidine and methionine residues is most common in antibodies with oxidation also possible at other amino acids such as cysteine and tyrosine. [263] Oxidation of key residues on antibodies have been linked to impaired Fc effector function and an increased propensity to aggregate. pH is known to affect the solvent accessibility of a number of oxidizable residues, thus extreme pHs can drive oxidation. [263]

High and low pH stress can cause conformational changes to a protein, which can result in exposure of hydrophobic regions as well as reactive residues that previously were not solvent accessible. [263] Furthermore, high and low pH stress can cause hydrolysis. Hydrolysis can lead to deamidation. [263] Hydrolysis of amino acids

can result in isomerisation, the transition of naturally occurring L form amino acids to the D forms. [268] Isomerisation in the CDR regions of an antibody have been found to negatively affect antigen-antibody interaction, reducing binding efficacy. [270]

Solvent accessible asparagine and glutamine residues can be deamidated into aspartic acid. [263-266] Deamidation of asparagine residues in the CDR regions of IgG antibodies have been reported to affect antigen binding [265] and deamidation has also been associated with changes to Fc receptor dissociation. [266]

Protein can become adsorbed onto liquid-solid and liquid-air interfaces such as the plastic containers material via hydrophobic interaction. [263, 264, 267] While adsorbed onto surfaces antibodies have an increased chance of further aggregating due to stabilising atypical conformations. [264, 267]

Glycation is the attachment of a sugar molecule to a protein without enzymatic regulation. Reports on the effect of glycation of antibodies is mixed, with some studies showing no effect, while others have found loss of antigen affinity and mannose receptor activity. [272] At 2-8 °C glycation was found to be negligible for at least 21 months, while at 40 °C glycation was significant within 1 week, although no difference in aggregation was found between glycated and control mAb at 40 °C. [272]

Glycosylation is also important for antibody stability, studies have found that deglycosylation of an antibody significantly increases the rate of unfolding and aggregation, however deglycosylation of an antibody typically requires enzymes such as PNGase F, rather than occurring naturally. [273]

Biopharmaceutical formulations often contain protective excipients, described in the next section.

1.6.2 Protective excipients

To help reduce the level of degradation to antibodies, excipients are added to the medicinal formulations. These excipient mixtures commonly include non-ionic surfactants, such as polysorbate 20 and 80; [263, 264, 268] pH stabilisers such as sodium citrate buffer, sodium phosphate buffer and L-histidine buffers; [263, 268, 268] and sugars such as sucrose or trehalose. [269]

Non-ionic surfactants are believed to form protein-surfactant complexes and surface-surfactant complexes, thus inhibiting the formation of protein-surface complexes. [126, 150, 238, 240, 263, 264, 267] Surfactants have been shown to reduce the rate of antibody aggregation and dilution will reduce the stabilising effect of the surfactant. [126, 150, 238, 240, 267]

Antibodies are typically most stable between pH 6.5 and 7.5. [148, 149] Use of pH buffers helps ensure the pH remains in this optimum zone during prolonged storage and upon dilution. [268]

Sugars are sometimes added to antibody formulations as they can form interactions with the proteins and reduce their mobility, thus reducing their reactivity with other proteins and surfaces. [268, 269] Addition of sugars to antibody formulations has been shown to reduce the rate of oxidation and deamidation. [268] Studies have shown that relative to other sugars such as glucose, trehalose has a much lower propensity for glycating antibodies. [271]

While mechanisms of degradation and protective excipients overlap for antibodies and ADCs, there are some antibody specific stability issues, discussed in the next section

1.6.3 ADC specific stability issues

ADCs have additional stability concerns over antibodies, as the linker and warheads could detach as well as the conjugation reactions affecting the stability of the antibody. ADCs, such as brentuximab vedotin, utilize a Michael addition reaction between a free thiol of cysteine residues, with a maleimide group on the linker. [273, 274] This causes an addition on a double bond of the maleimide. However, to generate solvent accessible cysteines, the intermolecular disulphide ridges are reduced, and the addition of a linker reduces the number of disulphide bridges holding the ADC's antibody together. [273] High DAR brentuximab vedotin has a much lower stability than low DAR brentuximab vedotin, for example, the rate of aggregation is higher, and the melting temperature is much lower. [90, 91]

Trastuzumab emtansine does not use cysteine to attach it's linkers, and instead uses the solvent accessible thiols of lysine residues. [273] The linker SMCC contains an NHS ester group which reacts with free thiols on lysines, to form an amide bond. [273] This means that there is no need to reduce the disulphide bridges that hold the ADC together and thus ADCs that attach their linkers via lysines have improved stability compared to ADCs that utilise conjugation via cysteines. [273]

The attachment sites of linker to thiol are both prone to retro-Michael reactions. [273, 275] Where present, free thiols found on glutathione, albumin or free amino acids such as cysteine exchange with the linker-warhead species. [273, 275] This phenomenon is reported to be responsible for *in vivo* premature payload release from ADCs such as trastuzumab emtansine and brentuximab vedotin. [273] However, during prolonged storage free thiols containing compounds should not be present to facilitate maleimide exchange/retro-Michael reactions.

The payloads of ADCs are also known to be hydrophobic, as discussed previously, hydrophobic interactions are key to antibody aggregation, which is why partial unfolding, stabilisation of partially unfolded antibody and hydrophobic surface

interaction, such as air-liquid and liquid-solid, have such significant impacts on biopharmaceutical aggregation. [274] The addition of up to eight hydrophobic payloads increases the rate of aggregation compared to the naked antibody, for example model ADCs aggregate faster than their parent antibodies. [90, 91, 274]

Scientists have already been testing alternative linkers which are hydrophilic, which reduces payload hydrophobicity and cysteine re-bridging, such as the THIOMAB linker, which prevents loss of disulphide structural integrity when using cysteine thiols to conjugate to. [274] Additionally, experimentation with self-hydrolysing maleimides in linkers has found that retro-Michael reactions can be prevented, improving the *in vivo* stability of ADCs and reducing premature payload release via retro-Michael reactions. [275] However, currently licensed ADCs do not yet use these technologies.

ADCs clearly have some additional stability issues compared to antibodies, with evidence pointing towards an increased propensity for aggregation via hydrophobic protein-protein and protein-surface interactions.

1.7 The high cost of modern medicines

Cancer therapy has come a long way since the 1940's. The advent of chemotherapy and the discovery that combination therapy improved patient outcomes made untreatable diseases treatable. In the 1960's non-cytotoxic small molecule drugs such as tamoxifen saw use alongside cytotoxic chemotherapy agents. In the 1990's monoclonal antibodies emerged and revolutionized not only cancer therapy but also many immune disorders too. Trastuzumab, marketed as Herceptin made headlines as it helped treat HER2 positive breast cancers and had a much less severe side effect profile. Trastuzumab was found to work best when combined with traditional chemotherapy and is still a very popular drug when used alongside lapatinib or capecitabine for treating HER2 positive breast cancer. However, data from the clinical trials TH3RESA and EMILIA

have shown the new antibody drug therapies such as trastuzumab emtansine outperform gold standard therapies such as trastuzumab combined with lapatinib [103,104].

Cancer therapy has also become more expensive since the 1940's. Trastuzumab emtansine's problem is its £90,000 price tag per patient. The national institute for health care excellence informs the NHS if a therapy is cost effective and has struggled to justify trastuzumab emtansine, which even after multiple "special deal" between the NHS and Roche, is above the top of the extended range of cost effectiveness.

As previously mentioned, anticancer therapies are getting more and more expensive. According to the online British National Formulary, [257] the small molecule cytotoxic drug doxorubicin costs ~£20 per mL, rituximab costs ~£350 per mL, and ocrelizumab costs ~£4800 per mL. With limited funding, getting approval from the national institute for health care excellence is harder which makes it harder from patients to benefit from these ground-breaking new drugs.

As already mentioned, vial wastage is a big problem, which can cost the NHS hundreds of thousands a year. The problem is when a drug is dosed according to patient weight, it is very likely that not all of the drug in a vial will eb needed, thus extremely valuable drug is discarded due to the short, typically 24-hour, shelf life if the manipulated drug. This wastes money that could be spent on funding more cancer therapy. A 2016 report on USA hospital overspending due to biopharmaceutical drug wastage reported, that over $23 million is spend on unused trastuzumab emtansine, $29 million is spent on unused brentuximab vedotin. [278] The authors state drug wastage could vary between 1% and 33% for the 10 most expensive drugs used in oncology. [278] The authors also suggest vial sharing as a practice that could reduce wastage. [278]

A key way to reduce the level of wastage is to manufacture multiple patients doses simultaneously, to reduce the amount of left over, thus wasted drug per patient, this is known as vial sharing. As most drugs have an SPC stipulated shelf life of only 24

hours once manipulated, the practice of batch manufacturing is hard to facilitate, and potential cost savings can be hard to achieve. However, if the shelf life was extended to at least a week, this would reduce the difficulty in timing the manufacture of multiple patients' medicines within 7 days of their administration date, thus increase cost savings. Even better is to increase the shelf life to at least one dose cycle, this enables the manufacture of at least two products, both for the same patient which can enable cost savings even if only one patient exists. Furthermore, outsourcing this work to external aseptic compounders enables the manufacture and supply to multiple hospitals thus increasing the chance of having multiple patients requiring the same drug.

Shelf life extensions bring a wealth of non-financial benefits too such as: driving costs per dose down due to batch manufacturing benefits and improving logistical and supply issues as the time limit for manufacture, shipping and administration is not as restrictive as 24 hours, with some drugs having three-month shelf lives, enabling hospitals to be stocked up and prepared for their patients. Additionally, stability can be demonstrated in environments previously not investigated, such as room temperature stability. Room temperature stability data can save the NHS and aseptic manufacturers a lot of money if stock is left out of the cold-chain. Anecdotal evidence from Bath ASU and NHS employees highlights how power cuts, fridge failures, absent minded staff and errors during delivery of stock can happen surprisingly often. Evidence of stability for 24-96 hours at 25 °C can save tens of thousands of pounds per event. Furthermore, with long enough room temperature stability, for example seven days, some drugs can be moved from high cost hospital administration settings to low cost home healthcare administration, this also has the benefit of improving a patients quality of life as they do not need to travel to a hospital to receive their healthcare, [276] studies have reported improved clinical outcomes for patients who receive the same antibody therapy via home infusion services vs traditional hospital clinic services. [276, 277]

Due to the reasons described above, the NHS desires shelf life extensions, where possible and places product shelf life as a high priority when considering working with

external compounding units, such as Bath ASU. However, to ensure that the shelf lives applied to pharmaceuticals are just and proper, they have created and published their own guidance on deriving and assessing stability of small molecule and biopharmauticals drugs. [101, 102] These are described in the next section.

1.8 NHS stability guidance

The NHS has published two documents called “Standard Protocol for Deriving and Assessment of Stability, Part 1: Aseptic Preparations (Small Molecules), Edition 4, April 2017 (Yellow Cover)” [101] and “Standard Protocol for Deriving and Assessment of Stability, Part 2: Aseptic Preparations (Biopharmaceuticals), Edition 4, April 2017 (Yellow Cover)” [102]. Yellow Cover part 1 deals only with non-peptide drugs with a molecular weight (MW) less than 2000 Dalton, and the Yellow cover part 2 covers biopharmaceuticals such as peptides, antibodies and fusion proteins.

The yellow cover documents were written by the R&D subgroup of the NHS Pharmaceutical Aseptic Services Group, the NHS Pharmaceutical Quality Assurance Committee and the NHS Pharmaceutical Production Committee, and subsequently updated by the NHS Pharmaceutical Research and Development Working Group. The NHS state “Published stability data may be of limited value because of inappropriate or inadequate analytical methodology, limited study duration, or improper processing of analytical data”, this is as the standards to satisfy the NHS stability documents are higher than in pre-existing stability assessments of pharmaceuticals. [101,102] The documents then list a range of key considerations when assessing or designing a study such as: relevant storage conditions, sample numbers, sampling frequency and minimum required sampling timepoints, as well as 10 critical quality attributes of a biopharmaceutical product: Visible changes, pH, chemical degradation, active pharmaceutical ingredient concentration, sub-visible particulates, Higher order structure, degradant product concentration, biological activity, active excipient concentrations, moisture loss and container extractables and leachables. These will be discussed in greater detail later in this thesis.

These documents enable assessment of stability data to ensure that NHS staff, such as pharmaceutical quality assurance officers for hospitals, are able to adequately review stability data and determine if it is of sufficient quality to be used to justify an extended shelf-life for a product. Conversely, the guidance documents can be used to ensure stability studies can be appropriately designed to justify shelf life extensions. Many published stability studies do not meet all the criteria, though this has improved with time. For example, a 2011 paper title "Physiochemical stability of diluted Trastuzumab infusion solutions in polypropylene infusion bags" fails on a great number of point, such as not characterising: higher order structure, levels of sub-visible particulates or changes to functional activity. The NHS guidance documents set a level of scientific rigour that must be met, otherwise no shelf life extension can be applied to products sold to NHS hospitals.

It should be noted that that it is the customer, typically a chief hospital pharmacist, who is ultimately responsible for the products shelf life, however they come to their own conclusions based on the research and data provided by companies such as Bath ASU or those found in published literature of a suitable quality, hence the importance of the NHS part 1 and 2 guidance.

Both NHS stability guidance documents draw heavily from pre-existing documentation written by the International council for harmonization of technical requirements for Pharmaceuticals for human use (ICH). These are covered in the next section.

1.9 ICH guidance documents

ICH is project that brings together the regulatory authorities of Europe, Japan and the Unites States, as experts of pharmaceuticals. The purpose of this council is to discuss scientific and technical aspects of pharmaceutical product registration, which

cover quality, safety, efficacy and multidisciplinary guidance. Multiple documents about stability study requirements they produced are of interest.

The ICH have released numerous documents since the 1990's that have shaped the NHS yellow cover documents. However, the ICH guidance is less detailed and focussed than the NHS guidance, and much older. Important documents such as Q2 (R1) are over 20 years old and the most recently published document that applies to stability research, Q1E, is over 15 years old. The NHS yellow cover documents are more recent and have been strongly influenced by the ICH guidance, specifically: Q1A (R2) "Stability Testing of New Drug Substances", Q1B "Stability testing: Photostability of New Drug Products and Substances", Q5C "Stability Testing of Biotechnological/Biological Products", Q6B "Specification: Test Procedures and Acceptance Criteria for Biotechnological/Biological Products" and Q1E "Evaluation and Stability Data". The NHS yellow cover documents collate most relevant information from the five aforementioned ICH documents.

A sixth document Q2 (R1) "Validation of Analytical Procedures: Text and Methodology" is referenced by the NHS yellow cover documents but Q2 (R1) is not encompassed by them. Both NHS yellow cover documents state that analytical techniques should be validated to the standard set out in Q2 (R1). ICH Q2 (R1) covers how to perform tests of linearity, precision, specificity, accuracy, robustness, and limits of detection and quantitation.

Following the NHS stability guidance documents and the ICH Q2 (R1) guidance enables the design and validation of studies to investigate the stability of small molecule and biological drugs to performed to a standard enabling shelf life extensions for the NHS and private UK hospitals.

1.10 Aims and objectives

ADCs have unique structural characteristics unlike conventional biopharmaceuticals and stability studies of ADCs are not covered by any existing guidance, though many similarities do exist between antibodies and ADCs. The NHS part 2 guidance states "Currently this group of products is outside of the scope of this document, although the principles may be relevant in assessing the antibody component of the conjugate". [102]

The overall aim of this thesis was to develop methods for the characterisation of an ADC trastuzumab emtansine product. These methods must be stability indicating and must encompass all 10 stated critical characteristics of biopharmaceuticals in the NHS guidance, [102] as well as any additional critical quality attributes that ADCs have. These methods would then enable a stability study to be performed on trastuzumab emtansine, for the purpose of applying an extended shelf-life, beyond its current 24 hours.

An extended shelf life trastuzumab emtansine product would have several benefits, such as enabling batch production of trastuzumab emtansine which will save thousands of pounds per patient, as well as loosening the logistical constraints between manufacturing and administration of the product. Ideally the shelf life would be extended beyond 21 days, which is a full dose cycle for trastuzumab emtansine, thus enabling cost savings on a single patient basis. Remember that trastuzumab emtansine drug wastage is estimated to cost the USA over $23 and it is estimated that on average 8 mg of trastuzumab emtansine is wasted per dose, which is worth £1312, [278] furthermore each patient receives an average of 40 doses. [103, 104] Therefore the average cost of drug wastage per patient is £52,480.

It would be beneficial for sufferers of HER2 positive breast cancer, the NHS, private UK hospitals and Bath ASU to be able to extend the shelf life of trastuzumab emtansine. Extended shelf life trastuzumab emtansine will provide Bath ASU with a competitive edge in the aseptic manufacturing business, increasing their chance of sales to hospitals

and reducing their own waste costs. The NHS and private hospitals will benefit due to reduced cost per patient due to reduced wastage and reduced risk to staff, as concentrated trastuzumab emtansine will not need to be handled by their staff. Both Bath ASU, and hospitals will benefit due to the increased window of time available between manufacture and administration, greatly reducing scheduling conflicts and the cost burden of missed deliveries or missed administrations due to sickness. A 2015 study found 13% of chemotherapy infusions were cancelled late, causing high cost drug wastage. [279]

This stability study cannot be easily performed, as ADCs are not covered by current stability guidance, and it is already known that some current characterisation techniques used for antibodies are affected when applied to ADCs. [173]

Chapter 2 of this thesis describes the methods and materials used during the project, though some experimental detail is also presented in subsequent chapters, especially where method optimisation is involved.

Chapter 3 describes work carried out towards identifying critical characteristics that must be assessed during an ADC stability study, selection of appropriate methods for assessing each characteristic, validation of these methods on the standard therapeutic antibody infliximab, and results from a published stability study using these methods.
The published stability study was performed on a mAb (infliximab) as an easy starter project, to practice validating methods that ought to work and to get a publication. This involved literature research, focussing on the NHS yellow cover documents Part 1 [101] and Part 2 [102] as well as research papers that have fully or partially characterised a mAb or ADC. This is critical for the project as it is known that the structure of ADCs makes them unsuitable for frequently used antibody characterisation techniques. Furthermore, the structure of ADCs means there are additional characteristics, such as the DAR that may be vital to assess during a stability study that could have implications regarding safety or stability.

Chapter 4 details the work carried out to validate the developed methods described in Chapter 3 towards application on trastuzumab emtansine, as well as developing methods using mass spectrometry for characterising characteristics unique to ADCs, such as using mass spectrometry to assess payload binding on reduced ADCs. This chapter also includes results from a full stability study carried out on trastuzumab emtansine.

Chapter 5 describes an investigation into the effect that container (infusion bag) material and construction has on biopharmaceutical stability. Three biopharmaceuticals are subjected to extended storage in three different types of infusion bags, and the impact on stability are investigated. This work was an outcome of Bath ASU's customer feedback, requesting products with extended stability be stored in containers different to those which had been used during the stability study.

Chapter 6 describes some preliminary investigations carried out into the in-use environmental safety of trastuzumab emtansine. Theoretically, the cytotoxic warheads of an ADC could become detached upon prolonged storage, or upon exposure to certain handling conditions such as spill clean-up. This poses a potential health risk as the warheads cytotoxic activity is typically kept in check by being bound to the antibody, but once detached it has implications for the safety of any persons involved in compounding, transporting, or administrating the final product.

Chapter 7 describes preliminary work carried out in determining the compatibilities of methods developed for trastuzumab emtansine towards brentuximab vedotin. Both trastuzumab emtansine and brentuximab vedotin share the overall design of an ADC, however the specific sites of attachment and linker chemistry of the two drugs are significantly are different and affect method suitability. This work is important as it will inform the next steps taken for a potential stability study on brentuximab vedotin.

Chapter 8 presents a conclusion to the thesis, summarising the main achievements to come out of this project, as well as a discussion about possible future work.

Chapter 2. Materials and methods

2.1 General reagents

Ultrapure Water with a resistivity of > 10 MΩ/cm was produced onsite by a Direct-Q 3 water purification machine (Merck Millipore, Massachusetts, USA). Analytical grade; Tris(2-carboxyethyl)phosphine (TCEP), sodium monophosphate, sodium diphosphate, potassium monophosphate, potassium diphosphate, sodium azide and sodium chloride were purchased from Sigma Aldrich (Sigma Aldrich, Dorset, UK). Amicon ultra 0.5 mL 100 kDa centrifugal filters, *Bos taurus* albumin, *Bos taurus* catalase, *Bos taurus* RNase A, *Homo sapien* Haemoglobin, *Equus ferrus* Myoglobin, *Amoracia rusticana* Peroxidase I, *Gallus gallus domesticus* Lysozome, *Leporidae* Aldolase, *Glycine max* Lipoxidase, *Pichia Pastoris* Alcohol Oxidase, *Aspergillus niger* Glucose Oxidase, *Saccharomyces cerivisae* Alcohol Dehydrogenase I, *Sus* Trypsin, and *Canavalia enisformis* Concanvalin A were purchased from Sigma Aldrich (Sigma Aldrich, Dorset, UK).

MAbPac HIC-10 LC columns, Fisherbrand 0.5 mL, 0.6 mL and 1.5 mL microcentrifuge tubes, Fisherbrand 15 mL and 50 mL centrifuge tubes, Roswell Park Memorial Institute (RPMI)-1640 cell media, Dulbecco's modified eagle media (DMEM) cell media, cell culture grade penicillin 10,000 units/mL, cell culture grade streptomycin 10 mg/mL, cell culture grade heat inactivated foetal calf serum, pH 7.4 Phosphate Buffered Saline, HyQTase cell detachment solution, desiccated MTT powder, Hellmannex III cuvette cleaning solution and Fisherbrand T75 cell culture treated flasks were purchased from (ThermoFisher Scientific, Massachusetts, USA). Analytical grade Hipersolv CHROMANORM brand isopropanol, methanol and acetonitrile were purchased from VWR Scientific (VWR Scientific, Fontenay, France).

Injekt BBraun syringes (1 mL, 5 mL and 10 mL) were obtained BBraun (BBraun, Sheffield, UK). Brentuximab vedotin (Adcetris) 50 mg vials and Vedolizumab (Entyvio) 300 mg vials were obtained from Takeda (Takeda UK Ltd, High Wycombe, UK).

Natalizumab (Tysabri) 300 mg vials were obtained from Biogen (Biogen Idec Ltd, Maidenhead UK). Ofatumumab (Arzerra) 100 mg vials were obtained from Novartis (Novartis Pharmacuticals UK Ltd, Camberley, UK). Nivolumab (Opdivo) 40 mg vials were obtained from Bristol-Myers Squibb (Bristol-Myers Squibb Pharmaceuticals limited, Uxbridge, UK). Bevacizumab (Avastin) 100 mg vials, Obinituzumab (Gazyvaro) 1000 mg vials, Pertuzumab (Perjeta) 420 mg vials, Rituximab (Mabthera) 100 mg vials, Trastuzumab (Herceptin) 150 mg vials and Trastuzumab emtansine (Kadcyla) 100 mg vials were obtained from Roche (Roche Products Limited, Hertfordshire, UK). Abatacept (Orencia) 250 mg vials were obtained from Bristol-Myers Squibb Pharma EEIG (Uxbridge, Greater London, UK). Infliximab (Remsima) 100 mg vials were obtained from Napp (Napp Pharmaceuticals, Cambridge, UK). Cetuximab (Erbitux) 100 mg vials were obtained from Merck (Merck Serono Ltd, Middlesex, UK). Denosomab (Prolia) 60 mg vials were obtained from Amgen (Amgen Ltd, Cambridge, UK).

Viaflo infusion bags of sodium chloride 0.9% sterile solution for infusion were obtained from Baxter (Thetford, Norfolk, UK). Freeflex infusion bags of sodium chloride 0.9% sterile solution for infusion were obtained from Fresenius Kabi (Runcorn, Cheshire, UK). Macoflex-N infusion bags of sodium chloride 0.9% sterile solution for infusion were obtained from MacoPharma (Tourcoing, Nord, France).

Tosoh TSKgel G3000SWxl size exclusion HPLC columns, Tosoh TSKgel Butyl-NPR columns, BIA Separations CIM r-Protein G DISKs, BIA Separations CIM r-Protein A DISKs and BIA Separations CIM C4 DISKs were purchased from Hichrom (Hichrom Ltd, Reading, UK). BioSep-SEC-s3000 columns and Yarra-SEC-s3000 columns were purchased from Phenomenex (Phenomenex, Cheshire, UK).

PNGase F and PNGase F Rapid were purchased from New England Biolabs (New England BioLabs, Massachusetts, USA).

BT-474 human mammary gland epithelial cells, HaCaT human keratinocyte epidermal cells, HepG2 human liver epithelial cells and WEHI 164 murine fibroblast cells

were purchased from ATCC via LGC (LGC Standards, Middlesex, UK). GCT-27 human testicular germ cell tumour cells were purchased from DSMZ (Leibniz-Institut DSMZ-Deutsche Sammlung von Mikroorganismen und Zellkulturen GmbH, Braunschweig, Germany). Recombinant human TNF-alpha protein (97%) and actinomycin-D (98%) were purchased from R&D Systems (R&D Systems Inc, Minneapolis, Cananda).

Lidl brand cotton buds were purchased from Lidl (Lidl UK, Wimbledon, UK). Klercide 70|30 Denatured Ethanol (Ecolab Ltd, Northwich, UK), Actichlor Chlorine disinfectant (Ecolab ltd, Northwich, UK) Sterile Prochlor stabilised hypochlorous acid spray (Contec, Vannes, France), InSpec N10 non-sterile prediluted detergent solution (Redditch Medical, County Durham, UK) were purchased via CleanRoomShop (Connect 2 Cleanrooms Ltd, Lancaster, UK).

2.2 General methods for analysis

2.2.1 Moisture loss

During both stability studies carried out for this thesis, the infusion bag masses were recorded for each sample before and after sampling at each time point to check for moisture loss upon storage. This was performed using an Ohaus Adventure Pro laboratory balance (Ohaus, Greifensee, Switzerland). The masses were recorded by contemporaneous printouts via an Ohaus SF40A printer (Ohaus, Greifensee, Switzerland). The balance was zeroed, and a measurement taken before placing a bag and taking a reading once the mass was stable.

2.2.2 Visual inspection

Prior to any analytical methods being performed, samples were checked according to 'Method 2.9.20 Appendix XIII B. Particulate Contamination' from the British Pharmacopeia. [110] The method detects visible particulates distinguished by the unaided

eye under normal laboratory fluorescent light against dark and white backgrounds as well as changes in colour and/or turbidity. Digital photographs of test sample syringes (e.g. after sampling from storage bag containers) were collected at each timepoint using a Canon Ixus 230 HS camera (Canon, Middlesex, UK).

2.2.3 pH analysis

Samples were tested using a Mettler-Toledo Seven Compact pH Meter equipped with a Mettler Toledo InLab Micro electrode (Mettler-Toledo, Leicestershire, UK). These were calibrated with Certipur® pH 4.00, 7.00 and 10.00 25 °C buffers, (Merck KGaA, Darmstadt, Germany) immediately prior to the first analysis of everyday. The calibration standards are purchased from Sigma Aldrich (Gillingham, Dorset, UK). The electrode were stored in a 15 mL centrifuge tube containing 10 mL of Mettler-Toledo KCL 3 mol/L Electrolyte Solution (Mettler-Toledo, Leicestershire, UK). Sample measurements are recorded using the Mettler Toledo LabX Direct software (Mettler-Toledo, Leicestershire, UK). The electrode was rinsed with ultrapure water before being dipped into the sample ensuring the electrode did not touch the centrifuge tube. The electrode was agitated until the pH reading stabilises, then a reading was taken and recorded by LabX Direct.

2.2.4 Dynamic light scattering analysis of subvisible particles

Each sample (0.2 mL) was analysed on a Zetasizer Nano-S instrument (Malvern Instruments, Worcestershire, UK) using a red laser at a wavelength of 633 nm and a Hellma Quartz-Suprasil cuvette, Type 105.251.005-QS, Light path 3 x 3 mm, Centre 9.65 mm (Hellma Analytics, Essex, UK). Samples were tested in triplicate at 20 °C. All data was recorded based on intensity and converted to relative percentage by volume using Zetasizer software v.6.20 and cumulants fit analysis. The cuvettes were filled with and soaked in a 5% w/v Hellmannex cuvette cleaning solution (Hellma Analytics, Essex, UK) for two minutes, before being rinsed out with ultrapure water. The cuvette was rinsed out with ultrapure water between each sample. A mean was calculated from the three repeated measurements taken.

2.2.5 Nanoparticle tracking analysis

Nanoparticle tracking analysis was performed using a Nanosight-LM10 (Malvern Instruments, Worcestershire, UK), set up with the version C red laser unit. The detection threshold was set at 30. Samples were analysed in triplicate, and measurements were recorded from runs of 60 seconds in duration. The camera level was optimised manually for each concentration on Day 0. It was then kept fixed at that level for the duration of the study to ensure no change in the image contrast. A mean average was calculated from the three repeated measurements taken.

2.2.6 Microflow imaging analysis of microparticles

Microflow imaging (MFI) was performed with a Fluid Imaging Technologies FlowCAM VS instrument (Fluid Imaging Technologies, Massachusetts, USA) fitted with an FC100 flow cell. The FC100 width is 2000 µm and the depth is 100 µm. The FC100's tubing is cut to the following specified dimensions, length above flow cell = 105 mm, length below tubing = 175 mm. The flow rate was set at 0.15 mL/min, with an imaging rate of 20 frames/second, a volume of analysis of 250 µL and a calculated efficiency of 34.5 %. Visual focus calibration was manually performed with 10 µm polystyrene beads and data analysed using Visual Spreadsheet software version 4.2. All samples were measured in triplicate and a mean average is calculated from the three repeated measurements taken.

Results were binned using digital filters into three categories sequentially. These were as follows, 'Total Reading' which has no filters, effectively generating a raw total reading. '>10 µm' which only includes particles from the 'Total Reading' which conform to the following three filters: an aspect ratio between 0.0 and 0.8, a circle fit between 0.0 and 0.8 and a length of 10 µm to 1000. '>25 µm' which only includes particles from the '>10 µm' which conform to the following three filters: an aspect ratio between 0.0 - 0.8, a circle fit between 0.0 and 0.8 and a length of 25 µm to 1000. While these filters

reduce the number of oil droplets and air bubbles, as well as rapidly removing particles less than 10 or 25 µm, often manual particle removal is required. This was done via visual inspection of the data from the '>10 µm' bin and '>25 µm' bin.

2.2.7 Gel Electrophoresis

Gel electrophoresis was performed with an Agilent 2200 series TapeStation system (Agilent Technologies, Waldbronn, Germany), in combination with the Agilent Screen Tape P200 Protein Standard Kit Part number: 5067-5371 (Agilent Technologies, Waldbronn, Germany). Samples were analysed under reducing and non-reducing conditions using P200 Reagents (Part number: 5067-5372). These were used according to the manufacturer's instructions. The pre-stained reagent P200 Marker was used as a molecular marker (Agilent Technologies, Waldbronn, Germany).

Samples were diluted to a concentration of 0.5 mg/mL with sodium chloride 0.9%. 2 µL of diluted sample was mixed with 2 µL of P200 stain reagent. This resultant mixture was centrifuged for 10 seconds with a Heathrow benchtop 'Sprout' centrifuge (Heathrow Scientific LLC, Illinois, USA). Then transferred to an IKA MS 3 Vortexer (IKA England LTD, Oxford, UK), the sample was vortexed for 15 seconds, then transferred to a 'PRO-LAB Benchmark myBlock Mini Dry Bath' (PRO-LAB, Toronto, Canada) preheated to 70 °C. After 7 minutes the samples were removed from the dry block and spun in the sprout centrifuge for another 10 seconds. The sample then had 4 µL of either P200 reducing sample buffer or P200 non-reducing sample buffer added, depending on if the sample was to be reduced or not. This resultant mixture was then centrifuged for 10 seconds with the sprout centrifuge, then transferred to the vortexer and vortexed for 15 seconds, then transferred to the dry bath. After 7 minutes the samples were removed from the dry block and spun in the sprout centrifuge for another 10 seconds. Then 2 µL of pre-stained reagent P200 Marker was added. This resultant mixture was then centrifuged for 10 seconds with the sprout centrifuge, then transferred to the vortexer and vortexed for 30 seconds, then centrifuged for 10 seconds with the sprout centrifuge.

This final mixture is what was run on the Tapestation and this process is in accordance to the manufacturer's instructions.

2.2.8 Circular dichroism analysis of secondary structure

Circular dichroism analysis was performed using a Chirascan spectrophotometer (Applied Photophysics Ltd, Surrey, UK) in conjunction with the software 'Chirascan' and 'Pro-Data Viewer' (Applied Photophysics Ltd, Surrey, UK). 250 µL of each sample from a single concentration were pooled and diluted to a concentration of 0.3 mg/mL with sodium chloride 0.9%. 400 µL was transferred to a Quartz Suprasil Cuvette (Hellma Analytics, Essex, UK) with a pathlength 0.1 cm. The cuvettes were filled with and soaked in a 5% w/v Hellmannex cuvette cleaning solution (Hellma Analytics, Essex, UK) for two minutes, before being washed and rinsed out with ultrapure water, prior to being used to measure any sample. CD spectra were collected in the far-UV region (205 to 260 nm) over a temperature range of 25-90 °C in steps of 1 °C at a rate of 1 °C / minute. Final CD spectra had blank subtraction using the diluent NaCl 0.9% w/v as the blank. The spectra were then smoothed using the Pro-Data viewer. The smoothed data was then converted from a dsx file to a txt file using 'APL Data Converter' (Applied Photophysics Ltd, Surrey, UK). This txt file cold then be analysed by the CDNN software version 2.1 (Gerald Bohm, Magderburg, Germany). CDNN estimates secondary protein structure composition using the accurate mass of the protein, the number of amino acids, the CD spectrometers path length and the sample's concentration. CDNN was set to use the 33-base spectra library during the deconvolution process.

2.2.9 Infrared spectroscopy secondary structure determination

The secondary structure of the trastuzumab emtansine protein was measured using a Tensor II Fourier Transform Infrared Spectrophotometer (Bruker, Coventry, UK) fitted with a supercooled HgCdTe photovoltaic detector and BioATR II sample interface device. These are controlled using the OPUS software version (Bruker, Coventry, UK). The instrument is purged with purified, dried air using a CleanAIR pump (Aariac, Italy),

maintained at 25 °C using a Ministat-125 water-circulation thermostat (Huber, Offenburg, Germany) and the HgCdTe detector reservoir has been filled with 300 mL of liquid nitrogen, for at least 30 minutes before analysis. Sample volume was 20 µL, applied using a pipette to the sample well. 120 scans were run between 4000-900 cm^{-1} with a resolution of 4 cm^{-1} and a scanning duration of 55 seconds. The sample well was rinsed with sodium chloride 0.9% solution, and the well physically dried and cleaned with a cotton bud between each sample. Sodium chloride 0.9% was used as a background sample, and five replicate measurements of each sample were made, with a fresh background reading taken between each sample measurement. Spectra are compared to a pre-processed quantitative data set to estimate the alpha helix and beta sheet structural content. The mean average is calculated for alpha helix and beta sheet for the quintuplicate measurements. The QDS was generated as part of this PhD project and design, construction and validation of the QDS is described in section 4.3.

2.2.10 UV Spectrophotometry

Total UV absorbance was measured using a FLUOStar plate reader (BMG Labs, Aylesbury, UK). Spectra (220-400 nm) were obtained to monitor for the accumulation of leachable substances. Absorbance at 280 nm was also recorded as a measure of protein concentration throughout the study period (single analysis only for each concentration). Samples were run undiluted and corrected for sodium chloride 0.9% absorbance which was run as a blank. 10 µL of each sample was transferred to a BMG UV-VIS microplate for UV plate analysis.

2.2.11 Cellular activity assay using MTT

This refers to the reading of a 96 well plate regardless of which experimental set up was used. The assay plates were removed from the incubator after incubation for 96 hours at 37 °C. Using a Fisherbrand FB70155 vacuum pump (ThermoFisher Scientific, Massachusetts, USA) the cell media and diluted drug were aspirated out of each well. 100 µL of 1 mg/mL Dimethylthiazol-2-yl diphenyltetrazolium bromide (MTT) (Sigma

Aldrich, Dorset, UK) and 10% foetal calf serum (ThermoFisher Scientific, Massachusetts, USA) in colourless cell medium was added to each well. The plates were then returned to the incubator for a further 4 hours. The plates were removed from the incubator and the MTT solution aspirated off. 100 µL of dimethyl sulfoxide (ThermoFisher Scientific, Massachusetts, USA) was added to each well and the plate then gently rocked on the IKA MS3 vortexer, before reading the plates absorbance at 540 nm in a FLUOStar OMEGA plate reader (BMG Labs, Aylesbury, UK. Percent cell viability was then calculated as (A540 sample/A540 negative control) × 100. Values were then indexed against values obtained for control samples, to control for inter-assay variability. Each sample was tested in quintuplicate and the mean and standard deviation calculated.

2.2.12 LC-MS sample preparation

Aliquots of samples (600 µL) were individually frozen in 0.6 mL microcentrifuge tubes at minus 80 °C until the day of analysis. Samples were thawed at room temperature over 1 hour. Samples were pooled by combining 125 µl of each sample from a single concentration group to give a total of 500 µL per concentration. This was transferred to an AMICON ultra® 100 kDa centrifugal filter tube (Merck KGaA, Darmstadt, Germany) which was subsequently spun at 14000 G for 10 minutes in a Heraeus Fresco 17 Microcentrifuge (ThermoFisher Scientific, Massachusetts, USA). The filtrate was discarded and 500 µL of ultrapure water was added to each sample. This removes 95% of salt in the sample and is repeated a further two times, removing 99.99% of the NaCl and excipients. The sample is then spun once more to concentrate the sample by 20x. The desalted and concentrated samples were then reduced by the addition 1 µL - 10 µL of tris-carboxyethylphosphine (TCEP) 10 mg/mL solution (Sigma Aldrich, Dorset, UK) , depending on drug concentration to achieve a 80 fold molar excess of TCEP relative to the molar concentration of the protein.

2.2.13 LC-MS measurement and data collection

Chip-based analysis was conducted using a HPLC-Chip Cube system coupled to a 6520-quadrupole time-of-flight (QTOF) mass spectrometer (Agilent Technologies, California, USA) operated in electrospray ionization positive-ion mode. Liquid chromatography was performed using a Protein-Chip (II) with a 40 nL enrichment column and analytical column of 43 mm x 75 µM with Zorbax 300SB-C8 packing material at 5 µm (Agilent Technologies, California, USA). The ChipCube source was operated at 365 °C with 5 L/min N_2 drying gas, the capillary voltage set to 2100 V and fragmentor at 400 V. The Time of flight MS scan range was from 100 – 4000 mass-to-charge ratio (m/z) at an acquisition rate of 1 spectrum per second. The source was interfaced with an Agilent 1260/1200 series HPLC system consisting of a 1260 Cap pump, 1200 Nano pump, 1200 Micro WPS and 1290 Infinity Thermostat (Agilent Technologies, California, USA). Between 0.2 and 1 µL sample was loaded on the enrichment column using the capillary pump flow with H_2O + 0.1 % formic acid (FA) at a flow rate of 4 µL/min. The sample was eluted onto the analytical column using the nanopump at a flow rate of 0.6 µL/min. Solvent A and B consisted of H_2O + 0.1 % formic acid (FA) and MeCN : H_2O 90:10 with 0.1 % formic acid. Gradient step were as follows: 0-4 min from 3 %B to 50 %B, 4-5 min to 100 %B, 5-11 min 100%B, 11-12 min from 100 % to 3 %B. Internal lock mass calibration during the run was done using one calibrant reference mass at 1221.9906 m/z.

2.2.14 LC-MS data processing

Data processing was performed using the MassHunter Workstation software version B.50.00 (Agilent, California, USA). LC-MS spectra (10-100 kDa) were generated at various timepoints and visually compared to spectra obtained on day zero or controls to show that no significant changes to the mass of the heavy or light chains was occurring.

2.2.15 Hydrophobic interaction chromatography

A ThermoFisher MAbPac HIC-10 (ThermoFisher Scientific, Massachusetts, USA), column dimensions 4.6 × 100 mm and particle size 5 µm was used for HIC analysis. The HIC-10 final method used a UV detection was set to 280 nm, flow rate was 0.5 mL/min, injection volume was 25 µL, column oven temperature was set to 30 °C, the method was a gradient from 100% 3M ammonium sulphate dissolved in 100 mM potassium phosphate + 15mM NaN_3 (pH 7.0) to 50 mM potassium phosphate + 15mM NaN_3 (pH 7.0). The gradient was over 180 minutes, the column was re-equilibrated for 10 minutes before the next injection at the starting conditions.

2.2.16 Size exclusion chromatography – mAb

Size Exclusion Chromatography (SEC) was performed on performed on Dionex Ultimate 3000 HPLC System (Dionex, Sunnyvale, California, USA). HPLC System 1 (HS1) consisted of an LPG-3400BM pump, a WPS-3000TBFC analytical autosampler, a TCC-3000SD column oven and a VWD-3100 detector. HS1 was operated via the Dionex Chromeleon software version 6.8. Detection was set at 280 nm, flow was isocratic, injection volume was 20 µL and sample trays were thermostated at 7 °C. The sample was eluted on a *TSKGel* G4000 SW_{XL} column with the dimensions 7.8 × 300 mm and particle size 8 µm, pore size 450 Å. The mobile phase was 300 mM NaCl + 50 mM Na_3PO_4 buffer at pH 6.8 in HPLC water. Samples were analysed in triplicate and a mean average including a standard deviation calculated from the three replicate measurements. Drug concentration was obtained from peak signal area using a linear regression curve of drug concentration vs absorption generated during drug specific method validations, see sections 3.4.8.

2.2.17 Size Exclusion Chromatography – ADC

Size Exclusion Chromatography (SEC) was performed on performed on Dionex Ultimate 3000 HPLC System (Dionex, Sunnyvale, California, USA). HPLC System 3 (HS3) consisted of an HPG-3200RS pump, a WPS-3000TSL analytical autosampler, a TCC-3100SD column oven and a DAD-3000RS detector. HS3 was operated via the Dionex Chromeleon software version 7.2. Sample trays were thermostated at 7 °C. a BioSep-SEC-s4000 with dimensions 300 mm × 7.8 mm, particle size 5 µm and pore size 500 Å fitted with a guard column. Isocratic elution was performed with the mobile phase being a 16:84 mix of propan-2-ol / 100 mM potassium phosphate buffer (pH 6.80) containing 15mM NaN_3 as an anti-microbial agent. The column temperature was 30 °C, the injection volume was 20 µL and UV detection was set at 280 nm. The flow rate was 0.75 mL/min and the run time was 25 min, with the monomer peak eluting at 12.5 minutes (**Figure 4.19**). Samples were analysed in triplicate and a mean average including a standard deviation calculated from the three replicate measurements. Drug concentration was obtained from peak signal area using a linear regression curve of drug concentration vs absorption generated during drug specific method validations, see sections 4.3 & Appendix I-III.

2.2.18 Forced degradation by acid

25 µL of 100 mM hydrochloric acid was mixed with 475 µL of sample. This is repeated three times. After 1, 2 & 3 hours at 25 °C, a sample is neutralised with 25 µL of 100 mM sodium hydroxide. The concentration of acid during degradation is 5mM.

2.2.19 Forced degradation by base

25 µL of 100 mM sodium hydroxide was mixed with 475 µL of sample. This is repeated three times. After 1, 2 & 3 hours at 25 °C, a sample is neutralised with 25 µL of 100 mM hydrochloric acid. The concentration of base during degradation is 5mM.

2.2.20 Forced degradation by oxidation

200 µL of a 30% w/v aqueous hydrogen peroxide solution was mixed with 400 µL of sample. The sample was stored at 25 °C, until testing. The concentration of hydrogen peroxide is 10% w/v, during degradation.

2.2.21 Forced degradation by photolysis

Sample was placed in an Adelphi Apollo 1 Lightbox (Adelphi Instruments, Haywards Heath, UK), exposing the sample to 20,000 lux. The sample was removed after 72 hours.

2.2.22 Forced degradation by thermolysis

Sample was placed in a myBlock Mini Dry Bath, at 60 °C. The sample was removed and sampled after 96 hours.

2.2.23 Unpaired students t-test

Data was assessed using a two tailed, unpaired, students t-test, performed using Graphpad Prism version 5.04. The confidence interval was set at 95%.

2.2.24 One-way ANOVA with post hoc Bonferroni

Data was assessed using a one-way analysis of variance (ANOVA) with a post hoc Bonferroni comparing all groups to D0 and D1 groups, this was performed using Graphpad Prism version 5.04. The confidence interval was set at 95%.

2.2.25 Validation of SEC HPLC method

Validation of SEC methods were performed as follows:

To demonstrate linearity, 5 concentrations of sample were tested covering the range of at least 20% below the lowest study concentration to at least 20% above the highest study concentration. These samples would be tested in triplicate and means taken. This is as defined in the ICH Q2 (R1) document. [103]

To calculate the limit of detection the mean standard deviation of the y-intercept was divided by the mean slope then multiplied by 3.3. This is as defined in the ICH Q2 (R1) document. [103]

To calculate the limit of quantification the mean standard deviation of the y-intercept was divided by the mean slope then multiplied by 10, this must be smaller than 20% less than the lowest study concentration. This is as defined in the ICH Q2 (R1) document. [103]

To calculate the precision, 3 measurements of 3 samples at each test concentration were made, the relative standard deviation was calculated and had to be less than 2% for each test concentration. This is as defined in the ICH Q2 (R1) document. [103]

As no standards exist for our drug samples, accuracy can be inferred if linearity, precision and selectivity have been demonstrated, as per ICH Q2 (R1). [103]

Selectivity can be demonstrated by forced degradation of samples to generate degraded samples for comparison to. According to ICH Q2 (R1), “As appropriate, this should include samples stored under relevant stress conditions: light, heat, humidity, acid/base hydrolysis and oxidation”. Thus, samples were subjected to light using method 2.1.20, heat using method 2.1.21, acid hydrolysis using method 2.1.17, base hydrolysis using general 2.1.18 and oxidation using method 2.1.19.

2.3 Experimental for Chapter 3

2.3.1 Preparation of infliximab validation samples

Remsima brand infliximab vials were reconstituted using validated pharmacy procedures and in full accordance with instructions outlined within the 'Summary of manufacturers Product Characteristics' for Remsima. The 10mg/mL stock solution was diluted 1/10, by adding 150 µL to 1350 µL of 0.9% NaCl for injection. The samples were then inverted several times to ensure good mixing, without over agitating the samples. This produces a 1.5 mL 1mg/mL sample of Remsima branded infliximab.

2.3.2 Infliximab 96 well plate set-up

Biological activity of infliximab was assessed by measuring the infliximab mediated 'rescue' of WEHI-164 cells grown in the presence of TNF-α and actinomycin D. WEHI-164 cells were grown in RPMI-1640 supplemented with 10% foetal calf serum with 100 U/mL penicillin and 0.1 mg/mL streptomycin. WEHI cells were harvested from culture and seeded in a Nunclon, cell culture treated, 96 well, flat bottomed, clear plastic, plate (ThermoFisher Scientific, Massachusetts, USA) at 1.5 x 10^4 cells/well and incubated for 2 hours at 37 °C in a Heraeus BBD 6220 incubator (ThermoFisher Scientific, Massachusetts, USA). To assess inhibition of TNF-α induced cell death, infliximab was diluted to 3 µg/mL in a 10 pg/mL solution of TNF-α. This solution was incubated in a Heraeus BBD 6220 incubator (ThermoFisher Scientific, Massachusetts, USA) at 37 °C for 30 minutes before adding 10 µL/well for a final well concentration of 1 µg/mL µg/mL. Finally, 10 µL of a 20 µg/mL actinomycin-D solution was added to each well, yielding a final concentration of 2 µg/mL actinomycin-D. The cell line, and concentrations of TNF-α and actinomycin-D are the same as those used in three published studies investigating activity of infliximab. [106-108] The actinomycin D induces a higher level of apoptosis, improving the sensitivity of the assay to TNF-α.

2.3.3 Preparation of Remsima study devices

Remsima products under study were prepared under aseptic conditions in line with Good Manufacturing Practice, using validated pharmacy procedures and in full accordance with instructions outlined within the Summary of manufacturers Product Characteristics for *Remsima*. Products were prepared at a clinically high, common and low concentration by reconstituting the vials with water for injection to give a 10 mL concentrated stock solution. The stock solution was added to a *Freeflex* polyolefin infusion bag of sodium chloride 0.9 % w/v and stored at 2-8˚C in light-protective bags. On the day of analysis, samples were removed from each test product bag using aseptic technique by withdrawing 4 mL into a lubricant-free syringe, which was capped and stored at 2-8˚C during the analysis period. All test products were prepared in quadruplicate thus a total of 4 bags at each test concentration were compounded and used for analysis.

2.3.4 Remsima sampling schedule

Samples were analysed on the day of test product preparation (Day 0) and then at days 1, 2, 4 and 7 for batches at the high and low concentration. Samples were analysed on the day of test product preparation (Day 0) and then at days 1, 2, 3 and 7 for the batch at the common concentration mg/mL. Test product samples were analysed using the listed range of physico-chemical and biological techniques to assess the physical, chemical and functional stability profiles of *Remsima* at each time point.

2.4 Experimental for Chapter 4

2.4.1 Preparation of validation samples

Kadcyla brand trastuzumab emtansine vials were reconstituted using validated pharmacy procedures and in full accordance with instructions outlined within the

'Summary of manufacturers Product Characteristics' for Kadcyla. The 20mg/mL stock solution was diluted 1/20, by adding 75 µL to 1425 µL of 0.9% NaCl for injection. The samples were then inverted several times to ensure good mixing, without over agitating the samples. This produces a 1.5 mL 1mg/mL sample of Kadcyla branded trastuzumab emtansine.

2.4.2 Trastuzumab emtansine 96 well plate set up

Biological activity of trastuzumab emtansine was assessed by measuring the trastuzumab emtansine mediated growth inhibition of three different cell lines. The cell line used for on-target toxicity was BT-474 cells, grown in RPMI-1640 supplemented with 10% foetal calf serum with 100 U/mL penicillin and 0.1 mg/mL streptomycin. The cell lines used to assess off-target toxicity were HepG2 and HaCaT, grown in DMEM supplemented with 10% foetal calf serum with 100 U/mL penicillin and 0.1 mg/mL streptomycin. Cells were harvested from culture and seeded in a Nunclon, cell culture treated, 96 well, flat bottomed, clear plastic, plate (ThermoFisher Scientific, Massachusetts, USA) at 1.5 x 10^4 cells/well and incubated for 4 hours at 37 °C in a Heraeus BBD 6220 incubator (ThermoFisher Scientific, Massachusetts, USA). Trastuzumab emtansine samples were diluted to 3000 µg/mL, 1000 µg/mL and 30 µg/mL in NaCl 0.9% for injection. 10 µL of these trastuzumab emtansine solutions were added to wells of HepG2 cells, HaCaT cells, and BT-474 cells, respectively. The final well concentration of trastuzumab emtansine was 300 µg/mL, 100 µg/mL and 3 µg/mL for HepG2 cells, HaCaT cells, and BT-474 cells, respectively. Assay plates were incubated for 96 hours at 37 °C before assessment via an MTT assay according to method 2.2.11.

2.4.3 Size exclusion c*hromatography – Yarra-SEC-3000*

This was performed on HS3, using a Phenomenex Yarra 3 µm SEC-3000 column, with dimension 300 x 4.6 mm. Detection was at 280 nm, flow rate was 0.35 mL/min for

20 minutes, injection volume was 2 µL, Mobile phase was 0.1 M sodium phosphate buffer (pH 6.8) + 0.3 M sodium chloride + 0.25% sodium azide. Autosampler thermostat was set at 7 °C. Column oven temperature 25 °C.

2.4.4 Size exclusion chromatography – Organic modifier

This is method 2.2.17 except, the mobile phase was a ratio of 0.1 M sodium phosphate buffer (pH 6.8) + 0.3M NaCl + 0.25% sodium azide to 5, 10, 15 and 20% ethanol, acetonitrile or propan-2-ol.

2.4.5 Size exclusion chromatography – Potassium vs sodium

This is method 2.2.17 except, the mobile phase was adjusted as part of this experiment. The mobile phase was 90% 0.1M sodium or potassium phosphate buffer (pH 6.8) + 0.3M NaCl + 0.25% sodium azide to 10% propan-2-ol.

2.4.6 Size exclusion chromatography - Alkali chloride concentration

This is method 2.2.17 except, the mobile phase was adjusted as part of this experiment. The mobile phase was 90% 0.1M potassium phosphate buffer (pH 6.8) + 0.3 or 0.0 M NaCl + 0.25% sodium azide to 10% propan-2-ol.

2.4.7 Size Exclusion Chromatography – Buffer concentration

This is method 2.2.17 except, the mobile phase was adjusted as part of this experiment. The mobile phase was 90-25% 0.1M potassium phosphate buffer (pH 6.8) + 0.25% sodium to 0-65% ultrapure water azide to 10% propan-2-ol.

2.4.8 Size exclusion chromatography – Isopropanol 0-30%

This is method 2.2.17 except, the mobile phase was adjusted as part of this experiment. The mobile phase was 85% -70% 0.1M potassium phosphate buffer (pH 6.8) + 0.25% sodium to 15-0% ultrapure water azide to 0-30% propan-2-ol. Exact combinations of propan-2-ol : water : buffer are below. 0:15:85, 5:10:85, 10:5:85, 15:0:85, 20:0:80, 25:0:75, 30:0:70.

2.4.9 Size exclusion chromatography – Isopropanol 14-17%

This is method 2.2.17 except, the mobile phase was adjusted as part of this experiment. The mobile phase was 85% -83% 0.1M potassium phosphate buffer (pH 6.8) + 0.25% sodium to 1-0% ultrapure water azide to 14-17% propan-2-ol. Exact combinations of propna-2-ol : water : buffer are below. 14:1:85, 15:0:85, 16:0:84, 16.5:0:83.5, 17:0:83.

2.4.10 Size exclusion chromatography – *Column temperature*

This is method 2.2.17 except, the column oven temperature was tested at 25 °C, 30 °C, 35 °C and 40 °C.

2.4.11 Size exclusion chromatography – *Flow rate*

This is method 2.2.17 except, the flow rate was tested at 0.5, 0.75, 1.0, 1.25 and 1.5 mL/min over 30 min, and UV absorbance measured at 280 nm.

2.4.12 Infrared spectroscopy QDS initial protein acquisitions

10 mg ± 0.1 mg of each of the 15 proteins was weighed out into a 10 mL volumetric flask. This was then reconstituted in 0.9% NaCl for injection to make a final

concentration of 1 mg/mL. The Tensor 2, with the BioATR fitted, was purged for 30 minutes before the sample well was cleaned using 5% v/v Hellmannex III solution. The well was rinsed out with ultrapure water and dried with soft cotton buds (Lidl, London, UK). 20 µL of 0.9% NaCl for injection was pipetted into the sample well, then a background reading was taken. The full settings for each sample measurement are described in (**Table 4.6**). Once the background had been fully acquired, the NaCl was completely drawn up and discarded using a 100 µL pipette (Gilson, Bedforshire, UK). Then 20 µL of a protein solution would be pipetted into the well. A measurement would be recorded, then the sample drawn up and discarded, the cell rinsed with ultrapure water, dried with a cotton bud then 20 µL of 0.9% NaCl for injection was pipetted into the sample well, then a background reading was taken. This was repeated until three spectra had been recorded for each protein solution. These 42 spectra were used to create the QDS.

2.4.13 Infrared spectroscopy vs Circular dichroism spectroscopy

Vials of bevacizumab, cetuximab, denosumab, infliximab, natalizumab, nivolumab, obinituzumab, ofatumumab, pertuzumab, rituximab, trastuzumab, vedolizumab and trastuzumab emtansine were reconstituted according to their individual summary of product characteristics, using sterile water for injection. These concentrated solutions were diluted in triplicate to 1 mg/mL and 0.3 mg/mL in 0.9% w/v NaCl for injection. The 0.3mg /mL samples were measured using circular dichroism

2.4.14 Infrared spectroscopy structure determination validation

A vial of obinituzumab and a vial trastuzumab emtansine were reconstituted according to their individual summary of product characteristics, using sterile water for injection. These concentrated solutions were diluted in triplicate to 1 mg/mL in 0.9% w/v NaCl for injection.

2.4.15 Hydrophobic interaction chromatography – TSKGel Butyl NPR

HIC was performed using HS2. HS2 consisted of an LPG-3400SD pump, WPS-3000 analytical autosampler, TCC-3000 column oven and DAD-3000 multiple-wavelength detector. The column used was a TSKgel Butyl-NPR (TOSOH BioScience, Stuttgart, Germany), column dimensions 4.6 × 35 mm and particle size 2.5 µm. The TSKgel final method used a UV detection was set to 280 nm, flow rate was 1 mL/min, injection volume was 25 µL, column oven temperature was set to 30 °C, the method was a gradient from 100% 1.5M ammonium sulphate dissolved in 100 mM potassium phosphate + 15mM NaN_3 (pH 6.80) to 100 mM potassium phosphate + 15mM NaN_3 (pH 6.80). The gradient was over 150 seconds and was held for 30 seconds before returning in 30 seconds to the starting conditions which were held to re-equilibrate for 150 seconds before the next injection.

2.4.16 Hydrophobic interaction chromatography - CIM r-Protein & C4

Dual HIC & Affinity chromatography using CIM r-Protein G/A Disks in combination with the CIM C4 A Disk. CIM disks were found unsuitable. No final method was achieved. However, the following method was used during early experimentation.

HIC was performed using HS2. HS2 consisted of an LPG-3400SD pump, WPS-3000 analytical autosampler, TCC-3000 column oven and DAD-3000 multiple-wavelength detector. UV detection was set to 280 nm, flow rate was 1.0 mL/min, injection volume was 50 µL, column oven temperature was set to 20 °C, the method was a gradient from 100% 2M ammonium sulphate dissolved in 100 mM sodium citrate buffer (pH 2.0) to 2M ammonium sulphate dissolved in 100 mM potassium phosphate (pH 7.0) to 100 mM potassium phosphate (pH 7.0). The gradient was over 60 minutes, the column was re-equilibrated for 10 minutes before the next injection at the starting conditions.

2.4.17 Intact LC-MS sample preparation

500 µL of sample was aliquoted into a 1.5 mL centrifuge tube and processed according to method 2.2.12, except no TCEP is added.

2.4.18 PNGase F deglycosylation protocol

425 µL of 1 mg/mL trastuzumab emtansine was mixed with 50 µL of the provided 'GlycoBuffer' and 125 µL of NEB PNGase F in a 1.5mL centrifuge tube. This sample was kept at 37 °C using a heat block for 24 hours. The sample would be removed and processed via experimental method 2.4.30.

2.4.19 PNGase F Rapid deglycosylation protocol

400 µL of 1.25 mg/mL trastuzumab emtansine was mixed with 200 µL of the 5X RAPID PNGase F in a 1.5mL centrifuge tube. This sample was kept at 75 °C using a heat block for 5 minutes. The sample would be removed and 50 µL of the Rapid PNGase F added and the sample placed at 50 °C for a further 10 minutes before being removed and processed via experimental method 2.4.30.

2.4.20 pH 9-11 at 50 °C buffer degradation of trastuzumab emtansine

75 µL of 100 mM Dipotassium phosphate adjusted to pH 9 with 1M hydrochloric acid or 10 or 11 with 5M potassium hydroxide was mixed with 25 µL of sample. After 180 minutes in the myBlock Mini Dry Bath at 50 °C**,** the samples were neutralised with 900 µL of 100 mM dipotassium phosphate, pH adjusted to 5.5 with 1M hydrochloric acid.

2.4.21 pH 7-9 at 40 °C buffer degradation of trastuzumab emtansine

75 µL of 100 mM Dipotassium phosphate adjusted to pH 7, 8 or 9 with 1M hydrochloric acid was mixed with 25 µL of sample. After 90 minutes in the myBlock Mini Dry Bath at 40 °C**,** the samples were neutralised with 900 µL of 100 mM dipotassium phosphate, pH adjusted to 5.5 with 1M hydrochloric acid.

2.4.22 pH 9 at 45 °C buffer degradation of trastuzumab emtansine

75 µL of 100 mM Dipotassium phosphate adjusted to pH 9 with 1M hydrochloric acid was mixed with 25 µL of sample. After 60, 90, 120 and 180 minutes in the myBlock Mini Dry Bath at 45 °C**,** the samples were neutralised with 900 µL of 100 mM dipotassium phosphate, pH adjusted to 5.5 with 1M hydrochloric acid.

2.4.23 Assessing DAR via heavy and light chain relative TICs

LC-MS was also used to evaluate the stability of cytotoxic 'payload' attachments to the trastuzumab antibody portion of the trastuzumab emtansine ADC. Total ion counts (TICs) per mass were exported at 1 Da resolution for each sample in the form of an XY plot (mass v abundance). Each XY plot was manually processed to sum all TICs related to a light or heavy chain bound to zero, one or two payloads. This produced 6 values: 3 describing the distribution of payloads on the light chain and 3 describing the distribution of payloads on the heavy chain. To improve data comparability the TICs pertaining to each chain are converted to TICs relative to the sum of all TICs pertaining to heavy or light chains respectively, these are then then expressed as a percentage. The mass range for TICs corresponding to naked light chains was 23422-23472 daltons. The mass range for TICs corresponding to single payload light chains was 24370-24440 daltons. The mass range for TICs corresponding to double payload light chains was 25324-25386 daltons. The mass range for TICs corresponding to naked heavy chains was 50525-50679 daltons. The mass range for TICs corresponding to single payload heavy

chains was 51483-51637 daltons. The mass range for TICs corresponding to double payload heavy chains was 52447-52577 daltons.

2.4.24 Preparation of study devices

Kadcyla products were prepared under aseptic conditions in line with Good Manufacturing Practice, using validated pharmacy procedures and in full accordance with instructions outlined within the Summary of manufacturers Product Characteristics for *Kadcyla*. Products were prepared at a clinically high, common and low concentration by reconstituting the vials with water for injection to give a 5 mL concentrated stock solution. The stock solution was added to a *Freeflex* polyolefin infusion bag of sodium chloride 0.9% and stored at 2-8˚C in light-protective bags. On each day of analysis, samples were removed from each test product bag using aseptic technique by withdrawing 5 mL into a lubricant-free syringe, which was capped and stored at 2-8˚C during the analysis period. All test products were prepared in quadruplicate thus a total of 4 bags at each test concentration were compounded and used for analysis.

2.4.25 Sampling schedule

Samples were analysed on the day of test product preparation (Day 0) and then at days 1, 4, 7, 11, 14, 18 and 20. After Day 20 samples were placed in a 25 °C oven and sampled after 24 hours (day 21) and then 96 hours (day 24).

2.5 Experimental for Chapter 5

2.5.1 Measuring bag dimensions

100 mL Baxter Viaflo, Fresenius Kabi Freeflex and Maco Pharma Macoflex-N infusion bags were emptied, and measurements using a steel rule were made of the inner chambers length and width.

2.5.2 Bag comparison study samples

Herzuma, Orencia and Mabthera products were prepared under aseptic conditions in line with Good Manufacturing Practice, using validated pharmacy procedures and in full accordance with instructions outlined within their own Summary of manufacturers Product Characteristics. Products were prepared at a clinically low concentration by reconstituting the vials with water for injection to give a concentrated stock solution. The stock solution was added to a *Fresenius Kabi Freeflex, Baxter Viaflo and Macopharma Macoflex-N* polyolefin infusion bags of sodium chloride 0.9% and stored at 2-8°C in light-protective bags. On each day of analysis, samples were removed from each test product bag using aseptic technique by withdrawing 3.5 mL into a lubricant-free syringe, which was capped and stored at 2-8°C during the analysis period. All test products were prepared in quadruplicate thus a total of 4 bags for each brand of polyolefin infusion bag were compounded and used for analysis.

2.5.3 Sampling schedule - Trastuzumab (Herzuma)

Samples were analysed on the day of test product preparation (Day 0) and then at days 3, 10, 21, and 30.

2.5.4 Sampling schedule - Rituximab (Mabthera)

Samples were analysed on the day of test product preparation (Day 0) and then at days 3, 10, 18, and 32.

2.5.5 Sampling schedule - Abatacept (Orencia)

Samples were analysed on the day of test product preparation (Day 0) and then at days 5, 10, 20, and 31.

2.5.6 SEC HPLC validation for trastuzumab, rituximab and abatacept

The HPLC assays validation were performed according to general method 2.2.24. This data has not been presented in the thesis, but is available in Appendices I-III.

2.5.7 Scanning electron microscopy

High magnification images were obtained using a JEOL JSM6480-LV scanning electron microscope (SEM) with EDX capability using an accelerator voltage of 10kV and a spot size of 25nm. The samples were coated with a thin layer of gold using an Edwards S150B sputter coater prior to SEM analysis.

2.6 Experimental for Chapter 6

2.6.1 Forced degraded and control sample preparation

250 µL of trastuzumab emtansine vial concentrate (20 mg/mL) was mixed at a 1:1 ratio with each of the common cleaning agents in a 0.5 mL centrifuge tubes, then placed on a heat block at 20 °C for 2 hours. The samples were then removed and immediately processed for LC-MS analysis

2.6.2 Brentuximab vedotin 96 well plate set up

Biological activity of brentuximab vedotin was assessed by measuring the brentuximab vedotin mediated growth inhibition of two different cell lines. The cell line used for on-target toxicity was GCT-27 cells, grown in DMEM supplemented with 10% foetal calf serum with 100 U/mL penicillin and 0.1 mg/mL streptomycin. The cell line used to assess off-target toxicity was HepG2, grown in DMEM supplemented with 10%

foetal calf serum with 100 U/mL penicillin and 0.1 mg/mL streptomycin. Cells were harvested from culture and seeded in a Nunclon, cell culture treated, 96 well, flat bottomed, clear plastic, plate (ThermoFisher Scientific, Massachusetts, USA) at 2.0 x 10^4 cells/well and incubated for 4 hours at 37° C in a Heraeus BBD 6220 incubator (ThermoFisher Scientific, Massachusetts, USA). Brentuximab vedotin samples were diluted to create a dose response curve from 3000 – 1 µg/mL in NaCl 0.9% for injection. 10 µL of these brentuximab vedotin solutions were added to wells of mL to both HepG2 cells, and GCT-27 cells. The final well concentration of brentuximab vedotin was 300, 100, 30, 10, 3, 1, 0.3 and 0.1 µg/mL for both HepG2 cells, and GCT-27 cells.

2.7 Experimental for Chapter 7

2.7.1 Control and forced degradation samples

A vial of brentuximab vedotin was reconstituted with water for injection according to its summary of product characteristics, to a 20 mg/mL. Two 1 mL aliquots were added to 9 mL of 0.9% w/v NaCl for injection, in a 15 mL centrifuge tube were made. One was degraded photolytically according method 2.2.20, while the other was kept protected from light and refrigerated at 2-8 °C for the same amount of time.

Chapter 3. Development and implementation of methods for the characterisation of a traditional monoclonal antibody

To design an appropriate stability study, it was first required to assess all relevant guidance. Then, identify analytical methods able to meet guidance requirements. It was considered appropriate to first implement these methods on a traditional mAb, as this would provide positive validation data to use as a point of reference when later investigating ADCs.

3.1 Critical characteristics and methods to measure them

There are 10 critical quality attributes of a biopharmaceutical product, that must be assessed, according to the NHS guidance [102] While they don't cover ADC's, they do provide a starting point. These attributes, methods for their measurement and a rational for choosing a technique are described in detail below.

3.1.1 Colour, clarity and visible particulates

Visible changes, such as colour change, can indicate the formation of a degradant species. Loss of clarity, or conversely an increase in turbidity indicates an increase in subvisible particulates or precipitation, and visible particulates could indicate precipitation. [224] Any of these observations could make a product unsuitable for administration, due to potential immunological responses and blockage of blood vessels and some visible changes are listed in British pharmacopeia (BP) monographs.

Visible changes can be measured by a visual inspection following a method set out in the British pharmacopeia "Method 2.9.20 Appendix XIII B. Particulate Contamination. Visible Particulates". [110] Inspecting products for 5 seconds under normal florescent light against a white and then a dark background should allow ample

opportunity to spot any changes to clarity, such as increased turbidity, or the development of a colour or change in colour. [111] It is also possible if colour is expected to compare the samples against colour standards. [112]

While it is possible to use a spectrophotometer to measure the total absorbance of visible light, delta max and absorbance spectrum, upon reviewing the NHS yellow cover documents and stability research papers for therapeutic small molecule studies and antibodies, typically only simple visual inspections were performed. [111,113,114] Consequently, the British pharmacopeia method, was used to assess colour, clarity and visible particulates and photographs of the samples were taken on each timepoint.

3.1.2 pH

The BP monograph for a drug states the acceptable pH for that drug at therapeutic concentrations. The pH of a drug can change slightly during long term storage, especially if the product has weak buffering or even no buffering excipients, such as cyclophosphamide 500 mg powder for injection which can have a pH anywhere between 3 and 9 as stated in its SPC.

The pH can be measured using indictor solution or paper but most commonly a calibrated pH probe. No studies found used indicator paper or solutions, most stability studies did not actually assess pH at all. All those that did measure pH, used a pH meter. [115, 116] Therefore, a pH meter calibrated with three pH standards will be used to assess the pH of samples on every timepoint.

3.1.3 Chemical degradation

Drugs may degrade in a variety of ways, resulting in degradants due to glycation, hydrolysis, oxidation, deamidation and fragmentation, with each chemical modification potentially affecting the rate of aggregation, and functional activity. It is important to assess all potential routes of degradation and identify any degradation products.

There are many ways of measuring the chemical degradation of an antibody, although over half of the published stability studies investigated did not assess it. Ion exchange chromatography (IEX), RP-HPLC following enzyme digestion and LC-MS are the most common methods of assessing antibody chemical stability found during literature research. [111,117-120]

IEX is able to separate charge-based variants of the monomer, often caused by oxidation, deamidation and hydrolysis. It has been demonstrated that charge heterogeneity impacts drug stability. [121] The method requires an HPLC system, an ion exchange column and associated mobile phase. It is one of the most common techniques used to assess chemical degradation.

RP-HPLC following enzyme digestion, also known as antibody digest analysis, requires an HPLC, a reverse phase column and associated mobile phase. It can separate antibody fragments, typically papain and pepsin, or trypsin are used to fragment the antibody. This method requires enzymes and creates highly complex spectra which can be hard to interpret as well as determining if changes have occurred. It is the least often used method found used to assess chemical degradation.

LC-MS is able to measure the exact mass of each species of antibody, to approximately 1 kDa. This allows new chemical forms of the antibody to be identified and the route of degradation can often be determined by calculating the change in mass. For example, glycosylation can be identified by the addition of a mass equal to a known sugar. LC-MS can also detect hydrolysis, glycosylation, deamination commonly of asparagine, oxidation commonly of methionine and even fragmentation, depending in the mass range that is observed. Use of reducing agents to cleave the inter-chain disulphide bonds can also be used to decrease the complexity of the samples and improve the resolution of species, although it does prevent fragmentation and oligermization being assessed. Typically, tris(2-carboxyethyl)phosphine (TCEP) or

tris(hydroxypropyl)phosphine (THPP) are used to reduce the disulphide bonds as they are known to reduce inter-chain disulphides but not intra-chain disulphide bonds. [122]

As stated in 3.2.4, size exclusion chromatography (SEC) was used and it was impractical to use a second chromatography-based method as that apparatus would not be available, the same is true for RP-HPLC following an enzyme digest. Furthermore, enzyme digests are complex and require more time than IEX. IEX does yield useful information without too much effort, however the additional information obtainable with LC-MS out-weighs the additional sample handling concerns and increased cost. Therefore LC-MS will be used to assess chemical degradation, this will be supported by pH readings and gel electrophoresis.

3.1.4 Active pharmaceutical ingredient (API) concentration

The API is the drug and most BP monographs state the acceptable loss of concentration which can range from 10% to only 2%. Some drugs do not have a drug or presentation specific monograph. For example, the British pharmacopeia's "General Monoclonal Antibodies Monograph" covers all mAbs for human use. In this instance 5% concentration loss is generally considered an acceptable limit.

The API is the antibody or antibody drug conjugate monomer. It is well known that antibodies aggregate into oligomers such as dimer and trimers, therefore it is important the method of characterisation can separate the monomer form oligomers. Size exclusion chromatography (SEC) is a common technique used that separates and sorts molecules by size, buffers are used to ensure the proteins are stabilised in their native form. All stability studies found determined the antibody concentration via SEC or UV absorbance. [111,123-125] SEC was the most common choice and is mentioned in the NHS yellow cover documents. SEC is a well-documented method able to separate the monomer from its oligomers, while total UV assays do not accomplish this. Consequently, SEC will be used to measure the API concentration, as well as assess levels

of dimer and trimer aggregates, this will be using analysis of the area under the curve of each species (monomer, dimer trimer) compared to a linearity curve.

3.1.5 Sub-visible particulates and aggregation

While visual checks can determine the level of visible particulates and aggregation, the majority of aggregates and particulates are sub-visible, or invisible to the naked eye. Sub-visible particles and aggregates can be of any size from 10 nm to about 100 µm. Aggregated drug is a problem as it can raise an immune response in patients, leading to: anti-drug antibodies, faster rates of drug clearance, impaired pharmacokinetics and reduced binding strength, ultimately resulting in a lower level of care being delivered to the patient. [225] Sub-visible particles are a cause of concern due to their ability to cause vein irritation, anaphylactic shock, phlebitis, pulmonary emboli, pulmonary granulomas, immune system dysfunction, pulmonary dysfunction, infarction, and death. [109]

Particles can be related to the packaging, such as rubber from a septum or plastic from an injection port. Alternatively, the particles could be undissolved, aggregated or precipitated drug/excipient material. Protein-based drugs aggregate, though excipients to prevent aggregation are included in many mAb formulations.

Sub-visible particles, whether aggregated drug or not, are of concern and the NHS specifically states a maximum number of particles per container at two size ranges, greater than 10 µm and greater than 25 µm, which are used when determining the shelf lives of small molecule drugs. However, those particles limits are not imposed upon biopharmaceuticals as the protein aggregates typically exceed those limits during the SPC shelf life (24 h from reconstitution). Consequently, no statistical difference to measurements made within the SPC shelf life is satisfactory as an acceptance criterion.

Oligermization was assessed by SEC, which covers the range of ~5 nm to about 50 nm. This covers antibody monomers and oligomers as antibody monomers have a length and width of about 8 by 14 nm. [228] Another technique must be used to assess 50 nm to 0.1 mm, which is about the limit of visible particulates. There are many methods of measuring sub-visible particles, the most common found in antibody stability research are summarised below.

Firstly, light obscuration is widely used in small molecules and there are limits established in the BP 'Appendix XIIIA. Particulate Contamination: Sub-visible Particles Ph. Eur. method 2.9.19'. Light obscuration methods are mentioned in the NHS yellow cover guidance, but it is also recognised that these methods require large volumes of sample as well as lacking sensitivity to the translucent protein aggregates.

Another test in the BP, known as microscopic particle count test, requires the use of an ocular micrometre and binocular microscope. The test involves counting particles in a known volume of solution against a known area and comparing these values to BP defined limits of 10 per mL for particles larger than 10 µm and 3 per mL of particles larger than 25 µm.

Microflow imaging (MFI) uses a camera, microscope, flow cell and pump to capture images of the sample while drawn through the flow cell. The images are used to detect particles via a comparison to a blank. MFI is one of the more common method of measuring particles in antibody stability studies. [126-130] This technique is widely used to measure particulates between 1 and 100 µm.

Resonant mass measurement (RMM) is a less common technique, though it is powerful, with the ability to detect particles from 50 nm to 5 µm. [129] RMM utilizes the inherent resonating frequency of the sample fluid as a background and detects changes as the sample flows past a cantilever, as particles have a different buoyancy depending on size, shape and material, which affects the frequency of resonance. Although this

technique is interesting and powerful, we do not have access to an RMM such as the Archimedes (Malvern Panalytical, Royston, UK).

Dynamic light scattering (DLS) is likely the most common technique used to assess protein particulates, greater than 50 nm. DLS measures the rate of change in laser light scattering, due particles present in a stationary sample, to determine the speed of particles due to Brownian motion. The particle speed can be used to calculate the estimate spherical size of said particles using the Stokes-Einstein equation. Thus, particle sizes can be calculated from 10 nm to 1000 nm. This technique does have poor resolution, grouping particles into peaks and presenting the average particle size of each peak and the polydispersity index, a measure of the peaks heterogeneity. However, the peaks need to be over three times the size of each other to be distinguished, meaning monomer, dimer and trimer are observed as a single peak, as well as any other particle peaks. Furthermore, DLS is hypersensitive to larger particles, a 10-fold increase in size results in a 1,000,000-fold increase in signal intensity. This makes DLS not very good at detecting smaller aggregates and if two peaks are near each other they can be grouped into one peak with an average particle size being produced. While DLS is widely used, a newer technique has been developed which appears superior in multiple ways. [117,123,129]

Nanosight Tracking Analysis (NTA) is a laser-based technique that tracks the motion of diffraction patterns due to particles and uses the Stokes-Einstein equation to calculate an estimated spherical volume. NTA differs from DLS for two reasons. Firstly, it can differentiate particles with a size difference of 0.5 nm and secondly its sensitivity, especially at the lower particle sizes is greater than DLS. [111, 126, 129] Meaning data produced is more detailed and accurate, however also more sensitive to sample heterogeneity. [131-134]

It is clear that, no single technique covers the complete range of subvisible particulates, although RMM comes the closest. Furthermore, the insensitivity of light obscuration and heavy workload required by the BP microscopic particle count test demonstrate neither BP methods are ideal techniques. MFI is the best technique to

replace these two BP methods, as it can count particles in the 1-100 micrometre range, which we could refer to as micro-particles.

NTA appears to be a step forward from DLS, although both are functional techniques that produce acceptable data, NTA is the preferred choice. And while RMM has very good range and sensitivity it is also unavailable to at Bath University and Bath ASU and expensive to buy (£100,000+). While NTA was the preferred technique, equipment was unavailable until Bath ASU funded the acquisition of a Nanosight LM10 (Malvern Panalytical, Royston, UK) in 2016. As such, DLS was used from 2014 – 2016 using a Zetasizer ZS (Malvern Panalytical, Royston, UK) which was available in the Bath University department of Biology.

3.1.6 Higher order structure

Protein function is inherently defined and controlled by its structure, from primary sequence of amino acids to its tertiary structure. The sequences of specific amino acids will generate secondary structures that interact with each other, for example due to hydrophobicity to form an entropically favourable tertiary protein structure. The tertiary shape of an antibody allows the CDR regions to bind to complementary antigens with specificity. If the shape of the Fab region changes, the CDRs may no longer align with the complementary regions of its target epitope, leading to loss of binding efficiency, potential loss of selectivity, or even new target selectivity, a facet of antibodies that is explored more using site directed mutagenesis to create structure function maps of an antibody and determine key amino acids. [226, 227] The shape of the Fc region affects the ADCC and CDC function as well as pharmacokinetic properties such as the half-life. The higher order structure refers to the secondary, tertiary and quaternary protein structure. The secondary structure consists mainly of alpha-helices and beta sheets (parallel and anti-parallel) and random coils, although random coils is a term used to describe irregular structure. There are other known secondary structures such as 3_{10} helices and π helices, but these are only observed in minute amounts. Tertiary structure is less definable but is the three-dimensional shape

generated by the secondary structure. Tertiary structure is not always fixed, many proteins have flexible regions, such as the hinge region of an antibody. These makes measuring tertiary structure more difficult though not impossible.

Protein higher order structure refers to either secondary, tertiary or quaternary structure. Techniques that can assess these include, circular dichroism spectroscopy (CDS), infra-red spectroscopy (IRS), X-ray crystallography (XRC), NMR spectroscopy (NMRS), Cryo 3D electron microscopy (C3DEM) and lastly primary sequence prediction algorithms (PSPA) such as PredictProtein (EMBL, München, Germany).

Firstly, sequencing a large protein such as an antibody is laborious, expensive and takes more time than is practical, therefore PSPA's are not useful in this instance. Furthermore, the primary sequence is unlikely to change during a stability study, while the conformation may change, so even if it was practical to measure the entire primary sequence it would not help us assess changes to the higher order structure.

XRC requires the growth of crystals which is difficult and time consuming furthermore analysis is incredibly complicated with large proteins, such as antibodies. XRC does produce very good information on proteins and is one of the best techniques for measuring a proteins structure [135-138] but in this instance, it is not practical to use, and the level of detail is unnecessary.

NMRS can assess proteins suspended in liquid which is good as it means our antibodies can be assessed in their diluted state. [139-141] NMRS generates a detailed structural breakdown of a protein, although it becomes more complicated and difficult the larger the protein is. In fact, NMRS using typical NMR equipment is not used to assess proteins over 100 kDa. [142] A review of the use of NMR to assess large proteins in 2013 showed only 5 proteins over 100 kDa had ever been measured. [142] NMRS is best used on proteins with a mass of 50 kDa or less. Unlike LC-MS where reducing the disulphide bonds and assessing only the light or heavy chains in isolation is feasible, that process would have dire implication on the structure and would render the data collected

effectively useless in determining if the structure or conformation of the intact antibody had changed.

C3DEM is a technique that uses electrons to image proteins, frozen in non-crystalline ice. Multiple 2D images taken at different angles are combined to create a 3D image. The more images taken at each angle and the more angles that pictures are taken at increases the level of detail or resolution of the 3D image. [143-146] C3DEM can be used to create images of proteins to an atomic level. [147] C3DEM is now being used more than XRC to measure the structure of proteins, according to the number of new structures added to the international protein data bank. However, the technique is impractical to perform on a study day due to the amount of time it takes to prepare samples and image them. Furthermore, the equipment is expensive, and access was not readily available. Consequently, this method was not employed.

The most commonly used technique for stability studies is CDS, coupled with a CD spectrum to structure software such as CDNN (Gerald Bohm, Magderburg, Germany). CD spectroscopy is mentioned in the yellow cover documents and has successfully been used in many antibody stability studies. [139,148-151] Secondary structure composition is estimated based on the CD spectrum which can be tracked over time to assess degradation, as well as measuring the change in conformation associated with a temperature ramp. This gives structure at room temperature and conformational stability in one experiment. While the technique typically requires an hour to perform a temperature ramp there is minimal sample preparation involved, elucidating why this technique is used in so many stability studies and is mentioned in the NHS yellow cover document.

IRS has been used to assess chemical identity due to the unique “fingerprint” small molecules have in the 1500 to 500 cm^{-1} region. More recently fourier-transform infrared spectroscopy (FTIR) has been used with attenuated total resistance (ATR) sample cells to investigate the structure of proteins in liquid suspensions [139,148-151]. ATR increases the surface area of sample that can affect the IR laser. Furthermore,

supercooled mercury-cadmium-telluride alloy detectors are used which can detect single photons, drastically increasing the sensitivity of the technique. It has been demonstrated that two characteristic peaks on an IR spectrum the Amide 1 and Amide 2 bands are conformationally sensitive, that meaning as the structure changes the bands also change. Some sample holders can be used to perform temperature ramps like CDS experiments. Initially we did not have access to equipment suitable for performing IRS though later during the PhD we able to gain access to one.

Differential scanning calorimetry provides an insight into the thermal stability of a compound, [148,150,151] specifically heat enthalpies during state changes and the temperatures required to cause state changes. However, while these would correlate with structure and structural stability, these measurements are not a directly translatable to higher order structure and so this technique is unsuitable for assessing antibody higher order structure in isolation. [152]

Multiple papers acknowledge all these techniques produce an estimation of the proteins higher order structure. [153,154] These estimations will not necessarily be the same although they should be similar and certain proteins will have high levels of comparability while others will have lower levels of comparability. [155,156] This is thought to be due to protein flexibility as well as inherent flaws in each technique, such as the suitability of original library of proteins that sample data is compared to. Some structural prediction algorithms are known to over predict certain secondary structural features and under predict on others. [157] However, as the purpose of the stability study is to monitor for change over time ensuring the predicted value is 100% accurate is not necessary if the readings are precise and stability indicating.

The first-choice technique is CDS, as it meets all criteria set out in the yellow cover document and the required equipment is available at the University of Bath. Furthermore, it is the most widely used technique in antibody stability studies, with regards to higher order structure characterisation. As covered in chapter 4, CDS proves problematic with ADCs, and IRS is investigated as the best alternative.

3.1.7 Degradation product concentration

British pharmacopeia drug monographs state an acceptable amount of API concentration loss, typically up to 10%, however there are rarely limits on the presence of specific degradants listed in a drugs BP monograph. Some monographs do list limits on impurities formed during API manufacture, which may also be formed as degradation products, but this is unlikely to be an exhaustive list of potential degradation products. Furthermore, the BP doesn't have antibody specific monographs and instead has a general monograph. Defining 5% total degradation products and no more than 2% of any individual degradation product, even when the concentration loss of API can be 10%. The main degradants observed in antibodies are oligomers, most commonly dimers and trimers, although some fragmentation has been observed. [125-129]

Degradants in biopharmaceutical formulations including dimers, trimers and other oligomers would be appropriately measured by SEC. Chemical degradation, leading to new glycol-forms or oxidised / reduced forms can be detected by LC-MS. Nanoscale aggregates and microscale aggregates can be assess using NTA and MFI respectively. Reduced DAR ADCs could be tracked using LC-MS. And free payloads may show up in LC-MS or SEC, and their toxicity or lack thereof can be monitored in the bio-assays. It was felt all possible degradants would be assessed using the chosen methods.

3.1.8 Biological activity

The NHS biopharmaceutical stability guidance [102] requires a measure of biological activity, stating biochemical assays, cell culture-based assays and animal models as methods that can indicate biological activity. Animal based models are not useful for chimeric or humanised antibodies due to the immunogenic response likely to be raised, not to mention the ethical and financial burdens they come with. Biochemical based assays such as binding assays are acknowledged as useful but not giving the whole picture, for example an Enzyme Linked Immuno-Sorbent Assay (ELISA) may reveal the

binding efficacy but not the receptor activity. Therefore, biochemical assays are not recommended in isolation.

Cell Culture Based Assays measure physiological response at the cellular level. A cell-based assay needs to show that the molecule will have the defined biological activity for its function. The cellular response to be measured also must be determined and may include cell signalling, cell death or cell proliferation. It is usual to use a high number of replicates for cell-based assays to allow for inherent variation in the assay performance and to improve the robustness of the results obtained. Other considerations include a good understanding of the methodology including validation to demonstrate that the cell-based assays will correlate with in vivo activity. Appropriate controls should be incorporated to validate the assay and should include positive reference standards in addition to negative controls.

The biological activity of antibodies and ADC used to treat cancer is typically to kill the aberrant cells. As explained in the introduction it is deemed inadequate by ICH and the NHS to perform simple biochemical tests as the only method of quantifying biological or functional activity. *In vivo* cellular assays provide a much more concrete demonstration that the drugs are still able to perform their intended function, while also providing a quantitative measure of their activity.

The cell assays we intend to use require incubation of target cell lines with defined concentrations of the ADC or antibody. The growth inhibition can be calculated by comparing either cell number, metabolic activity or DNA content for control cells not exposed to the drug against cells incubated with the drug. The concentration of drug the cells would be incubated with and the duration of incubation was determined during validation tests.

The three main types of cellular viability assays are cell number, metabolic activity or DNA content. Cell number can be determined with reagent such as trypan blue which is excluded from viable cells and a haemocytometer, however this is

incredibly labour intensive and has a high risk of operator error due to the physical strain associated. To overcome this cell counters are now commonly used in laboratories such as the Invitrogen Countess Automated Cell Counter (Invitrogen, California, USA). However, the cost of consumables required to perform this test and the labour required is still very high.

Rather than direct cell measurements via counting cells that exclude a reagent such as trypan blue, metabolic activity assays measure absorbance at a defined wavelength. This is because a reagent that is metabolized by active cells changes colour. The most ubiquitous metabolic activity reagent is MTT, which is metabolized from a yellow tetrazolium to a purple formazan. This colour change is easily measurable on a plate reader and allows 96 well plate assays to be performed. MTT is very cheap although the assay does require a few steps.

First the cells are seeded into each well and left to grow in the presence of a defined concentration of the antibody or ADC. After about 5 days the cell growth media is aspirated from each well and 1.2 mM MTT diluted in complete colourless growth media is added. After about 4 hours of incubation the growth media is aspirated and DMSO is added to solubilise the tetrazolium and formazan crystals. The plates can then be read using an absorbance plate reader. The MTT assay has been used by thousands of scientists and is quite an old assay.

Some other tetrazolium metabolic assay reagents have been developed such as XTT, MTS and WST 1-8 which do not require the addition of DMSO to solubilise the crystals as they are water soluble.

Resazurin is a blue reagent that can be used similarly to the water-soluble tetrazolium reagents, in that it is metabolized by active cells to the pink resorufin. It has been demonstrated as more sensitive than the tetrazolium assay reagents, requiring fewer cells per well. Resazurin was commonly used as the branded product Alamar Blue

which was a combination of Resazurin and additional reagent designed to prevent over metabolism of resazurin.

Alternatively, DNA content assays can be used to measure the total DNA content, assumed to be directly proportional to the cell number, like metabolic activity assays. SYBR green is a dye that binds to DNA allowing it to be measured using fluorescence, for example in a fluorescence plate reader. SYBR green is useful as it can be combined with other reagents that fluorescence such as resazurin or caspase activity reagents. Multiplex imaging of cells can be very useful in investigating cellular activity, however it is far beyond what is required for a measurement of the biological activity of drugs that cause apoptosis. Furthermore, MTT assays use a very cheap reagent and use of an automatic electronic pipette reduces the required effort, thus MTT assays will be used.

To assess off target activity in an ADC all that is required is to change the cell type to a non-target cell type and adjust the required concentration of drug added to the cells as theoretically they would be far less sensitive to the drugs than the target cells, thus requiring far greater concentrations of drug to initiate apoptosis.

3.1.9 Active excipient concentrations

Excipients, while not APIs can have active effects in the body, for example hyaluronidase, an enzyme that breaks down hyaluronic acid in the extracellular matrix to improve the permeability of a drug in subcutaneous forms can degrade reducing the effectiveness of the product without affecting the API concentration. Most formulations do not contain active excipients and only use excipients for controlling of pH, solubility and preventing aggregation.

No commercially available ADC's currently include active excipients in their formulations, so it was not considered necessary to investigate this aspect.

3.1.10 Moisture loss

Infusion bags are one of the most common containers for aseptically prepared products. Long term storage of infusion bags can lead to minor levels of moisture loss, generally accepted to be clinically insignificant during typically 24 – 48-hour storage time but worth monitoring upon extended storage.

Moisture loss can be measured by comparison of bag weights taken after the sample volume has been withdrawn from the bag on a study timepoint to bag weight taken immediately prior to the next sample withdrawal. From personal experience, moisture loss from infusion bags stored at 5 °C is less than 0.1% mass during a month, while storage at 25 °C is over 0.1% mass during a month.

3.1.11 Container extractables and leachables

Infusion bags contain additives, such as plasticisers, which may leach into drug products upon extended storage. This is more likely to occur in drug products that contain solubilising excipients, extractables are typically only important if the drug contains excipients that could cause extraction of into the drug solution, most drugs do not contain excipients able to extract chemicals from the container material. The UV absorbance of stored drug solutions can be measured to detect plastic additives, such di(2-ethylhexyl)phthalate, leaching into the stored product at

3.2 NHS yellow cover document compliant study design

Having identified the necessary quality characteristics that require evaluation, as well as appropriate analytical techniques for their evaluation, it was then decided to incorporate these aspects into the design of a compliant stability study.

3.2.1 Following the guidance

As mention in the introduction, the NHS yellow cover document outlines a series of study design choices that must be as specified in either the SPC of the drug under investigation or as specified in the yellow cover document itself. Some design parameters are more flexible as will be discussed. Where possible all guidelines must be followed and where not, it must be explained and justified.

3.2.2 Analytical methods

The development and validation of all analytical methods used must be described. Methods must be stability indicating, robust and fully validated in accordance with the International Conference on Harmonisation (ICH) Q2(R1) document. [105] The specificity of the method together with its ability to detect degradants must be described. The characterisation techniques we will be using are as defined in section 3.4.1 to 3.4.12, with general methodologies described in chapter 2, some experimental details will be in subsequent chapters as they are involved in method development.

3.2.3 Diluents

The diluents used and the rationale for their choice must be described. Typically, this is 0.9% w/v NaCl for injection, but will be specified in the API's SPC. The SPC for Kadcyla branded trastuzumab emtansine and Remsima branded infliximab states the powder must be reconstituted with sterile water, then the reconstituted drug concentrate must be diluted into 0.9% NaCl for injection. Therefore, only sterile water for injection will be used to reconstitute the lyophilized powders, and subsequently only 0.9% NaCl will be used as a diluent.

3.2.4 Container

Containers used and the rationale for their choice must be stated. Studies should be carried out in the specific containers to be used in clinical practice. It is recommended that non-PVC infusion bags be used instead of PVC infusion bags. This means polyolefin (PO) infusion bags are the most appropriate container. There are many types of polyolefin, such as polyethylene (PE) and polypropylene (PP).

3.2.5 Concentrations

The concentrations used and the rationale for their choice must be stated. Ideally a clinically high and low concentration can be used with interpolation between the two allowed but not extrapolation. According to each drug's SPC, there is a defined mass of drug to be administered as a multiple of the patient's weight. This means there is not an easily definable maximum or minimum concentration, as patient weight can vary. To overcome this, Bath ASU's extensive order history was utilized to identify which concentrations of each drug are ordered and made the judgement that if we could cover over 100% of the concentrations they had been requested to manufacture, we would be producing stability data applicable to almost all possible products. Furthermore, where a patient may be outside this range, it is possible to overfill or underfill an infusion bag to adjust the final dose while keeping the concentration of the product within the range. It is suggested in the NHS stability guidance that biopharmaceuticals demonstrate reduced stability at lower concentrations. It is suggested that this may be due to over dilution of stabilising excipients, resulting in a faster rate of degradation. To minimise the risk posed by studying only a high and low concentrations where the low concentration may degrades quickly while the high remains stable, a clinically common concentration in addition to the extremely low concentration was investigated too.
For the infliximab and trastuzumab emtansine study a clinically low, common and high concentration was assessed, that will not be stated in the thesis.

3.2.6 Storage conditions

The storage conditions used and the rationale for their choice must be defined, although the storage conditions are suggested to be 25 °C ± 2 °C or in the absence of light at 5 °C ± 3 °C. If the product is kept at 5 °C ± 3 °C, there must be a 24-48-hour period at 25 °C ± 2 °C at the end of the study to demonstrate in-use stability. As light and temperature can increase the rate of degradation of drugs, the optimal storage condition is refrigerated in the absence of light at 5 °C ± 3 °C, for the duration of the study, followed by a room temperature (25 °C ± 2 °C) exposure for at least 24 hours.

3.2.7 Storage duration

The NHS guidance states that studies should be between 48 hours and three months. It also recommends that the applied shelf life is no more than 80% of the maximum demonstrable shelf life, and if the shelf life of a product exceeds three months, the products will require an on-going sterility testing regimen, due to microbiological concerns. Therefore, the absolute maximum trastuzumab emtansine study duration would be 113 days so that 90 days is no more than 80% of the study duration. However, once trastuzumab emtansine has demonstrated instability the study can be stopped as the purpose of the study has been achieved. The infliximab study is designed to be published to allow UK hospitals to apply a 7 days shelf life to their Remsima branded infliximab.

3.2.8 Sample numbers

The number of samples and batches tested and the rationale for their choice must be stated. Ideally there will be at least three independently prepared batches for each concentration, although this can be one batch stored in three separate containers for the duration of the study. Each of these batches ought to be tested in triplicate. This meant a minimum of one vial of drug must be reconstituted and the required volume of

drug concentrate added to a minimum of three separate infusion bags (the storage containers). If one infusion bag were to be compromised, the study would not meet the criteria, therefore as long as the cost is not prohibitive, four individual containers will be used at each concentration.

3.2.9 Testing protocols

The minimum number of sampling timepoints is T = 0 (or day zero) followed by four other timepoints. A timepoint must occur at least every thirty days since the previous timepoint.

The infliximab study is designed to prove stability over seven days. Therefore, the timepoints chosen for analysis were T = 0, 1, 2, (3/4) and 7. The fourth timepoint was T4 for the low and high concentrations and T3 for the clinically common concentration.

3.3 ICH Q2 (R1) compliant method validation

3.3.1 Types of analytical test

The Q2 document defines four different types of analytical tests: an identification test, a quantitative test for impurities, a limit test for impurities, and a quantitative test of the API. Identification tests are tests that ensure the identity of an analyte. For example, checking the intact mass of an antibody via LC-MS. Limit tests for impurities are intended to accurately reflect the purity characteristics of the sample without quantifying the degradant. For example, gel electrophoresis which can detect the presence of antibody fragments but not quantify their amount. Quantitative tests for impurities are intended to accurately reflect the purity characteristics. For example, RP-HPLC analysis of a small molecule with known impurities, which can quantify the

concentration of said impurities during a stability study. Quantitative API tests measure the analyte present in a given sample for example SEC analysis of the monomer concentration. Each type of test requires a different level of validation as set out in (**Table 3.1**).

Impurity limits and quantification tests are not applicable to stability studies as the level of impurities are not going to change unless they are also degradants, which are characterised by the array of characterisation methods used.

Only the SEC assay could be classed as API quantification methods. This technique will require the most rigorous validation, assessing each characteristic as stated in Table 3.1.

LC-MS, gel electrophoresis and the total protein UV assay could be defined as identification tests, however in all cases this is not the primary purpose of the test. For example, the total UV assay could be used to identify the drug via its UV fingerprint over the 220 nm to 400 nm wavelength region, however its main purpose is to demonstrate no change to the UV absorption indicating no extractables are present. LC-MS could be used to identify which antibody we are looking at based on its unique molecular weight, but it is being used to detect the emergence of new molecular masses, which would indicate degradation. Gel electrophoresis could be used to identify the antibody, by comparison of the MW and the band pattern of the reduced antibody, however its primary purpose is to demonstrate no change in molecular weight, and no emergence of new bands, indicating no degradants.

Characteristic	Analytical Procedure			
	Identification	**Impurity Limit**	**Impurity Quantification**	**API Quantification**
Accuracy	-	-	+	+
Precision	-	-	+	+
Specificity	+	+	+	+
Detection Limit	-	+	-	-
Quantitation Limit	-	-	+	-
Linearity	-	-	+	+
Range	-	-	+	+

Table 3.1. Validation requirements for analytical procedures as set out by the ICH in Q2 (R1).

Characterisation Technique	Type of Analytical Procedure
pH	N/A
MFI	N/A
DLS	N/A
NTA	N/A
SEC	API Quantification
LC-MS	Identification
Gel electrophoresis	Identification
MTT Assay	N/A
Total Protein UV Assay	Identification
In vitro MTT assay	Identification

Table 3.2. Identification of each characterisation techniques type of analytical procedure.

MFI, NTA and DLS are used to characterise the size and concentration of particles, typically aggregated drug. The Q2 (R1) specifically states it does not address these techniques, and although it states the ICH *may* address these in a subsequent document, they have not.

The NHS yellow cover documents specify the use of forced degradation to induce the formation of typical degradation products. Forced degradation can be used to generate degraded samples which can be tested via the different methods required for the stability study. According to the NHS yellow cover documents, the ability to detect differences between control samples and degraded samples demonstrates the stability indicating nature of a technique. Furthermore, the ICH Q5C document [158] "Stability testing of Biotechnological/Biological products ", which is a document that informed the NHS yellow over documents mentions the use of methods for "the accurate detection of degradation changes that may result from deamidation, oxidation, sulfoxidation, aggregation or fragmentation during storage".

Therefore, forced degradation was used on infliximab and trastuzumab emtansine to validate the stability indicating nature of all methods, while also performing a full API quantification assay validation on the SEC method. It is noted in the NHS yellow cover document that bioassays suffer from inherent variability, so the acceptance criteria for the MTT assay may be more relaxed than the other assays.

Additionally, according the ICH guidance, measurement of pH is deemed a general measurement, and not drug specific, thus it requires no validation beyond a suitable and regular calibration.

3.3.2 Forced degradation

Compliant forced degradation required the use of heat, acid, base, light and oxidizers. Thermal degradation was used in multiple studies investigating antibody

degradation. [159,160] Subjecting antibodies to temperatures above 65 °C can initiate aggregation, likely due to protein unfolding and the exposure of typically inaccessible motifs. Altering the pH of the drug solution can cause hydrolysis of vulnerable residues and also cause aggregation and degradation of the monomer [161], typically it is best to neutralise the sample after a defined duration of adjusted pH. Light can degrade many drugs, the photostability is typically due to bonds than can be cleaved by UV radiation found in natural light. ICH guidelines states, "cool white fluorescent lamps with a lux over 20,000" can be used to expose samples to appropriate levels of light. Photodegradation can cause antibodies to aggregate, causing a loss of monomer and an increase in oligomers, as well as minor structural changes, however it can cause loss of biological function. [162,163] Light exposure has also been reported to cause the oxidation of amino acid residues in the Fc region. [162,164] Use of oxidising reagents such as hydrogen peroxide to degrade antibodies has been demonstrated and measured using LC-MS. [165] Furthermore it has been demonstrated that the propensity for degradation via adjusted pH, photodegradation and oxidative degradation is increased with temperature. [166] As stability studies will be based on therapeutic formulations of biopharmaceutics that also contain stabilising excipients, we could not use the same conditions used in the literature, however they did provide a good starting place.

3.3.3 Linearity validation

The linearity of the response must be determined. A linearity value determined via R^2 regression analysis must be at least 0.999. This is especially important for RP-HPLC and SEC where determining API concentration is crucial to the integrity of the study. Even if a study is performed on a single concentration of drug, the chromatography method must be linear on a range of concentration at least 20% above and below the test concentration. For a range of concentrations, the method must be proven to be linear over a range at least 20% below the lowest test concentration and 20% above the highest concentration. For the MTT assay, linearity is assessed via dose response curves. These curves are used for selecting the optimal concentration of drug to incubate the

cells with. Ideally the EC_{50} can be determined and used as it is the most sensitive to a change in the activity of the drug.

Linearity should be established across at least 5 different concentrations. Ideally, this should be performed independently three times, with the mean R^2 value being used as the metric of passing validation of linearity.

3.3.4 Precision

Precision can mean three different things under ICH Q2 (R2), it can mean intra-lab reproducibility, which is only relevant if the assay will be performed in multiple locations. It can mean intermediate precision, comparing precision after changes to the operator, day or equipment used. Or more commonly it can mean repeatability which is measured as a minimum of 6 determination of the single test concentration or at least 9 determinations covering the range of concentrations. It is the more common definition that we must meet. As each of our studies will have three concentrations we tested the precision of triplicate injections at each of the study concentrations.

3.3.5 Specificity

Ideally test a pure sample, then test the sample spiked with its known degradants and closely related compounds if applicable. If the API is discriminated from the degradants and/or closely related compounds the test can be considered specific. However as already stated there are no known degradants we could order and so forced degradation was utilized to generate degraded samples to compare against.

3.3.6 Accuracy

Accuracy can only be determined by testing a standard that has not formed part of your linearity and test it or test a sample on a previously validated method and the

un-validated method. Furthermore, if linearity, accuracy and specificity have been established accuracy may be inferred. As no pure standards are available and each batch of infliximab and trastuzumab emtansine can vary due to variable filling overage, the simpler approach of inferring accuracy was taken.

3.3.7 Robustness

This is a measurement of the ability of the method to handle small variations in the method, such as variations of the pH, flow rate, sample volume, temperature and buffer concentration. This is important if multiple operators or laboratories will be using the same method and comparing results, but as the methods are not designed to be transferred to other laboratories this was deemed unnecessary. To reduce any potential causes of variability, the operators for each technique were assigned and kept the same during each study. Flow rate, sample volume, and column temperature are controlled via Chromeleon and the inherent variability of the Dionex chromatography system. Each system is serviced annually and passes the required annual tests of conformity, linearity, precision and accuracy. Mobile phase pH is checked and adjusted to within 0.05 pH units of 6.8 and buffer concentration variability is controlled by following a buffer recipe and using a calibrated and serviced balance.

3.3.8 Limits of detection (LOD) and quantitation (LOQ)

There are five ways to determine these values, one using visual evaluation, one using signal to noise ratios and three ways using the standard deviation of the response and slope of the calibration curves created for the linearity determination. The LOD can be calculated as three times the standard deviation of the response divided by the slope of the calibration curve. The standard deviation of the response can be determined in two ways, the easiest is to determine the standard deviation of the y-intercepts. The LOQ can be calculated as ten times the standard deviation of the response divided by the slope of the calibration curve. The LOQ must be lower than 20% of the lowest test concentration.

3.4 Remsima study method validations

3.4.1 Introduction

To evaluate whether the chosen methods were stability indicating and that they were validated if necessary, samples produced according to general method 2.3.1 were tested using each method chosen in section 3.1. The ability to distinguish control samples from degraded samples is the minimum requirement for a method to be considered stability indicating as per ICH guidance, with the exception of size exclusion chromatography, which requires a full validation.[105] The stability indicating nature of each method was demonstrated through forced degradation studies. A range of degradation pathways were assessed by subjecting freshly prepared samples of diluted *Remsima* (1.5 mg/mL in 0.9 % NaCl solution) to several stress conditions which included low pH (according to method 2.2.18), high pH (according to method 2.2.19), oxidation (according to method 2.2.21) and exposure to 20,000 lux light (according to 2.2.22). All samples were analysed immediately following stress.

Remsima is an infliximab biosimilar. It is one of the first biosimilars to be licensed in the UK, along with biosimilars of rituximab and trastuzumab. Remsima is dosed at 5 mg/kg for most indications but may be 3 or 7.5 mg/kg in some circumstances. When diluted into infusion bags, the concentration of Remsima ranges between 0.6 mg/mL and 2.5 mg/mL. [236]

3.4.2 Visual inspection

Following method 2.2.2, no visual differences compared to the control samples were observed for any degraded samples. All samples remained clear and free of visible particulates. While this method has not been demonstrated as stability indicating, this method is used by healthcare professionals to detect visible changes such as

precipitation and colour change. Therefore, it is an acceptable method to use for visual inspection, it is likely harsher degradation would have generated visible changes.

3.4.3 pH

pH readings cannot be made for oxidisation, acid or base hydrolysis samples. This is because the pH can be altered by the reagents used to degrade the sample. Following method 2.2.3 the control samples, photolytically degraded and thermally degraded samples could be measured. The control was 6.62 ± 0.02, photolytically degraded samples were 6.19 ± 0.22 and the thermally degraded samples were 6.71 ± 0.10. This data demonstrates the pH measurement is stability indicating for at least photolytic degradation and the pH method is compatible with infliximab.

3.4.4 Microflow imaging analysis of microparticles

To evaluate whether microflow imaging analysis of microparticles (10-100 µm) was stability indicating, a control sample was compared to acid, base, oxidation and photolytically degraded samples following method 2.2.6 (**Figure 3.1**). All degradation samples had an increase in microparticle concentration for both size categories compared to the control. Base degradation had the least effect, about a one magnitude increase in microparticle concentration while acidic degradation had the most effect with a nearly three magnitudes increase in microparticles. This data demonstrates that microflow imaging analysis of microparticles (10-100 µm) is stability indicating.

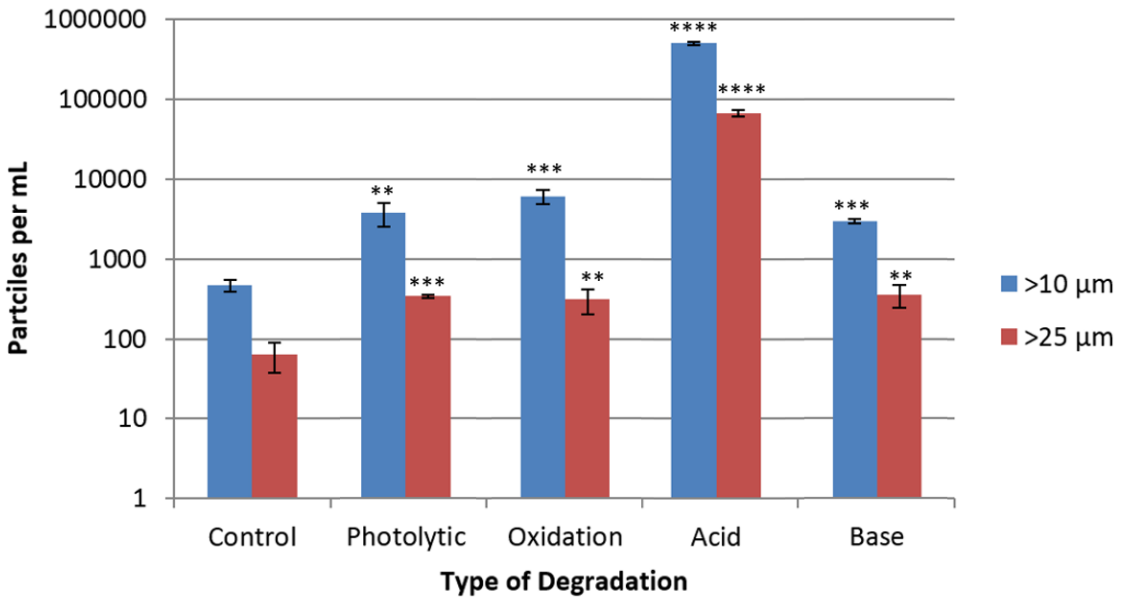

Figure 3.1. Microflow imaging comparison of microparticle concentrations (10 -100 µm) in infliximab control samples and forced degraded samples. Results are means (n=3) ± one standard deviation. All stressed conditions caused an increase in particles in both size categories, with the acid treated samples showing the most significant differences. Data was assessed using a one-way ANOVA, *, **, *** & **** indicate p values below 0.05, 0.01, 0.001 & 0.0001 respectively.

3.4.5 Dynamic light scattering analysis of sub-visible particles

To evaluate whether dynamic light scattering analysis of nanoparticles (1-10,000 nm) was stability indicating, following method 2.2.4, control samples were compared to acid, base, oxidation and photolytically degraded samples (**Figures 3.2 & 3.3**).

Photolytic degradation caused a decrease in the diameter, suggesting a loss of the dimer species (**Figure 3.2**). Oxidation and acid hydrolysis show a clear increase in the mean diameter, suggesting an increase in oligomers, such as dimers and trimers (**Figure 3.2**). The standard deviation for the base hydrolysis results are too wide to determine any real change (**Figure 3.2**).

While a decrease was noted for the % monomer particles by volume, the standard deviations do not indicate that is a real change (**Figure 3.3**). The base hydrolysed samples had a decrease in the percentage volume of monomer/dimer

particles, suggesting particles between 50nm and 10,000 nanometres are forming in a significant volume, ~5% (**Figure 3.2**).

This data indicates dynamic light scattering analysis of nanoparticles (1-10,000 nm) was stability indicating, with evidence of degradation for all types of degradation, however it was most sensitive for base hydrolysis (**Figure 3.3**) and oxidation (**Figure 3.2**).

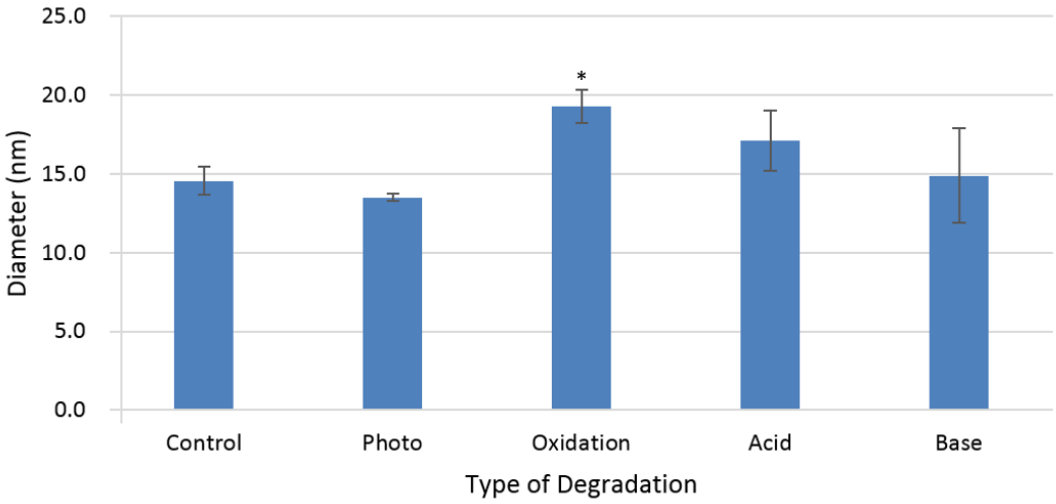

Figure 3.2. Dynamic light scattering analysis of the monomer/dimer peak mean diameter (nm). Results are means (n=3) ± 1 standard deviation. A statistically significant ($p < 0.05$) increase in particle diameter was observed for the oxidization samples, other differences observed where not statistically significant.

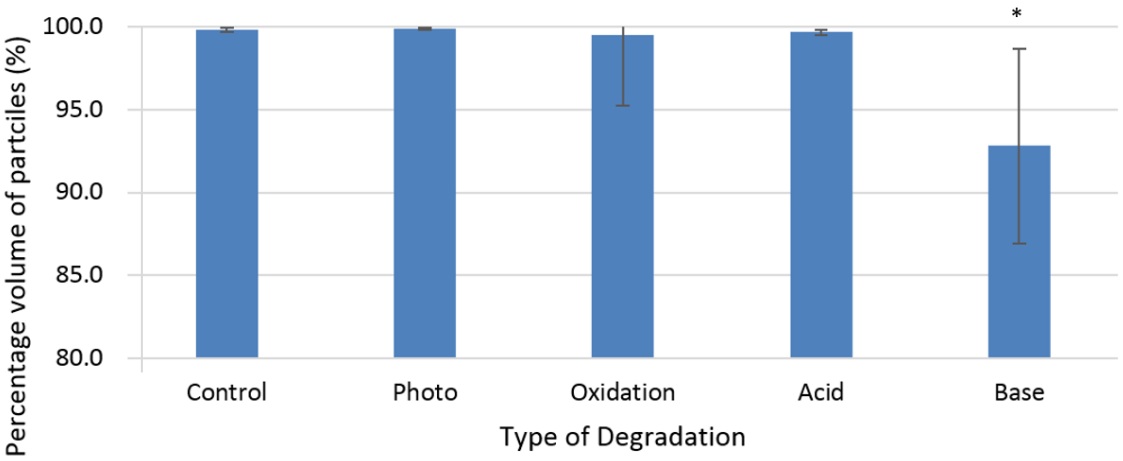

Figure 3.3. Dynamic light scattering analysis of monomer/dimer particles % volume of particles 1-10,000 nanometres. Results are means (n=3) ± 1 standard deviation. Only the base degraded sample had a statistically significant change from the control ($p < 0.05$), showing a decrease in % monomer particles by volume. This shows that under basic conditions a significant volume of non-monomer particles (aggregates and fragment) must be forming, and/or that the volume of monomer particles has decreased most likely via aggregation.

3.4.6 Circular dichroism analysis of higher order structure

To evaluate whether circular dichroism analysis of higher order structure is stability indicating for infliximab, a control sample was compared to acid, base, oxidation and photolytically degraded samples (**Tables 3.3 & 3.4**). This was performed in accordance to method 2.2.8. The higher order structure of the photolytically degraded sample did not appear different to the control (**Table 3.4**). Base hydrolysis and oxidation appeared to have the most effect, especially on Alpha helix and Antiparallel sheets. (**Table 3.4**). This data demonstrates that circular dichroism analysis of higher order structure is compatible with infliximab and stability indicating. Acid and base degradation appear to have a similar effect on structure to each other, presumably by changing the charge states of the exposed amino acid residues. Oxidation of methionine residues on antibodies creates negative charge variants which are known to aggregate more readily, which may explain why the oxidised samples have such a distinctly different structure.

Structure	Control	Photolysis	Oxidation	Acid Hydrolysis	Base Hydrolysis
Alpha Helix	5.80%	5.80%	9.00%	4.60%	4.10%
Antiparallel Sheet	39.60%	39.50%	32.00%	42.10%	43.30%
Parallel Sheet	5.50%	5.50%	5.50%	5.40%	5.30%
Beta-Turn	17.00%	17.00%	17.90%	17.80%	18.40%
Random Coil	34.80%	34.80%	34.90%	34.90%	34.90%
Total Sum	102.70%	102.60%	99.30%	104.80%	106.10%

Table 3.3. Infliximab secondary structure analysis via CDNN deconvolution of circular dichroism spectra at 25 °C. compared to the control the photolytic condition had no observable effect. Acid and base degradation appear to have a similar effect on structure to each other.

Secondary Structure	Photolysis	Oxidation	Acid Hydrolysis	Base Hydrolysis
Alpha Helix	0.00%	3.20%	-1.20%	-1.70%
Antiparallel Sheet	-0.10%	-7.60%	2.50%	3.70%
Parallel Sheet	0.00%	0.00%	-0.10%	-0.20%
Beta-Turn	0.00%	0.90%	0.80%	1.40%
Random Coil	0.00%	0.10%	0.10%	0.10%
Total Sum	-0.10%	-3.40%	2.10%	3.40%

Table 3.4. Absolute change from control in CDNN deconvolution of infliximab circular dichroism spectra at 25 °C. Acid and base degradation appear to have a similar effect on structure to each other.

3.4.7 Gel electrophoresis analysis of fragmentation and aggregation

To evaluate whether gel electrophoresis analysis of fragmentation and aggregation was stability indicating for infliximab, a control sample was compared to acid, base, oxidation and photolytically degraded samples (**Figure 3.4**). This was performed in accordance with method 2.2.7 The reduced control sample has clearly been reduced into its heavy (~50 kDa) and light (~25 kDa) chains while the intact sample has a strong band indicating the intact antibody (~150 kDa). The acid degraded samples had a new band at about 100 kDa when reduced and two very feint bands when reduced at about 50kDa and 100 kDa, as well as evidence of aggregation at 200 kDa. The base degraded sample has two new bands when reduced, one at about 100 kDa and one at about 125 kDa. When run intact the base degraded sample appears highly fragmented with multiple new bands at 25, 50, 75, 100 and 125 kDa as well as evidence of aggregation at 200 kDa. The oxidised sample did not appear to run. It is possible that the hydrogen peroxide interfered with the staining reagents used in the method. The photolytically degraded sample has numerous additional bands when reduced around 75, 100, and 125 kDa. The intact photolytic sample has a stronger band at 25 kDa compared to the control and an additional band around 50 kDa. This data demonstrates that electrophoresis analysis of fragmentation and aggregation is stability indicating for infliximab.

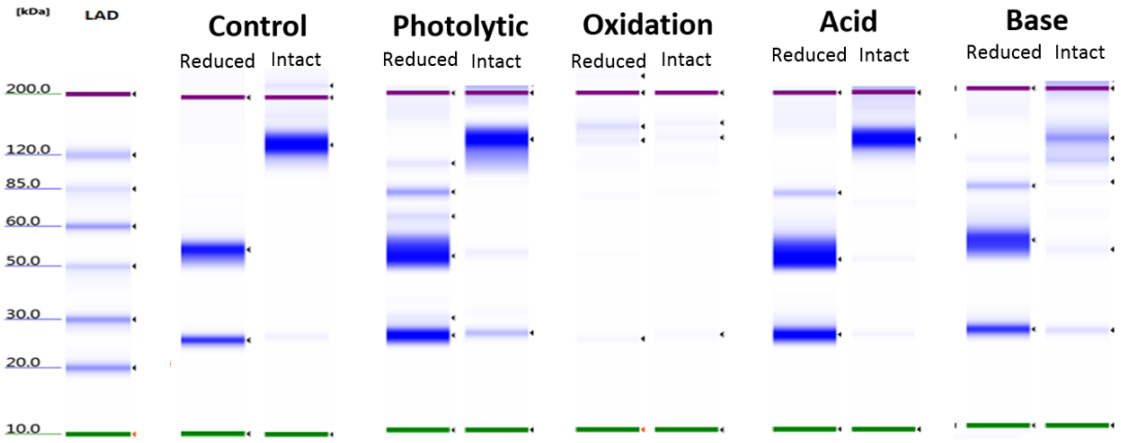

Figure 3.4. Gel electrophoresis analysis of fragmentation and aggregation of infliximab control and degraded samples. The reduced sample for the acid condition shows a new band with a mass around 100 kDa, this new band is most likely two heavy chains that still have a disulphide bond between them. This band is also present in the base degraded reduced samples. The acid degraded intact sample has feint bands that correlate with heavy and light, while the base degraded intact sample have feint bands that correlate with LC, HC, HC-LC, and HC-HC-LC, while also showing a marked loss of antibody monomer band intensity and an increase in aggregate intensity at the top of the gel. Oxidation may be interfering with the experiment as in both reduced and intact conditions the sample does not show up very well. Photolytic degradation shows HC-LC, and HC-HC-LC present in the reduced samples and heavy and light chain in the intact sample.

3.4.8 Size exclusion chromatography analysis of monomer concentration

Size exclusion chromatography analysis of monomer concentration was performed according to method 2.2.16, to determine the concentration of the active pharmaceutical ingredient, infliximab monomers. As such, it is outlined in the ICH guidance document Q2(R1) [105] that the linearity, precision, specificity and accuracy must be validated according to the limits stated in the ICH Q2(R1) document. This was performed in accordance to method 2.2.25.

The method must be demonstrated as having a linearity with an R^2 value of at least 0.999 for a range covering at least 20% higher and lower than the test concentrations. (**Figure 3.5**), plots the mean absorbance (n=3) of samples from 0.3 mg/mL to 3.0 mg/mL. The R^2 value is greater than 0.9999 and is rounded up to 1 by Excel. This linearity result exceeds the required minimum linearity for a concentration range greater than required for the proposed stability study.

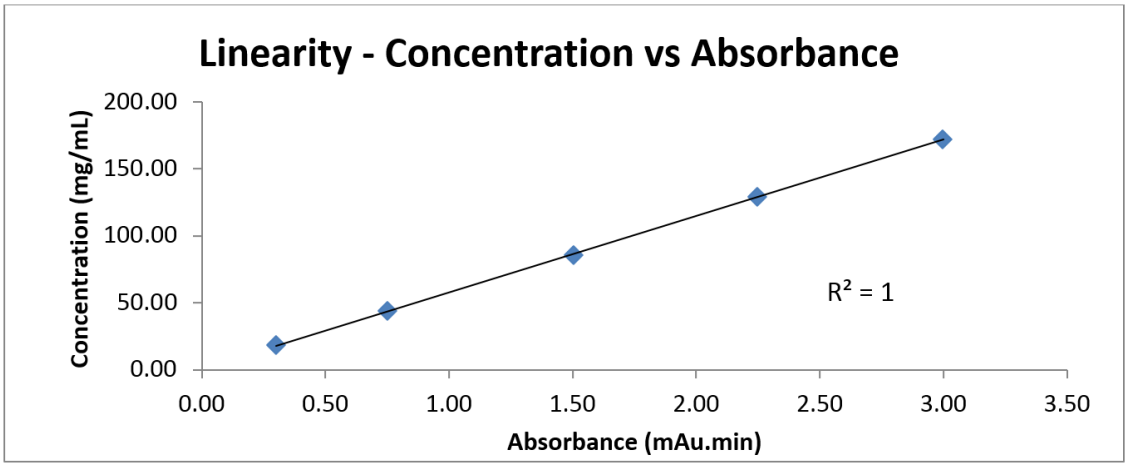

Figure 3.5. Size exclusion chromatography analysis of monomer concentration. Results are a mean (n=3).

The method must be demonstrated as having a precision with a relative standard deviation of no more than 2% at each test concentration. **Tables 3.5 - 3.7** below, show the measured precision from six repeat injections at the clinically low, common and high concentration respectively. The determined relative standard deviations are all below 2%, indicating the method has suitable precision.

Concentration	Injection	Peak Area (mAu.min)	Relative SD (%)
Low	1	43.03	**1.51**
	2	42.83	
	3	42.48	
	4	43.83	
	5	43.83	
	6	44.09	
	Mean	**43.20**	

Table 3.5. Size exclusion chromatography precision determination at the clinically low concentration. The relative standard deviation is acceptable as the limit is 2.00 %, although this is still a high result, this is most likely due to the errors being magnified at lower concentrations where the method is less sensitive.

Concentration	Injection	Peak Area (mAu.min)	Relative SD (%)
Common	1	86.03	**0.23**
	2	86.33	
	3	86.14	
	4	85.99	
	5	85.77	
	6	85.87	
	Mean	86.02	

Table 3.6. Size exclusion chromatography precision determination at the clinically common concentration. The result of 0.23% is very good, as the limit is 2.00 %.

Concentration	Injection	Peak Area (mAu.min)	Relative SD (%)
High	1	128.26	**0.32**
	2	128.42	
	3	129.08	
	4	129.31	
	5	128.75	
	6	128.46	
	Mean	**128.46**	

Table 3.7. Size exclusion chromatography precision determination at the clinically high concentration. The result of 0.32% is very good, as the limit is 2.00 %.

The size exclusion chromatography method must also be demonstrated to be specific. Meaning able to differentiate degradants, such as dimers and trimers from the monomer. This is demonstrated by analysis and comparison of control samples of infliximab to force degradation samples. When photolytically degraded, a loss of monomer and increase in dimer is detectable (**Figure 3.6**). When degraded via acid hydrolysis, a detectable loss of monomer and a probable increase in oligomer is observed (**Figure 3.7**). When degraded via oxidation a detectable loss of monomer is apparent but no increase in dimer, trimer or higher order oligomers (**Figure 3.8**). When degraded via base hydrolysis a loss of monomer is detected and a large peak due to higher order oligomers can be noted (**Figure 3.9**). This data indicates this method is specific and stability indicating.

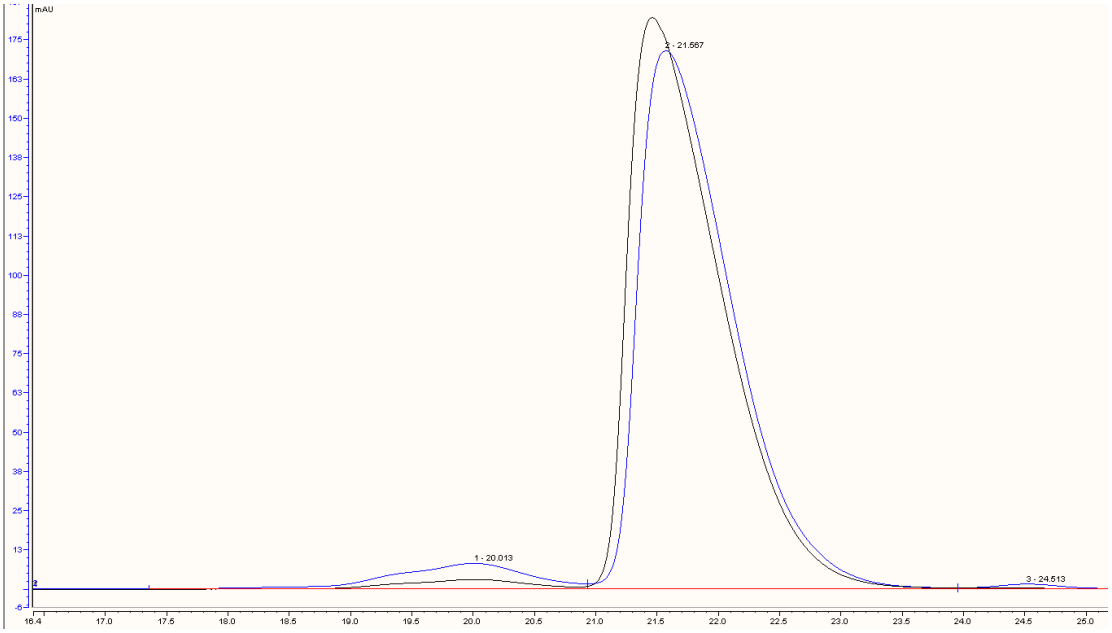

Figure 3.6. Size exclusion chromatogram of infliximab control (**Black**) vs infliximab photolytically degraded (**Blue**). The X-axis is time (minutes). The photolytically degraded main peak at 21.6 minutes is markedly decreased in area compared to the control. The peak at 24.5 minutes is due to a lower molecular weight fragment and is only present in the photolytically degraded sample. The broad peak at 20 minutes is due to the dimer and trimer and while it is present in the control, the peak is larger in the photolytically degraded sample.

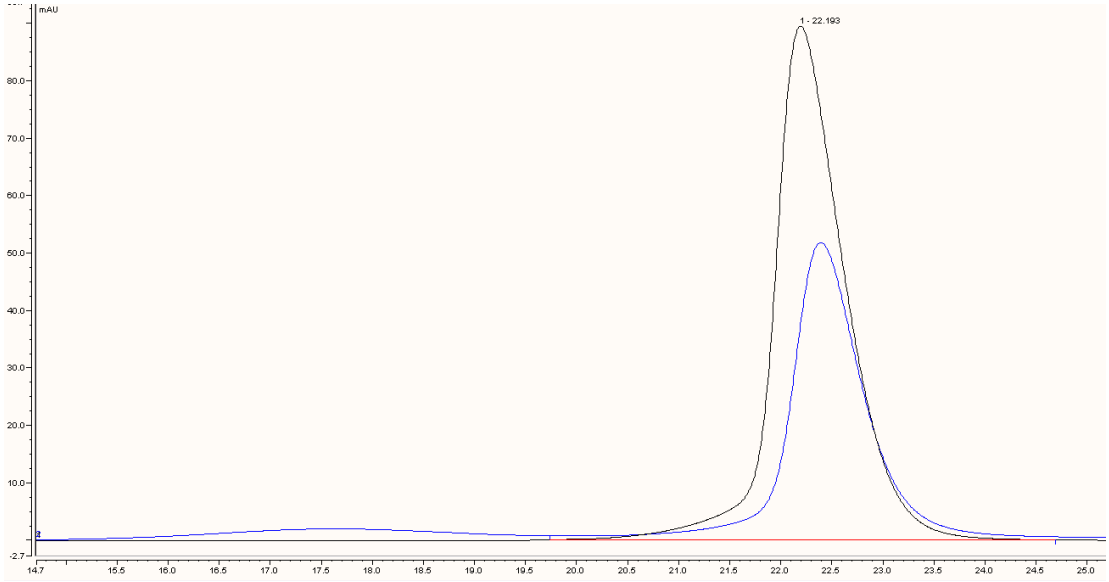

Figure 3.7. Size exclusion chromatogram of infliximab control (**Black**) vs infliximab acidically degraded (**Blue**). The X-axis is time (minutes). The main peak at 22.2 minutes is markedly decreased in peak area in the acidically degraded sample, and there is a new very broad band at 17.5 minutes, this is most likely due to oligomers.

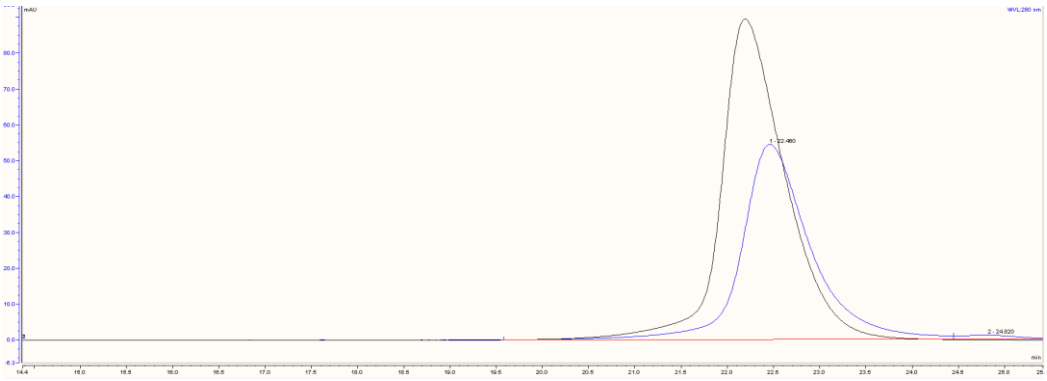

Figure 3.8. Size exclusion chromatogram of infliximab control (**Black**) vs infliximab degraded via oxidation (**Blue**). The X-axis is time (minutes). The main peak at 22.4 minutes is markedly decreased in peak area in the oxidised sample.

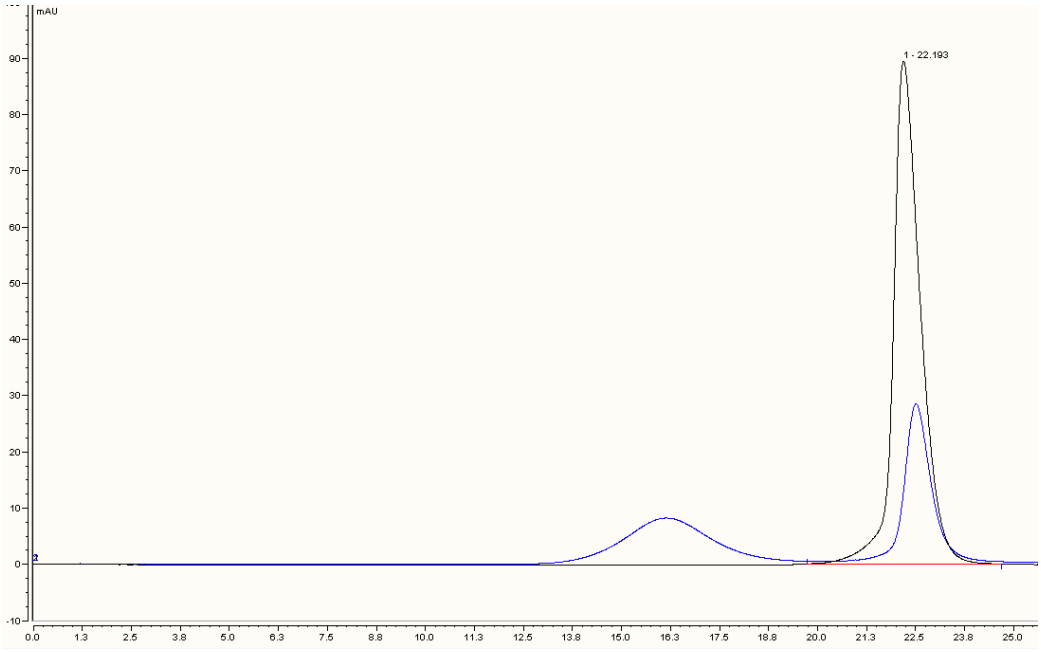

Figure 3.9. Size exclusion chromatogram of infliximab control (**Black**) vs infliximab degraded via base hydrolysis (**Blue**). The X-axis is time (minutes). There is a dramatic loss of monomer peak area coupled with an equally dramatic formation of a new peak at 16.3 minutes.

If the size exclusion chromatography method is demonstrated as linear, precise and specific the accuracy can be inferred, following ICH Q2 (R1). [105] This is useful, as no standards exist for testing accuracy of infliximab.

The limit of quantification (LOQ) must be less than 80% of the lowest test concentration. The LOQ can be calculated as the standard deviation of the y-intercept of the linearity graph, divided by the slope then multiplied by 10, as outlined in the ICH

Q2 (R1) document [105]. The calculated LOQ is 0.04 mg/mL, less than 80% of the clinically low test concentration.

This size exclusion method (method 2.2.16) has been demonstrated as linear, precise, specific, stability indicating, which allows the inference of suitable accuracy. This method is compatible with infliximab and validated to ICH Q2 (R1) standards.

3.4.9 LC-MS analysis of chemical degradation

To evaluate if LC-MS analysis of chemical degradation is stability indicating, control samples of infliximab were compared to degraded samples. Following method 2.2.12-2.2.14 produced acceptable spectra for heavy and light chains (**Figures 3.10 & 3.11**).

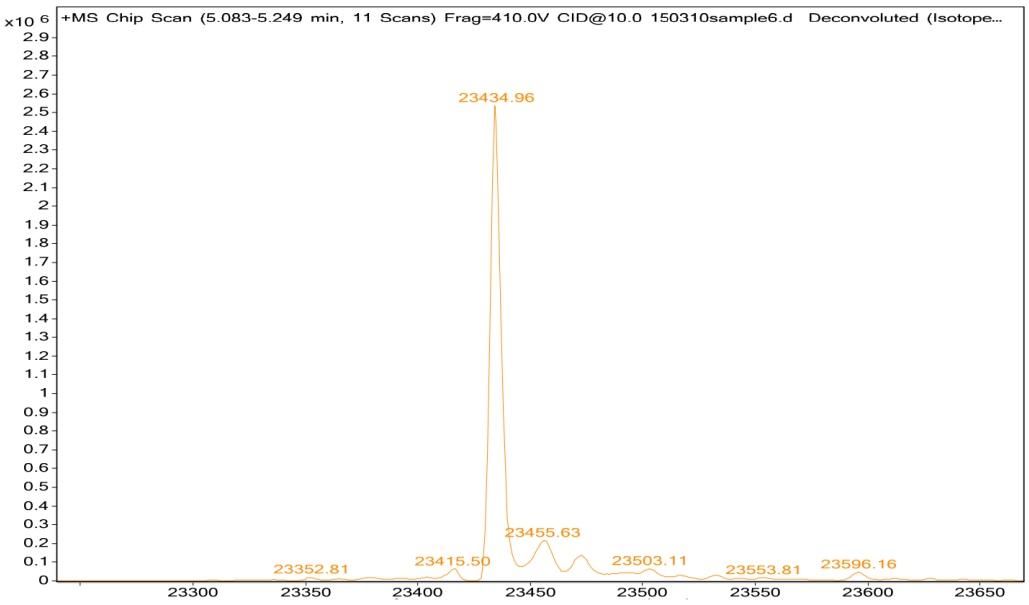

Figure 3.10. LC-MS spectra for infliximab control sample light chain. Y-axis = TICs, X-axis = Mass (Daltons) This figure shows molecular weight for single Remsima light chain is 23434.96 daltons. There is also the presence of a few variants with masses of 23415, 23455 and 23475 daltons.

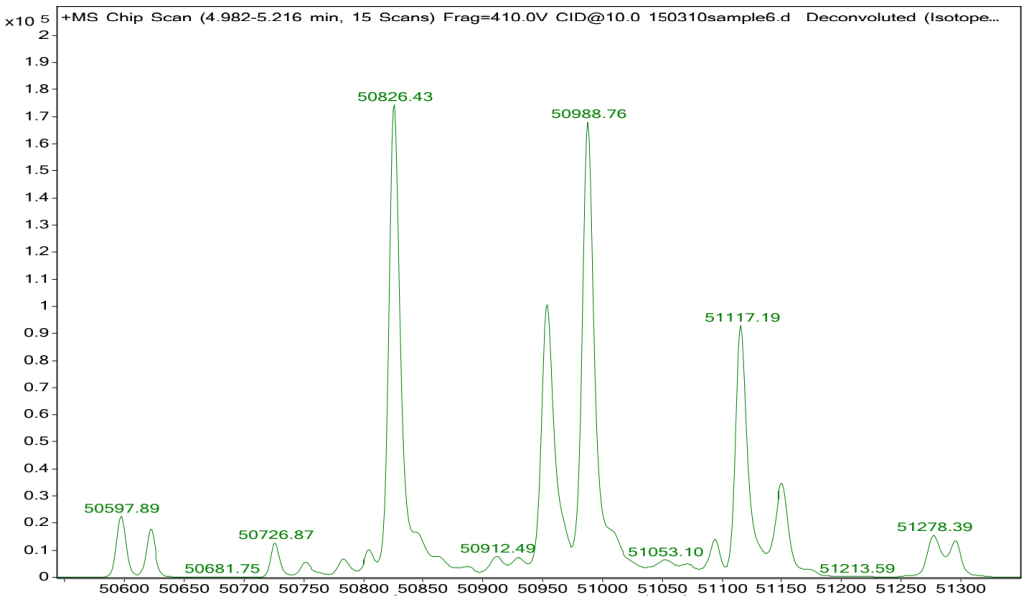

Figure 3.11. LC-MS spectra for infliximab control sample heavy chain. Y-axis = TICs, X-axis = Mass (Daltons) This figure shows molecular weight for Remsima heavy chain is 50826 daltons. There is also the presence of a few glycovariants with masses such as 50988 and 51117 daltons.

Acid hydrolysis, base hydrolysis and photolytic degradation did not produce any observable changes to the light chain. But oxidation degradation caused two new peaks to appear at 23451 daltons and 23499 daltons, these masses correlate with a single oxygen addition and a quadruple oxygen addition (**Figure 3.12**). There are peaks that may be due to a double and triple oxygen adducts but were too small to be labelled.

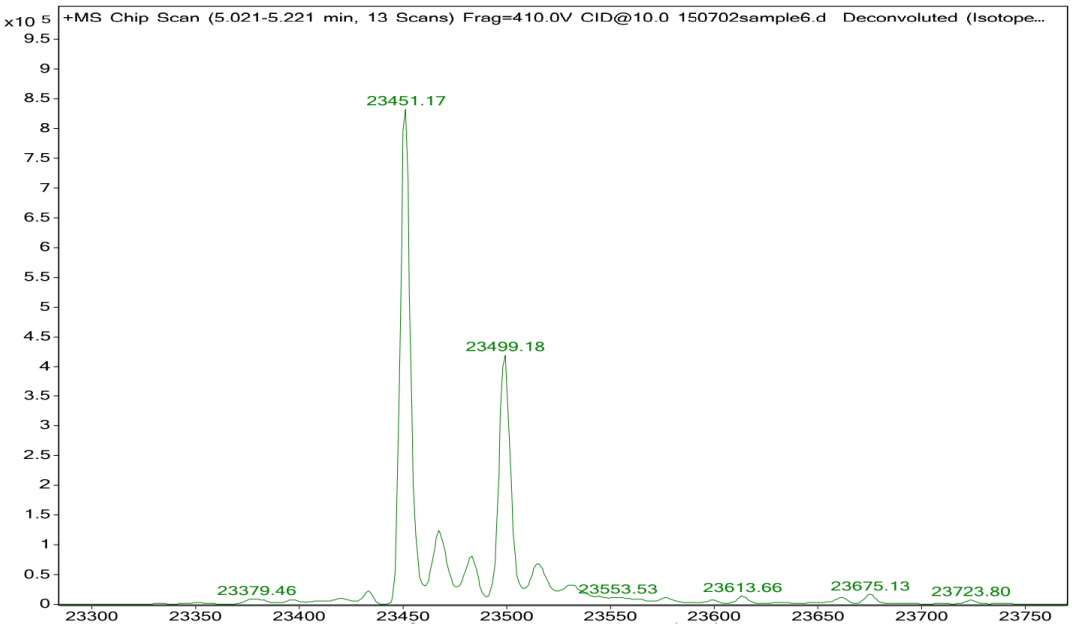

Figure 3.12. LC-MS spectra for infliximab oxidation sample light chain. Y-axis = TIC, X-axis = Mass (Daltons). The peak at 23451 is 17 daltons greater than the mass of light chain in figure 3.10. Furthermore, there are another four peaks with masses with 16 daltons differences, indicating oxygen addition, most likely at methionine residues.

Acid hydrolysis, base hydrolysis and photolytic degradation all cause slight shifts in heavy peak masses, but no more than 5 daltons for any peak (**Figure 3.13 A, C & D**). Oxidative degradation of the heavy chains (**Figure 3.13 B**) caused a drastic change in the spectra, with multiple new peaks corresponding to oxidised heavy chains.

This data indicates that this LC-MS based method of chemical degradation analysis is compatible with infliximab and stability indicating.

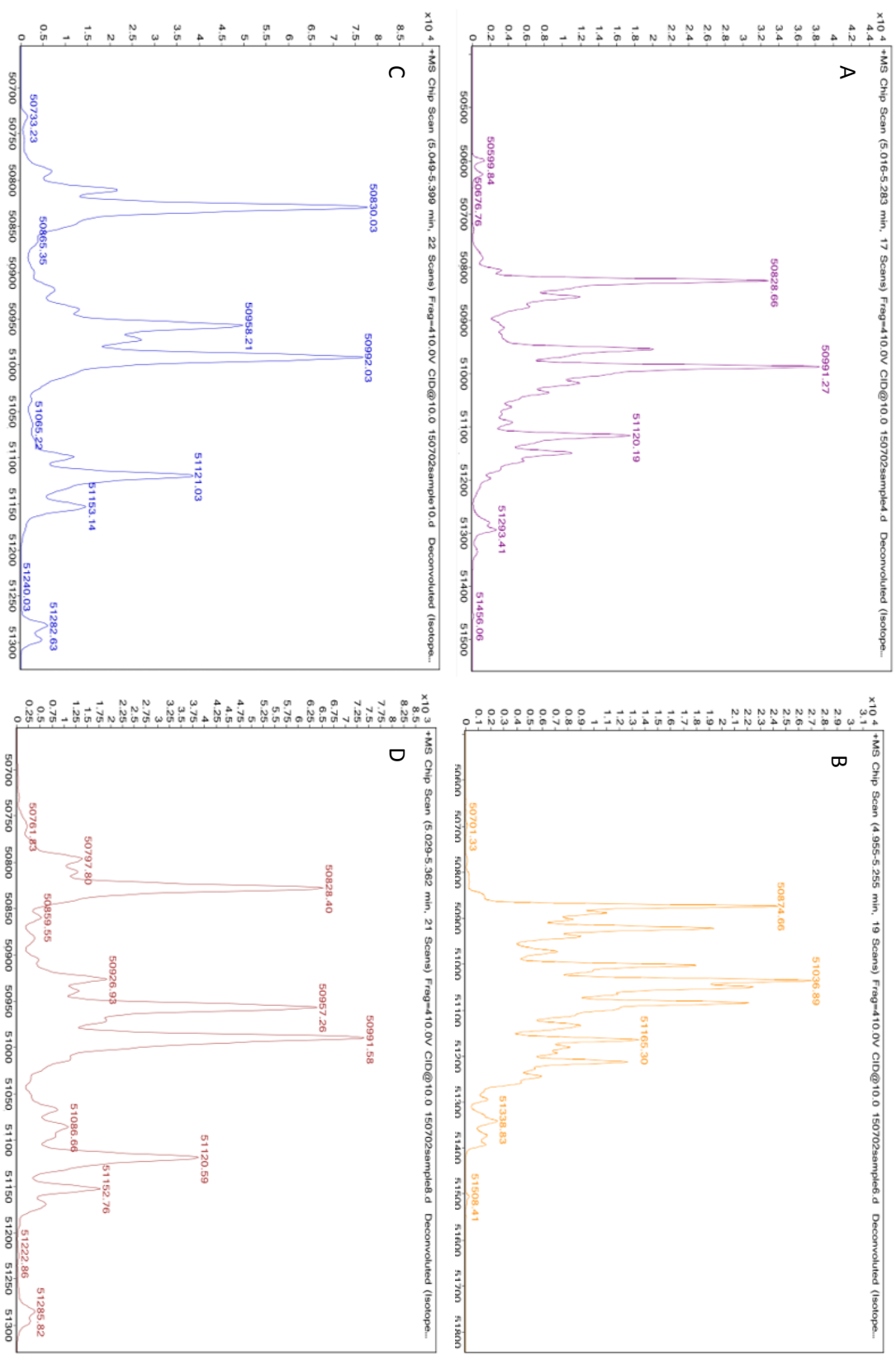

Figure 3.13. LC-MS spectra for infliximab heavy chain degraded via (**A**) photolysis, (**B**) oxidation, (**C**) acid hydrolysis and (**D**). Y-axis = TICs, X-axis = Mass (Daltons).

3.4.10 Cellular assay (MTT) of functional activity

This cellular assay measures the difference in the growth of WEHI-164 cells grown in the presence of actinomycin D and tumour necrosis factor alpha (TNF-α). Together, TNF-α and actinomycin D, induce apoptosis in the WEHI-164 cells. However, infliximab binds to the TNF-α, preventing TNF-α from binding to and activating CD30 signalling in the WEHI-164 cells. Infliximab can 'rescue' the cells, and allow them to grow, with more growth theoretically possible at higher concentrations of infliximab. This was demonstrated by creating a dose response curve of infliximab mediated 'rescue' of WEHI-164 cells incubated in the presence of TNF-α and actinomycin D (**Figure 3.14**), this method has previously been used by Augustin *et al* [107], Kabhar *et al* [106] and more recently Song *et al* [108]. Plate set up was performed according to method 2.3.2, and plate reading was performed according to 2.2.11. The dose response curve shows concentrations of infliximab below 1000 ng/mL don't completely 'rescue' the cells. Below 10 ng/mL no 'rescue' of cell growth is observed. 100 ng/mL appears to be the EC_{50} for cell growth rescue. Another IgG1 antibody, cetuximab, was used as a negative control, as it has no affinity for TNF-α. Cetuximab had no effect on cell growth. This work validates the assay as a method of measuring functional activity for infliximab.

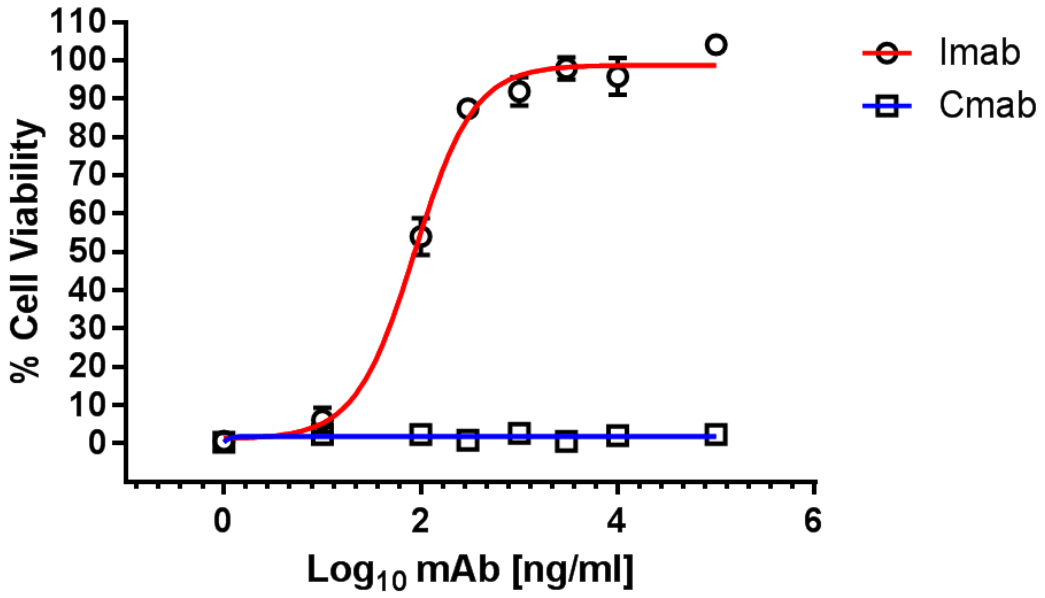

Figure 3.14. A dose response curve for infliximab (red) and cetuximab (blue) in a WEHI-164 cell growth assay using TNF-α and actinomycin D. The dose response produced a sigmoidal curve for infliximab with an EC_{50} of 94 ng/µL. (n=3) with five repeats of each sample. The data was plotted using GraphPad Prism 5, and the curve was fitted using non-linear regression with variable slope and four parameter modelling.

3.5 Remsima stability study

3.5.1 Study purpose

First, this study was performed to demonstrate that the methods and study design chosen are all appropriate, and provided experience running a stability study, highlighting problems that could occur and be better planned for in the trastuzumab emtansine study. Secondly, it was hoped the data collected would enable justification for a shelf-life extension to Remsima branded infliximab for Bath ASU and all UK compounders with a specials license or section 10 exemption. This study was published in the International Journal of Pharmaceutics in 2015. [167] All results in this section are taken from that paper.

Remsima is a biosimilar of Remicade and the excipients for both are identical according to their SPCs. It was expected that Remsima have near identical stability to Remicade and as papers existed evidencing stability beyond 7 days for Remicade diluted

to clinical concentrations it was expected to generate similar data for Remsima, but this time in full compliance with NHS guidance. [229, 102]

3.5.2 Study design

The analytical techniques used, and study design is as described in chapter 3 and methods used as stated in section 2. To briefly recap, a clinically low, common and high concentration of Remsima brand infliximab were diluted in 0.9% NaCl solution for infusion, stored in four polyolefin infusion bags each at 5 °C ± 2 °C in the absence of light. Samples were withdrawn and tested from each bag on five separate days during a seven-day period. Furthermore, to reduce cost burden, the total volume was scaled down from 250 mL to 25 mL and the bag size was reduced from a 250 mL bag to a 50 mL bag. This reduced the cost of required Remsima from £28,000 to only £3000.

3.5.3 Visual inspection

Performed according to method 2.2.2. All samples remained clear for the duration of the study with no precipitates or particulate matter detected with the naked eye. No change in colour or turbidity was observed over the study period. Representative photographs are in appendix IV.

3.5.4 pH

Performed according to method 2.2.3. No significant change was observed for the pH of samples at any of the concentrations tested throughout the study period (**Figure 3.15)**. The pH of samples at the high and common concentration were very similar at around pH=6.9, while the pH of the most dilute samples at the low concentration was noticeably lower at pH=6.6, possibly reflecting the buffering capacity of excipients. Slight variability in pH readings (±0.1 pH units) was observed for all

concentrations, however this variability was not significant as the observed pH's at day 7 showed almost no change from their respective pH's at day 0, for all concentrations.

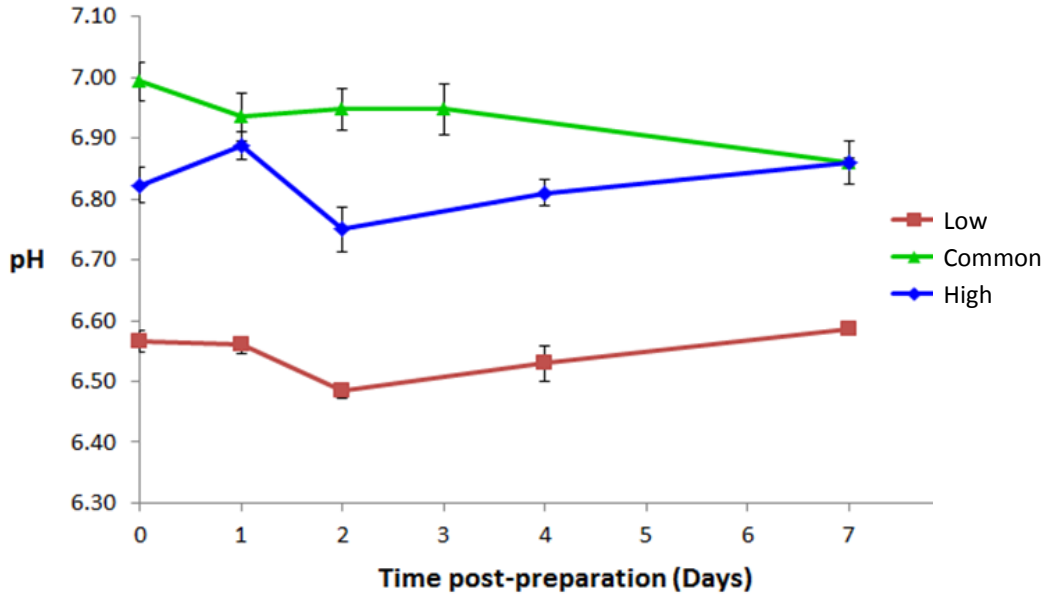

Figure 3.15. pH profile of infliximab for clinically low, common and high concentration solutions over the study period (n = 4). Error bars represent ±1 SD. There is no statistically significant difference when comparing each data point to both the day 0 and day 1 measurements of each concentration. There was no clear trend across all concentrations although the common concentration does show a downward trend.

3.5.5 Microflow imaging analysis of microparticles

Performed according to method 2.2.6. Quantification of particle numbers was carried for particles >10 μm and > 25 μm in size (**Figure 3.16**). At all concentrations tested, the number of particles >10 μm was significantly higher than the number of particles > 25 μm for all time points. Also, as is common with flow imaging techniques, the standard deviations for replicate samples was found to be quite large, making a detailed statistical analysis of results difficult. However, for all concentrations tested the largest variations in particle numbers appeared to be between the early time points (day 0, 1 and 2), with particle numbers appearing to remain relatively constant past day 2. Importantly, there appeared to be no appreciable change in average particle numbers between samples at day 0 and day 7, for any of the concentrations tested.

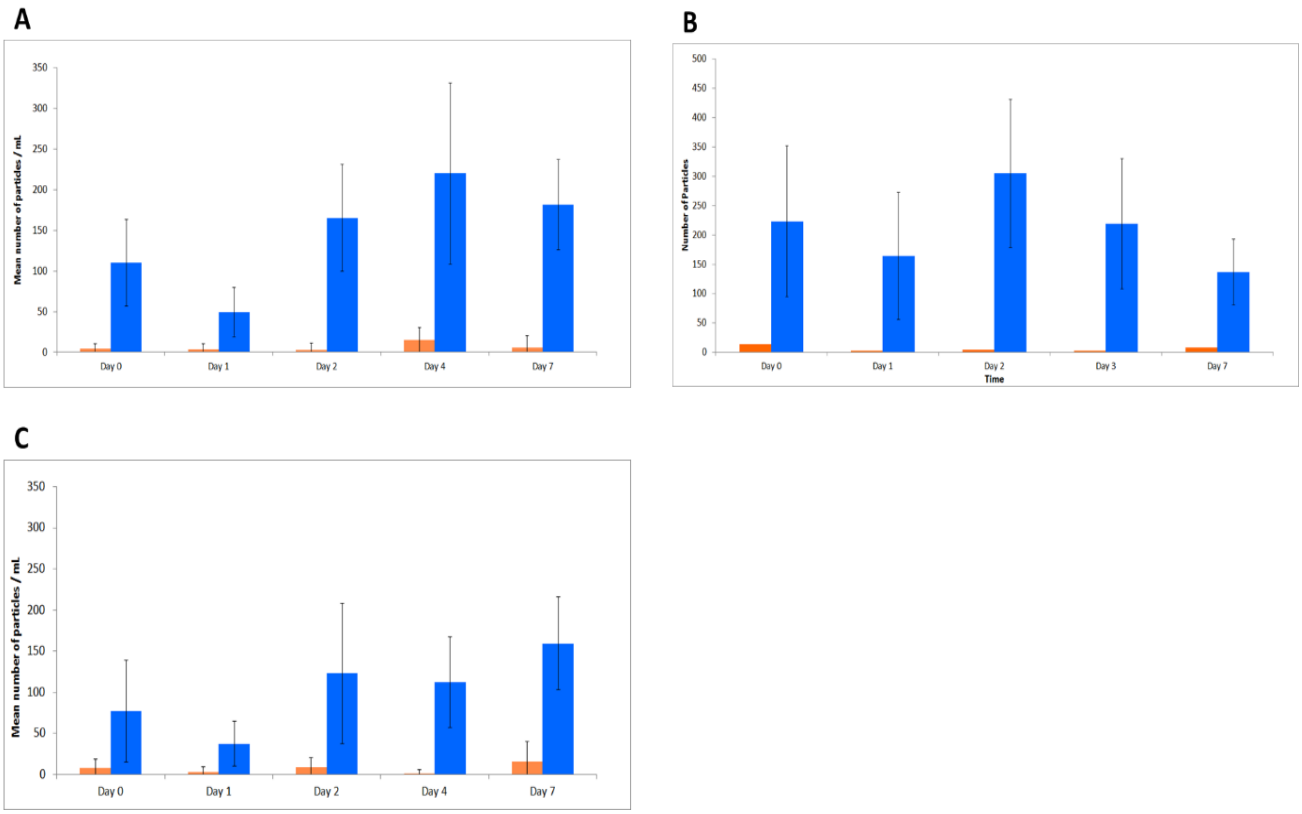

Figure 3.16. Mean particle number results from FlowCam imaging of Remsima at clinically (**A**) Low, (**B**) Common and (**C**) High concentrations (n=4), over the period of the study. Particles >10 µm are shown in blue and particles > 25 µm are shown in orange. Error bars represent ±1 SD. There was no statistically significant difference observed. There was also no clear trend across all concentrations.

3.5.6 Dynamic light scattering analysis of nano-particles

Performed according to method 2.2.4. Dynamic light scattering results are expressed as the mean radius and percentage abundance of detected drug particles within the test solution (**Figure 3.17**). A significantly larger mean radius could suggest the formation of aggregates which have a greater spherical volume, while a decrease in percentage abundance of drug could be attributed to larger aggregate formation. The measured drug radii were found to be similar for all concentrations throughout the study, ranging from 14.3 - 15.1 nm immediately after preparation on day 0, to 12.9 – 15.2 nm on day 7.

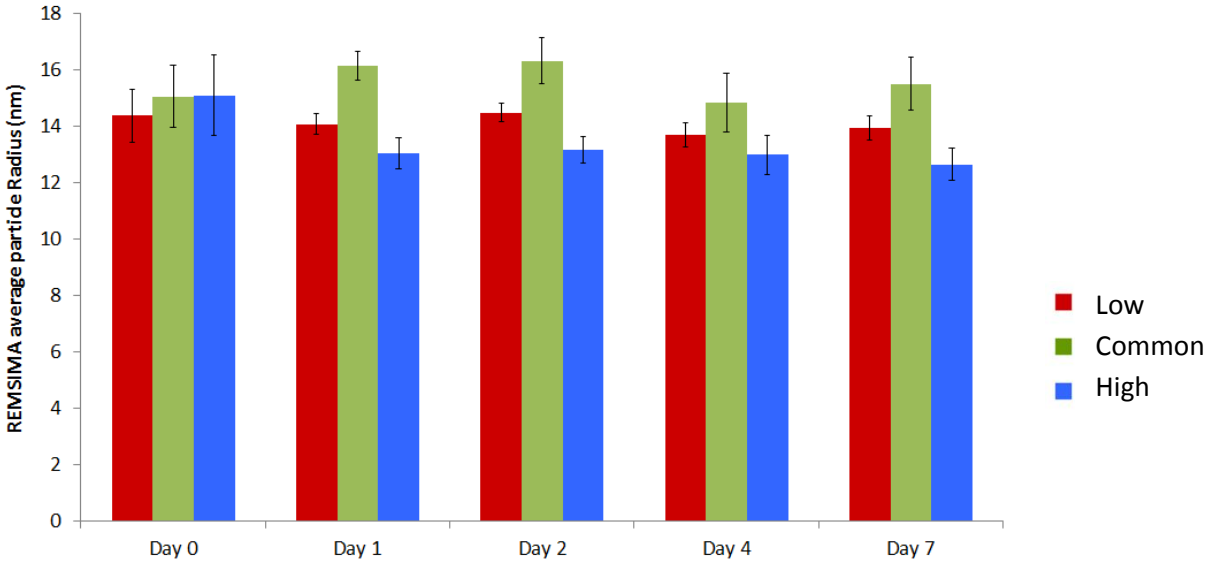

Figure 3.17. Averaged particle radius of clinically low, common and high Remsima samples over the course of 7 days as determined by dynamic light scattering. Each time point consisted of 4 different samples at each concentration, which in turn were run in triplicate to provide an average measurement for each bag (n = 4). There was no statistically significant difference observed. The only trend was a slight decrease in average particle radius for the high concentration, while not statistically significant this could suggest loss of trimer and/or dimer relative to the monomer, either through further aggregation into higher order aggregates or through separation of the trimer and dimer into monomer.

Additionally, the percentage abundance of drug particles remained constant over the study period, demonstrating that there was no significant increase in the number of larger particles (<6 µm) at any of the concentrations (**Table 3.8**).

	D0	D1	D2	D4	D7
High	99.82 (±0.12)	99.85 (±0.03)	99.98 (±0.02)	99.92 (±0.04)	99.92 (±0.02)
Common	99.52 (±0.24)	99.28 (±0.12)	99.59 (±0.05)	99.65 (±0.29)	99.77 (±0.05)
Low	99.83 (±0.10)	99.93 (±0.06)	99.9 (±0.06)	99.79 (±0.09)	99.84 (±0.05)

Table 3.8. Averaged drug abundance (percentage) of clinically high, common and low concentrations of Remsima samples over 7 days, as determined by DLS. No statistically significant changes are observed. This indicates very few, if any, new aggregates are being formed. While the volume remains the same it is still possible for pre-existing aggerates to combine, changing the size and number distribution of sub-micron particles, however the total volume of sub-micron aggregates remains statistically unchanged.

3.5.7 Size exclusion chromatography

Performed according to method 2.2.16. All HPLC chromatograms of Remsima were characterised by a single major peak with an elution time of 21.6 minutes (**Figure 3.18**). For the clinically high concentration batch this comprised, on average, 99.28% (± 0.15%) of all detected signals over the course of the study. A minor signal with a retention time around 20.0 min was also observed at this concentration, which comprised the remaining 0.73% of observed signals. This minor peak was assigned as Remsima dimer on the basis of the retention time equating to a molecular weight of 300 kDa. Chromatograms obtained from samples at common and low concentrations were comprised of only a single peak corresponding to the Remsima monomer. Importantly, no change in the intensity of signals was observed for any of the batches over the period of the study, indicating that the concentration of Remsima remained constant throughout (**Table 3.9**).

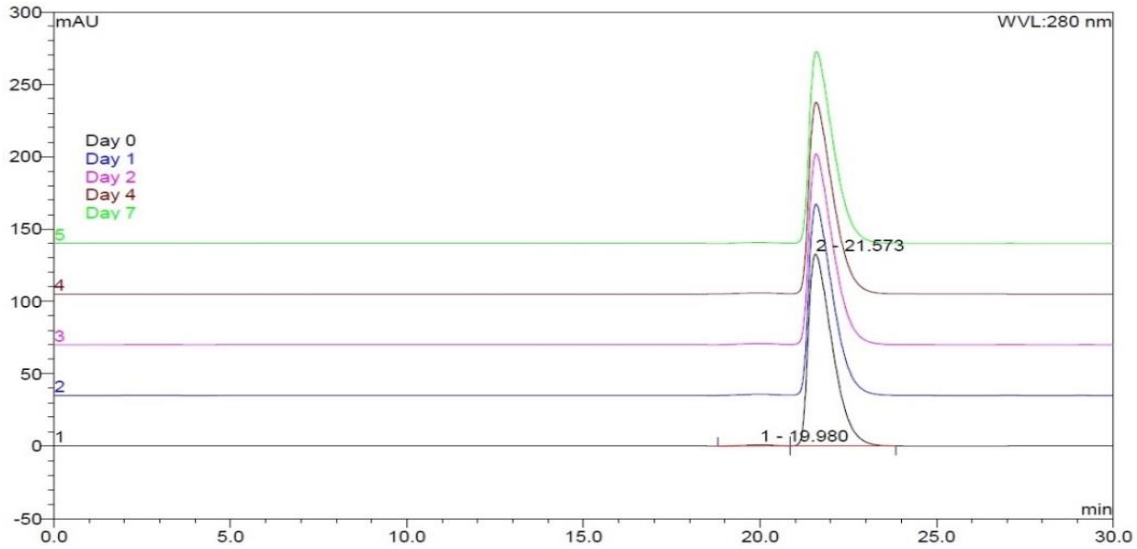

Figure 3.18. Representative overlay of SE-HPLC chromatograms of clinically high concentrations of Remsima at Days 0, 1, 2, 4, and 7. Samples at each time point were run in triplicate and an average peak-signal calculated. No loss of peak area was observed, thus the concentration of the monomer remained constant, with no statistically significant change in monomer concentration observed.

	Day				
	0	**1**	**2**	**4**	**7**
High	100.20	100.07	99.39	100.06	100.08
	97.05	96.82	96.59	96.91	96.58
	100.26	99.72	99.26	98.96	99.69
	102.48	102.44	101.79	101.72	101.92
% Mean Day 0 Concentration	**100.00**	**99.76**	**99.26**	**99.41**	**99.57**
S.D.	2.23	2.30	2.13	2.02	2.22

	Day				
	0	**1**	**2**	**3**	**7**
Common	101.20	101.35	101.09	101.11	101.20
	98.78	98.69	98.32	99.00	98.54
	100.28	99.74	99.85	99.93	99.65
	99.72	99.04	99.39	99.63	98.76
% Mean Day 0 Concentration	**100.00**	**99.71**	**99.66**	**99.92**	**99.54**
S.D.	1.01	1.18	1.15	0.89	1.21

	Day				
	0	**1**	**2**	**4**	**7**
Low	97.75	96.89	96.12	96.60	97.10
	102.96	101.98	102.60	101.75	102.04
	96.66	97.01	96.24	95.71	96.63
	102.60	102.10	101.98	101.57	101.95
% Mean Day 0 Concentration	**100.00**	**99.50**	**99.24**	**98.91**	**99.43**
S.D.	3.25	2.94	3.54	3.20	2.97

Table 3.9. SEC of Remsima monomer concentration given as mean % of the mean average D0 concentration over the period of the study for clinically high, clinically common and clinically low concentration batches. Each batch contains 4 replicate devices, with each device tested in triplicate. No statistically significant change in monomer concentration relative to day 0 was observed.

3.5.8 Variable temperature circular dichroism

Analysis of variable temperature circular dichroism spectra indicates the protein undergoes its most significant changes to secondary structure induced by thermal degradation over the temperature range 74-78 °C (**Figure 3.19**). This temperature range

remained largely constant throughout the study period for all concentrations tested. Testing was performed according to method 2.2.8.

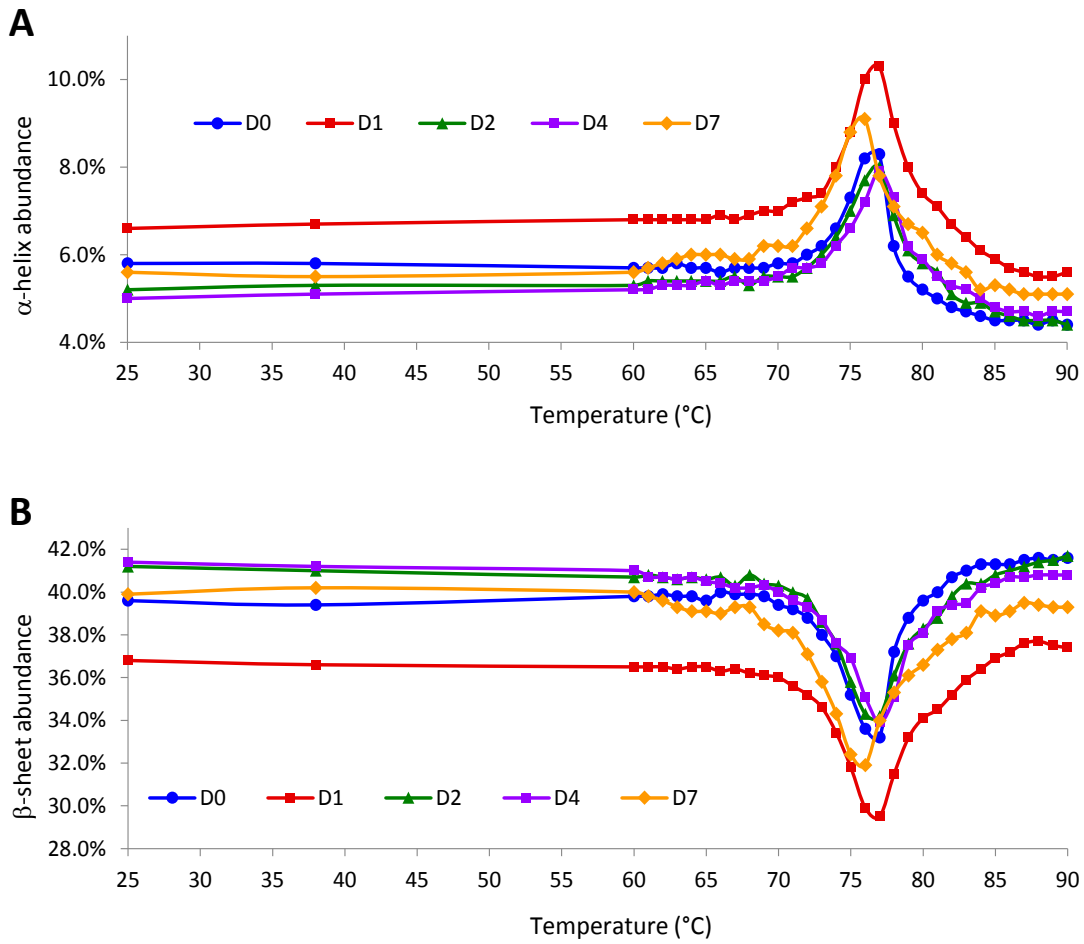

Figure 3.19. Variable temperature circular dichroism data for Remsima samples at a clinically high concentration showing structural abundance of (A) α-helix, and (B) β-sheet as a percentage of the total protein. Measured over a temperature range of 25 to 90 °C. While the heat ramp profiles of D1 and D7 are different from D0, 2 and 4, as D1 forms the SPC limit, no clinically relevant changes are presumed to have occurred between D0 and D7

The percentage composition of secondary structures α-helix, and β-sheet measured at 76 °C was found to vary slightly over the course of the study, though no appreciable changes were observed. For the high concentration samples, α-helix content varied between 7.2 % and 10 % during the study, while β-sheet varied between 29.9 % and 35.1 %. At this concentration, the samples at day 1 showed the greatest deviation from results at other time points whilst, importantly, day 7 data fell between the range of day 0 and day 1 (**Table 3.10**).

For the low concentration samples, slightly less variation in secondary structure was observed, with α-helix content varying between 8.3 % and 9.7 % during the study, while β-sheet varied between 30.7 % and 33.2 %. At this concentration it was the day 2 samples that showed the greatest deviation from results at other time points, indicating that changes to secondary structure may be occurring slower than for the higher concentration samples. Additionally, for both the high and low concentrations, it is the early time points in the study that exhibit the greatest degree of variations in secondary structure (**Table 3.10**).

	Day 0		**Day 1**		**Day 2**		**Day 3**		**Day 4**		**Day 7**	
Conc'	**α**	**β**	**α**	**β**	**α**	**β**	**α**	**β**	**α**	**β**	**α**	**β**
Low	8.3	33.2	8.6	32.7	9.7	30.7			9.3	31.7	9.0	31.7
Common	8.2	33.1	8.4	32.9	7.9	33.6	7.9	33.7			8.0	33.8
High	8.2	33.6	10	29.9	7.7	34.3			7.2	35.1	9.1	31.9

Table 3.10. Deconvoluted CD data for Remsima samples at low, common and high concentrations (acquired at 76 °C) over the period of the study. All values stated are given as the percentage of total structural abundance in α-helix or β-sheets. No clear trend is observed across all concentrations, with only small and reversible changes being noted during the study period.

3.5.9 Gel electrophoresis

Performed according to method 2.2.7. Protein separation of day 0 samples for all concentrations was characterised by a single band of approximately 150 kDa for the native (non-reduced) samples and two bands of approximately 50 kDa and 25 kDa for the reduced samples (**Figures 3.20 A & C**). No change to either the molecular weight or intensity of the bands was observed for any samples throughout the study period for all concentrations, as is demonstrated by the day 7 samples shown (**Figures 3.20 B & D)**. The purple and green bands are the upper and lower markers respectively.

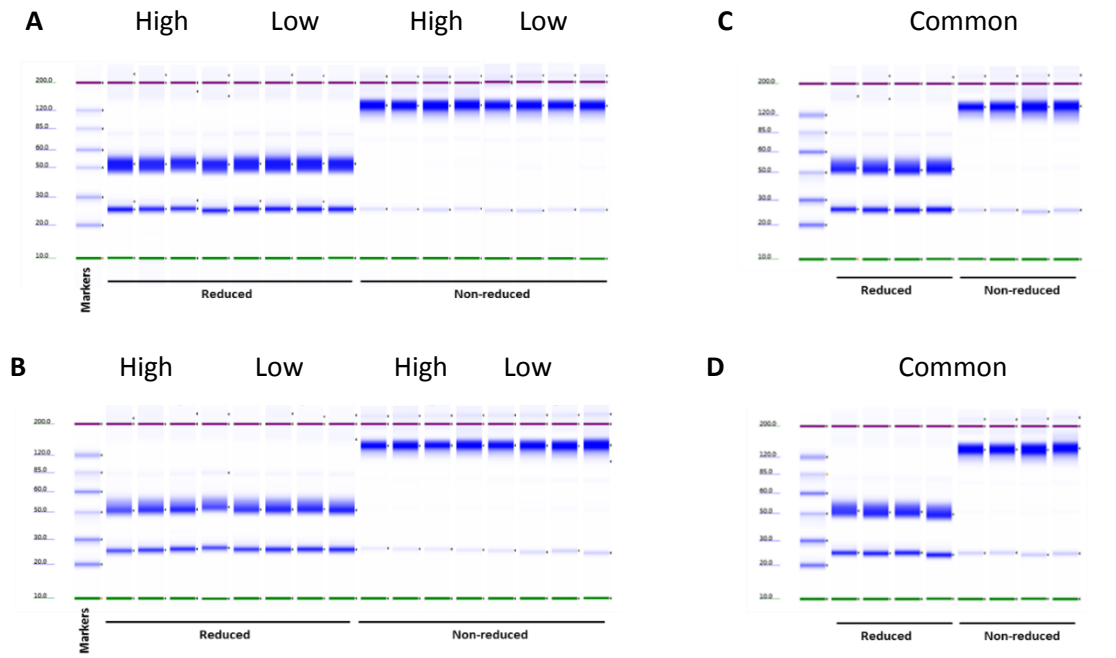

Figure 3.20. Protein separation analysis of Remsima samples (5 µg per well) showing (**A**) Day 0 for the clinically high and low concentrations, (**B**) Day 7 for clinically high and low concentrations, (**C**) Day 0 for the clinically common concentration and (**D**) Day 7 for the clinically common concentration. Lane 1 in all gels is a protein ladder standard. No changes are observed between D0 and D7, no new peaks or changes in band intensity were seen, suggesting Remsima's disulphide bonds remain intact and the level of aggregation does not increase.

3.5.10 LC-MS analysis

Performed according to methods 2.2.12-2.2.14. Mass spectral analysis of the light chain of Remsima on day 0 across all concentrations is characterised by a single major species of mass 23.4 kDa (**Figure 3.21 A**). The mass of this species remained constant over the study period, with no additional peaks appearing, indicating that the chemical identity of the light chain did not change.

The mass spectrum of the heavy chain of Remsima is characterised by a series of molecular ion peaks of around 51 kDa in mass (**Figure 3.21 B**). The complexity of this spectrum is characteristic of antibody heavy chains owing to the heterogeneity of N-linked glycan profiles. Comparison of the heavy chain mass spectra at day 0 and day 7, for all concentrations, revealed no obvious change in chemical composition at any point

during the study period. Importantly, this technique demonstrates the stability of the primary peptide chain, as well as the glycan profile of the antibody which can influence functional activity and pharmacokinetics of the protein.

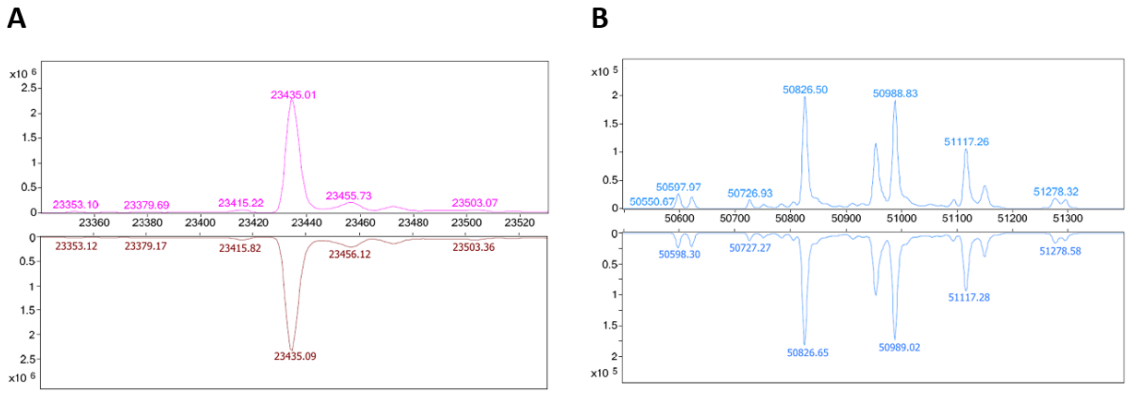

Figure 3.21. Comparison of LC-MS spectra for samples of Remsima stored at 0.60 mg/mL. Day 0 (top) versus Day 7 (bottom) spectra are compared for (A) light chain and (B) heavy chain. Y-axis = TICs, X-axis = Mass (Daltons). No changes are observed between the D0 and D7 samples, the glycosylation pattern appears to remain identical.

3.5.11 Biological activity

Plate set up was according to method 2.3.2 and plate reading was performed according to method 2.2.11. Samples of diluted Remsima typically prevented around 80% of the TNF-α induced death of WEHI cells when tested at 1 µg/mL in this assay. This level of biological activity was equivalent to that observed for freshly prepared samples of Remicade (1 µg/mL), the bio-originator that Remsima is based on. Samples of Remsima tested at Day 0 showed the most dramatic variability in biological activity, both across the three concentrations and within each batch (**Figure 3.22**). This variability in activity appeared to diminish over the period of the study, such that Day 7 data demonstrated the least amount of inter- and intra- batch variability. Owing to the variability in the data, statistical analysis (t-test) was performed to identify changes of significance in the biological activity of the drug, Day 1 (SPC limit) data was compared to both Day 0 and Day 7 data (**Table 3.11**). Analysis demonstrated a statistically significance in biological activity between Day 0 and Day 1 samples (within the SPC assigned shelf-life) at all concentrations tested. However, no significance was assigned to differences between activities at Day 1 and Day 7, across all concentrations. This is most likely due

to the smaller error bars on day 0 than day 7, as well as the mean day 0 data point for the common concentration appearing erroneous, compared to the activity of the low and high concentrations.

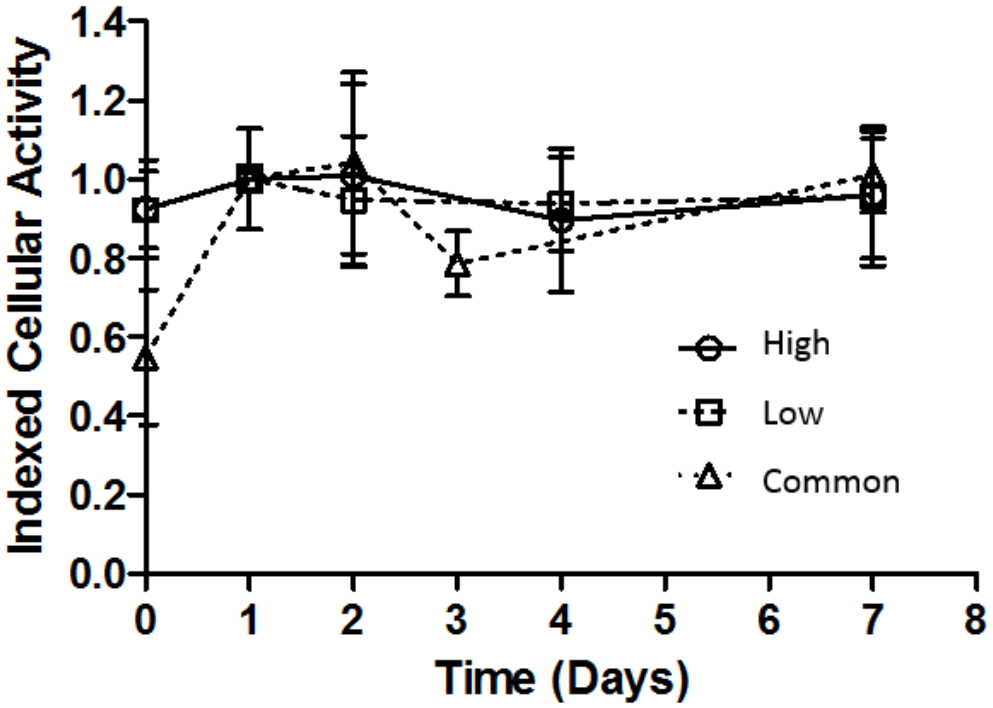

Figure 3.22. Functional activity of Infliximab was tested by its ability to neutralise TNF-alpha in a WEHI cell death assay. Infliximab was tested at 1 µg/ml and results indexed against results for Remicade to control for inter assay variation. Data shown are mean (n=3) with SD of pooled results for each concentration. No trend is observed for any of the concentrations. Comparison of D1 to D7 suggest no statistically significant difference occurs.

	Data tested	D1 vs D0	D1 vs D7
High	p-value	0.011	0.2877
	Are means sig diff?	yes	no
	Summary	*	ns

	Data tested	D1 vs D0	D1 vs D7
Common	p-value	<0.0001	0.3053
	Are means sig diff?	yes	no
	Summary	****	ns

	Data tested	D1 vs D0	D1 vs D7
Low	p-value	0.0016	0.2777
	Are means sig diff?	yes	no
	Summary	**	ns

Table 3.11. Statistical analysis of functional activity. Data shown in (**Figure 3.22**) were subjected to an unpaired t-test using Prism 5 software, comparing Day 7 with Day 1 (the SPC limit) and subsequently, Day 7 with Day 1.

3.5.12 Remsima study discussion

This study has employed study design and testing methodology which are compliant with NHS guidance requirements for performing a robust evaluation of antibody stability over a period of extended storage. We have used a number of analytical and biological techniques to evaluate the stability of diluted solutions of Remsima stored at 4 °C for a period of 7 days. Overall, no chemical or physical instability was observed, while the drug was also found to retain full biological activity.

The techniques of LC-MS, SE-HPLC and gel electrophoresis showed no change for any sample examined throughout the study, indicating that full integrity of the chemical structure (protein and carbohydrate) of the drug is retained.

However, variable temperature circular dichroism does indicate minor changes in the secondary structure of the drug immediately following dilution, which appears to be accompanied by greater variability in numbers of particles >10 μm in size. Initial dilution of infliximab results in dilution of excipients, such as polysorbate 80, as well the polyolefin bag surface to interact with resulting in reorganisation of protein surface interactions. This fact is further supported by results from DLS spectra which demonstrates a measurable drop in hydrodynamic volume of the antibody immediately following dilution. In all cases however, the observed variability is reduced over time as the drug gradually reaches equilibrium under new conditions.

It is also of interest to note that, although minor, the initial changes to secondary structure and variability in particle number do appear to show a measurable impact upon the biological activity of the drug. A statistically significant difference can be attributed to the mean activities of day 0 and day 1 samples, whilst no such difference is present between day 1 and day 7 samples. In totality, these results suggest that the process of drug dilution contributes a more dramatic impact on drug quality than does extended storage, at least over the storage period studied here.

3.5.13 Remsima study conclusions

Here we have demonstrated the stability of Remsima brand infliximab over a 7-day period when diluted in sodium chloride solution and stored in polyolefin bags at 2 - 8 °C. A range of analytical techniques were used to assess the physico-chemical and functional integrity of the drug over time. Furthermore, the methods and techniques used here are fully compliant with NHS guidance for evaluating the stability of biologicals, enabling this data to be used for the application of 7-day shelf-life to Remsima products, when prepared under a Section 10 exemption or a Specials License. This work demonstrates the validity of the study design and characterization methods in assessing a simple antibody's stability, to NHS guidance standards.

Chapter 4. Evaluation and development of methods for characterisation of trastuzumab emtansine

4.1 Additional critical characteristics for an ADC

4.1.1 Introduction

Compared to antibodies, ADCs have unique critical stability characteristics due to the conjugation of warheads via linkers. Off-target toxicity is also an important issue if the warheads become detached via hydrolysis of an ester or amide, as the warheads rely solely on the targeting provided by the antibody. Section 4.1 details the additional critical characteristics ADCs possess compared to antibodies.

4.1.2 DAR

The DAR is one of the most distinguishing characteristics an ADC has compared to a regular antibody. We know that an individual trastuzumab emtansine molecules DAR will not be the same as all the other molecules. We know there are ADCs in a trastuzumab emtansine vial with DARs ranging between 1 and 8 as well as naked antibody in the mixture too. [87 - 89] We also know that high (7-8) DAR ADCs have reduced biological half-lives, and low (1-2) DAR ADCs have reduced potency. [90] That is why ADCs are typically designed to have a mean DAR of about 4, and the majority of DAR species to be between 3 and 6. [87-89] Monitoring the mean DAR or payload binding would indicate if payloads are detaching. Increased off target activity, or loss off on target activity could also indicate change in DAR. Lastly the concentration of free payloads and warheads should be relative to the mean DAR.

4.1.3 Positional isomers

Positional isomers refer to variations in binding sites of ADCs with the same DAR. For example, a DAR of 1 trastuzumab emtansine ADC could be one of about 30 possible positional-isomers. The level of complexity increases, and it is quite possible that it is unpractical to attempt to assess positional-isomers. However, enzymatic fragmentation of an antibody coupled with a method of separation and detection with enough resolution may be able to provide some measure of the positional-isomers. However, this will only change from batch to batch of the trastuzumab emtansine. Once linkers and warheads have been attached to the antibody, the payloads should not rearrange during storage. It is possible we could observe functional activity and/or physico-chemical stability differences between positional-isomers, but this information will unlikely be useful in determining the overall stability of trastuzumab emtansine as we have no control over the positional-isomers present. As such, while positional-isomers are important regarding stability and even potency of ADCs, as specific binding locations may affect the binding of the ADC to the receptor or affect CDC and ADCC, they are not under our control or going to change during storage, therefore will not be investigate further. [197]

4.1.4 Free payloads / warheads

As the payloads can become detached, and the warheads are extremely cytotoxic, they have the potential to be hazardous degradation products. Trastuzumab emtansine's payloads contain amide bonds and ester bonds. These are bonds which may be hydrolysed, liberating a portion of the payload. Amide and ester bonds are most to acid and base hydrolysis. As the linker is stable in human lysosomes, which have a pH of about 4.5, the ester and amides must require more acidic conditions to be degraded. The payload can also be liberated at the ester via a retro-Michael reaction involving any species capable of acting as a proton acceptor such as the thiol containing albumin or glutathione. [230]

4.1.5 Off target toxicity

The trastuzumab antibody is very specific for HER2, however off target toxicity could arise if fragments of the payloads, detach and diffuse into non-target cells. Payloads could detach due to ester or amide hydrolysis, trastuzumab emtansine is most likely to detach from its payloads under more basic conditions than it is stored and formulated at. While it could be possible to detect free payloads, determining if there is an increase in off target activity would require a cell-based assay. The activity of trastuzumab emtansine to kill target cells that express high levels of HER2 compared to the activity of trastuzumab emtansine to kills non-target cells, ideally that express normal low levels of HER2.

4.2 Evaluating an ADC with infliximab validated methods

4.2.1 Introduction

To evaluate whether the methods used in the infliximab study are compatible with the ADC trastuzumab emtansine, control samples and force degraded samples of trastuzumab emtansine, made following method 2.4.1, were tested using each method successfully used on infliximab in chapter 3. The ability to distinguish the control from at least one type of degradation is the minimum requirement for a method to be considered stability indicating as per ICH guidance. [105] Samples of trastuzumab emtansine were degraded using acid hydrolysis, base hydrolysis, oxidation, photolysis, and thermal degradation according to methods 2.2.17 - 2.2.21 respectively.

Trastuzumab emtansine is dosed at 3.4 mg/kg or 2.4 mg/kg. When prepared into an infusion bag, according to its SPC, the concentration ranges between 0.5 and 1.5 mg/mL. The concentration of samples used in this validation was 1 mg/mL.

4.2.2 Visual inspection

Following the procedures set out in method 2.2.2, no visual differences compared to the control samples were observed for any degraded samples. All samples remained clear and free of visible particulates. This technique appears entirely unaffected by the change to testing the ADC trastuzumab emtansine. The structure of trastuzumab emtansine was not expected to have an effect on the compatibility of the visual inspection method

4.2.3 pH

Because pH is altered by oxidative, acidic and basic reagents, only control samples, photolytically degraded and thermally degraded samples were measured following method 2.2.3. The control was 5.67 ±0.03, photolytically degraded samples were 6.61 ± 0.09 and the thermally degraded samples were 6.04 ± 0.61. This demonstrates pH can be stability indicating and the pH method is compatible with trastuzumab emtansine.

4.2.4 Microflow Imaging analysis of microparticles

When measured following method 2.2.6, all investigated paths of degradation were observed to cause an increase in microparticles (10-100 µm) of both size categories, except those >25 µm for the 'Acid Degraded' condition (**Figure 4.1)**. These results clearly demonstrate the stability indicating nature of the MFI method. This technique is entirely unaffected by the change to testing the ADC trastuzumab emtansine. Note the photolytic control is only for comparison to the photolytic degraded sample, and was a control kept at 5 °C ± 3 °C for 96 hours.

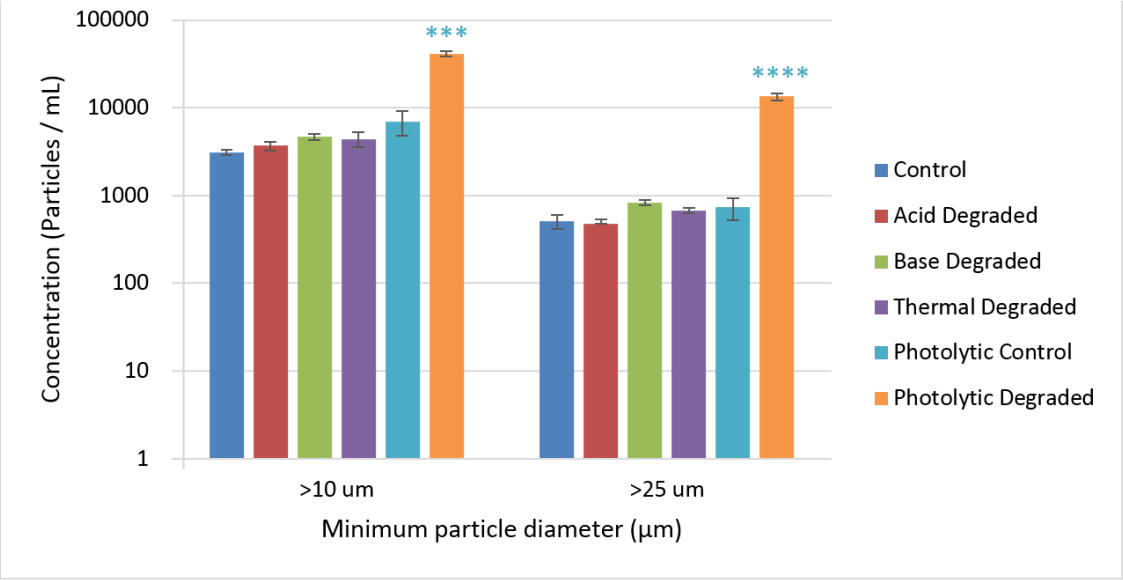

Figure 4.1. Microparticles / mL for trastuzumab emtansine controls and degraded samples, as measured by MFI. Effect of various methods of degradation on microscale particles per mL. For both size categories of microparticle, only the photolytically degraded sample was significantly different from the photolytic control. results are a mean (n=3) with error bars reporting 1 standard deviation. The effect of photolytic degradation was statistically more significant on the number of particles greater than 25 µm than the number of particles greater than 10 µm. *** = p <0.001, **** = p <0.0001

4.2.5 UV assay for extractables and leachables

The purpose of this techniques is to detect plasticisers that have leached into the drug solution. **Figure 4.2** below, shows UV scans of the three concentrations used in the stability study, obtained following method 2.2.10. UV absorption at 280 nm is caused primarily by amino acids with aromatic rings, such as tyrosine, tryptophan and phenylalanine. Trastuzumab emtansine's warhead, DM-1, contains only affects lysine residues for trastuzumab emtansine, which an aromatic ring which slightly increases the molar absorption co-efficient at 280 nm. Leachables, such as DEHP, would cause an increase in the absorbance at 226 nm and above 300 nm. [231, 232] This technique is compatible when testing trastuzumab emtansine.

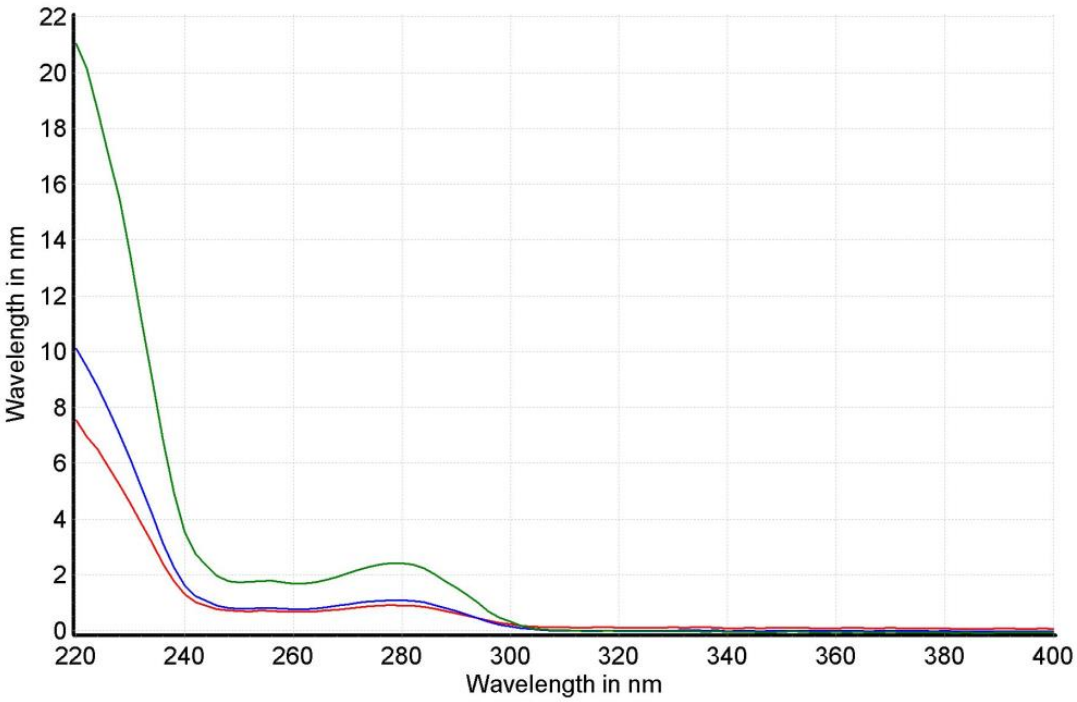

Figure 4.2. UV absorbance from 220 nm to 400 nm of a clinically High (**Green**), Common (**Blue**) and Low (**Red**) concentration of trastuzumab emtansine. No absorbance from 300 nm to 400 nm means common plasticisers such as DEHP should be detectable even in small amounts.

4.2.6 Gel electrophoresis

Following method 2.2.7, The photolytic and thermal samples had discernible differences compared to the control (**Figure 4.3**). No difference was noted with the acidic and basic hydrolysis methods, while the oxidized sample failed to either stain or run properly, the hydrogen peroxide is likely interfering with the staining reagents.

The thermally degraded samples each had a new band below 10 kDa, suggesting fragmentation in addition to greater intensity of the wide band above 200 kDa, indicative of aggregation. The photolytically degraded samples each had an additional band around 120 kDa, suggesting incomplete reduction as well as an increase in intensity of the wide band above 200 kDa, indicative of aggregation. This data indicates the gel electrophoresis method is compatible with trastuzumab emtansine and is stability indicate, however these findings also suggest thermal stress is driving aggregation, perhaps through partial unfolding of the antibody exposing

hydrophobic regions that would normally be inaccessible, as well as causing fragmentation of sub 10kDa species, this could be payloads. While photolytic stress also drives aggregation, the fragmentation of species with a molecular weight between 10 and 20 kDa is very curious, as no fragment of an ADC is that size, suggesting intra-chain fragmentation may be occurring, though this has not been confirmed.ng.

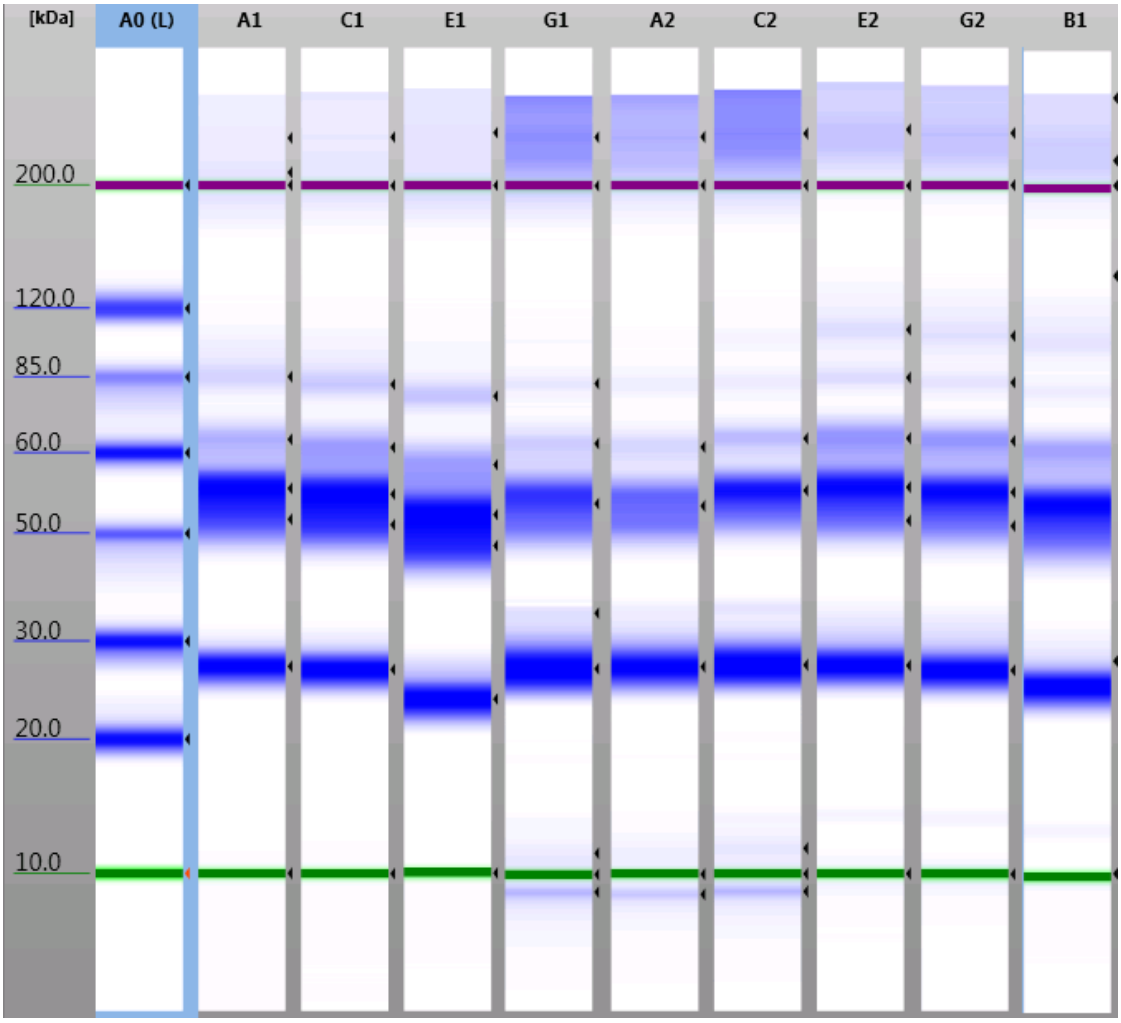

Figure 4.3. Gel electrophoresis images of reduced trastuzumab emtansine: sample controls [A1, C1, E1], thermally degraded samples [G1, A2 & C2] and photolytically degraded samples [E2, G2 & B1]. Compared to the control samples, the thermally degraded samples show a marked increase in aggregate band intensity, (bands above the 200 kDa marker), as well as new bands below the 10 kDa marker. Compared to the control samples, the photolytically degraded samples show a slight increase in aggregate band intensity, (bands above the 200 kDa marker), as well as feint new bands between the 10 and 20 kDa marker.

4.2.7 Dynamic light scattering analysis of nano-particles

This technique was not used as a better technique, Nano-tracking analysis, became available after the Infliximab study had been performed. However, work by Cockrell *et al* [168] used DLS analysis, to assess aggregation of a model antibody drug conjugate after photodegradation. Their model ADC was trastuzumab linked to eosin via its lysine residues. Cockrell *et al* found they were able to detect aggregation following photolytic degradation of their model ADC, but not for trastuzumab. That work indicates DLS would likely have been compatible and stability indicating.

4.2.8 Nano-tracking analysis of nano-particles

Following method 2.2.5, NTA was able to measure the concentration (per mL) of nano-particles (1-1000 nm) in trastuzumab emtansine control and degraded samples (**Figure 4.4**). The stability indicating nature of the technique was demonstrated by the ability to detect differences in the degraded samples compared to the controls. All conditions increased the concentration of nano-particles. With acidic and thermal degradation having the most significant effect. NTA appears compatible and stability indicating. Acidic degradation caused the most statistically significant amount of change, suggesting that acid hydrolysis affects the structure of trastuzumab emtansine the most while basic degradation appears to have had the least statistically significant effect on particle concentration. This is interesting as acid and base stress will cause hydrolysis of the linker however that is not likely to drive aggregation. It appears that acidic environments cause the conformation of the antibody to expose hydrophobic residues that would typically be inaccessible to a greater extent than basic environments. Oxidation of methionine residues is known to cause aggregation in antibodies and it is reasonable to assume the same is true for ADCs. Thermal degradation can also cause unfolding of proteins which appears to be true of ADCs too.

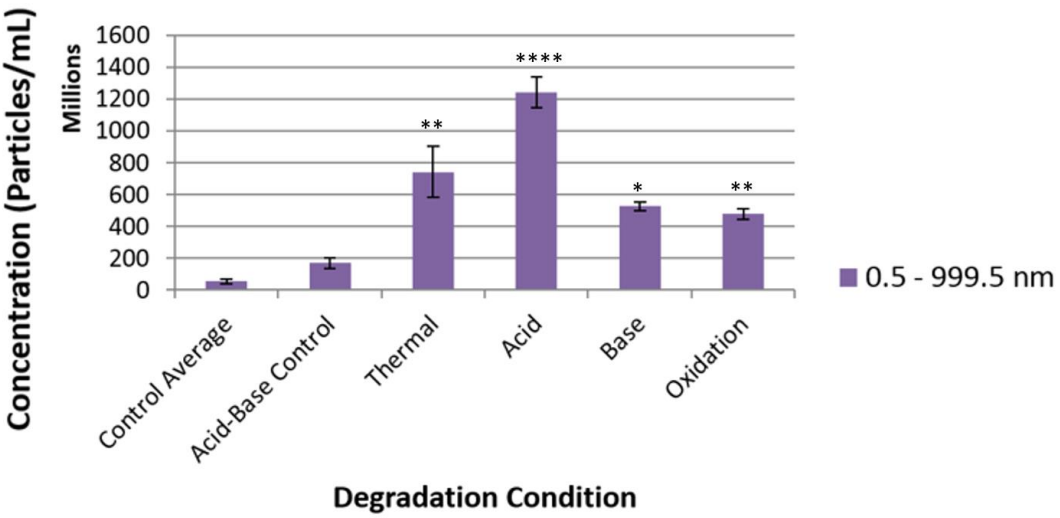

Figure 4.4. Nano-particles per mL for control and degraded trastuzumab emtansine. Plots are a mean average (n=3) ± 1 standard deviation. All stress conditions increased the concentration of nanoparticles. *, ** & **** indicate $p < 0.05$, 0.01 & 0.0001 respectively.

4.2.9 LC-MS analysis

Trastuzumab emtansine was reduced into its heavy and light chains and analysed using method 2.2.12. (**Figures 4.5 & 4.6**). Heavy and light chains with up to two payloads are detectable with mass differences matching molecular weight of a single payload. The samples were run according to method 2.2.13 and the data was processed according to method 2.2.14

Degradation using heat and photolysis could be detected as a loss in peak intensity compared to the controls, as well as an increase in peak intensity at about 50650 kDa, (**Figures 4.5 & 4.6**). Peak intensity loss appears more prevalent on chains with more payloads Furthermore, an increase in peak intensity is observed at 50650 daltons, indicating successful detection of a chemically different heavy chain species formed during photolytic degradation (**Figure 4.6**). Therefore, this method appears to be compatible with trastuzumab emtansine and is stability indicating for at least thermal and photolytic degradation.

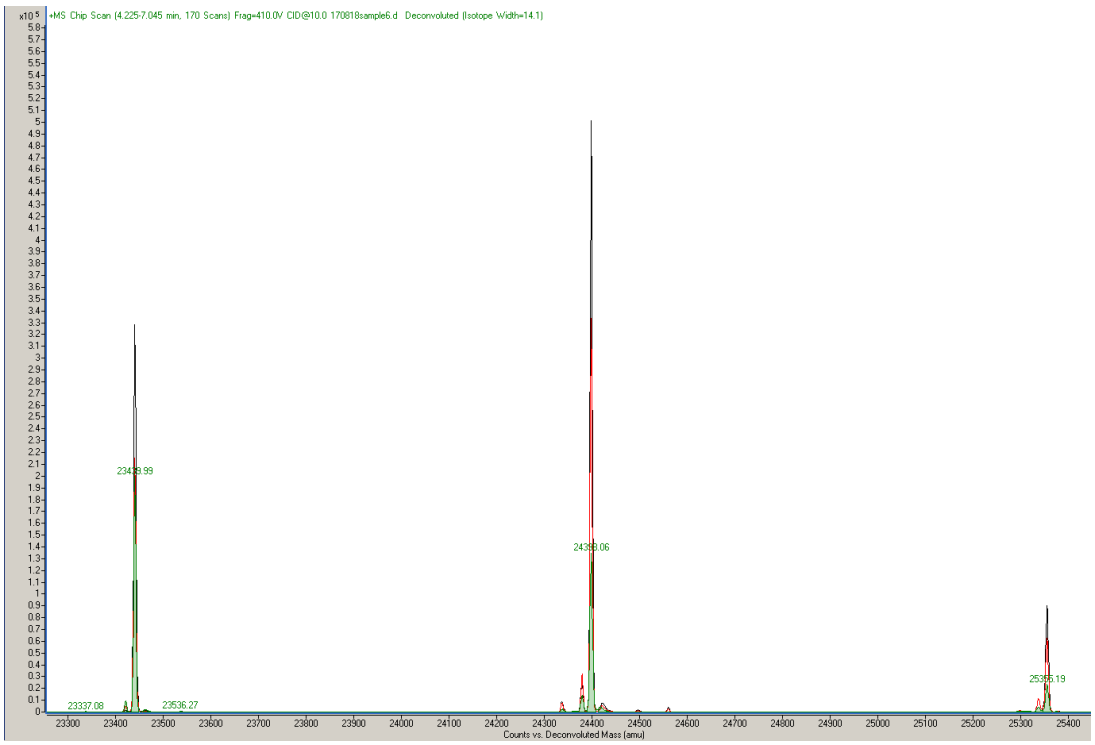

Figure 4.5. Mass spectra between 23300 and 25400 daltons of trastuzumab emtansine light chains, following TCEP reduction. Control sample spectra are (**Black**), thermally degraded sample spectra are (**Red**) and photolytically degraded samples are (**Green**). First, there are three distinct peak clusters, each pertaining to light chain with either 0, 1 or 2 bound payloads. Second, it is notable that the peak cluster patterns, which are due to variable glycosylation, are not identical between the peak clusters. It could be possible that specific glycosylation profiles influence linker conjugation for trastuzumab emtansine, however this has not been investigated further. Third, in the thermally and photolytically degraded samples the signal intensity of the peaks is reduced compared to the control. Finally, in the thermally and photolytically degraded samples some peaks are greater in magnitude while the main peaks of the clusters have decreased, indicating that this technique is able to detect changes in the glycosylation peak profiles for trastuzumab emtansine.

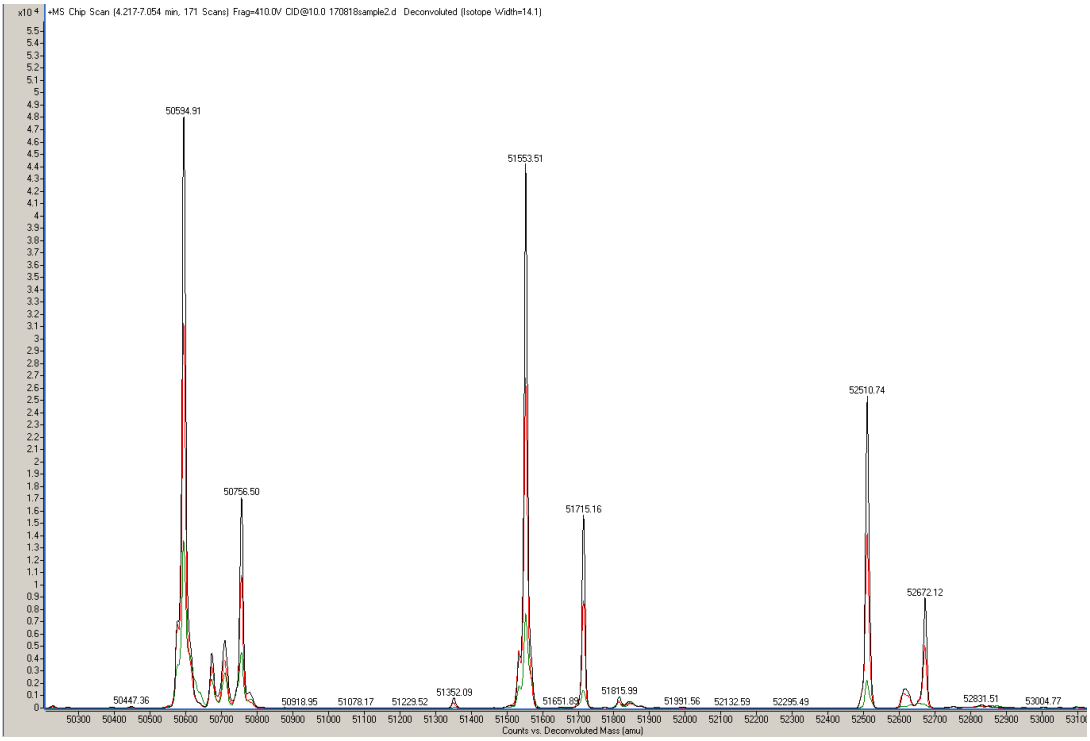

Figure 4.6. Mass spectra between 50300 and 53100 daltons of trastuzumab emtansine heavy chains, following TCEP reduction. Control sample spectra are (**Black**), thermally degraded sample spectra are (**Red**) and photolytically degraded samples are (**Green**). First, there are three distinct peak clusters, each pertaining to heavy chain with either 0, 1 or 2 bound payloads. Second, it is notable that the peak cluster patterns, which are due to variable glycosylation, are not identical between the peak clusters. It could be possible that specific glycosylation profiles influence linker conjugation for trastuzumab emtansine, this was also noted for the light chains. Third, in the thermally and photolytically degraded samples the signal intensity of the peaks is reduced compared to the control. Finally, in the thermally and photolytically degraded samples some peaks are greater in magnitude while the main peaks of the clusters have decreased, indicating that this technique is able to detect changes in the glycosylation peak profiles for trastuzumab emtansine, though this is far less prevalent than on the light chains.

4.2.10 MTT cellular assay

The plate was set up according to 2.4.2, the plates were read according to method 2.2.11. Theoretically, trastuzumab emtansine should only bind, become internalised and then initiate apoptosis in cells with a high HER2 expression. Therefore, on-target activity and can be well modelled with the cell line BT-474. BT-474 is a breast cancer cell line with a highly upregulated HER2 expression, that has been used by numerous studies to investigate trastuzumab activity and model breast cancer since 1979. [169-172] A $\log_{10}$ dose response curve of percentage cell death of a control sample vs a photolytically degraded sample of trastuzumab emtansine demonstrates a loss of activity via a shift of the dose response curve to the right (**Figure 4.7 A**). Off target activity is a concern for ADCs as their payloads can become detached and cause apoptosis in any cells the payloads are able to diffuse or get transported into. To assess off target activity a human epidermal skin cell line known as HaCaT's was used to measure off target activity on the skin (**Figures 4.7 B**), while hepatic cell line HepG2, was used to assess off target activity at the liver (**Figures 4.7 C**). Note the loss of activity at the lower concentrations for the photolytically degraded trastuzumab emtansine is significant for the on-target cell line but insignificant for the off target cell line.

MTT analysis of biological activity appears to be unaffected when measuring the ADC trastuzumab emtansine, however the cell lines used are completely different to those used in the infliximab study. This data suggests this method is valid and stability indicating for detecting off target and on target toxicity.

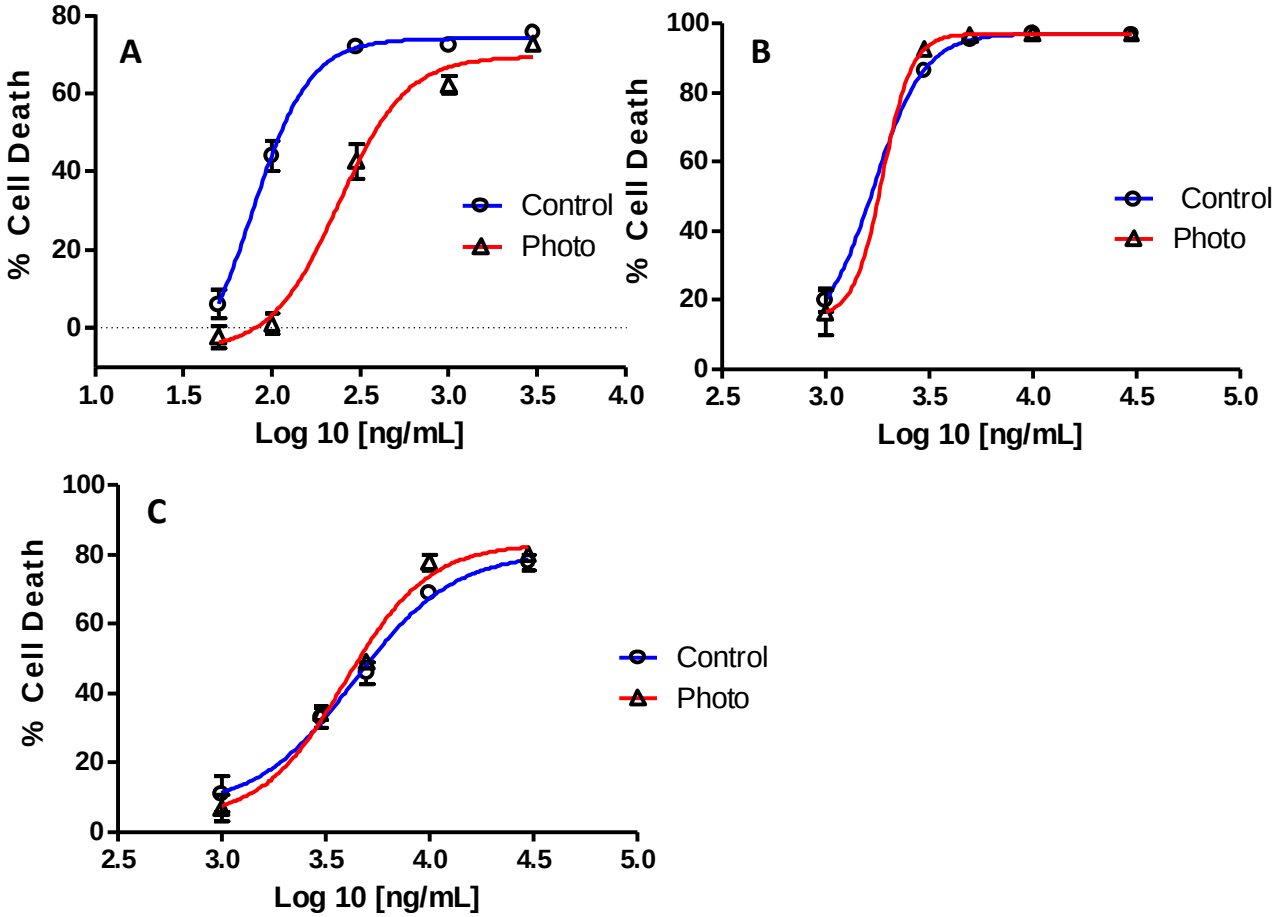

Figure 4.7. Log[10] dose response curves of (**A**) BT-474 cells, (**B**) HaCaT cells and (**C**) HepG2 cells to control samples and photolytically degraded trastuzumab emtansine. Samples were tested in quintuplicate. Results are means (n=5) ± 1 standard deviation. All dose response curves exhibit the classic sigmoidal curve associate with a dose response that crosses the EC_{50}. The control and degraded dose response curves for BT-474 cells do not overlay, with a shift towards the right on the X-axis, seen when photolytically degraded. The EC_{50} for the control trastuzumab emtansine against the BT-474 cells was 77.3 ng/mL which dramatically increased to 239.7 ng/mL for the degraded drug. The control and degraded dose response curves for HaCaT and HepG2 cells overlay, with minimal change in the EC_{50}. The EC_{50} for the control trastuzumab emtansine against the HaCat cells was 4.4 µg/mL which slightly decreased to 3.6 µg/mL. The EC_{50} for the control trastuzumab emtansine against the HepG2 cells was 1.7 µg/mL which slightly increased to 1.9 µg/mL when photolytically degraded.

4.2.11 Size exclusion chromatography analysis of monomer and oligomers

To investigate compatibility of size exclusion chromatography analysis, trastuzumab emtansine and its parent antibody, trastuzumab were analysed using method 2.2.16, previously used for infliximab (**Figure 4.8**). The monomer peak has clearly been affected, with the plate number dropping from 5394 to 596 and the asymmetry increasing from 1.2 to 1.7. An asymmetry of 1 is a perfectly symmetrical peak, while an asymmetry above 1.5 is bad for analytical chromatography and an asymmetry above 2.0 is unacceptable. Any secondary interaction to the stationary phase (column material) will cause peak tailing, leading to an unacceptable degree of peak asymmetry as well as a loss of resolution and theoretical plate number. Trastuzumab emtansine's payloads appear to be interacting with the stationary phase, resulting in a drastically impaired peak unsuitable for a full validation. This finding agrees with work by Wakankar *et al,* [173] who found impaired peak shape for ADCs analysed using traditional methods. This method is not compatible with trastuzumab emtansine and cannot be validated to determine its stability indicating nature.

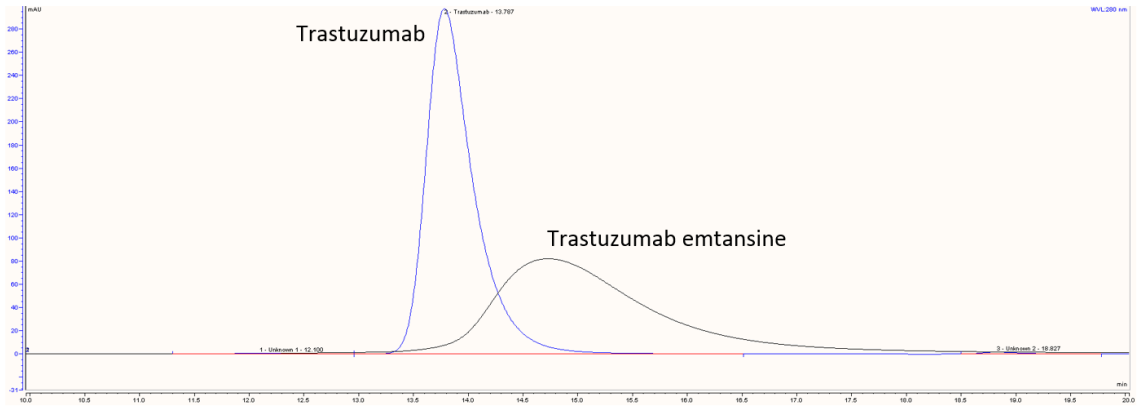

Figure 4.8. A chromatographic overlay of the mAb trastuzumab in (**Blue**), and the ADC trastuzumab emtansine in (**Black**) both at 2 mg/mL using the same method. The X-axis is time (minutes). The peak for trastuzumab is resolved from the dimer peak and fragment peak, and has acceptable peak shape, while the peak for trastuzumab emtansine has a much broader peak that has unacceptable levels of fronting and tailing, with no resolution of the monomer peak from the dimer or fragment.

4.2.12 Circular dichroism analysis of higher order structure

To investigate the compatibility of circular dichroism analysis of higher order structure, trastuzumab emtansine, its parent antibody trastuzumab and denosomab, an IgG2 antibody with a different target antigen, were analysed using method 2.2.8, previously used for infliximab (**Figure 4.9 & Table 4.1**).

It was found that the CD spectra of trastuzumab and trastuzumab emtansine were similar which made sense but when processed using CDNN into a prediction of secondary structure, the prediction did not appear correct (**Table 4.1**). Although trastuzumab emtansine has payloads bound to the lysine residues, the secondary structure of the antibody should not be affected significantly. It is likely that High DAR forms of trastuzumab emtansine would exhibit the most altered structure, or trastuzumab emtansine with payloads bound to lysine residues around the hinge region may have reduced flexibility, affecting the most favourable resting conformation. However, these effects should be minimal, and there are no reports of trastuzumab emtansine having a significantly different secondary structure to trastuzumab. When measuring trastuzumab and trastuzumab emtansine CD they appear similar (**Figure 4.9**).

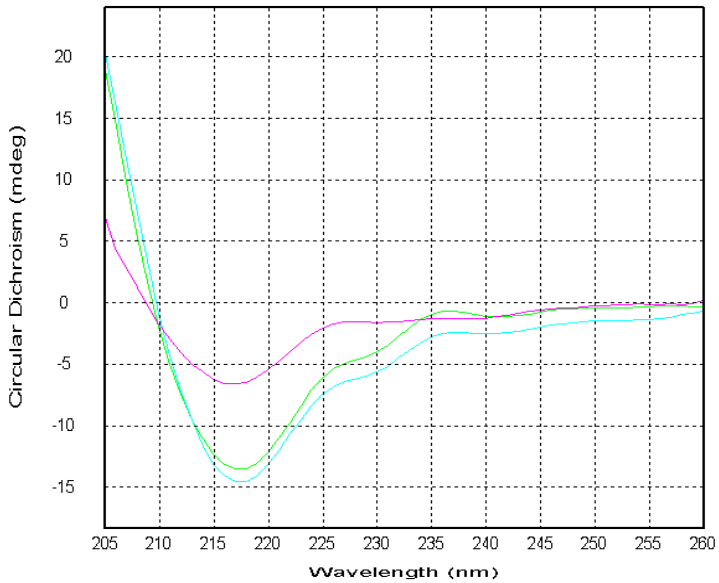

Figure 4.9. The CD spectra for 0.3 mg/mL trastuzumab in (**Green**), trastuzumab emtansine in (**Blue**) and denosumab in (**Pink**). The spectra for trastuzumab and trastuzumab emtansine are very similar in shape, though the signal intensity appears to be stronger for trastuzumab emtansine, even though they are at the same concentration. Denosumab has a completely different CD spectra.

However, when deconvoluted via CDNN, the predicted structure does not correlate with a realistic estimation of secondary structure, see (**Table 4.1**). Note that denosumab which is an IgG2 antibody that binds to a completely different receptor and has a different primary sequence has a more similar structure to trastuzumab than trastuzumab emtansine, according to CDNN estimation.

Secondary Structural Motif	Trastuzumab	Denosumab	Trastuzumab Emtansine
Helix	5.3%	5.8%	14.3%
Antiparallel	41.0%	40.7%	35.4%
Parallel	5.6%	5.5%	5.5%
Beta-Turn	14.8%	14.0%	20.8%
Random Coil	33.4%	34.7%	36.7%
Total Sum	100.1%	100.7%	112.7%

Table 4.1. CDNN structural estimation from the CD spectra for 0.3 mg/mL trastuzumab, trastuzumab emtansine and denosumab. Trastuzumab and denosumab have well predicted structures with the total % of secondary structure summing to approximately 100%. Trastuzumab emtansine has a secondary structure that adds up to over 112%, which highlights something must be wrong. The most notable differences between trastuzumab and trastuzumab emtansine occur at the alpha helix, which increase 9%, beta turns, which increase 6%, random coil which increases 3%, and antiparallel sheet, which decreases 5.6%.

The secondary structure composition does not look right for trastuzumab emtansine. As well as the specific structural estimations not matching up, the structural sum adds up to 112.7%, while trastuzumab and denosomab only add up to 100.3 and 100.6 respectively.

There are two ideas that may partially explain why this is observed. Proteins have chiral centres that contribute to their inherent circular dichroism (the degree to which they preferentially absorb left or right handed polarised light). This is conformationally sensitive and using CDNN to deconvolute the spectra based on a comparison to a known

library of proteins, along with the specific concentration, exact number of amino acids and molecular weight with an accuracy of 0.1 daltons.

The first idea was, the mass being used in the deconvolution calculations was wrong, as CDNN is based only on proteins and not ADCs, which have additional mass not due to protein but due to payloads. The second idea was, the payloads themselves were affecting the circular dichroism of the ADC, as the payloads contain a chiral centre that is unrelated to the antibody's circular dichroism.

Attempts to spoof CDNN by using the mass of trastuzumab instead of trastuzumab emtansine were made, but the results still had Total structural sums over 110%. This leads me to believe that the chiral centres in the payloads are interfering with the CDNN structural deconvolution.

This method of determining secondary structure was not feasible to use with the ADC trastuzumab emtansine and is predicted to be incompatible to any ADCs with payloads containing chiral centres, which includes all four currently licensed ADCs. Thus, a new method of determining secondary structure is required.

In summary, analysis of higher order structure using the circular dichroism based method previously applied to infliximab is unsuitable for trastuzumab emtansine and therefore cannot be determine to be stability indicating.

The issues with deconvolution of CD spectra to secondary structure predictions is not reported in literature, although the only published papers that used CD to investigate ADC structure did not attempt to deconvolute the data to estimate secondary structure, as is typically done for normal antibodies, and instead reported the mean residue ellipticy. [233, 234] In 2016, Arakawa *et al* identified differences between a model ADC and its parent antibody in the near-UV region as well as claiming that many cytotoxic drugs have many cytotoxic drugs have UV absorbance that can interfere with optical properties of ADCs. [234]

4.3 Optimisation of a SEC method for API quantification

4.3.1 Literature research

SEC is an essential method, required for characterising a mAb or ADC. A stability indicating method can quantify the concentration of the monomer, dimer and trimer. Oligermization of antibodies is known to affect their activity, immunogenicity and pharmacokinetics. [174] Thus, monomer, dimer and trimer concentrations are critical characteristic, as stated in the NHS biopharmaceutical stability guidance. [102]

Standard SEC methods for mAbs, have been demonstrated as unsuitable to characterise the ADC trastuzumab emtansine, it is believed this is due to secondary interactions of the ADCs payloads with the stationary phase. To reduce the effect of payload secondary interactions Wakanker *et al* added varying amounts of different organic modifiers, such as acetonitrile and propan-2-ol. [173] They found 15% propan-2-ol to 85% 200mM potassium phosphate / 250mM potassium chloride adjusted to pH 6.95 minimised the secondary interactions and produced suitable chromatograms. An issue regarding the addition of organic solvents to a mobile phase is salt precipitation. This can affect HPLC modules as well as cause irreparable damage to a size exclusion chromatography column. The column manufacturer Phenomenex claim their SEC columns could quantify ADCs without the need to add organic modifiers at all, with published data showing addition of organic modifier did not change the chromatograms. [175]

4.3.2 Experimentation with Phenomenex's Yarra and BioSEP columns

Phenomenex have a public technical note demonstrating the use of their Yarra SEC-s3000 column to separate monomer and dimer of a model ADC without using organic additives to prevent secondary interaction of the payloads with the column. [175] Using trastuzumab emtansine and following method 2.4.3, the results could not be

replicated (**Figure 4.10**). When organic phase was added the peak shape improved, showing the column was affected by the non-specific interactions caused by the payloads. Phenomenex make a BioSep-SEC-s4000 column marketed as an equivalent or superior to the Tosoh G3000 SWxl, which had been used for the infliximab analysis in chapter 3. As we had a negative experience with the Yarra, we were given a BioSep-SEC-s4000 as compensation. Preliminary testing confirmed the BioSep was equivalent to the Tosoh G3000 SWxl. Due to the significant difference in price, (£800 cheaper), the BioSEP-4000 was selected for the SEC method instead of the Tosoh G3000 SWxl used for the infliximab study.

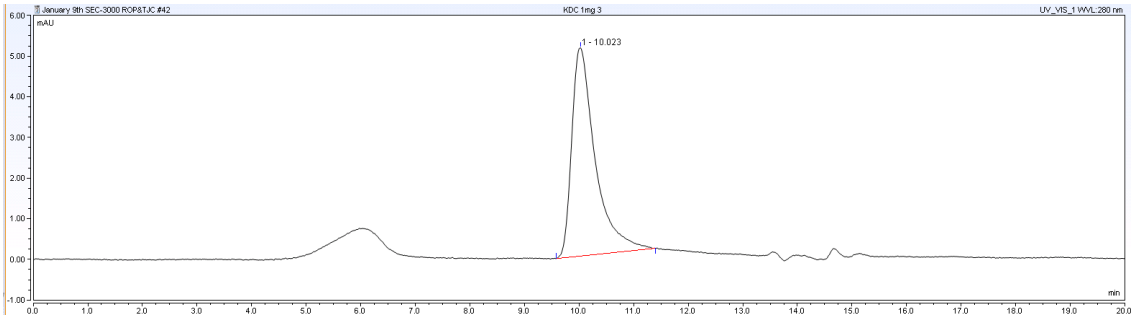

Figure 4.10. A SEC chromatogram of trastuzumab emtansine, tested on the Yarra SEC-3000 with the manufacturers recommended method. The X-axis is time (minutes). The monomer elutes at about 10 minutes, with a poor peak shape due to tailing. An aggregate peak elutes around 6 minutes, which also exhibits poor peak shape, with both fronting and tailing.

4.3.3 Adjusting the mobile phase

The effects of different organic modifiers, such as acetonitrile and propan-2-ol (IPA) were investigated, as well as the effect of altering the: buffer salts, final pH, buffer strength, SEC column type and flow rate.

Trastuzumab emtansine's payloads are hydrophobic, causing hydrophobic interaction with the SEC column stationary phase. [173] Addition of organic modifiers reduces the tailing observed due to hydrophobic interaction. [173] Method 2.4.4 was used to compare 0, 5, 10 15 and 20% acetonitrile, IPA and ethanol (**Figure 4.11**). Ethanol least improved the peak shape, while acetonitrile and propan-2-ol had more similar effects. Addition of 10% propan-2-ol produced the best results, according to retention time,

peak resolution and asymmetry, thus propan-2-ol was selected as the most suitable organic modifier. These findings reflect Wakankar's original work. [173] IPA is notably more viscous than acetonitrile or ethanol and is also cheaper than ethanol or acetonitrile. As the modifier is being used in sub 25% amounts the potential increase on backpressure is negligible, but the difference in price of IPA over acetonitrile makes the decision to use IPA much easier.

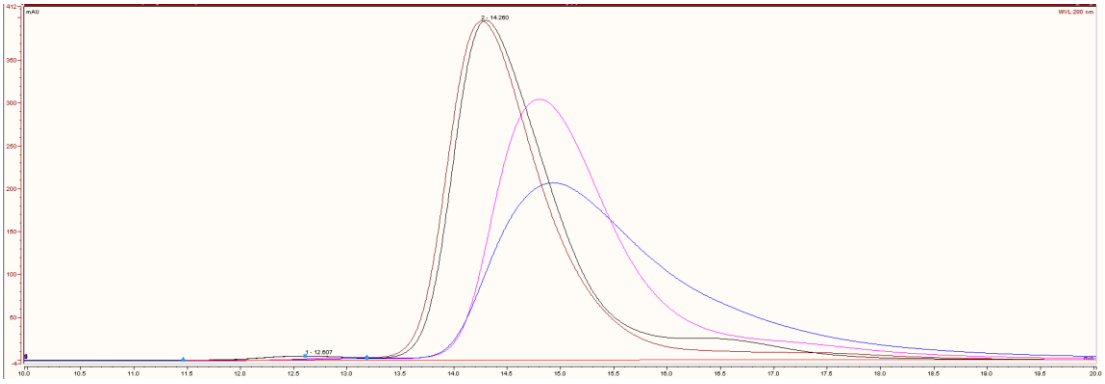

Figure 4.11. Chromatograms of trastuzumab emtansine with 0 % organic modifier in (**Blue**) which has clear peak tailing and the worst peak shape, 10 % ethanol in (**Pink**) which had the second worst peak shape due to tailing, 10 % acetonitrile in (**Black**) with the second-best peak shape and 10 % propan-2-ol in (**Brown**) which had the best peak shape according to asymmetry calculated by Chromeleon. The X-axis is time (minutes).

One of the biggest risks of adding organic modifiers is precipitation. There were three approaches to minimising this risk: reduce the concentration of salt in the mobile phase, reduce the amount of organic solvent in the mobile phase, use more soluble and miscible reagents. The American USP standard method for antibodies uses potassium-based buffers, while most other countries use sodium-based buffers. Previous work had used sodium phosphate as the buffer but it has been shown that sodium is less soluble in organic solvents than potassium. [176] When comparing potassium-based buffers to sodium-based buffers following method 2.4.5, no discernible difference could be noted with no change in peak asymmetry, plate number, retention time or absorbance (**Figure 4.12**). Thus, potassium phosphate was selected as the optimal buffer.

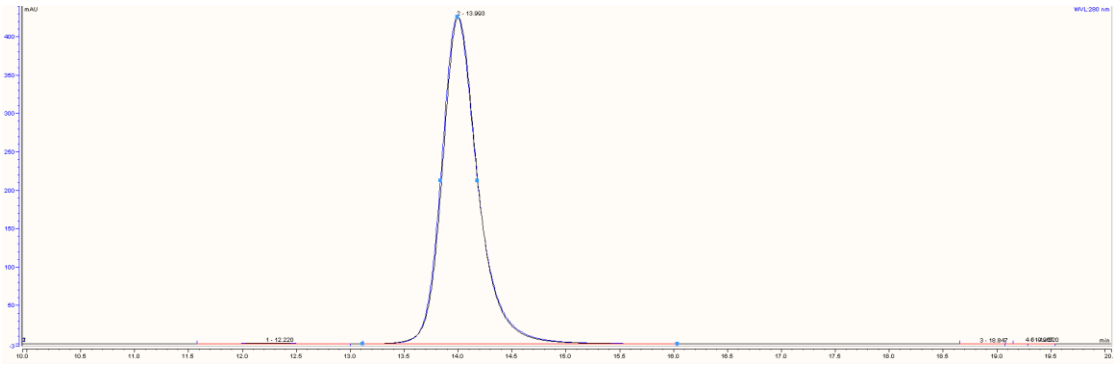

Figure 4.12. Chromatograms of a mAb using a sodium-based buffer in (**Blue**) and a potassium-based buffer in (**Black**). The X-axis is time (minutes). Both peaks exhibit good peak shape, with low asymmetry, excellent signal to noise, however both do also have small amounts of fronting and tailing.

An alkali chloride such as sodium or potassium chloride is typically added to antibody mobile phases. The alkali chloride inhibits non-specific interactions of the proteins with the stationary phase. [235] However more modern columns are designed to minimise these interactions and with the addition of an organic modifier it was decided to investigate the effect of the alkali chloride concentration. Following method 2.4.6, we found that mobile phases with organic modifier use in conjunction with a more modern BioSep-SEC-s4000 column there was no effect on the peak quality (**Figure 4.13**) and noted a slight decrease on HPLC backpressure as well. There was no change in peak asymmetry, and a 1.6% loss of peak area and a 0.3% loss of theoretical plates, but these differences are trivial. Thus, it was decided not to include any alkali chloride in the mobile phase.

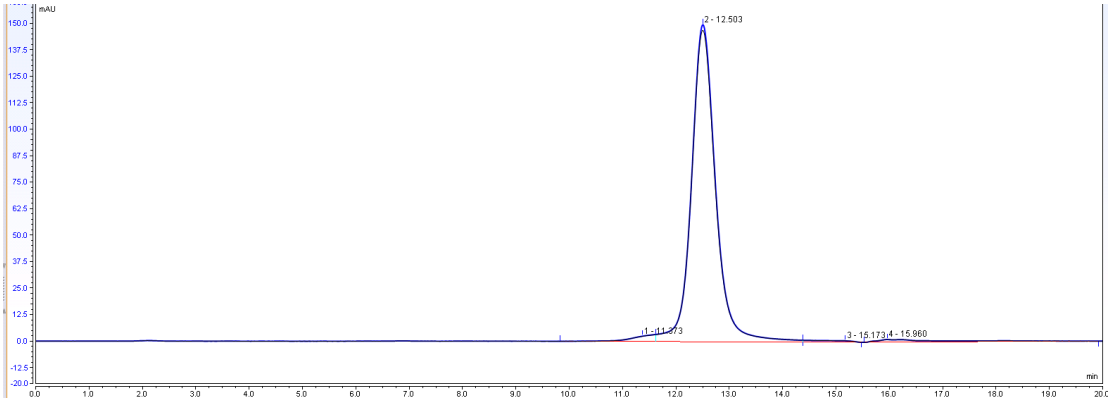

Figure 4.13. Chromatograms of trastuzumab emtansine with 300mM sodium chloride in the buffer in (**Blue**), and with 0mM sodium chloride in the buffer in (**Black**). The X-axis is time (minutes). Both chromatograms overlay with the 300 mM NaCl condition having a slightly higher peak height and correspondingly a slightly higher peak area, though the effect was very small.

The buffer salt concentration is different in many published HPLC methods but is most often 100 mM. [111, 123-125, 173, 175, 235] Ideally, the lowest concentration as possible would be used, as this is the least likely to cause a precipitation event and is a more economical use of reagents. Following method 2.4.7, we investigated the use lower concentrations (**Figure 4.14**). 25 mM buffer drastically impairs peak shape and peak metrics, the 50 mM buffer has visually impaired peak shape and peak metrics, while the 75 and 85 mM buffers appear visually almost identical. The 85mM buffer produced better plate numbers and resolution, as well as a larger absorbance for the dimer peak (Peak 1, 6.027 mins). 85 mM was the best concentration based on asymmetry and peak area, therefore, 85mM potassium phosphate was chosen as the optimum pH buffer.

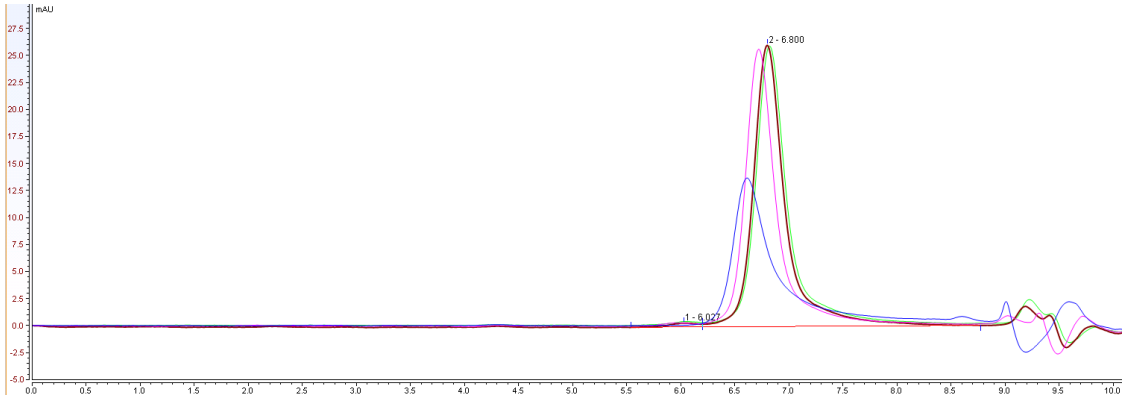

Figure 4.14. Chromatograms of an ADC using a phosphate buffer that is 25 mM (**Blue**), 50 mM (**Pink**), 75 mM (**Brown**) and 85 mM (**Green**). The X-axis is time (minutes). The stronger the concentration of phosphate buffer, the greater the peak height, peak area and lower the asymmetry.

The last way to reduce the risk of a precipitation event is to reduce the % of organic modifier in the mobile phase. Following method 2.4.8 we investigated the effect of different ratios of potassium phosphate buffer to IPA, (**Figures 4.15 and 4.16**). Increasing the concentration of IPA up to 20% was found to improved the peak shape and absorbance, but above 20% was found it increase asymmetry and reduce absorbance (**Figure 4.15**).

To find the optimal % of IPA we needed to identify the best balance of all peak metrics, including total absorbance, peak shape, plate number and column backpressure. While column backpressure is a limiting factor, the most important factor for us was the peak shape or the asymmetry, followed by absorbance or peak area and

then plate number. While following method 2.4.9, we found the column backpressure was inversely proportional to the IPA% and was unacceptable above 20%. Chromatograms at 14-17% IPA were compared and it was found above 16% plate number and asymmetry worsened, and below 16% asymmetry and total absorbance worsened. Thus 16% IPA was selected as the optimal percentage of IPA to use, see (**Figure 4.16**).

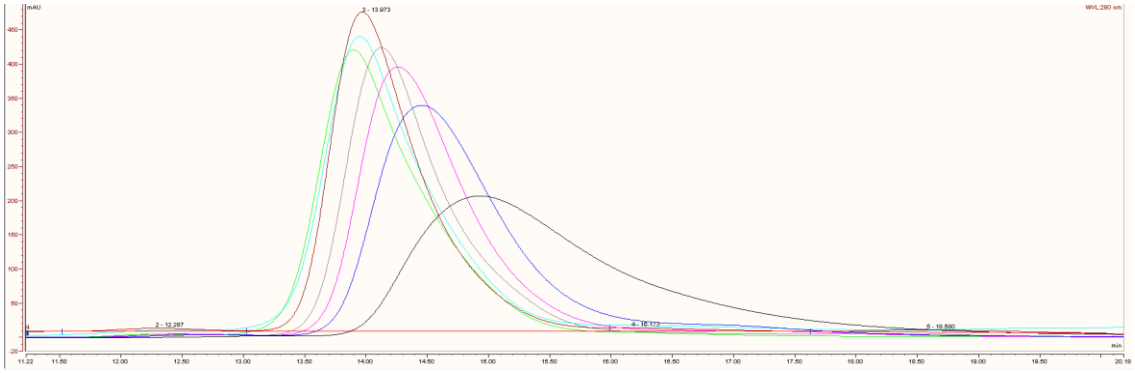

Figure 4.15. Chromatograms of trastuzumab emtansine with different total % of IPA in the mobile phase. 0% (**Black**), 5% (**Dark Blue**), 10% (**Pink**), 15 % (**Grey**), 20% (**Brown**), 25% (**Light Blue**), 30% (**Green**). The X-axis is time (minutes). 20% acetonitrile (**Brown**) gives the best result, with the greatest peak height, largest peak area and lowest asymmetry. It is a dramatic difference between 20% and 0%, demonstrating how much tailing occurs with no acetonitrile present.

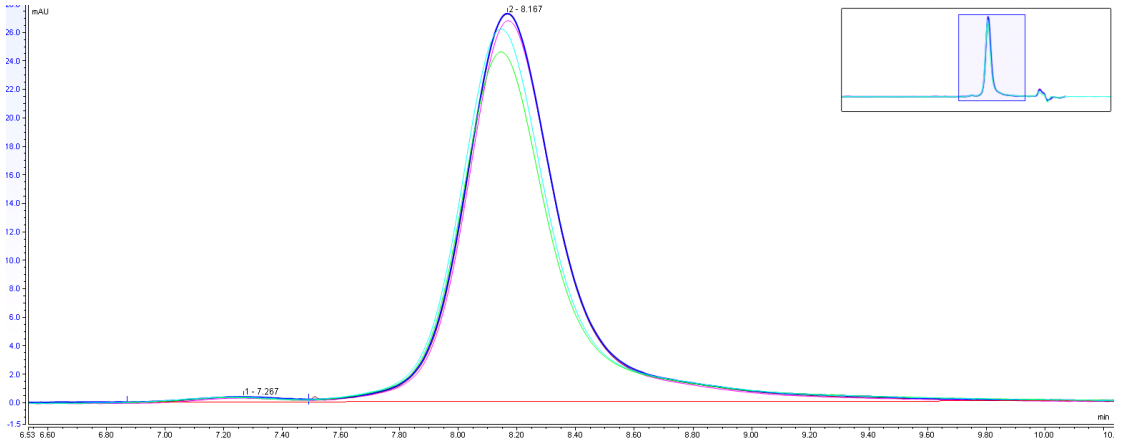

Figure 4.16. Chromatograms of trastuzumab emtansine with different total % of IPA in the mobile phase. 14% (**Green**), 15% (**Light Blue**), 16% (**Pink**), 16.5 % (**Brown**), 17% (**Dark Blue**). The X-axis is time (minutes). When the acetonitrile contact was 17 % (**Dark Blue**) has the greatest peak height and peak area but at 16 % (**Pink**) it had the best peak shape, with the lowest asymmetry and highest number of thermotical plates, between the dimer and monomer.

4.3.4 Adjusting HPLC running parameters

Column temperature for antibody SEC methods is typically set at room temperature, or 20/25 °C. Increasing the temperature of SEC analysis of proteins has been shown to improve the efficiency of separation but only at extremely elevated temperatures (150 °C). [177] This was not due to affecting the relative separation but by improving the fluid dynamics inside the column. [177,178] At more normal temperatures (<40 °C), the effects are very minimal, although it has been demonstrated that peak absorbances can be affected, as well as reducing column backpressure. The Bio-SEP 4000 column has a maximum operational backpressure of 1500 psi, and the method was running between 1000 and 1400 (depending on flow rate). Therefore, the effects of adjusting the temperature of the column oven were investigated, following method 2.4.10 (**Figure 4.17**). Pressure was inversely proportional to temperature, but total absorbance was greatest at 30 °C. Furthermore, peak shape at 40 °C was significantly affected with poor tailing. 30 °C was the optimum column oven temperature.

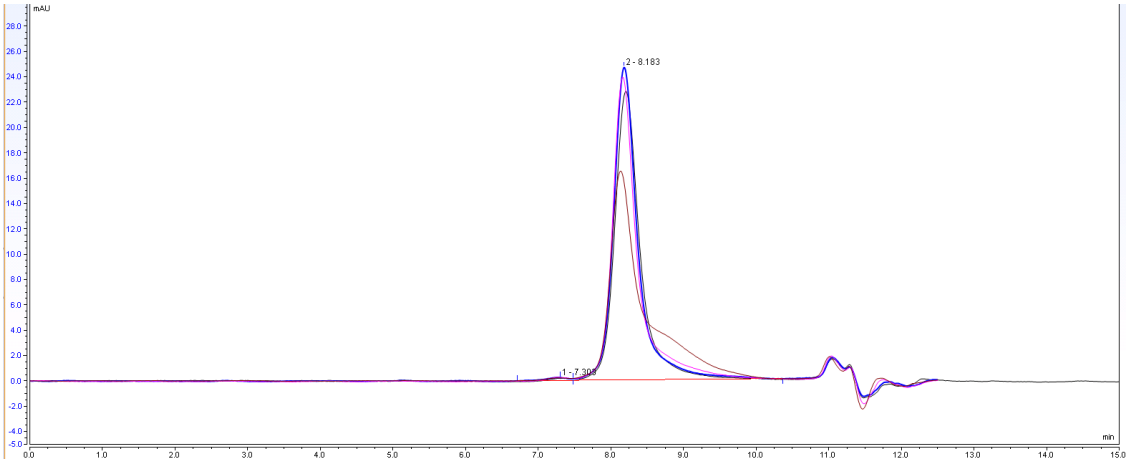

Figure 4.17. Chromatograms of an ADC method at 25 °C (**Black**), 30 °C (**Blue**), 35 °C (**Pink**) and 40 °C (**Brown**). The X-axis is time (minutes). At 40 °C (**Brown**) there is a very large increase in tailing, or possibly even a new peak emerging in the tail of the monomer peak. At 30 °C (**Blue**) the peak has the greatest height, area and lowest asymmetry.

Flow rate is directly proportional to backpressure, and it is known to affect, retention time, peak shape and even separation. [178] Ideally an HPLC method will be as short as possible, therefore the method ought to be as high a flow rate as possible, without compromising the separation or peak quality. The effect of varying the flow rate

between 0.5 and 1.5 mL/min was investigated, following method 2.4.11 (**Figure 4.18**). It was found increasing the flow rate improved the retention time and column asymmetry, but also decreased the total peak area and plate number. Retention time, plate number, peak area, resolution and asymmetry are inversely proportional to flow rate while backpressure is directly proportional to flow rate. As a high flow rate caused: higher pressure, reduced sensitivity of the method for dimers and trimers, and reduced peak resolution, 0.75 mL/min was chosen, as it appeared to be the best balance for overall method suitability.

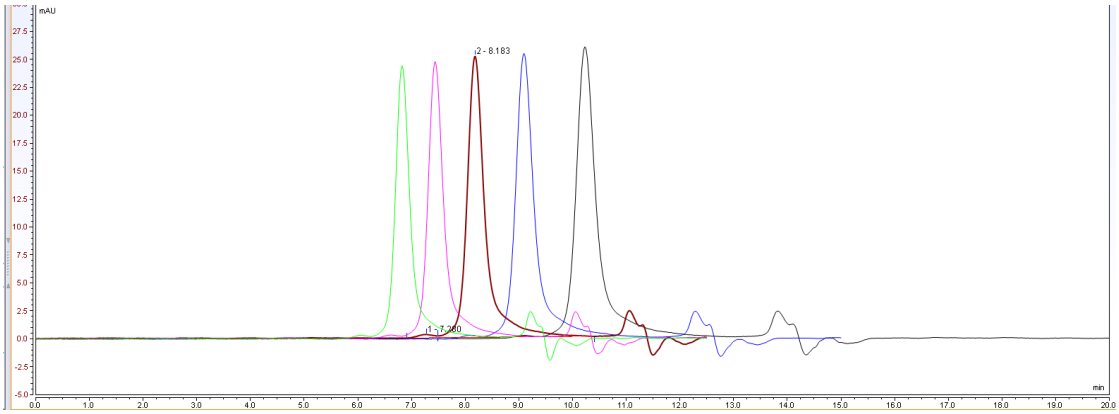

Figure 4.18. Chromatograms of an ADC run with different flow rates. 1.5 mL/min (**Green**), 1.25 mL/min (**Pink**), 1.0 mL/min (**Brown**), 0.75 mL/min (**Blue**) and 0.5 mL/min (**Grey**). The X-axis is time (minutes). Retention time is inversly proportional to the flow rate. With the shortest retention time of 6.8 minutes for 1.5 mL/min and the longest retention time of 10.5 minutes at 0.5 mL/min. Peak height and are was inversely proportional to flow rate too, with 0.5 mL/min producing the largest peaks.

4.3.5 The fully optimise' SEC method

The final method is as follows. Column of choice is a Phenomenex BioSep SEC-s4000 with dimensions 300 mm × 7.8 mm, particle size 5 µm and pore size 500 Å fitted with a guard column. Isocratic elution was performed with the mobile phase being a 15 : 85 mix of propan-2-ol / 100 mM potassium phosphate buffer (pH 6.80) containing 15mM NaN_3 as an anti-microbial agent. The column temperature was 30 °C, the injection volume was 20 µL and UV detection was set at 280 nm. The flow rate was 0.75 mL/min and the run time was 25 min, with the monomer peak eluting at 12.5 minutes (**Figure 4.19**). Compared to using the infliximab method, the asymmetry was 1.1, down from 1.7 and the plate number was 4597 up from 530.

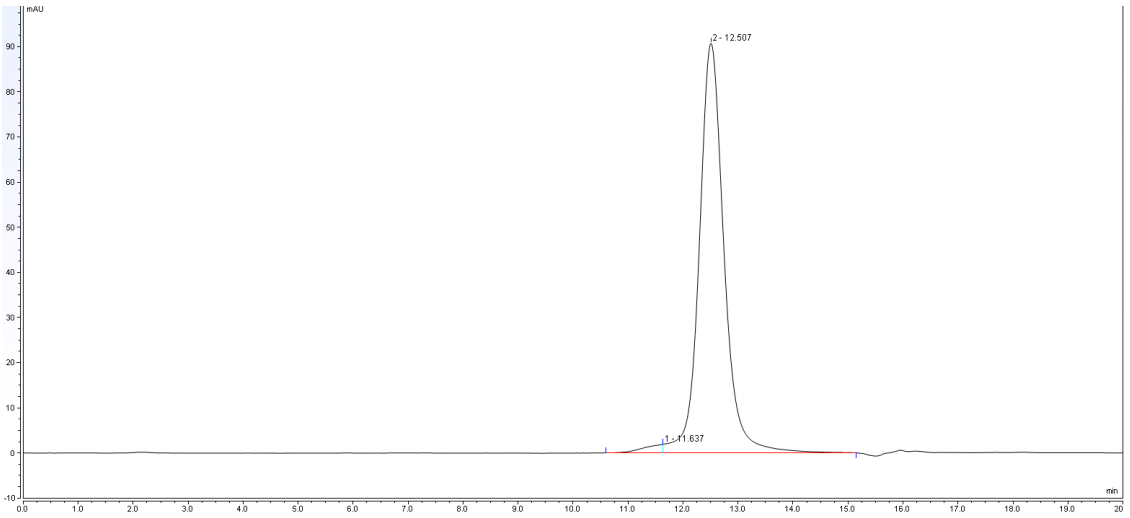

Figure 4.19. A chromatogram of a clinically high concentration of trastuzumab emtansine run using the final study method. The X-axis is time (minutes). Retention time of 12.5 minutes for the monomer and 6.5 minutes for the dimer.

4.3.6 Validation of the optimized size exclusion chromatography method

Size exclusion chromatography analysis of monomer concentration is a method used to determine the concentration of the active pharmaceutical ingredient, trastuzumab emtansine monomers. As such, it is outlined in the ICH guidance document Q2(R1) [105] that the linearity, precision, specificity and accuracy must be validated according to the limits stated in the ICH Q2(R1) document. Validation samples were prepared according to method 2.4.1 and degraded using methods 2.2.18 to 2.2.22.

The method must be demonstrated as having a linearity with an R^2 value of at least 0.999 for a range covering at least 20% higher and lower than the test concentrations. (**Figure 4.20**), plots the mean absorbance (n=3) of samples from 0.2 mg/mL to 2.0 mg/mL. The R2 value is greater than 0.9999 and is rounded up to 1 by Excel. The linearity exceeds the required minimum linearity for a concentration range greater than required for the proposed stability study.

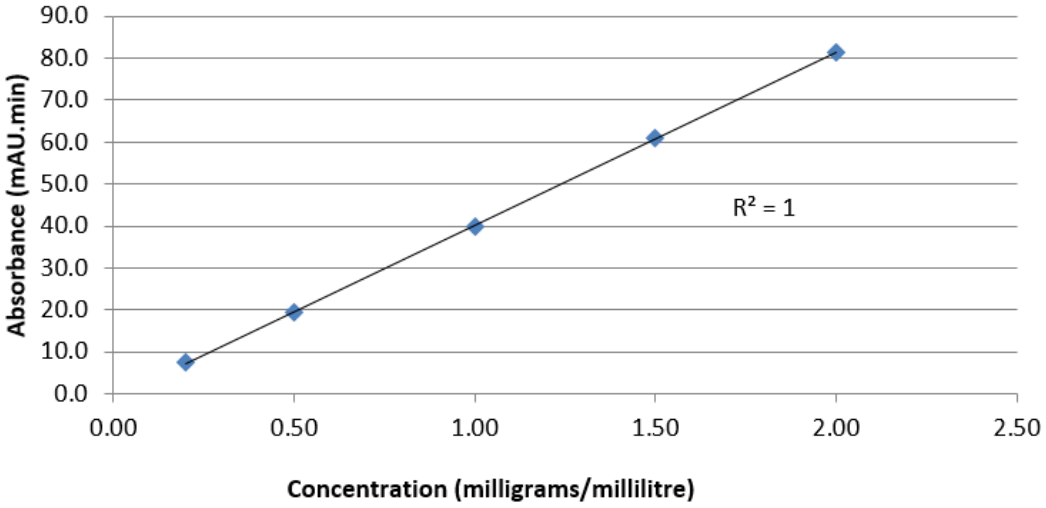

Figure 4.20. Size exclusion chromatography analysis of trastuzumab emtansine monomer concentration. Results are a mean (n=3). The R^2 = 0.9999 across the entire range

The method must be demonstrated as having a precision with a relative standard deviation of no more than 2% at each test concentration. (**Tables 4.2 - 4.4**) below, show the measured precision from six repeat injections at the clinically low, common and high concentration respectively. The determined relative standard deviations are all below 2%, indicating the method has suitable precision.

Concentration	Injection	Peak Area (mAu.min)	Relative SD (%)
	1	19.54	
	2	19.63	
	3	19.41	
Low	4	19.29	**0.60**
	5	19.41	
	6	19.47	
	Mean	**19.46**	

Table 4.2. Size exclusion chromatography precision determination at the clinically low concentration. The RSD of 0.6 % is well below the limit of 2.0 %, indicating the method is precise enough at the lowest concentration to be tested during the study.

Concentration	Injection	Peak Area (mAu.min)	Relative SD (%)
Common	1	41.90	**1.12**
	2	43.00	
	3	42.92	
	4	42.76	
	5	42.89	
	6	43.32	
	Mean	**42.80**	

Table 4.3. Size exclusion chromatography precision determination at the common concentration. This RSD will pass the limit of 2%, but it's the closest to failing of all the concentrations tested.

Concentration	Injection	Peak Area (mAu.min)	Relative SD (%)
High	1	62.43	**0.47**
	2	62.33	
	3	62.42	
	4	62.01	
	5	62.20	
	6	61.67	
	Mean	**62.18**	

Table 4.4. Size exclusion chromatography precision determination at the clinically high concentration. The RSD of 0.47 % is the best obtained for all concentrations of trastuzumab emtansine tested.

The size exclusion chromatography method must also be demonstrated to be specific, meaning it is able to detect degradants such as dimers and trimers. This is demonstrated by analysis and comparison of control samples of trastuzumab emtansine to force degradation samples. When photolytically degraded, a loss of monomer is detectable (**Figure 4.21**). When degraded via acid hydrolysis, a loss of monomer is detected (**Figure 4.22**). When degraded via base hydrolysis a large loss of monomer is observed along with the emergence of multiple fragments of trastuzumab emtansine with lower molecular weights than the monomer (**Figure 4.23**). When degraded via oxidation a loss of monomer is detected (**Figure 4.24**) and a large peak eluting at 16 minutes is due to a preservative in the hydrogen peroxide, it is not a degradation product. This data indicates this method is specific and stability indicating. Furthermore, it highlights the potential for fragmentation following base hydrolysis.

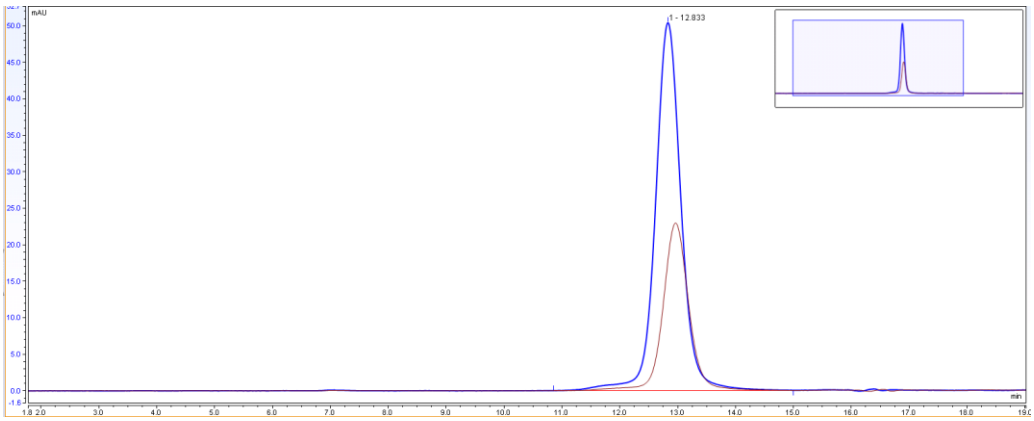

Figure 4.21. Size exclusion chromatogram of trastuzumab emtansine control (**Blue**) vs trastuzumab emtansine photolytically degraded (**Brown**). The X-axis is time (minutes). Peak height and peak area is reduced when comparing the control to degraded sample.

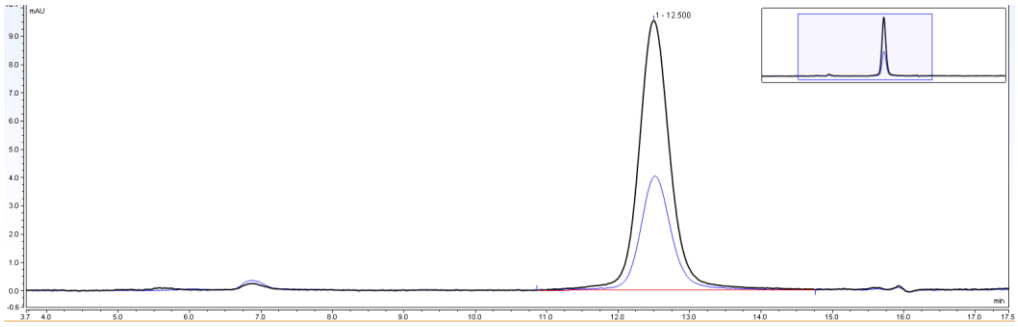

Figure 4.22. Size exclusion chromatogram of trastuzumab emtansine control (**Black**) vs trastuzumab emtansine acidically degraded (**Blue**). The X-axis is time (minutes). Peak height and peak area is reduced when comparing the control to degraded sample.

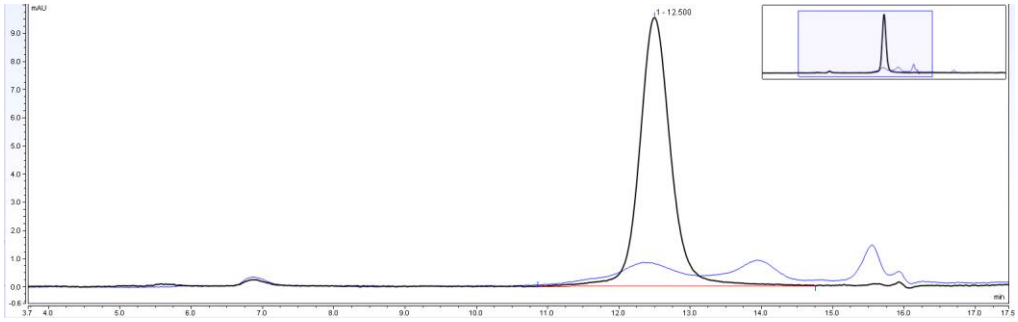

Figure 4.23. Size exclusion chromatogram of trastuzumab emtansine control (**Black**) vs trastuzumab emtansine degraded via base hydrolysis (**Blue**). The X-axis is time (minutes). Base degradation has caused a large loss of monomer peak area, as well induce the formation of more aggregates, show as larger peak areas to the left of the monomer peak, and more notably, the formation of fragments, seen at new peaks eluting to the right of the main peak.

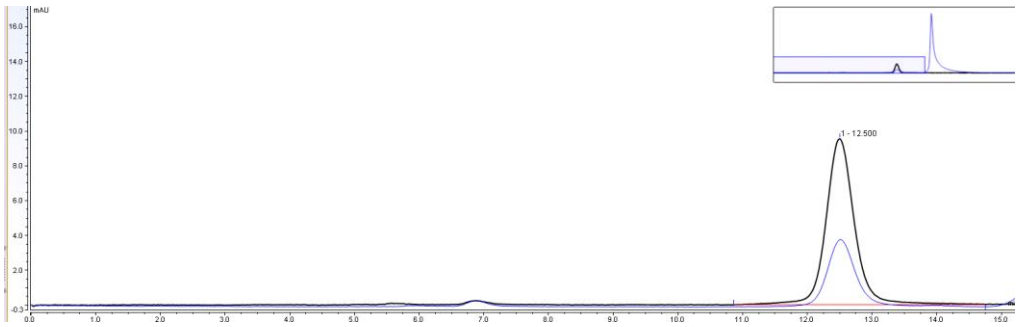

Figure 4.24. Size exclusion chromatogram of trastuzumab emtansine control (**Black**) vs trastuzumab emtansine degraded via oxidation (**Blue**). The X-axis is time (minutes). Degradation has presented itself as a loss of monomer peak height. No aggregates or fragments were detected.

If the size exclusion chromatography method is shown to be linear, precise and specific the accuracy can be inferred. This is useful, as no standards exist for testing accuracy of trastuzumab emtansine.

The limit of quantification (LOQ) must be less than 80% of the lowest test concentration. The LOQ can be calculated as the standard deviation of the y-intercept of the linearity graph, divided by the slope then multiplied by 10, as outlined in the ICH Q2 (R1) document. [105] The calculated LOQ is 0.09 mg/mL, less than 80% of the clinically low test concentration.

This size exclusion method has been demonstrated as linear, precise, specific, stability indicating, which allows the inference of suitable accuracy. This method is compatible with trastuzumab emtansine and validated to ICH Q2 (R1) standards.

4.4 Developing new methods for characterising secondary structure

4.4.1 Reviewing initial literature research

The next best alternative to CD was IR, as IR spectra can be compared to quantitative data sets (QDS) to estimate the amount of beta sheet and alpha helix present. This is due to the conformational sensitivity of the Amide 1 and 2 bands,

detected via IR spectroscopy. However, we did not have access to an appropriate instrument.

4.4.2 IR in practice – Visiting Bruker

Bruker has a UK based purpose-built facility for the demonstration and testing of their equipment. We travelled to Coventry multiple times with a selection of diluents, antibodies, infusion proteins and ADCs to test on their infra-red spectrometers. The samples needed to be tested were all liquids and even clinically high concentrations are low concentrations for most IR spectrometers. Initially a spectrophotometer fitted with a Bruker AquaSpec transmission cell module was tested. Mason *et al* have previously used a Bruker AquaSpec to analyse antibody structure. [148] The AquaSpec could be purchased with a prebuilt quantitative data set created and validated by Bruker. At clinically high concentrations (2 mg/mL) it was able to detect trastuzumab and a few other antibodies, but not trastuzumab emtansine. At supra clinical concentrations (10 mg/mL), it could detect trastuzumab emtansine, and could use the integrated QDS to estimate the structure of both trastuzumab emtansine and trastuzumab. The predictions were close to each other and similar to what would have expected for an antibody.

However, this set up was unsuitable as we would certainly need to assess structure at much lower concentrations than the AquaSpec was able to. It was found that at clinically low concentrations (<1 mg/mL) most of their spectrometers could not detect the protein, and many that could, had abysmal signal to noise ratios, most likely due to too short an absorbance pathlength.

The best equipment configuration was the Bruker Tensor 2 infra-red spectrophotometer (Bruker, Coventry, UK) fitted with a Harrick BioATR Cell 2 sample holder (Harrick Scientific Products, New York, USA) connected to a Huber Ministat 125 Peltier (Huber, Offenburg, Germany). The Harrick BioATR Cell 2 uses attenuated total reflectance to increase the contact area of the sample with the IR beam, therefore

increasing sensitivity. With this set up trastuzumab below clinically relevant concentrations was detectable, as well as above clinically relevant concentrations. However, there was no prebuilt QDS for the BioATR module.

Following discussions with my supervisor Dr Andrew Watts and Bruker UK's lead infra-red applications scientist Dr Christopher Stapleton, Bath ASU purchased the Tensor 2, with a BioATR module and Ministat peltier. The task of using these to construct and validate a new quantitative data set became a crucial part of the PhD project.

4.4.3 QDS – Design

A quantitative data set (QDS) is a library of spectra with known values. A QDS can be used to perform many functions depending on which samples are used to create the library and which characteristics or dimensions are known to affect FT-IR spectra. FT-IR spectra are conformationally sensitive, specifically to alpha helices and beta sheets. Furthermore, 1000s of published protein structures are freely available on the "Research Collaboratory for Structural Bioinformatics" (RCSB) "Protein Data Bank" (PDB). The PDB website contains published structural conformation data based on NMR, XRC & 3DCEM methods as well as primary sequences and prediction algorithms. A list of proteins with known structures on the PDB was constructed. Structures with at least two or three independent and close if not identical predicted structures were used. It was important to note the type of technique used to make these measurements, and the resolution of the technique, as these can be causes for dissimilar structure estimations. Thus, only XRC based atomic structure predictions were used. The atomic structure, as defined by XRC, is then processed by an algorithm such as DSSP [179] which generates a percentage of secondary structural features, such as alpha-helix and beta-sheet. To ensure consistency only the DSSP based estimations from PDB was used. STRIDE [180] and DSPP are the two main secondary structure prediction methods and have been demonstrated to have a 95% agreement on secondary structure[181], though DSSP tends to overpredict alpha-helices, while STRIDE overpredicts beta-sheet. DSSP data was used as it is the default algorithm on PDB. Furthermore, these exact proteins had to be

available to purchase at a reasonable price from Sigma Aldrich, many proteins can be produced by different organisms, and these proteins can have different structural conformations, even though they have the same name. While Brukers AquaSpec QDS is based on 43 proteins, only 14 proteins were selected, see (**Table 4.5**), which covered alpha-helix structures from 1% to 76%, and beta-sheet from 0% to 46%. CD structure predictions for antibodies and the AquaSpec's structure prediction for trastuzumab and trastuzumab emtansine informed us a range from about 4% alpha helix to 15% and from 30% beta sheet to 40% beta sheet was required. Furthermore, this QDS would be usable on more than just antibodies and ADCs. The QDS can work on any protein, therefore we expanded the range beyond what would have been required for just ADCs and mAbs to cover to improve future applicability of the QDS.

Protein Name	Organism	Size (kDa)	Alpha Helix (%)	Beta Sheet (%)	PDB Code	Literature Source
Hemoglobin	*Homo sapiens* (Human)	65.0	76	0	2DN1	Park *et al* 2006 [182]
Myoglobin	*Equus ferus* (Horse)	16.7	74	0	5CN5	Barends *et al* 2015 [183]
Albumin	*Bos taurus* (Cattle)	66.5	73	0	3V03	Majorek *et al* 2012 [184]
Peroxidase I	*Armoracia rusticana* (Horseradish)	44.0	49	4	1HCH	Berglund *et al* 2002 [185]
Lysozyme	*Gallus gallus domesticus* (Chicken)	14.3	41	10	5WRB	Sugahara *et al* 2017 [186]
Aldolase	*Leporidae* (Rabbit)	161.0	44	14	3B8D	Maurady *et al* 2002 [187]
Lipoxidase	*Glycine max (Soybean)*	*6.5*	40	14	3PZW	Chruszcz *et al* 2008 [188]
Catalase	*Bos taurus* (Cattle)	0.3	31	17	3RGS	Purwar *et al* 2011 [189]
Alcohol Oxidase	*Pichia pastoris* (Yeast)	0.7	30	20	5HSA	Koch *et al* 2016 [190]
Glucose Oxidase	*Aspergillus niger* (Fungus)	0.2	34	23	1CF3	Wohlfahrt *et al* 1999 [191]
Alcohol dehydrogenase I	*Saccharomyces cerevisiae* (Yeast)	146.0	28	29	4W6Z	Raj *et al* 2014 [192]
RNase A	*Bos taurus* (Cattle)	13.7	20	35	6ETK	Vergara *et al* 2018 [193]
Trypsin	*Sus* (Pig)	23.8	5	41	1S81	Transue *et al* 2004 [194]
Concanavalin A	*Canavalia ensiformis* (Jack bean)	52.0	3	46	1JBC	Parkin *et al* 1996 [195]

Table 4.5. The 14 proteins in the QDS, with their DSSP derived % alpha-helix and beta-sheet, molecular weight, species of origin, protein data bank code and the primary data source.

4.4.4 QDS – Construction

10 mg ± 0.1 mg of each of the 15 proteins was weighed out into a 10 mL volumetric flask. This was then reconstituted in 0.9% NaCl for injection to make a final concentration of 1 mg/mL. The Tensor 2, with the BioATR fitted, was purged for 30 minutes before the sample well was cleaned using 5% v/v Hellmannex III solution. The well was rinsed out with ultrapure water and dried with soft cotton buds (Lidl, London, UK). 20 µL of 0.9% NaCl for injection was pipetted into the sample well, then a background reading was taken. The settings for each sample measurement are described in (**Table 4.6**). Once the background had been fully acquired, the NaCl was completely drawn up and discarded using a 100 µL pipette (Gilson, Bedforshire, UK). Then 20 µL of a protein solution would be pipetted into the well. A measurement would be recorded, then the sample drawn up and discarded, the cell rinsed with ultrapure water, dried with a cotton bud then 20 µL of 0.9% NaCl for injection was pipetted into the sample well, then a background reading was taken. This was repeated until three spectra had been recorded for each protein solution. These 42 spectra were used to create the QDS. Once all the protein spectra had been captured, they were collated inside a QDS file using the OPUS "Setup Quant 2 Method" feature. Each protein's triplicate spectra were grouped together and assigned their alpha-helix and beta-sheet content inside the QDS builder. Then the 'Interactive Region Selection' tool was used to specify which regions of the spectra were to be calibrated and used for the conformational identification. The amide 1 and amide 2 bands were selected, (**Figure 4.25**), with a spacing set at 1 cm^{-1}.

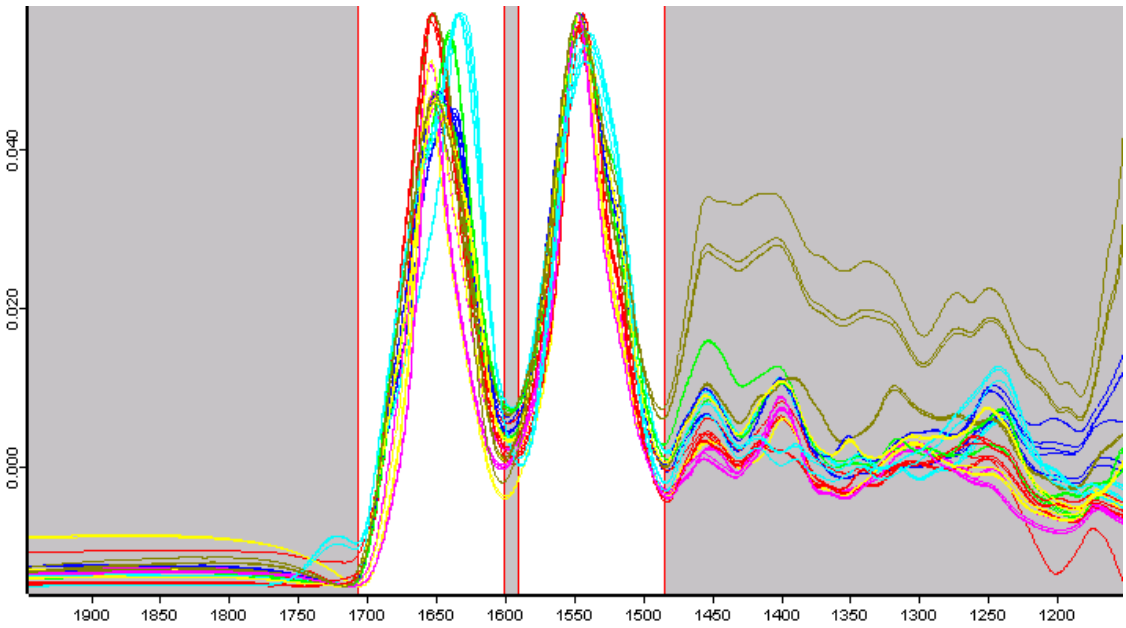

Figure 4.25. QDS spectra integration region selection for all 14 proteins that constitute the QDS. Amide 1 is detected between 1705 cm^{-1} and 1600 cm^{-1}, amide 2 is detected between 1590 cm^{-1} and 1485 cm^{-1}. X-axis is wavenumber (cm^{-1}). Y-axis is absorbance (AU). All 14 proteins have slightly different amide 1 and 2 bands.

Once the Amide 1 and 2 bands had been selected, investigations into the effect of the different pre-processing methods on the QDS were possible. OPUS offers 11 types of spectral pre-processing, with some options having further levels of optimisation.

The following quote is taken directly form the OPUS Quant User manual [196] "In quantitative analysis, the effective pathlength of the infrared light in the sample (sample thickness) is assumed to identical in all measurements. A lack of reproducibility in sample preparation can easily cause variations in sample thickness. If the thicknesses are different or unknown, this effect can be eliminated by a normalization of the spectra. The purpose of data pre-processing is to ensure a good correlation between the spectral data and the concentration values." Normalisation stretches a spectra along its y-axis to reduce visible differences based on magnitude, which is a factor dependent on concentration rather than structure.

Parameter	Setting
Resolution	4 cm^{-1}
Scans / sample	120
Scans / background	120
Scan Range	4000 cm^{-1} to 900 cm^{-1}
Result spectrum	Absorbance
Additional data treatment	H2Ocomp ([<FILE>:ScSm], [<FILE>:ScRf], [H2O=7]);
Data blocks to be saved	Absorbance / Single Channel / Background
External Synchronisation	Off
Source Setting	MIR
Beamsplitter	KBR
Optical Filter	Open
Aperture Setting	6 mm
Measurement Channel	Sample Compartment
Detector Setting	LN-MCT Photlovlotaic [Internal]
Scanner velocity	15 KHz
Measurement Signal Gain	Automatic
Measurement preamp Gain	Reference
Delay before measurement	0 seconds
High pass filter	ON
Low pass filter	Automatic
Acquisition mode	Double Sided, Forward-Backward
Correlation Mode	OFF
Phase resolution	32
Phase correction mode	Power Spectrum
Apodization Function	Blackman-Harris 3-Term
Zerofilling Factor	4

Table 4.6. Table detailing the IR acquisition settings for each measurement.

The following methods can be applied within the OPUS quant builder:

- Linear Offset Subtraction shifts the spectra to set the y-minimum to zero.
- Straight Line Subtraction fits a straight line to the spectrum and subtracts it. This accounts for a tilt in the recorded spectrum.
- Vector Normalization normalizes a spectrum by first calculating the average intensity value and subsequent subtraction of this value from the spectrum. Then the sum of the squared intensities is calculated, and the spectrum is divided by the square root of this sum. This method is used to account for different samples thickness, for example.
- Min-Max Normalization first subtracts a linear offset and then sets the y-maximum to a value of 2 by multiplication with a constant. Used like the vector normalization.
- Multiplicative Scatter Correction performs a linear transformation of each spectrum for it to best match the mean spectrum of the whole set. This method is often used for spectra measured in diffuse reflection.
- First Derivative calculates the rate of change of the spectrum. This method emphasizes steep edges of a peak. It is used to enhance small features over a broad background. Spectral noise is also enhanced. (To exemplify, the first derivative of a distance time graph is speed)
- Second Derivative calculates the rate of change of the first derivative graph. It is used to greatly enhance small features over a broad background. Spectral noise is also greatly enhanced. (To exemplify, the second derivative of a distance time graph is acceleration)

Furthermore, first derivative method can be used in combination with Min-max, straight line subtraction or vector normalisation. No general recommendation can be given whether a given data set should be pre-processed or which method is suited best for it. Therefore, the optimal data pre-processing method can only be found empirically by applying several methods to your spectral data and comparing the results.

There are four metrics that can be used to evaluate the QDS method. The R^2 value, the root mean square error of the coefficient of variation (RMSECV), the residual

predictive deviation (RPD) and bias. According to the Bruker Quant manual, the most capable QDS method will be the one with the lowest RMSECV and highest RPD. Although R^2 and bias can also be useful indicators when methods have similar RPDs and RMSECVs. A cross validation within OPUS to measure these values for each type of pre-processing possible was performed (**Table 4.7**). First derivative + Vector normalization and First derivative + Multiplicative scattering appeared to be the best. The five best methods were taken and the mean cross validation metrics of alpha and beta compared to select the best pre-processing method available (**Table 4.8**). The best method was 'First derivative + Vector Normalisation'. This method has an adjustable smoothing at 5, 9, 13, 17, 21 and 25. Effect of this smoothing were investigated (**Table 4.9**) and found that higher levels of smoothing improved the Alpha helix prediction but worsened the beta sheet prediction. An average of the alpha and beta sheet metrics was calculated (**Table 4.10**), finding 25 levels of smoothing was better overall as alpha helix prediction improvement is greater than loss in beta sheet.

Pre-processing method	Structure	R^2	RMSECV	RPD	Bias
None	Alpha	73.46	11.3	1.95	0.987
	Beta	68.32	7.88	1.79	-0.899
Linear Offset Elimination	Alpha	57.7	14.2	1.55	1.53
	Beta	45.54	10.3	1.37	-1.42
Straight line subtraction	Alpha	60.31	13.8	1.6	1.6
	Beta	53.67	9.52	1.48	-1.34
Vector Normalization	Alpha	84.91	8.48	2.59	-0.929
	Beta	84.14	5.57	2.51	0.008
Min-Max Normalization	Alpha	88.78	7.31	2.99	-0.272
	Beta	84.58	5.5	2.55	0.336
Multiplicative scattering correction	Alpha	87.78	7.63	2.86	-0.299
	Beta	86.67	5.11	2.74	0.233
First Derivative	Alpha	67.75	12.4	1.76	0.136
	Beta	76.78	6.74	2.08	-0.336
Second Derivative	Alpha	73.72	11.2	1.95	-0.333
	Beta	74.84	7.02	2	0.567
First Derivative + Straight line subtraction	Alpha	67	12.5	1.74	-0.17
	Beta	72.5	7.34	1.91	0.219
First Derivative + Vector Normalization	Alpha	88.26	7.48	2.92	-0.445
	Beta	89.43	4.55	3.08	0.066
First Derivative + Multiplicative Scattering	Alpha	87.29	7.78	2.81	-0.028
	Beta	88.15	4.82	2.91	-0.027

Best
Good
Average
Bad
Worst

Table 4.7. QDS cross validation evaluation metrics. First derivative + vector normalisation produced the best measurements, while linear offset produced the least linear estimations.

Pre-processing method	Structure	R^2	RMSECV	RPD	Bias
Vector Normalization	Total	84.53	7.03	2.55	-0.46
Min-Max Normalization	Total	86.68	6.41	2.77	0.03
Multiplicative scattering correction	Total	87.23	6.37	2.8	-0.03
First Derivative + Vector Normalization	Total	88.85	6.02	3	-0.19
First Derivative + Multiplicative Scattering	Total	87.72	6.3	2.86	-0.03

Best
Good
Average
Bad
Worst

Table 4.8. QDS cross validation evaluation metrics averaged between alpha helix and beta sheet. First derivative + vector normalisation produced the best measurements, while linear offset produced the least linear estimations.

Method	Structure	Smoothing	R^2	RMSECV	RPD	Bias
First Derivative + Vector Normalization	Alpha Helix	5	87.26	7.79	2.81	-0.43
		9	87.38	7.76	2.82	-0.44
		13	87.55	7.70	2.84	-0.44
		17	87.77	7.64	2.86	-0.44
		21	88.01	7.56	2.89	-0.44
		25	88.26	7.48	2.92	-0.45
	Beta Sheet	5	89.67	4.50	3.11	0.16
		9	89.67	4.50	3.11	0.15
		13	89.65	4.50	3.11	0.13
		17	89.62	4.51	3.10	0.11
		21	89.55	4.52	3.09	0.09
		25	89.43	4.55	3.08	0.07

Table 4.9. QDS cross validation evaluation metrics for alpha helix and beta sheet individually. Alpha helix is best estimated with a larger degree of smoothing, produced the best R^2, RMSECV and RPD, however beta sheet is best estimated using the least amount of smoothing.

Method	Structure	Smoothing	R^2	RMSECV	RPD	Bias
First Derivative + Vector Normalization	Total	5	88.47	6.15	2.96	-0.14
		9	88.53	6.13	2.97	-0.15
		13	88.60	6.10	2.98	-0.16
		17	88.70	6.08	2.98	-0.17
		21	88.78	6.04	2.99	-0.18
		25	88.85	6.02	3.00	-0.19

Table 4.10. The mean QDS cross validation evaluation metrics of alpha helix and beta sheet. Comparing the effect of different smoothing values on prediction capability. It is clear now that the improvement to alpha helix prediction at higher levels of smoothing outweigh the detriment to beta-sheet prediction.

Overall, structure prediction is better with more smoothing, being best at level 25 for all evaluation metrics except bias, which favours a smoothing value of 17, and gets worse with more or less smoothing applied.

The last variable is the partial least squares (PLS) rank fit, which can vary from 1-10, but is automatically chosen for alpha helix and beta sheet, though they can be manually adjusted if necessary, see (**Figure 4.26 A & B**). Quant builder automatically identifies the optimal rank as 2 for alpha helix and 1 for beta sheet. The final pre-processing method was First Derivative + Vector Normalization, with a smoothing level of 25, see (**Figure 4.27 & Table 4.11**).

Structure	R^2	RMSECV	RPD	Bias
Alpha	88.26	7.48	2.92	-0.445
Beta	89.43	4.55	3.08	0.066

Table 4.11. The R^2, RMSECV, RPD and Bias for alpha helix and beta sheet are listed in (**Figure 4.27**). The prediction for beta sheet is better than the prediction for alpha helix but both have excellent levels of bias and have R^2 values of almost 90.

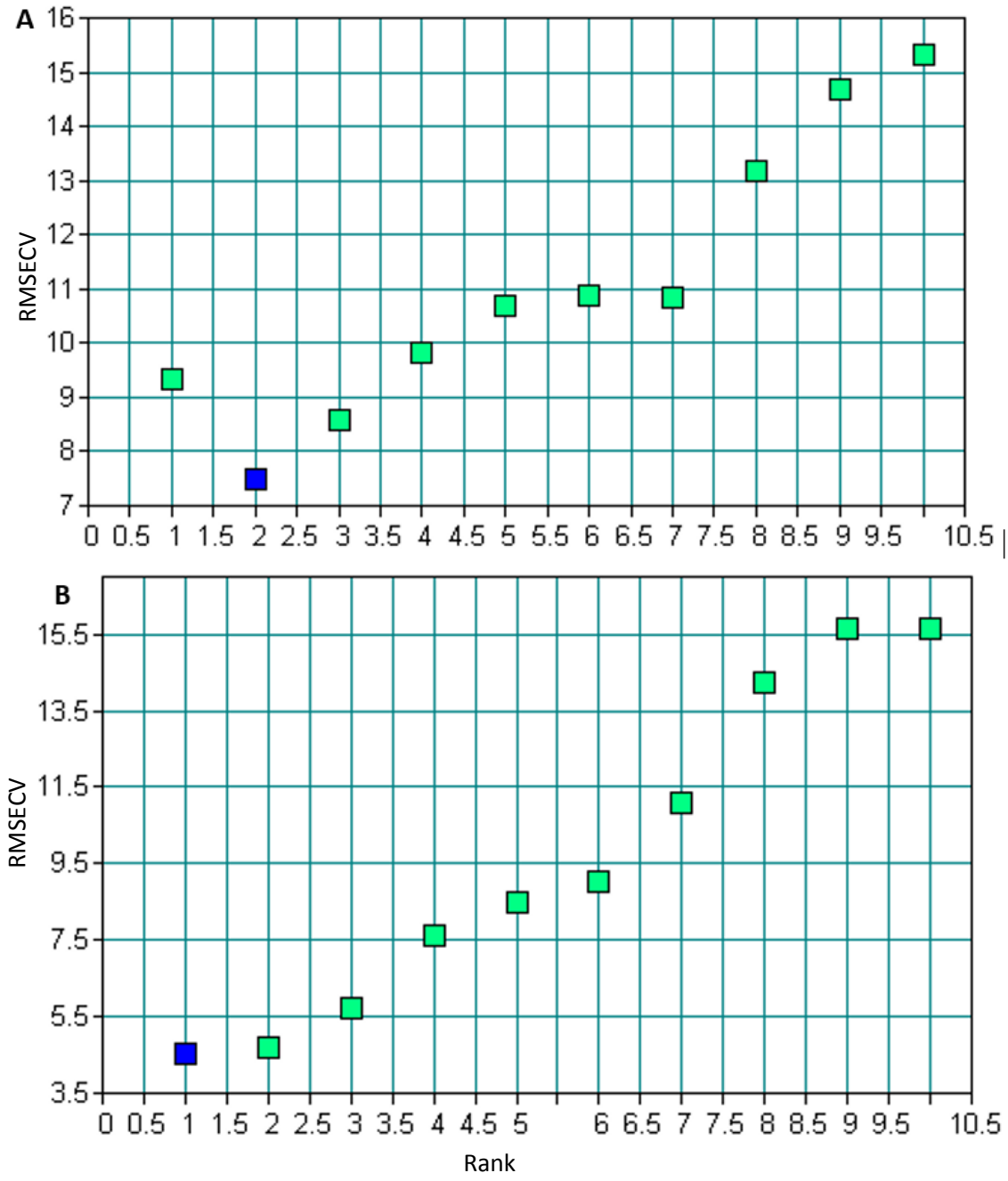

Figure 4.26. The RMSECV (Y-Axis) vs Rank (X-Axis) for alpha helix (**A**) and beta sheet (**B**). The lowest value of RMSECV at any rank

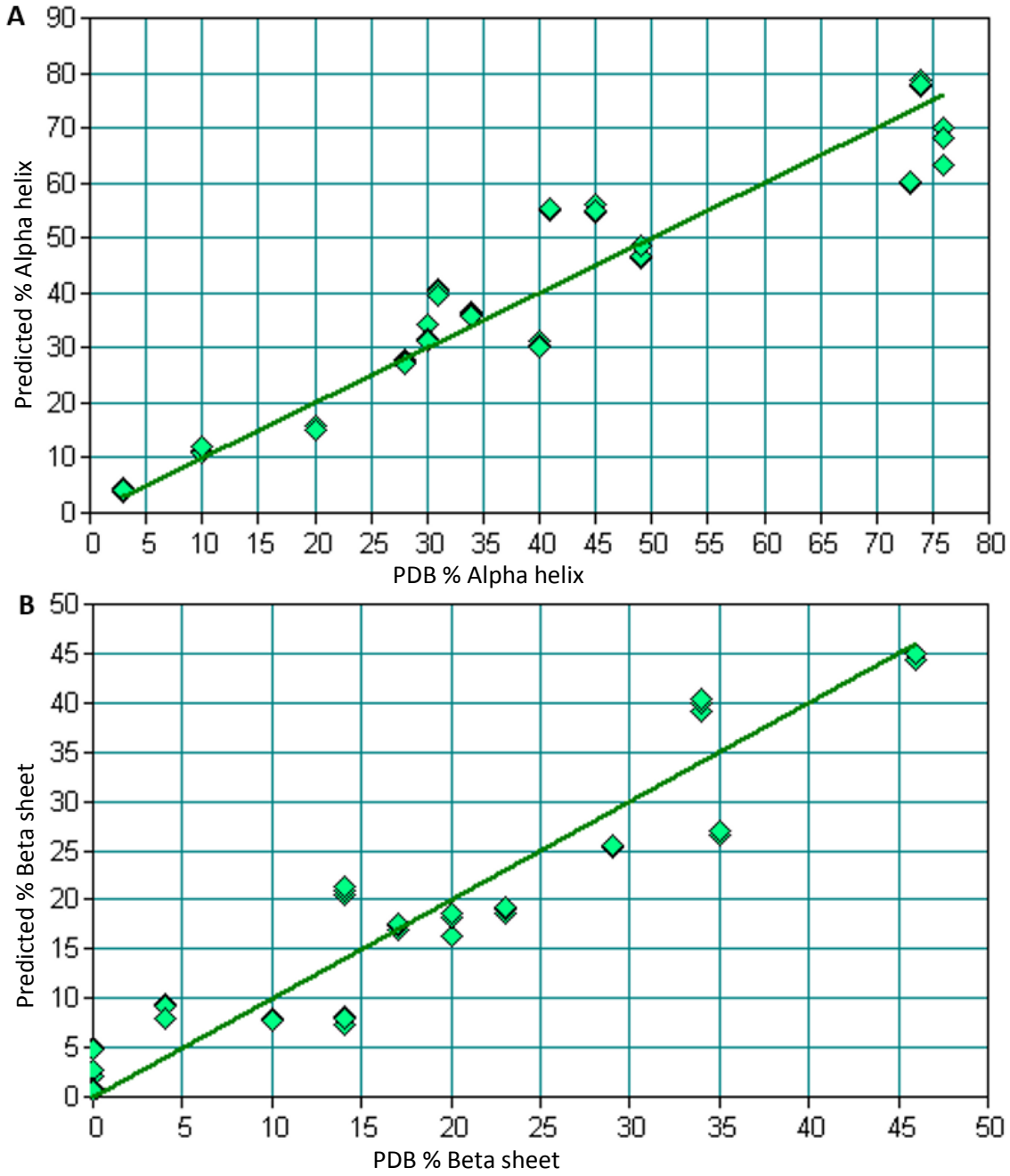

Figure 4.27. Plots of the predicted (Y-axis) vs PDB (X-Axis) values of % alpha helix (**A**) and beta sheet (**B**). Both alpha helix and beta sheet predicted values correlate well with the protein data base values.

4.4.5 QDS – Validation

While the QDS method had already been through an extensive cross validation it is important to compare results to validated method, such as circular dichroism spectroscopy, to ensure the predictions for antibodies are not too dissimilar, as that may suggest the pre-processing method is over-fitting the data causing false structures to be predicted. To do this, 12 different therapeutic antibodies were measured in triplicate via IRS and then tested via CDS, following method 2.4.13. The results showed mostly similar structures (**Figure 4.28**) with pertuzumab and infliximab having the greatest and smallest difference in % alpha helix respectively (**Table 4.12**) and bevacizumab and cetuximab having the greatest and smallest difference in beta sheet respectively (**Table 4.12**). It is not required for these methods to be statistically equivalent, as it is well documented no secondary structure predictive test is 100% accurate, and even the most commonly used do not have 100% agreement. However, it is promising to see that almost two thirds of the antibodies had statistically insignificant differences for either alpha helix or beta sheet and a third had no statistically significant difference at all.

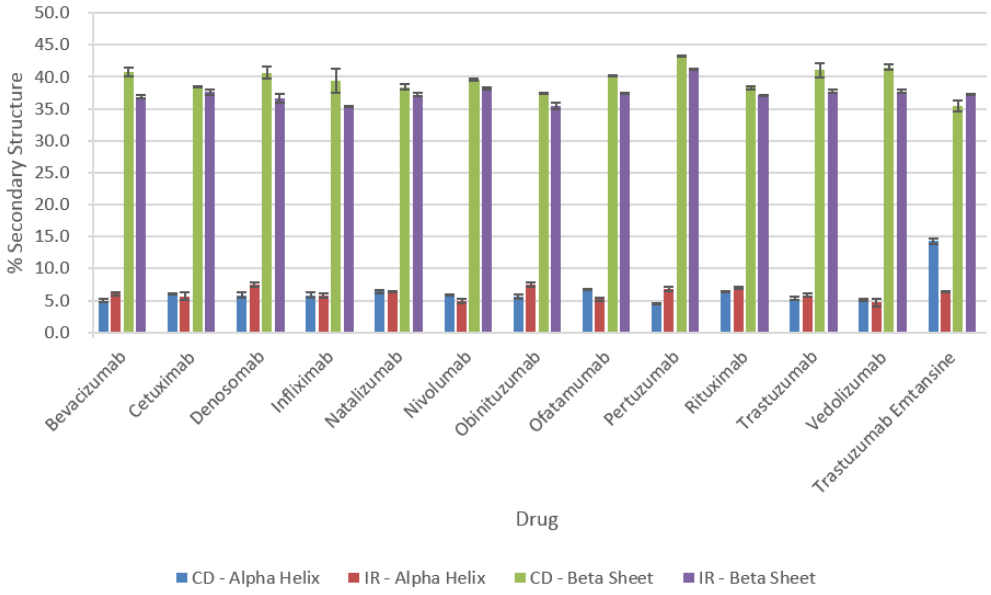

Figure 4.28. A comparison of CD secondary structure predictions vs IR secondary structure predictions. Note the difference in alpha helix prediction for trastuzumab emtansine. Statistics are presented in (**Table 4.12**). Both techniques predict similar secondary structure values for most of antibodies for example cetuximab or natalizumab, but in some circumstances are notably different for example ofatumumab or pertuzumab.

IR prediction difference from CD prediction				
Sample	**Alpha Helix**	**SD**	**Beta Sheet**	**SD**
Bevacizumab	+1.1 ***	0.5	-3.9 ****	0.9
Cetuximab	-0.3	0.7	-0.8	0.6
Denosomab	+1.6 ****	0.8	-4.0 ****	1.6
Infliximab	+0.0	0.8	-4.1 ****	2.0
Natalizumab	-0.1	0.3	-1.2	0.7
Nivolumab	-0.9 *	0.5	-1.4	0.4
Obinituzumab	+1.9 ****	0.6	-2.0 **	0.7
Ofatumumab	-1.5 ****	0.4	-2.6 ****	0.2
Pertuzumab	+2.2 ****	0.4	-2.1 **	0.2
Rituximab	+0.5	0.2	-1.2	0.3
Trastuzumab	+0.5	0.5	-3.3 ****	1.4
Vedolizumab	-0.4	0.7	-3.8 ****	0.7
Average mAb	***+0.4***	***0.5***	***-2.5***	***0.8***

No Significant Difference
One Significant Difference
Both Significantly Different

Table 4.12. Absolute difference between the IR prediction and the CD prediction of alpha helix and beta sheet including standard deviation and results of statistical analysis. The alpha helix and beta sheet content are significantly different for 4 of the antibodies tested, either a alpha or beta was different for 5 of the antibodies tested and there were no significant differences for 3 of the antibodies tested. *, **, *** & **** indicate a p value < 0.05, 0.01, 0.001 & 0.0001 respectively.

Comparing trastuzumab to trastuzumab emtansine via IR shows results that agree with the literature (**Figure 4.29**). A two-way ANOVA showed a statistically significant difference between the alpha-helix prediction between trastuzumab and trastuzumab emtansine via CD but not IR.

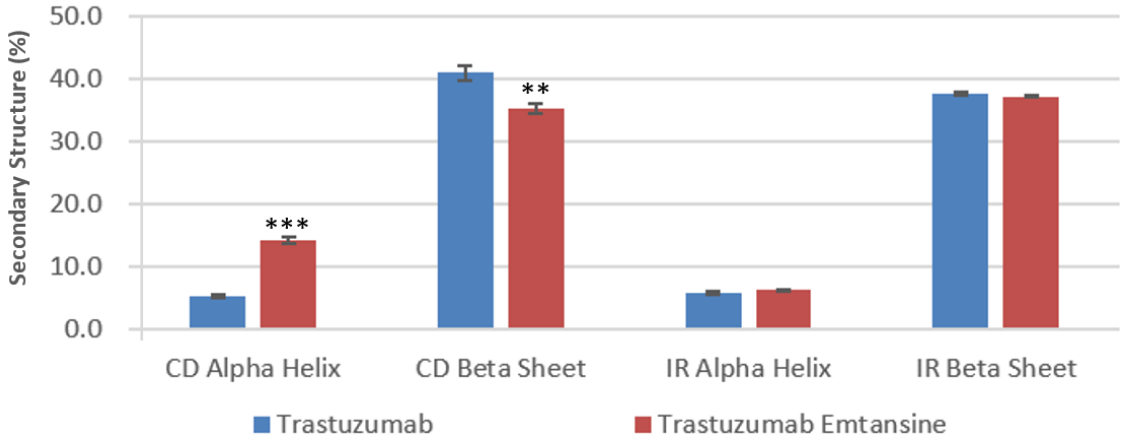

Figure 4.29. IR and CD prediction of alpha helix and beta sheet for trastuzumab and trastuzumab emtansine. IR analysis of trastuzumab emtansine's alpha helix and betas sheet content shows no significant differences compared to the trastuzumab structure. CD analysis shows significant levels of difference for both alpha helix and beta sheet. ** & *** indicate a p value < 0.01 & 0.001 respectively.

IR secondary structure determination using the QDS has been shown to predict very similar values to CD based methods when testing antibodies (**Figure 4.28 & Table 4.12**). However, unlike CD methods, the IR method detects no significant difference between the secondary structure of trastuzumab vs trastuzumab emtansine.

The IR method has been demonstrated as stability indicating, following method 2.4.14 (**Figures 4.30 & 4.31**), and a good predictor of both alpha helix and beta sheet secondary structure composition. By designing, building and validating this quantitative data set for infrared spectroscopy analysis, the problems encountered with the original circular dichroism analysis method had been overcome. Now characterisation of an ADCs higher order structure is possible using a rapid IRS test, a big step towards enabling an NHS compliant stability study to be performed. While secondary structure characterisation won't detect tertiary structure events such as misfolding, it still meets the required guidance requirements, and IR is a viable alternative to the traditional CD based secondary structure determination.

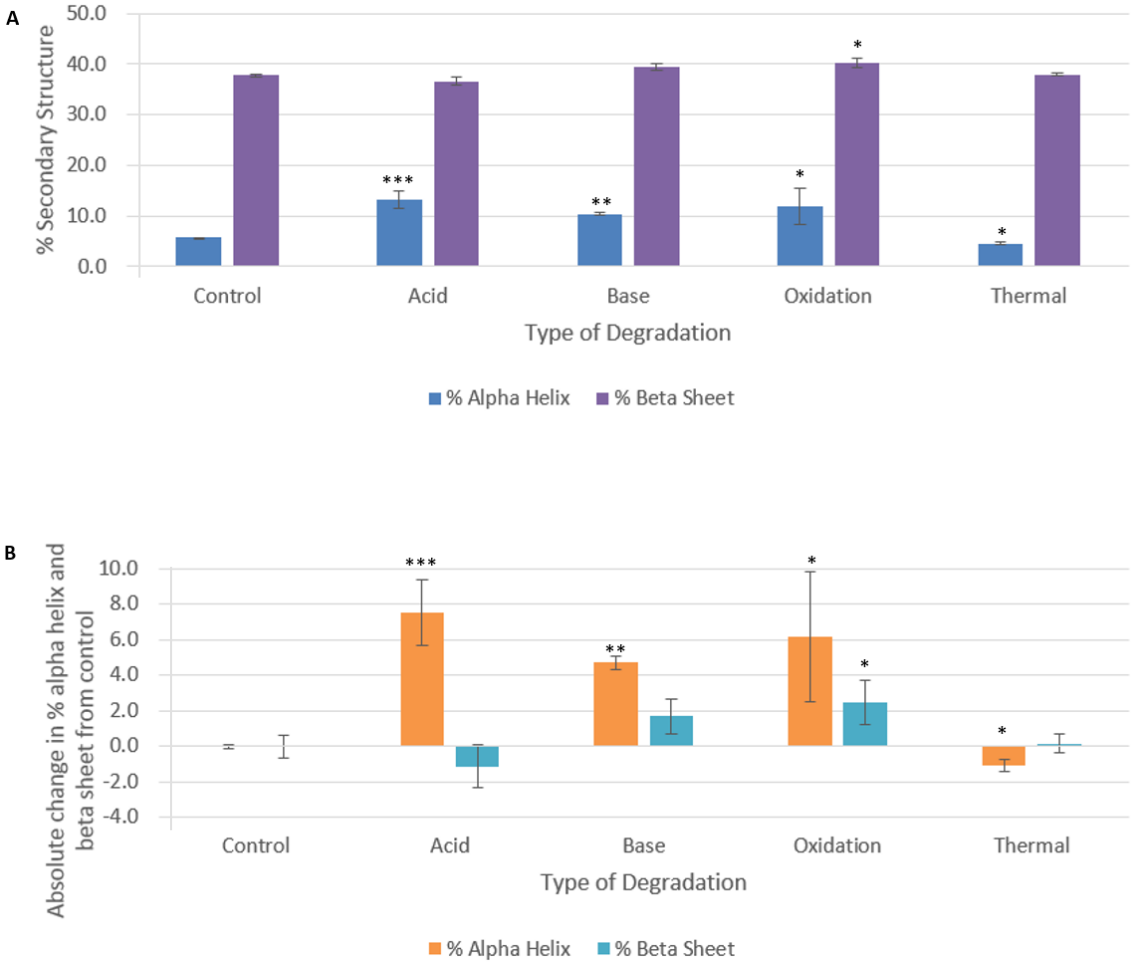

Figure 4.30. IR analysis of forced degradation of obinituzumab higher order structure presented as total % alpha helix and beta sheet (**A**) and (**B**) absolute change in % alpha helix and beta sheet from control. Acid and base hydrolysis had the most significant effect on alpha helix content while oxidation had the most significant impact of beta sheet. Only thermal degradation caused a significant decrease in alpha helix. *, ** & *** indicate a p value < 0.05, 0.01 & 0.001 respectively.

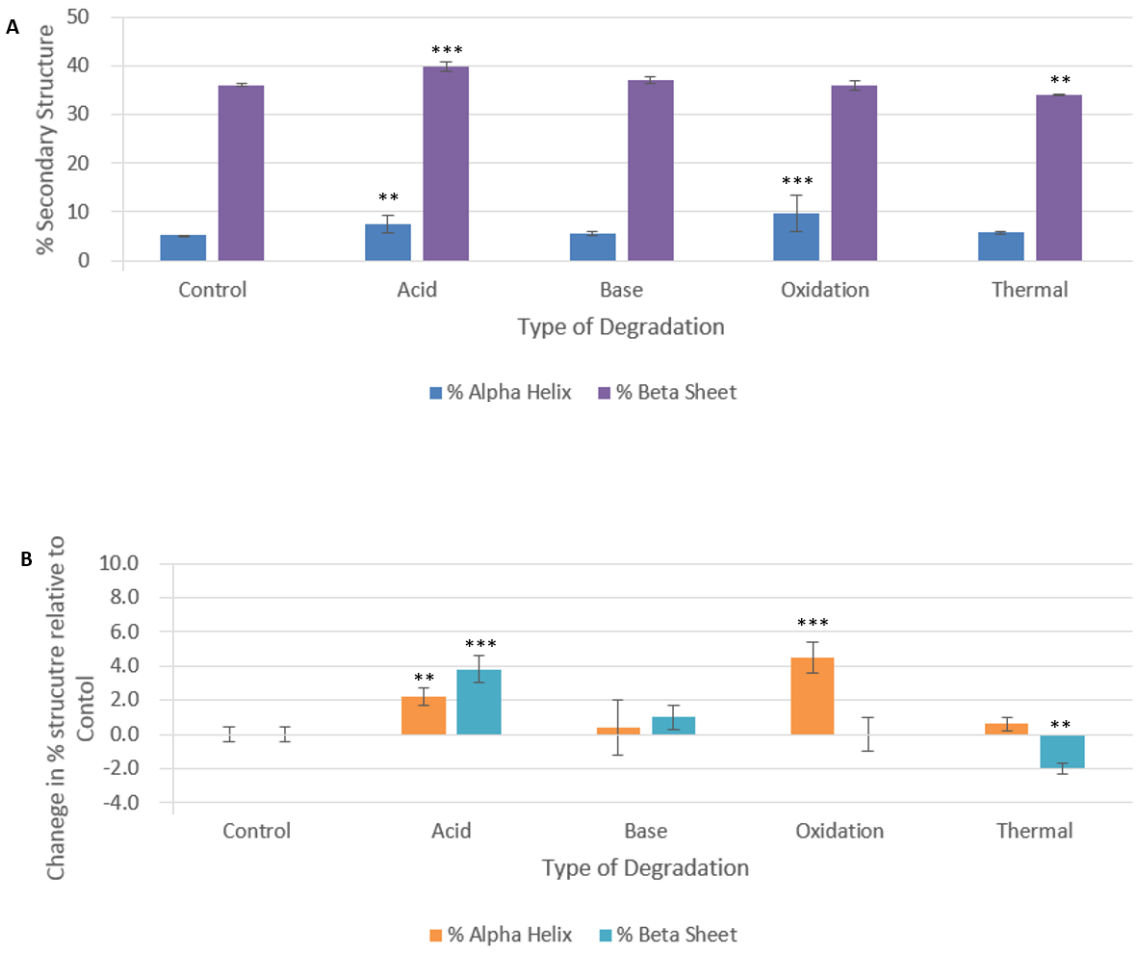

Figure 4.31 IR analysis of forced degradation of trastuzumab emtansine's higher order structure presented as (**A**) total % alpha helix and beta sheet and (**B**) absolute change in % alpha helix and beta sheet from control. Acid degradation caused the most significant change, with differences noted in the alpha helix and beta sheet, while oxidation and thermal only caused significant changes to either alpha helix or beta sheet. Base degradation did not cause any significant changes, however slight increases to both alpha helix and beta sheet are seen. *, ** & *** indicate a p value < 0.05, 0.01 & 0.001 respectively.

4.5 Methods to measure DAR

4.5.1 Reviewing initial literature research

No standard method is used for measuring an ADCs DAR is listed in the NHS or ICH guidance. That is because ADCs are not covered by these documents. Furthermore, literature research has shown that the site of payload attachment, currently either a lysine or cysteine residue, has a significant effect on drug heterogeneity. More specifically, ADCs that utilize attachment via lysine are dramatically more variable due the number and location of accessible lysine residues.

For ADCs with cysteine linked residues either high resolution mass spectrometry or hydrophobic interaction chromatography (HIC) can be used to measure the DAR. HIC is favoured due to its much lower entry cost, running costs and level of required expertise. For lysine linked ADCs HIC struggles to work due to the vast heterogeneity causing a near infinite spread of hydrophobicity. Therefore, no resolution of peaks is possible. Hence, high resolution mass spectrometry, more specifically MALDI-TOF MS is the only technique that appears to be used to assess DAR in lysine linked ADCs. [89,197,198]

4.5.2 HIC trials

In 2005 and 2011 Hamblett *et al* [199] *and Wakanker et al* [173] used HIC methods to quantify the DAR of a cysteine linked ADC. It was decided to replicate that work and to investigate if using more modern column technologies could separate the different DARs of trastuzumab emtansine using HIC.

Wakanker used a Tosoh Butyl-NPR column and was able to separate the DAR 0, 2, 4, 6 and 8 peaks, of a cysteine linked ADC, from each other at 280nm. This work was repeatable, following method 2.4.15 (**Figure 4.32**). We were also able to identify the

DAR 1, 3, 5, and 7 peaks, although these are so small they are hard to identify, especially DAR 5 and 7.

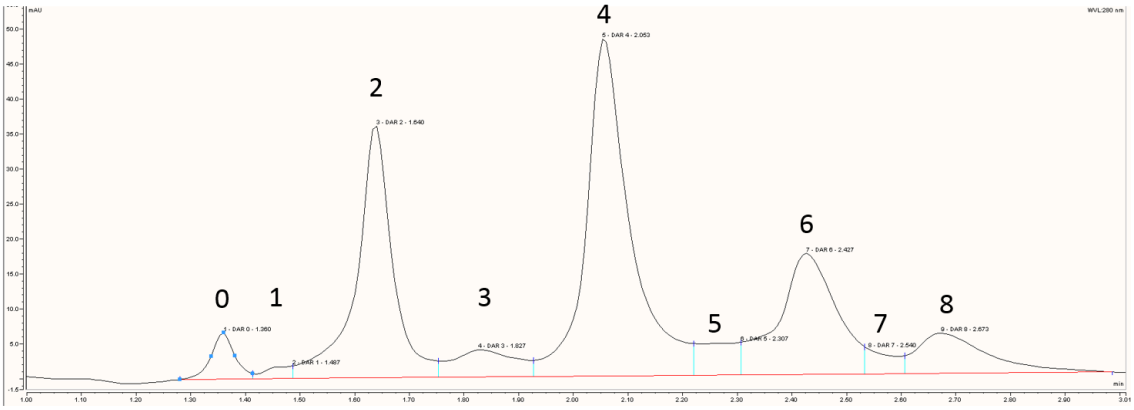

Figure 4.32. HIC analysis of a cysteine linked ADC (brentuximab vedotin), showing full separation of DARs 0, 2, 4, 6 and 8. Peaks for DARs 1, 3, 5 and 7 have been labelled. The X-axis is time (minutes).

The method was repeated on trastuzumab emtansine, but it only produced a single large band with no separation of any DARs (**Figure 4.33**). This agrees with the literature as HIC has not been successfully used to assess a lysine linked ADCs DAR [173].

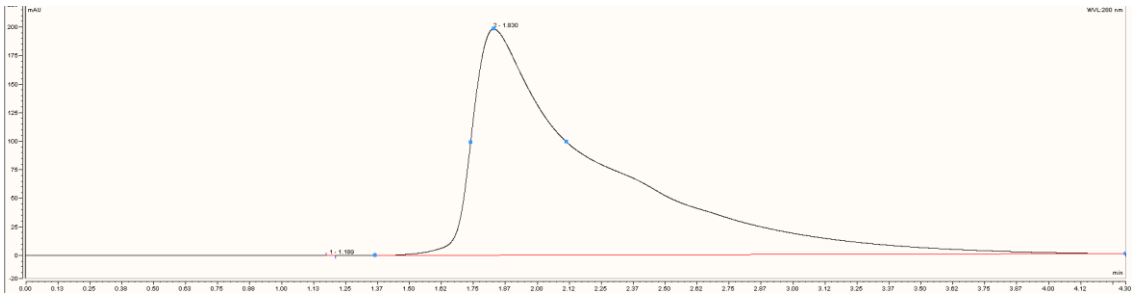

Figure 4.33. HIC analysis of a lysine linked ADC (trastuzumab emtansine) on a TOSOH Butyl-NPR, showing no separation of DARs 0, 1, 2, 3, 4, 5, 6, 7 and 8. The X-axis is time (minutes).

To investigate if more modern chromatography technology could improve the separation of trastuzumab emtansine, a ThermoFisher Scientific MAbPac HIC-10 column with pore size of 5 µm, internal diameter of 4.6 mm and length of 100 mm, was purchased. This column had been advertised in the literature as able to separate and produce peaks of a cysteine linked antibody with all DAR forms resolved and producing distinguishable peaks, a clear improvement over the methods that Wakankar and Hamblett had been using and compared to the Tosoh-Butyl-NPR column. Following the method used in the ThermoFisher application note (method 2.2.15) , it was not possible to generate acceptable spectra for trastuzumab emtansine, though there were hints of

peaks. To improve the separation, the concentration of ammonium sulphate in mobile phase A, was increased from 1.5 M to 3 M, the concentration of sodium phosphate was reduced from 100 mM to 50 mM in mobile phase B. The flow rate was reduced to 0.5 mL/min and the gradient increased from 28 minutes to 3 hours. This was a highly impractical method but did enable the detection of some peaks for trastuzumab emtansine's different DAR forms. However, the peaks were only visible after a blank subtraction and the quality of the peaks was poor, with little to no resolution and a drifting baseline (**Figure 4.34**).

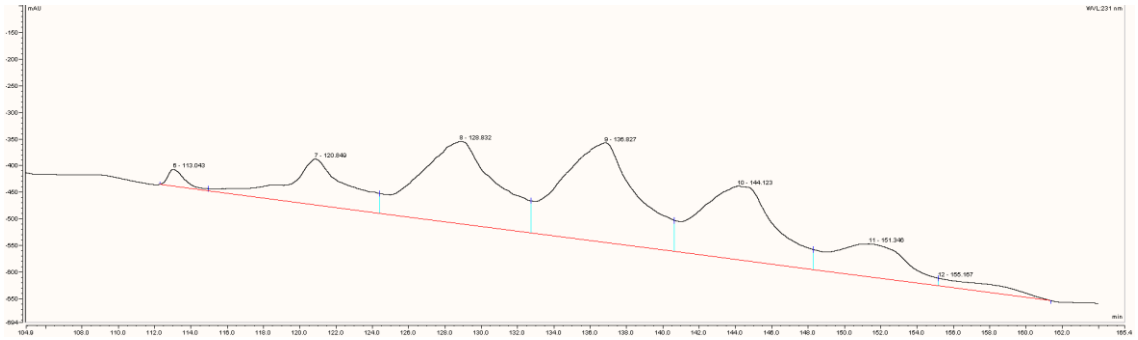

Figure 4.34. HIC analysis of a lysine linked ADC (trastuzumab emtansine) on a MAbPac HIC-10 column, showing 7 peaks with poor peak quality and resolution. The X-axis is time (minutes).

BIA separations monolith disk technology was also investigated. Monolith disks are hard sponge-like materials with interactive chemistry all over the monolith surface. This gives monoliths a huge increase in effective interaction area compared to normal columns. This means the "columns" don't need to be as long as a typical HPLC column 50mm-300mm, and are about 5mm long, explaining why they are called monolith disks. These 'disks are so short that multiple discs (up to 4) can be inserted into a disc holder. Following method 2.4.16, investigations using C4, protein G and protein A disks found them to be worse than normal columns for HIC DAR analysis.

All of the work with HIC only demonstrated that HIC still cannot be used to asses DAR for lysine linked ADCs. The 'best' modern HIC column was only able to separate trastuzumab emtansine DARs with an entirely impractical method. Therefore, LC-MS methods had to be tried.

4.5.3 Intact ADC LC-MS

LC-MS can be used to detect the accurate mass of compounds, this theoretically allows detection of different DAR forms, as each form will be at least 957 daltons different, the mass of a complete trastuzumab emtansine payload. LC-MS analysis of mAbs is often performed under reducing conditions to separate the heavy and light chains, increasing the signal to noise ratio. However, ADCs are analysed intact as the DAR is a ratio of drug to antibody and reducing the antibody into heavy and light chains would prevent that being measured.

To establish a baseline for trastuzumab emtansine with no payloads attached (naked trastuzumab), trastuzumab was run intact on the same LC-QTOF mass spectrometer following method 2.4.17 (**Figure 4.35**). Mass differences noted here are likely due to heterogeneous binding of sugars, as the masses of mannose, glucose and galactose residues are 162 daltons. The same sample of trastuzumab was also run reduced to help with structural identification (**Figures 4.36 & 4.37**). The mass of trastuzumab, which is equivalent to a DAR 0 trastuzumab emtansine, was established as ranging between 147.8 kDa and 148.7 kDa depending on the level of glycosylation at the heavy chains. Mass differences are likely due to heterogenic binding of sugars, as the masses of mannose, glucose and galactose residues are 162 daltons. One peak shows a difference of 204 daltons, which matches either an N-acetylgalactosamine or an N-acetylglucosamine. Attempts at running trastuzumab emtansine intact produced spectra that did not match this, (**Figure 4.38**). Mass differences, approximately equivalent to a single payload, are observed between peaks in clusters of variable glycosylation. The mass spectrometry technician stated the deconvolution algorithm was struggling with the complexity and low sensitivity.

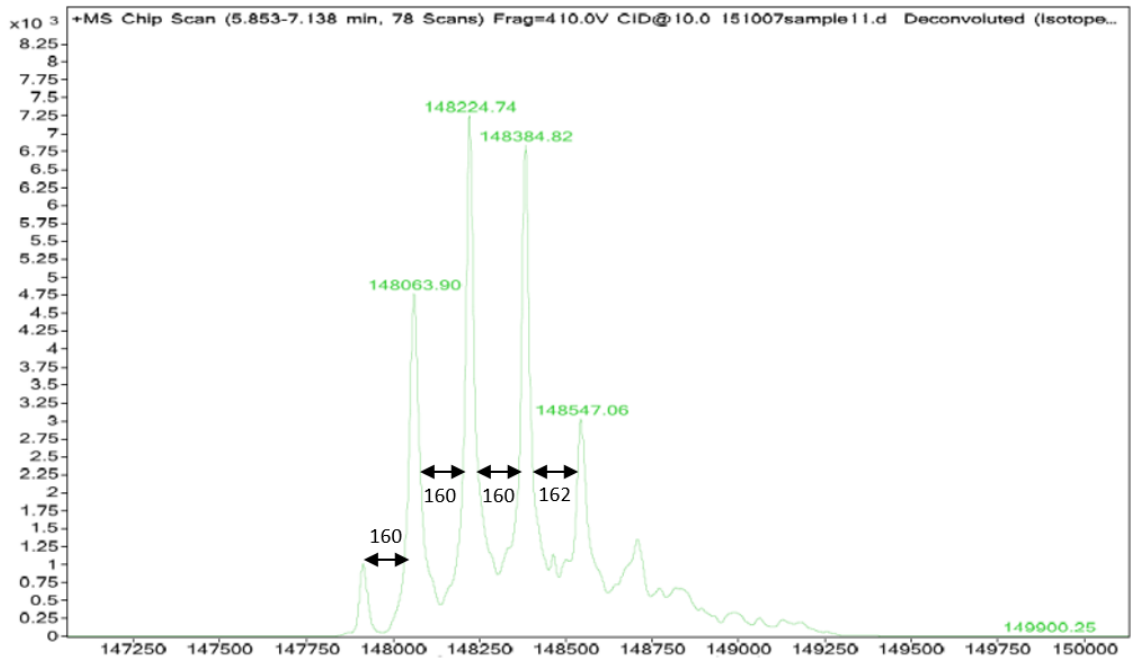

Figure 4.35. Intact LC-MS analysis of trastuzumab. Y-axis = TICs, X-axis = Mass (Daltons). Peaks around 148 kDa are detected, with 160 dalton differences.

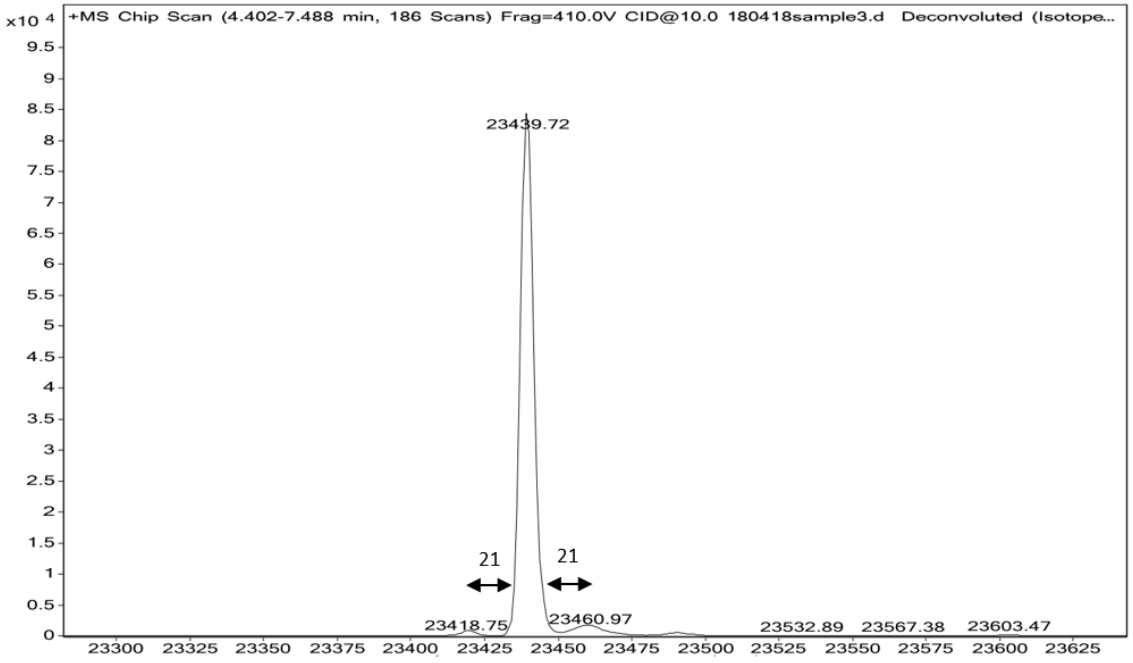

Figure 4.36. LC-MS analysis of trastuzumab light chains. Y-axis = TICs, X-axis = Mass (Daltons). Only three peaks were detectable with one peak dominating at 23439 daltons, and with mass differences of 21 daltons from the other detected species.

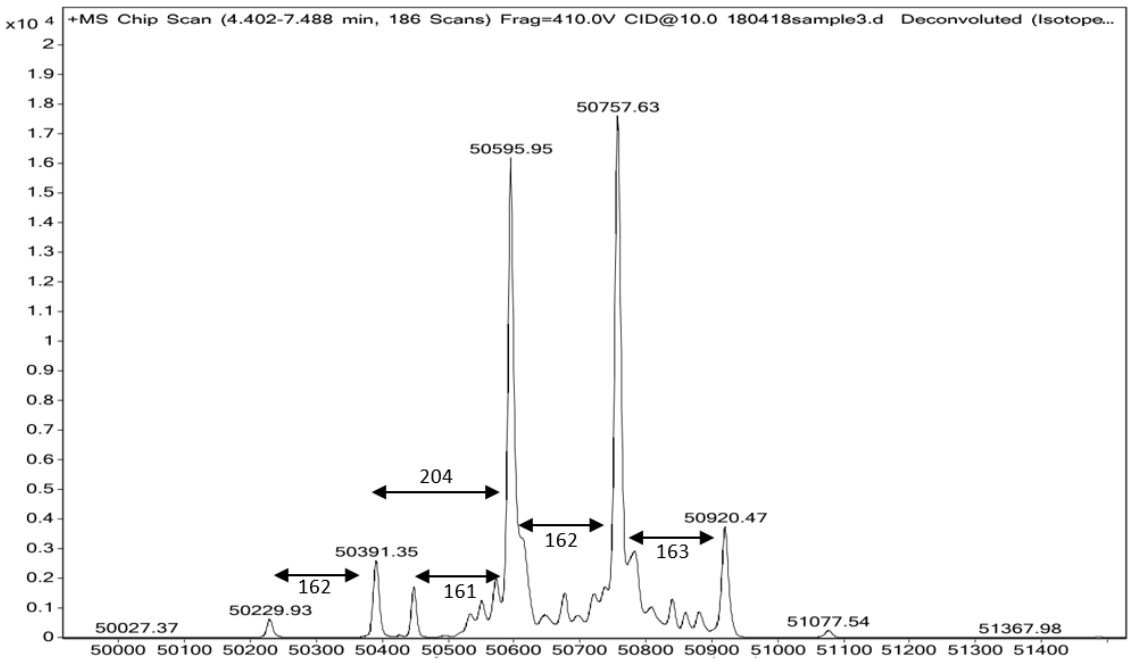

Figure 4.37. LC-MS analysis of trastuzumab heavy chains. Y-axis = TICs, X-axis = Mass (Daltons). Multiple peaks were detected due to the varying glycosylation of trastuzumab. Differences of around 162 daltons were observed.

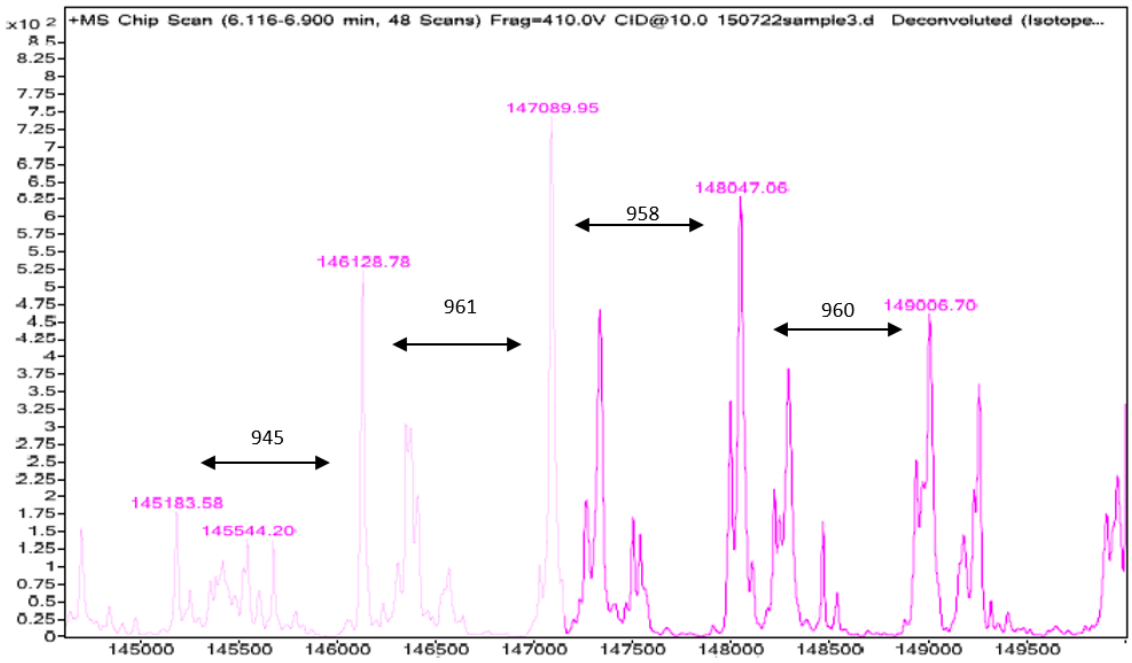

Figure 4.38. LC-MS analysis of intact trastuzumab emtansine. Y-axis = TIC, X-axis = Mass (Daltons). Multiple peak clusters were observed with peak height differences of about 960 daltons, which matches the mass of trastuzumab emtansine's payload. The signal to noise ration was very poor, with signal levels ten times lower compared to the intact trastuzumab

4.5.4 PNGase F

To reduce sample complexity, the enzyme 'Peptide N-Glycosidase (PNGase) F' was used to cleave the N-linked oligosaccharides from the heavy chains. PNGase F was purchased from New England Biolabs (New England BioLabs, Massachusetts, USA), and used according to the non-denaturing enzyme protocol (Method 2.4.18). However, the method was only partially successful, not ever fully deglycosylating the antibody, and used large amounts of PNGase F, while also taking a full day of incubation, which is unpractical for a stability study method intended to be run on the day.

PNGase F Rapid, an improved enzyme designed with activity equivalent to PNGase F over 24 hours at 37 °C in only 15 minutes at 75 °C and then 50 °C, was then investigated. Following method 2.4.19 the deglycosylation was underwhelming. Both PNGase F and PNGase F rapid recommend the addition of denaturing reagents to reduce steric hinderance of the enzyme. However, those protocols are designed for analysis of the glycan groups and not the protein. Furthermore, PNGase F rapid was even more expensive and had not worked better in any observable way, while adding heating steps and a buffer exchange step to remove the PNGase F from the sample before LC-MS analysis. While other enzymes were available for protein deglycosylation it was decided not to pursue deglycosylating enzymes further.

4.5.5 A new way of thinking about LC-MS data and DAR

Following method 2.2.12-2.2.14 had already satisfactorily characterised the glycosylation of antibodies such as infliximab and trastuzumab emtansine **(Figures 4.5 & 4.6**). Below are spectra for the light and heavy chains of trastuzumab emtansine (**Figure 4.39 & 4.40**). Mass differences of 957, exactly matching a single trastuzumab emtansine payload, are observed between peaks.

The data for light chains confirms that there are no more than two lysine residues with payloads bound on the light chain, and that double payload binding is less common. The data for heavy chains confirms that there are no more than two lysine residues with

payloads bound on the heavy chain, and that double payload binding is less common. This makes sense, as it is known that trastuzumab emtansine has a maximum DAR of 8, which would be made from two light chains with two payloads and two heavy chains with two payloads. If we had found heavy or light chains with bound three payloads it would suggest the possibility of DAR 10-12 trastuzumab emtansine could be present but that has not been reported in any literature. [85, 86, 89] The reaction to attach the payloads results in a heterogeneous mixture of DARs and to create a mixture with a mean DAR between 3 and 4, the linker attachment reaction is controlled to prevent under or over linking. As we don't see peak differences equivalent to a single linker, it appears the linker to warhead attachment step is designed to ensure maximum yield of conjugated antibody.

While looking at this data the reasons why DAR needed to be measured were thought about in detail. For an API manufacturer such as Lonza (Lonza, Basel, Switzerland) which makes trastuzumab emtansine for Roche, or a drug research company such as Genentech (Genentech, California, USA) who designed trastuzumab emtansine for Roche, knowing the exact DAR is important. However, a stability study does not need to measure the exact DAR. Change in DAR would be matched by a change in the peak heights for the heavy and light chains. Once manufactured, an ADC can only lose payloads. If the DAR were to decrease, the intensity of light and heavy chain peaks corresponding to zero payloads bound, will increase while the intensity of peaks corresponding to chains with 1 or 2 payloads bound will decrease. However, the values would need to be comparable from sample to sample, timepoint to timepoint. Experience with this method had taught me that variability in sample signal intensity was common, due to inconsistencies in sample recovery from the centrifugal spin filters. Usually, this is not a problem as absolute peak intensity is not important for monitoring that glycosylation profile. However, the DAR profile needs to be quantified even if it is not the DAR value itself. To normalise samples, the ratio of masses corresponding to naked (payload = 0), single (payload = 1), and double (payload = 2) chains could be compared. To do this an XY plot of the deconvoluted mass spectrum, with X being mass and Y being total ion count (TIC) could be extracted. Then the TICs for all masses

corresponding to naked, single and double chains for heavy and light chains summed separately. Then we could express the total naked light chain TICs as a % of the total TICs for light chain and express the total naked heavy chain TICs as a % of the total TICs for heavy chain. Doing this enables the capturing of count data for all masses corresponding to naked, single or double chains.

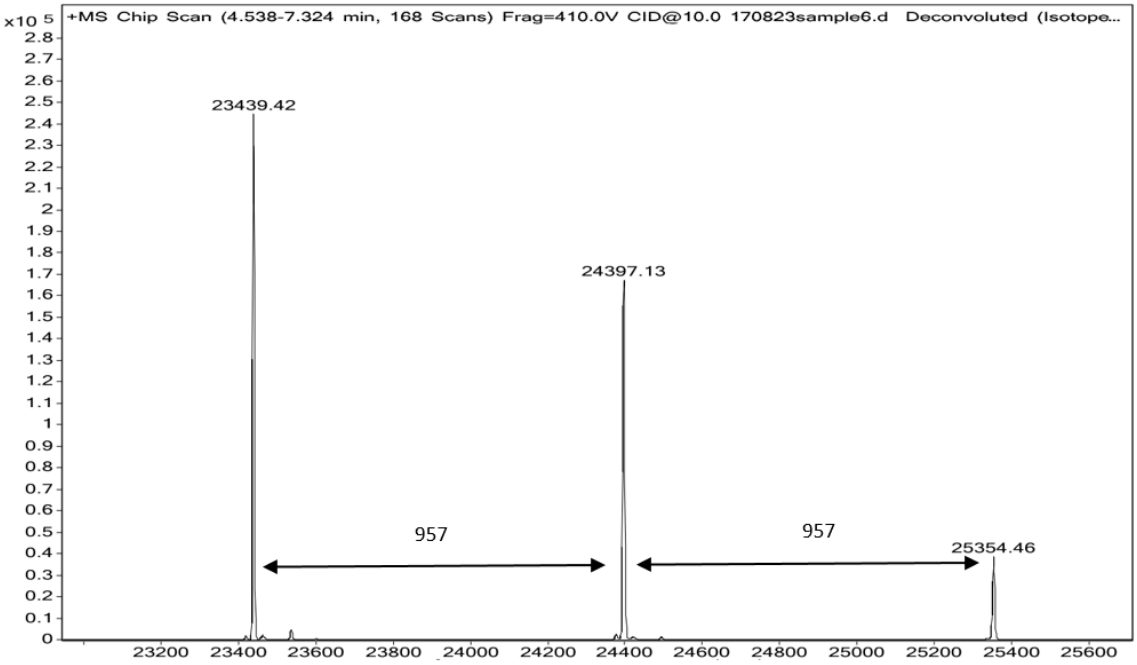

Figure 4.39. LC-MS analysis of trastuzumab emtansine light chains. Y-axis = TIC, X-axis = Mass (Daltons). Three main peaks were detected with mass differences of about 960 daltons. One peak matches the mass of trastuzumab light chain, suggesting the heavier two peaks correspond to a light chain with one or two bound payloads.

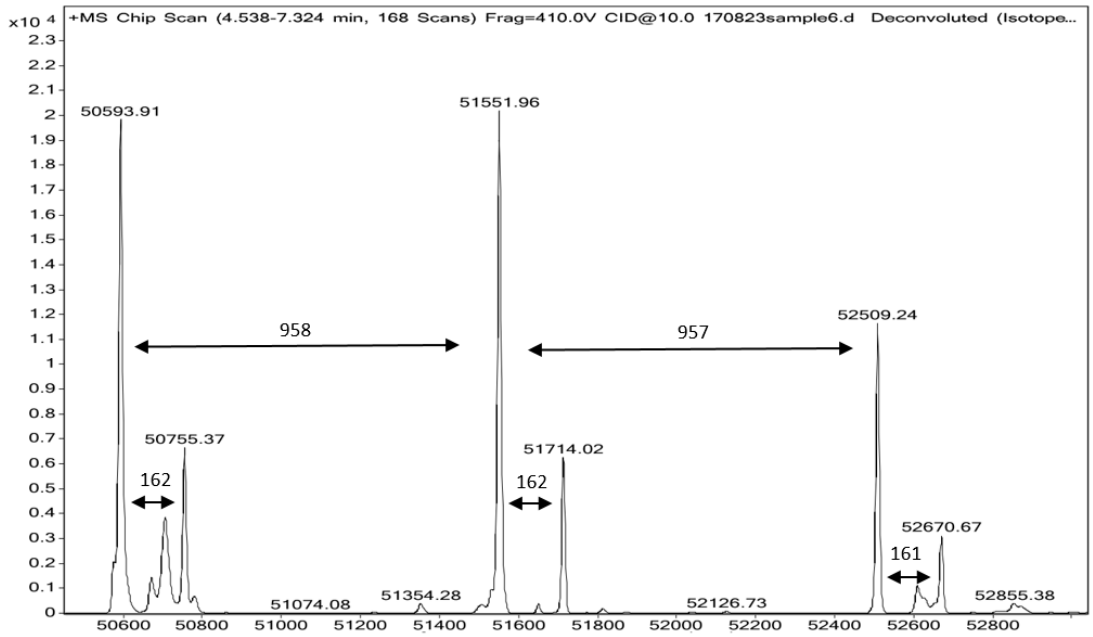

Figure 4.40. LC-MS analysis of trastuzumab emtansine heavy chains. Y-axis = TIC, X-axis = Mass (Daltons). Three main peaks were detected with mass differences of about 960 daltons. One peak matches the mass of trastuzumab heavy chain, suggesting the heavier two peaks correspond to a light chain with one or two bound payloads. Furthermore, like trastuzumab heavy chain, mass differences of about 160 daltons are observed.

4.5.6 Validation of new method using forced degradation

To test this theory, trastuzumab emtansine was degraded following method 2.42, specifically to liberate the payloads. The structure of trastuzumab emtansine has been identified and drawn, in chapter 1. The bonds most likely to break and liberate the payload are the amide and ester bonds (**Figure 4.41**). This could create three different masses of payload fragment. Hydrolysis at the ester would create a fragment with a molecular weight of 564 daltons, hydrolysis of the amide in DM-1 would create a fragment with a molecular weight of 650 daltons, and hydrolysis of the amide on the linker would create a fragment of around 958 daltons. 958 daltons is just an entire payload, so peaks with a mass difference of 650 or 564 daltons were of interest. Upon reviewing the forced degradation data for trastuzumab emtansine it was found there were no exact matches for these mass losses, the closest matches would often be 10-20 daltons off or well below the signal to noise ratio. As hydrolysis was the main route of degradation It was decided to use phosphate buffers to degrade trastuzumab emtansine at an elevated temperature before neutralising it. The intention was to cause hydrolysis

at the amides and/or ester in DM-1 and the SMCC linker and cause fragmentation. Following method 2.4.20, trastuzumab emtansine was exposed to pH 9-11 at 50 °C for 3 hours, this over degraded trastuzumab emtansine (**Figure 4.42**) resulting in dramatic loss of payload and at visual aggregation at pH 11. Then degradation was the assessed at less extreme conditions, using pH 7, 8 and 9 at 40 °C for only 90 minutes, following method 2.4.21 (**Figure 4.43**) but degradation was underwhelming, except at pH 9.

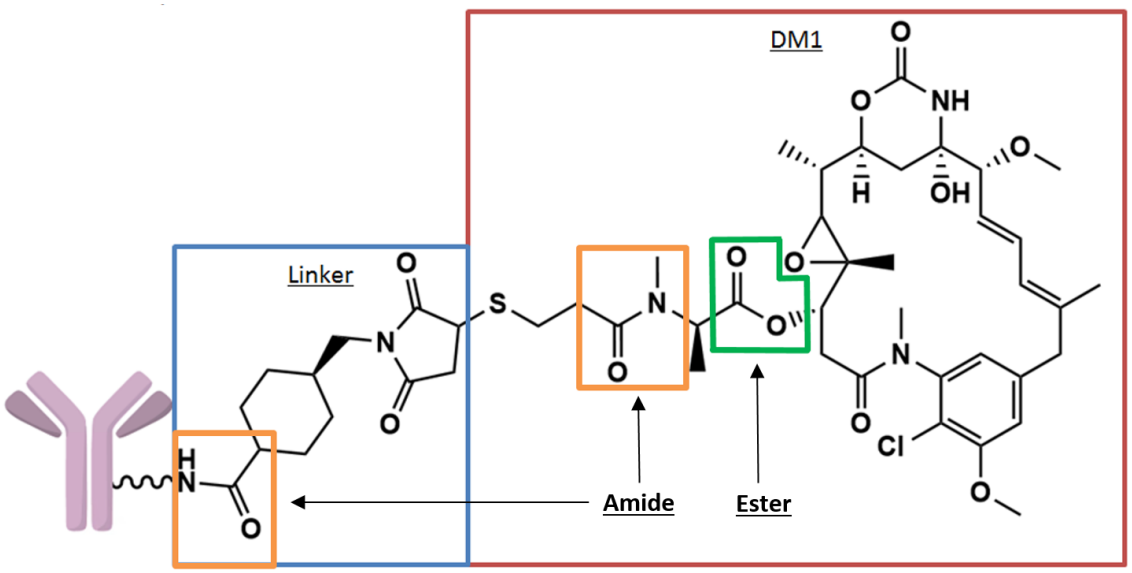

Figure 4.41. Chemical structure of trastuzumab emtansine's payload. Amide bonds are shown in orange, while the ester is shown in green.

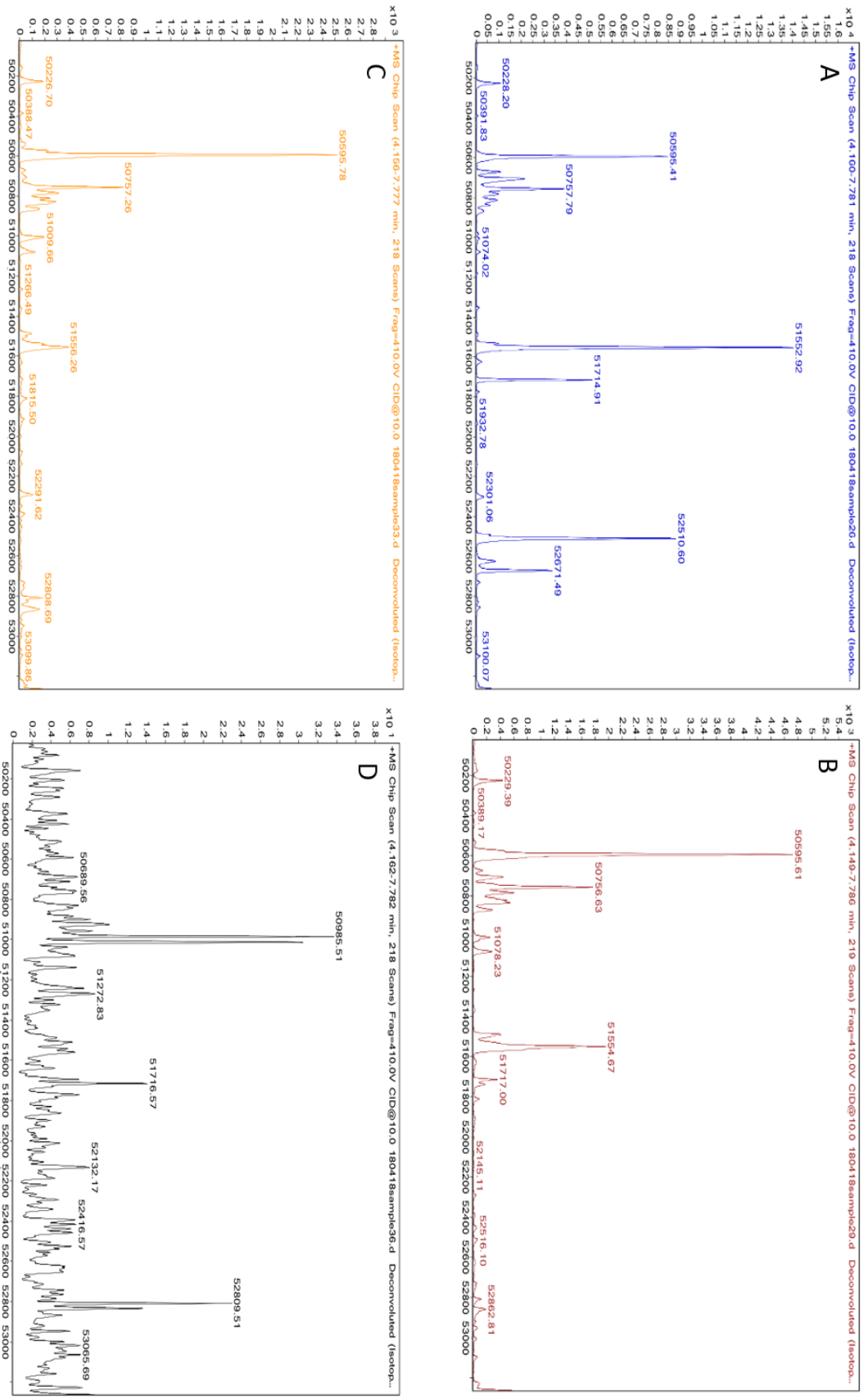

Figure 4.42. LC-MS spectra of trastuzumab emtansine heavy chains after 3 hours incubation at 50 °C. (**A**) is the control, (**B**) was at pH 9, (**C**) was at pH 10 and (**D**) was at pH 11. Y-axis = TIC, X-axis = Mass (Daltons). The higher the pH the smaller the peaks for bound payloads were, and the smaller the overall signal.

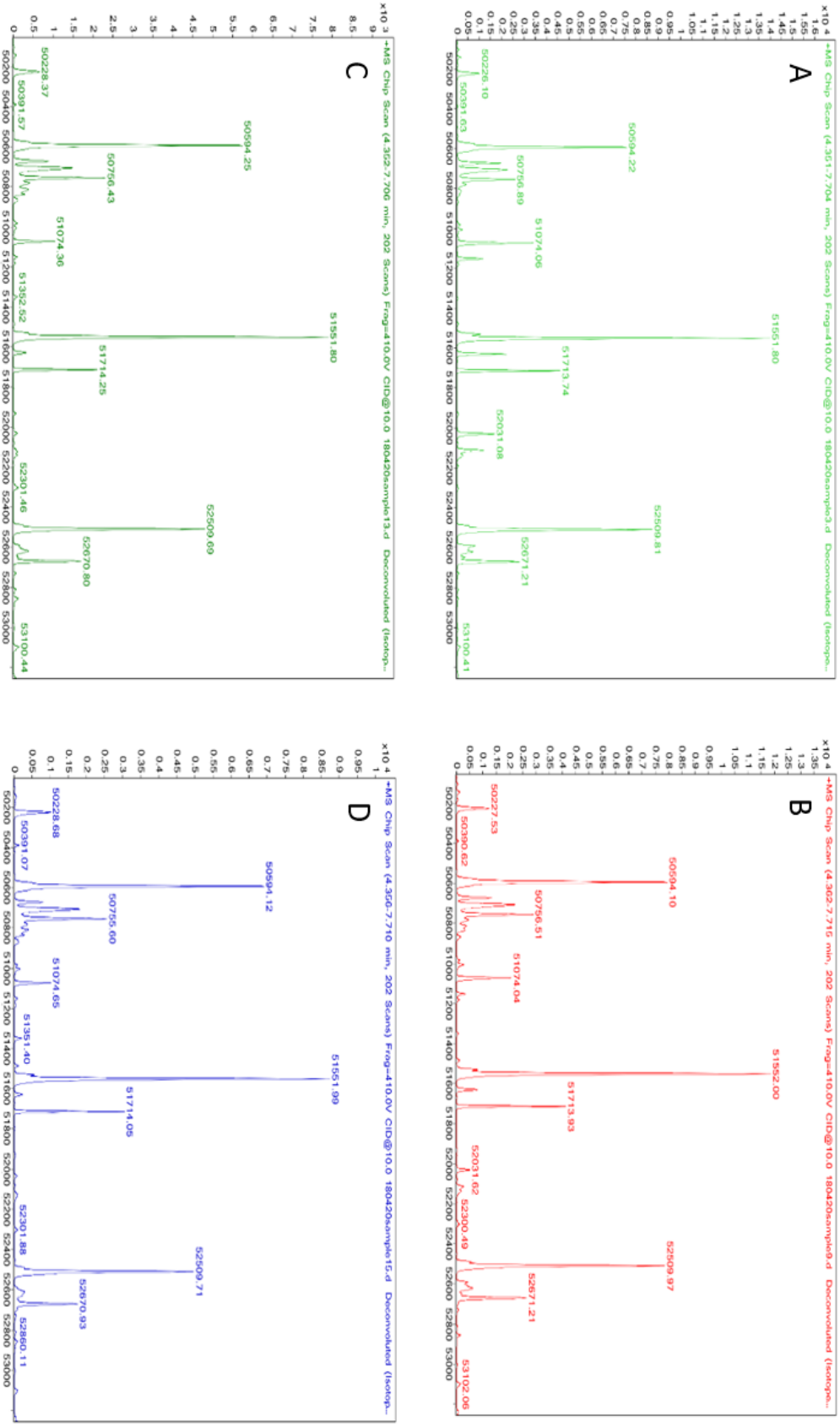

Figure 4.43. LC-MS spectra of trastuzumab emtansine heavy chains after 1.5 hours storage at 40 °C. (**A**) is the control, (**B**) was at pH 7, (**C**) was at pH 8 and (**D**) was at pH 9. Y-axis = TIC, X-axis = Mass (Daltons). The higher the pH the smaller the peaks for bound payloads were. Signal intensity was not lost.

Finally, following method 2.4.22, trastuzumab emtansine samples were pH adjusted to pH 9 and stored for 1-3 hours on a heat block at 45 °C before being removed and neutralized. This degraded the heavy and light chains without stripping them completely (**Figure 4.44 & 4.45**). Increased duration of storage at pH 9 and 45 °C caused greater amounts of degradation for both heavy and light chains. The intensity of peaks corresponding to double payload chains are more affected than peaks corresponding to single payload chains. This is accompanied by an increase in signal intensity for naked chain peaks.

All of the degradation experiments for this were performed in triplicate and the data processed, according to method 2.4.23, to compare the relative ratios of the TICs to calculate means for each condition (**Figure 4.46 & 4.47**). Payloads on the light chains appear to be more easily hydrolysed than those on heavy chains, both double and single payload chains are easily hydrolysed. 180 min at pH 10 & 50 °C causes over 95% of light chains to lose their payloads. Also, it is noticeable that the single payload heavy chains do not appear to be affected until much harsher conditions are used. 180 min at pH 10 & 50 °C causes 100% of double payload chains to be degraded but only ~50% of the single payload chains. 180 min at pH 9 & 45 °C and gentler conditions do not appear to affect the single payload heavy chains. It is more likely that when a double payload heavy chain is hydrolysed, only one payload is liberated while the other payload is unaffected. This means if a double and single chain are both hydrolysed, it will appear as though the double payload was completely hydrolysed while the single payload chain was not hydrolysed. This could explain why the double payload heavy chain appears to degrade directly to naked heavy chain. This phenomenon could also explain why the single payload chain appears to increase in some instances.

This work demonstrates that the payload binding profile can be monitored using this method. And that it is stability indicating and quantitative. While the payload binding profile of heavy and light chains is not the exact DAR, it is directly related. And change in DAR will be associated with a change in the payload to chain binding profile.

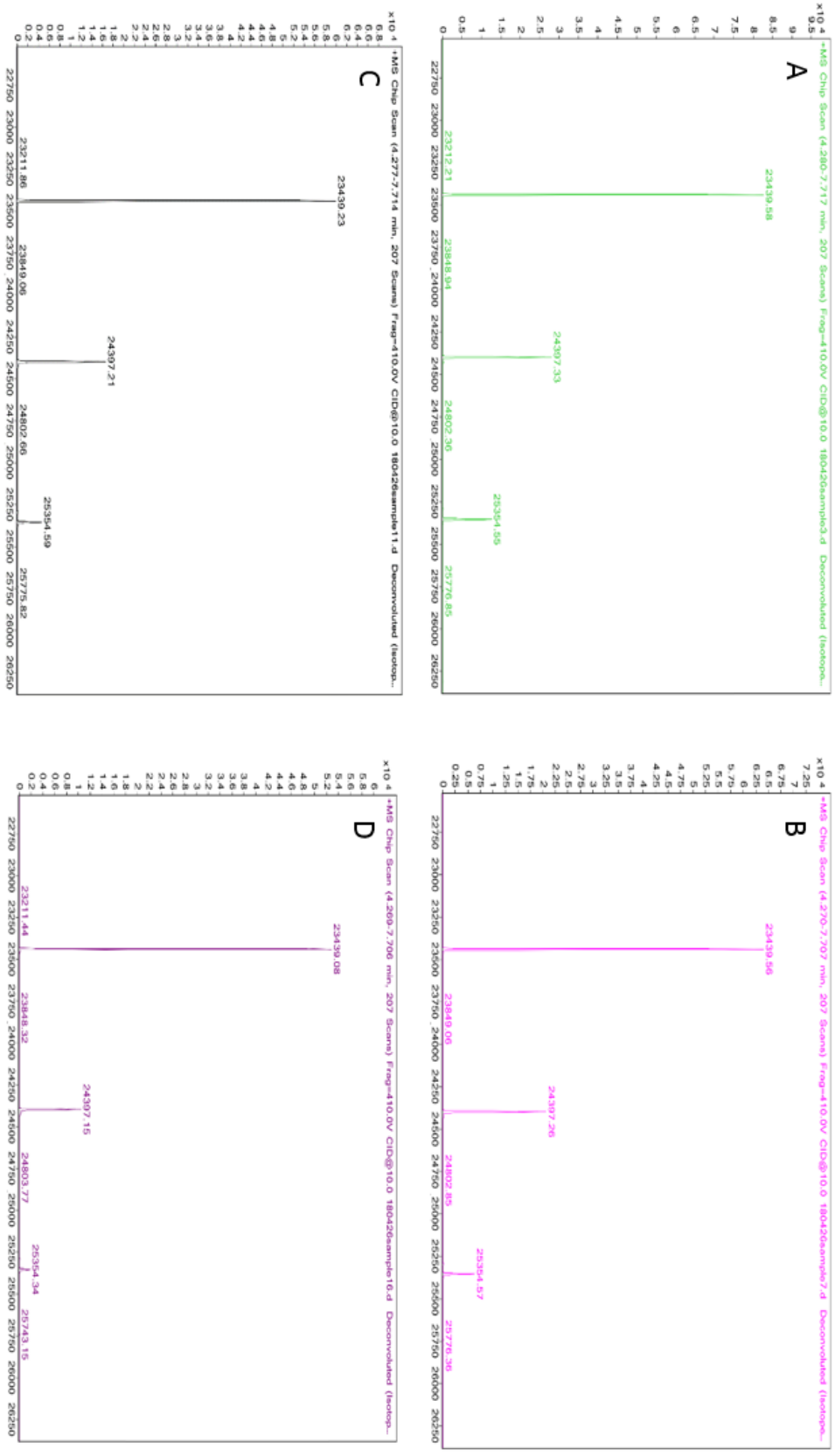

Figure 4.44. LC-MS spectra of trastuzumab emtansine heavy chains stored at pH 9 and 45 °C. Samples were neutralized after 1 hour (**A**), 1.5 hours (**B**), 2 hours (**C**), and 3 hours (**D**). Y-axis = TIC, X-axis = Mass (Daltons). Incubation time is inversely proportional to bound payload peaks height.

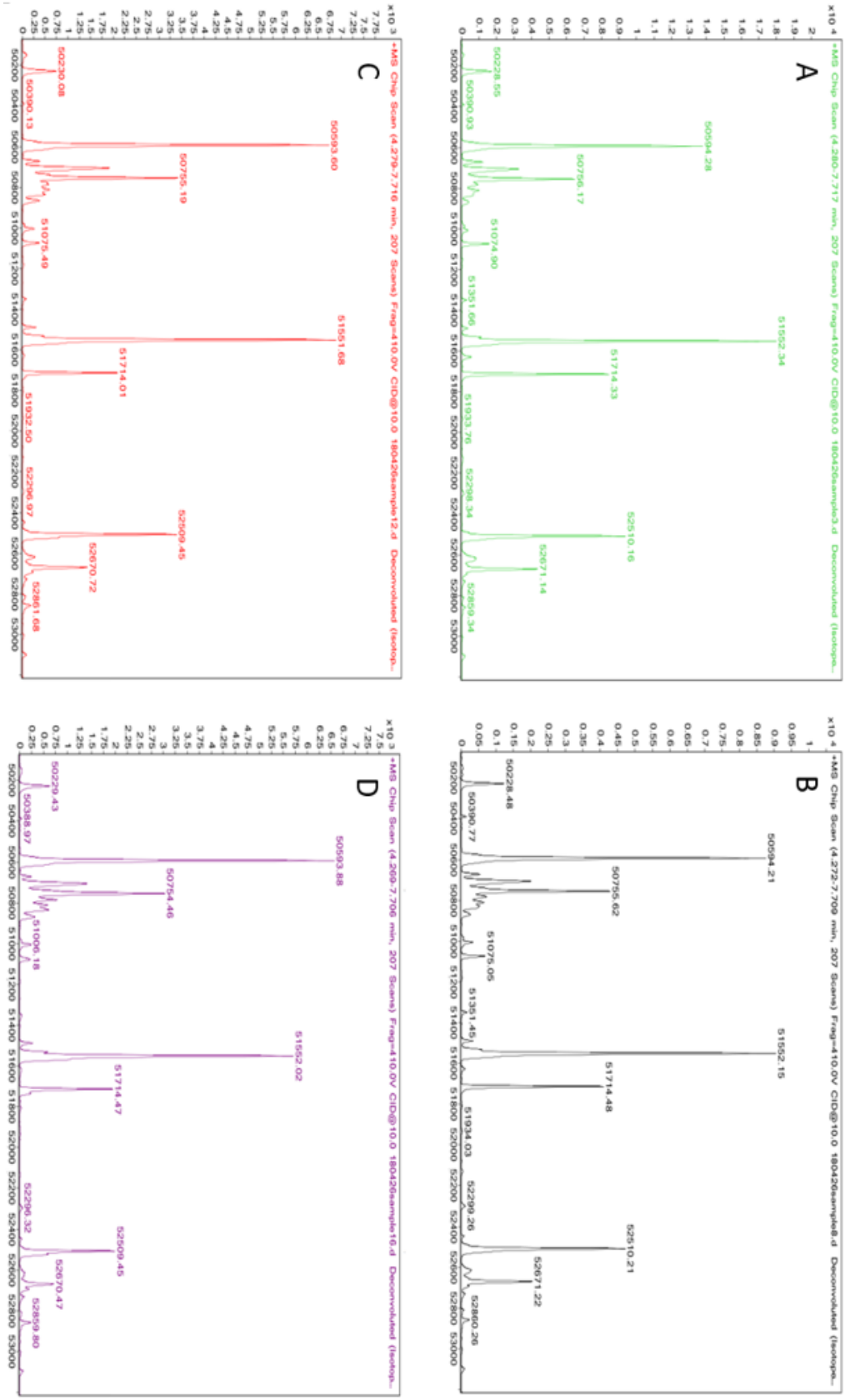

Figure 4.45. LC-MS spectra of trastuzumab emtansine heavy chains stored at pH 9 and 45 °C. Samples were neutralized after 1 hour (**A**), 1.5 hours (**B**), 2 hours (**C**), and 3 hours (**D**). Y-axis = TIC, X-axis = Mass (Daltons). Incubation time is inversely proportional to bound payload peaks height.

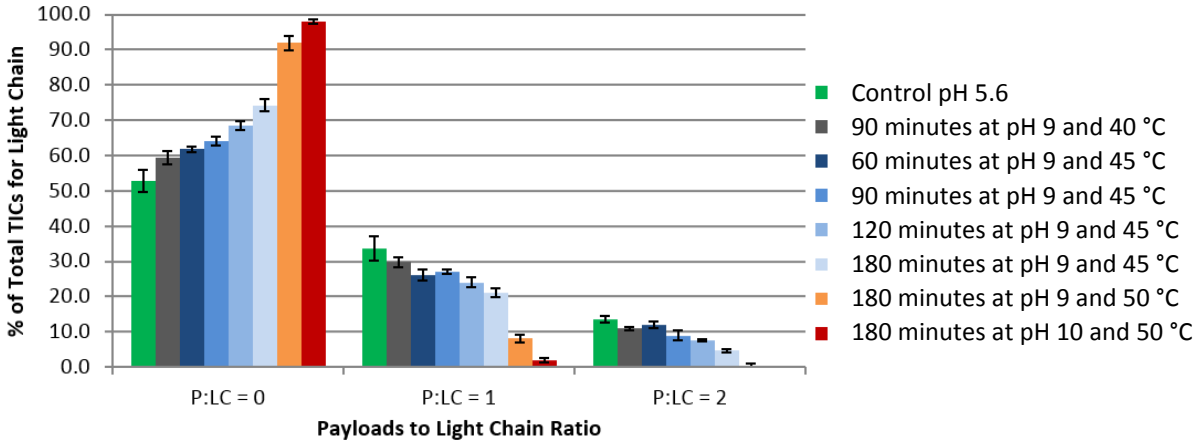

Figure 4.46. Bound payload profiles of trastuzumab emtansine light chains, following base hydrolysis. Incubation time and pH are inversely proportional to bound payload peaks height.

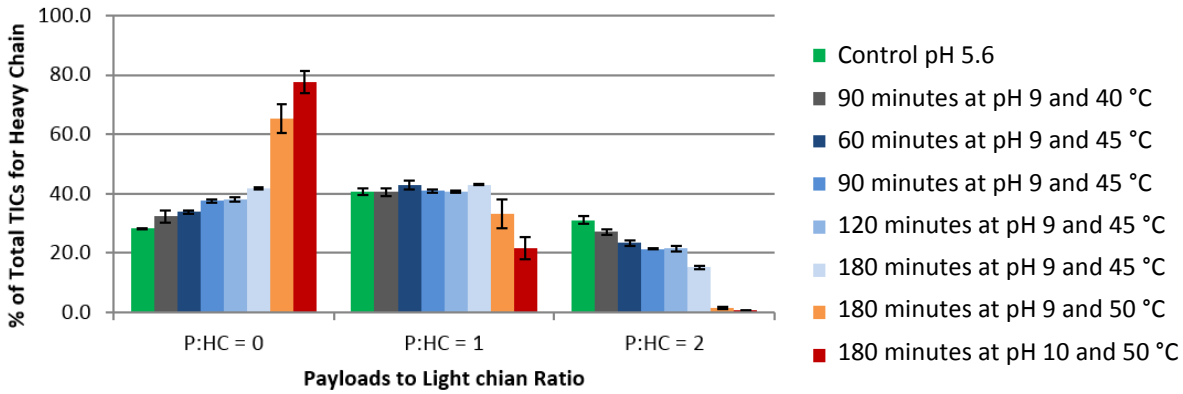

Figure 4.47. Bound payload profiles of trastuzumab emtansine heavy chains, following base hydrolysis. Incubation time and pH are inversely proportional to double payload peak height but not single payload peak height.

4.6 Trastuzumab emtansine stability study

4.6.1 Reasons for performing this study

Trastuzumab emtansine has been investigated in two clinical trials, 'EMILIA' [103,200] and 'TH3RESA'. [104] A review of trastuzumab emtansine from the Lancet stated,

"*Together with EMILIA, findings from TH3RESA substantiate the potential of antibody–drug conjugates to achieve a more favourable benefit-to-risk profile than that seen with traditional combinations of chemotherapy and targeted agents in epithelial cancers. Data from these two, large phase 3 studies suggest that trastuzumab emtansine is effective across the natural history of HER2-positive advanced breast cancer, spanning from disease with previous exposure only to adjuvant treatment, to progressive heavily pre-treated disease after regimens incorporating trastuzumab and lapatinib. Trastuzumab emtansine should be considered as a new standard for patients with HER2-positive advanced breast cancer"*

The EMILIA study demonstrated that trastuzumab emtansine provided 6 months extra median overall survival, a 50% increase in median progression free survival and a 50% increase in the duration of response, compared to the gold standard treatment of lapatinib + capecitabine. During the EMILIA study 4 patients from the lapatinib + capecitabine arm died due to coronary artery disease, multiorgan failure, coma, and hydrocephalus, while only one patient died in the trastuzumab emtansine arm, which was due to metabolic encephalopathy after CNS progression. The TH3RESA study also demonstrated 6 months of additional overall survival using trastuzumab emtansine vs the physician's gold standard choice, furthermore the physician's choice had a 17.5% increase in adverse effects, relative to trastuzumab emtansine. The evidence explains why Dr Krop said "Trastuzumab emtansine should be considered as a new standard". However as stated in a 2017 Lancet article [201], the UK's National Institute of Clinical Excellence (NICE) deemed trastuzumab emtansine too expensive to justify as an NHS treatment option.

In an unopened vial the product is stable for up to 3 years when stored at 2-8 °C. The reconstituted concentrated solution is stable for up to 24 hours when stored at 2-8 °C, followed by a further 24 hours at 2-8 °C when diluted in sodium chloride 0.45% or 0.9%. This stability is acceptable if compounding inside a hospital pharmacy, but it impedes the use of external aseptic compounders, as only 24 hrs is not enough to easily compound, transport and administer a product. However, with an extended shelf life the logistical issues can be overcome, the product can be made days to weeks in advance and be waiting at the hospital ready for the patient. An extended shelf life also enables wastage savings, estimated to be over £1300 per dose, by combining multiple patient orders together to maximise vial usage. There are also logistical benefits and cost benefits due to batch manufacture, lower overheads of external units and competition between external compounding units, lowering the overall cost per patient. Coupled with a 'special deal' that Roche is offering the NHS regarding trastuzumab emtansine, a shelf life extension should improve patient access and therefore the outcome for NHS patients with HER2-positive advanced breast cancer who have previously received trastuzumab and lapatinib.

4.6.2 Study design

A clinically low, common and high concentration of Kadcyla brand trastuzumab emtansine were stored in four polyolefin infusion bags each. To reduce the cost burden, the volume of trastuzumab emtansine solution stored was reduced from 250 mL to 50 mL, which saved £130,000. The bags were stored at 5 °C ± 2 °C in the absence of light. Samples were withdrawn and tested from each bag on days 0, 1, 4, 7, 11, 14, 18, 20, 21 & 24. After sampling the bags at day 20, the samples were kept at 25 °C and not returned to the fridge, thus day 21 samples, had 20 days refrigerated and one day at "room temperature", as per yellow cover specification, and day 24 had 4 days at room temperature. This study is designed to be compliant with Part 2 (biopharmaceuticals) of the current NHS yellow cover document: A Standard Protocol for Deriving and Assessment of Stability. [102] which means the measurement of all stated critical quality

attributes as defined by the NHS guidance document, [102] as well as off target toxicity and payload binding.

4.6.3 Test methodology

The methods used are as described in chapter 2 and have previously been used in the infliximab study other than SEC, IR and the additional data processing of the LC-MS data and NTA instead of DLS.

4.6.4 Visual inspection

Following method 2.2.2, all samples remained clear and colourless for up to 24 days with no evidence of precipitates or particulate matter. No change in colour or turbidity was observed over the 24-day study period. Representative photographs are available in appendix V.

4.6.5 Moisture loss

Following method 2.2.1, no cumulative moisture loss was observed throughout the course of the study, less than 0.1% relative mass difference was observed between each sampling timepoint. (**Figure 4.48**).

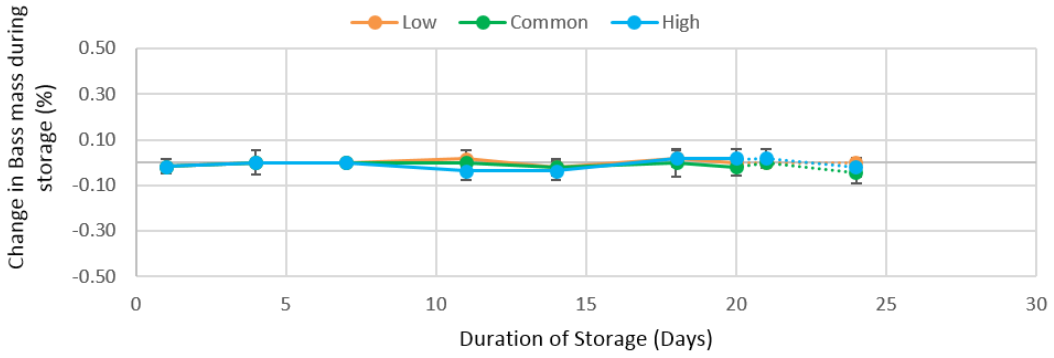

Figure 4.48. Moisture loss from infusion bags containing trastuzumab emtansine over time, no trend observed at any concentration. Storage at 25 °C is denoted with dashed lines.

4.6.6 pH

Following method 2.2.3, the mean pH of trastuzumab emtansine throughout the study is shown in (**Figure 4.49**). No strong trend is observed, though the mean pH on day 25 is 0.1 pH units lower for the low and common concentrations and 0.05 pH units for the high concentration. The pH is also lower the higher the concentration is, this is due to the pH of the trastuzumab emtansine vial concentrate being lower than the pH of the 0.9% NaCl diluent.

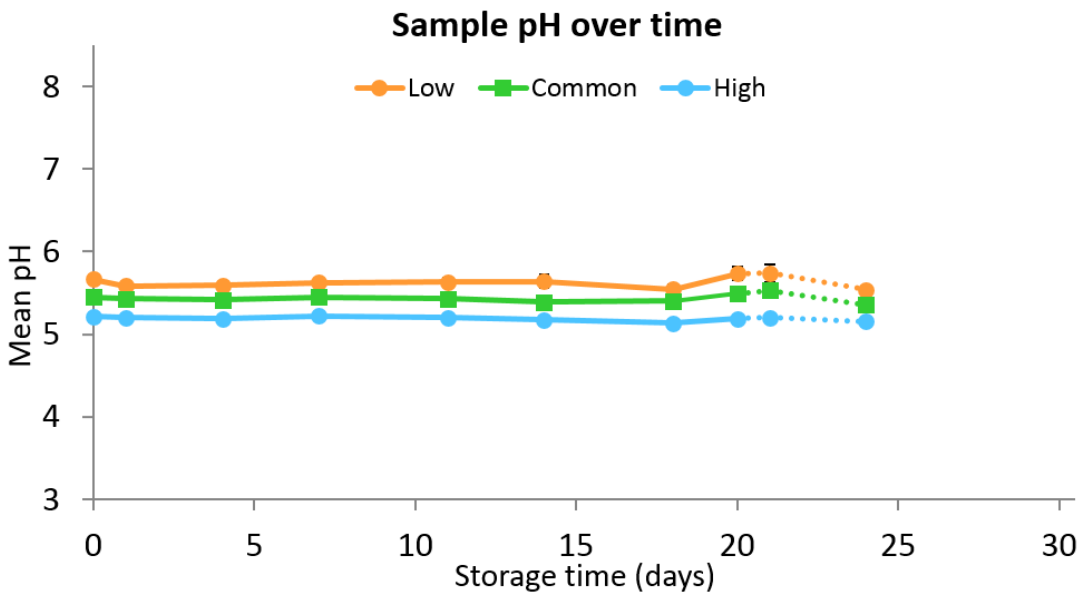

Figure 4.49. pH changes of trastuzumab emtansine over time, no strong trend observed at any concentration. Storage at 25 °C is denoted with dashed lines.

4.6.7 Gel electrophoresis

The macromolecular structure of trastuzumab emtansine was assessed by gel electrophoresis at each timepoint, according to method 2.2.7, as shown by representative runs from day 0 and day 24 (**Figure 4.50 & 4.51**). The results indicate that compared to day 0, no change to the mass of trastuzumab emtansine occurred throughout the study period for the Low, common or high concentration samples.

Thus, the antibody structure remains structurally intact upon extended storage and does not undergo fragmentation to any measurable extent.

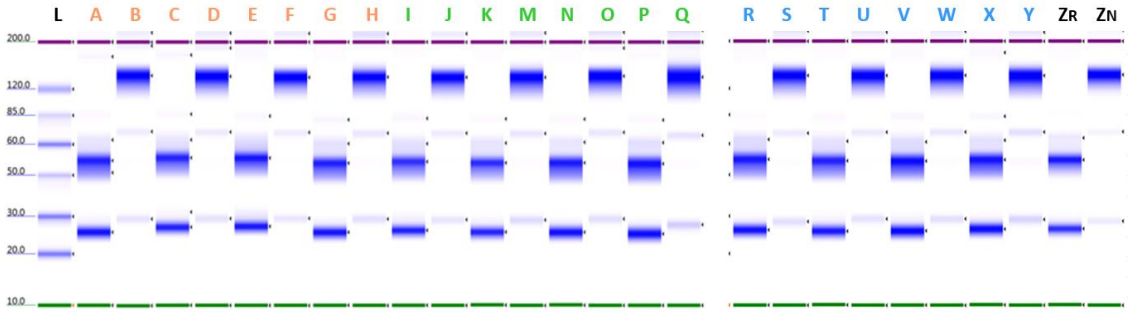

Figure 4.50. Gel electrophoresis profile of trastuzumab emtansine at a low (A-H), common (I-Q) and high (R-Y) concentration for day 0. L is a digital ladder, while Z is a fresh vial sample for comparison. All intact samples and control appear the same as each other as do all reduced samples.

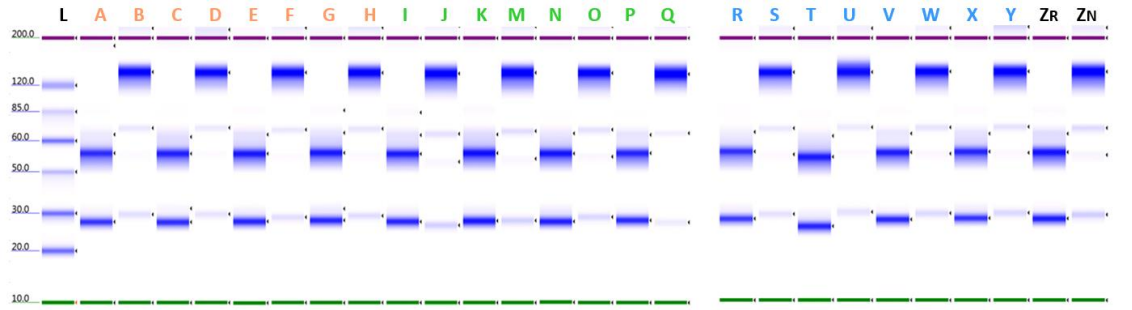

Figure 4.51. Gel electrophoresis profile of trastuzumab emtansine at a low (A-H), common (I-Q) and high (R-Y) concentration for day 24. L is a digital ladder, while Z is a fresh vial sample for comparison. All intact samples and control appear the same as each other as do all reduced samples.

4.6.8 Microflow imaging analysis of microparticles

The abundance of sub-visible particles above 10 µm was measured by microflow imaging, according to method 2.2.6, throughout the study period (**Figure 4.52, 4.53 & 4.54**) show the mean particle count per unit volume measured for the low, common and high trastuzumab emtansine solutions respectively. A common trend observed across all concentrations is that the mean particle count per mL reaches an apex at day 11 or 14, after which particle counts decrease to a level which is largely maintained to day 25. With the exception of a transient increase observed on D14 for the common concentration bags (**Figure 4.53**), at no point is a statistically significant increase in mean particle count observed compared to the SPC limit on day 1 ($p < 0.05$, one-way ANOVA

with post hoc Bonferroni). The data recorded therefore strongly suggests that trastuzumab emtansine undergoes reversible aggregation, perhaps as a result of adsorption onto the surface of the container material, and subsequent release. The increase in particulates observed around day 11 coincides with the decrease in API observed on day 11 with SE-HPLC analysis, when the measured monomer abundance drops by 2.0%, 1.1% and 1.7% for the low, common and high concentrations respectively. The decrease in observed concentration could be the result of aggregated protein being impeded by the HPLC guard column (5 µm pore size) or could be because of adsorption onto the bag surface and subsequent aggregation. Overall the abundance of sub-visible particles shows no sustained pattern of increase over the study (24 days).

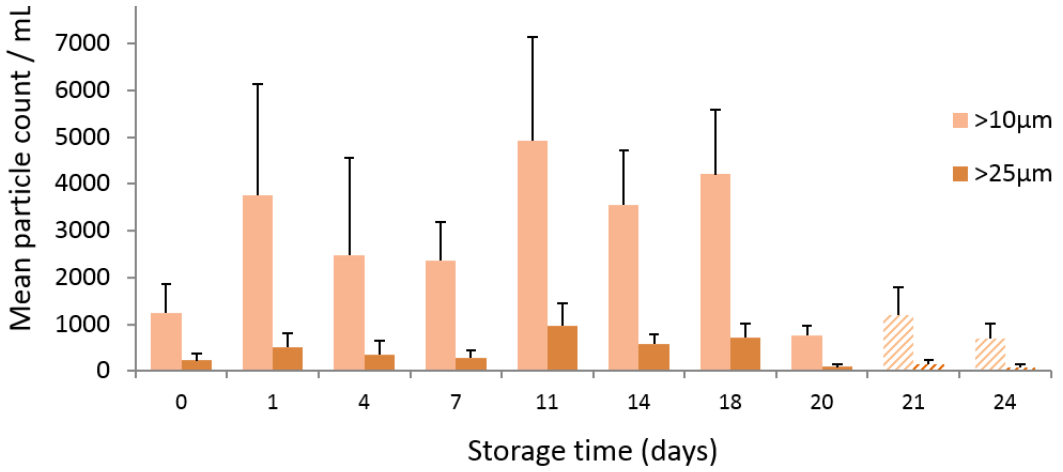

Figure 4.52. Mean particle count observed throughout the study period for the low concentration trastuzumab emtansine. Day 21 & 24 have dashed columns to indicate room temperature data points.

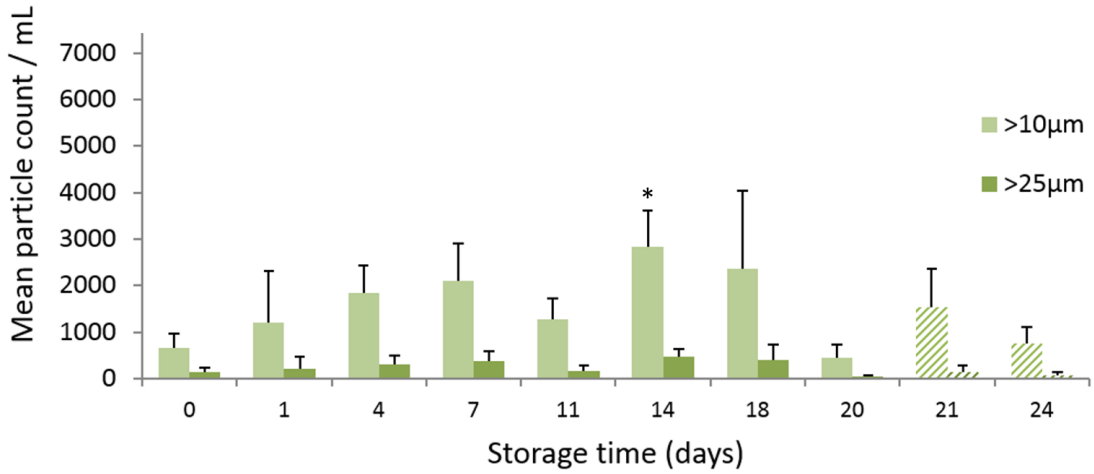

Figure 4.53. Mean particle count observed throughout the study period for the common concentration trastuzumab emtansine. Day 21 & 24 have dashed columns to indicate room temperature data points. The * indicates $p < 0.05$ compared to Day 0 and Day 1 results.

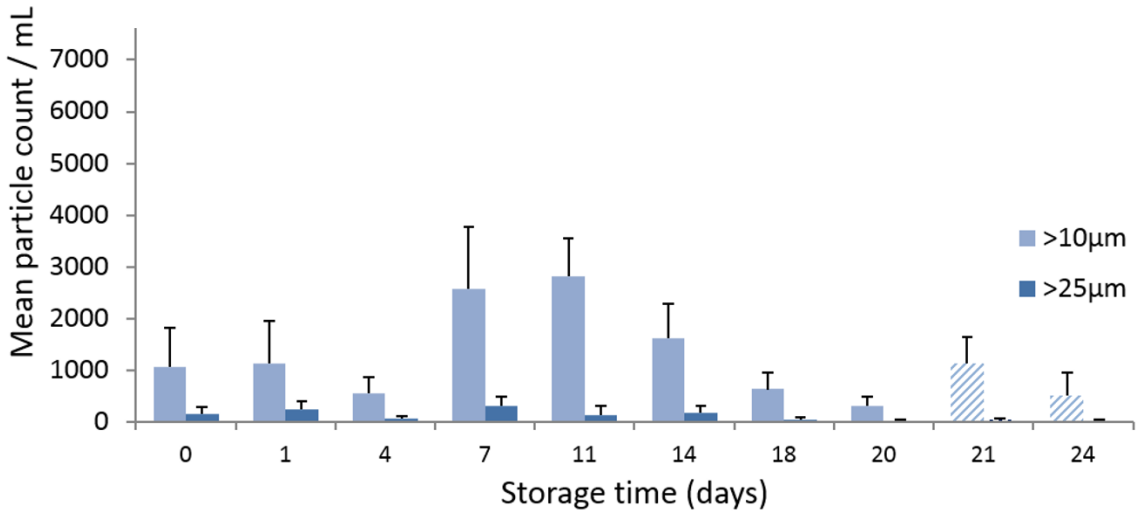

Figure 4.54. Mean particle count observed throughout the study period for the common concentration trastuzumab emtansine. Day 21 & 24 have dashed columns to indicate room temperature data points.

4.6.9 Infrared spectroscopy structure determination

The secondary structure of the trastuzumab emtansine protein was determined by analysis of FTIR spectra which were obtained throughout the study period accordein to method 2.2.9. The results are shown in (**Figures 4.55 & Table 4.13**) with data presented as the % of the α-helix or β-sheet abundance measured at each timepoint respectively. The results show that no significant change in the secondary structure of the trastuzumab protein is occurring upon extended storage at any concentration, and the antibody secondary structure remains conformationally stable for up to 20 days when stored at 2-8 °C, following storage at 25 °C for up to 120 hours. The trastuzumab emtansine powder for reconstitution contains sucrose and polysorbate 20, both help to stabilise the protein even when diluted to clinically relevant concentrations. The sucrose limits local mobilisation and the polysorbate 20 is a surfactant that protects the protein form liquid-air and liquid-solid interfaces. [237] Together, these two stabilisers ensure trastuzumab emtansine's higher order structure is protected when in solution.

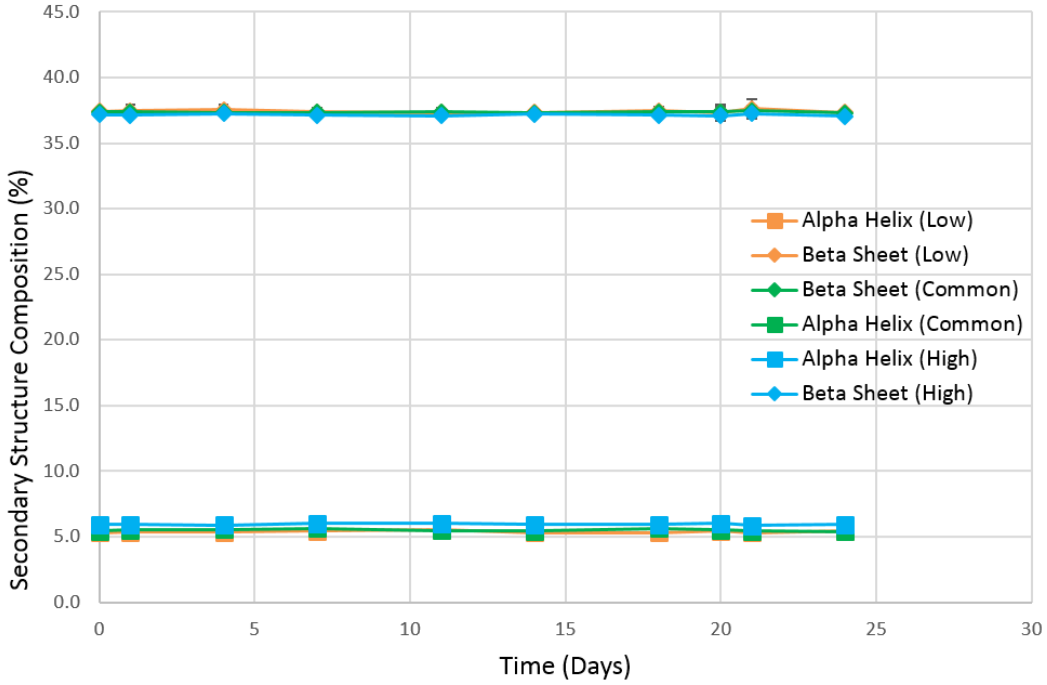

Figure 4.55. Change in α-helix and β-sheet abundance of trastuzumab emtansine throughout the study period. Both alpha helix and beta sheet content remained constant during the study. No significant changes occurred, and no trend of change was observed.

		Alpha Helix			Beta Sheet		
	Day	**0**	**20**	**24**	**0**	**20**	**24**
Low	**Mean**	**5.3**	**5.4**	**5.5**	**37.4**	**37.3**	**37.3**
	SD	*0.2*	*0.7*	*0.6*	*0.2*	*0.6*	*0.2*
Common	**Mean**	**5.5**	**5.5**	**5.4**	**37.4**	**37.4**	**37.3**
	SD	*0.3*	*0.3*	*0.3*	*0.2*	*0.4*	*0.2*
High	**Mean**	**5.9**	**6.0**	**5.9**	**37.2**	**37.1**	**37.1**
	SD	*0.2*	*0.3*	*0.2*	*0.2*	*0.3*	*0.3*

Table 4.13. Measured alpha helix and beta sheet for Day 0, 20 and 24. There was no statistical difference between day 0 and day 20 or day 24 (which includes 96 hours at room temperature).

4.6.10 SEC analysis of monomer concentration

SEC was used to measure the concentration of trastuzumab emtansine, and early oligomerization over the course of the study, by measuring the area of the peak associated with the trastuzumab emtansine monomer and dimer at each time-point, according to method 2.217. The results are summarised in (**Figure 4.56**), where they are expressed as % monomer relative to day 0. The absolute concentrations of each sample have been measured over the course of the study but will not be part of this thesis as that would circumvent the anonymisation of the concentrations.

The results indicate that after 20 days storage at 2-8 °C, no net loss in protein monomer was observed at low or common concentration samples; however, a small but statistically significant change was observed in the low concentration samples on day 11 compared to day zero and one ($p = < 0.05$, one-way analysis of variance with a post hoc Bonferroni). These results indicate that no aggregation or fragmentation of the antibody protein is occurring to any measurable extent throughout the refrigerated study period. After storage for 4 days at 25 °C, a small decrease in protein monomer was noted in all concentrations relative to day 0, decreasing by 0.2%, 0.3% and 1.4% in the low, common and high concentrations respectively, but this change was statistically insignificant.

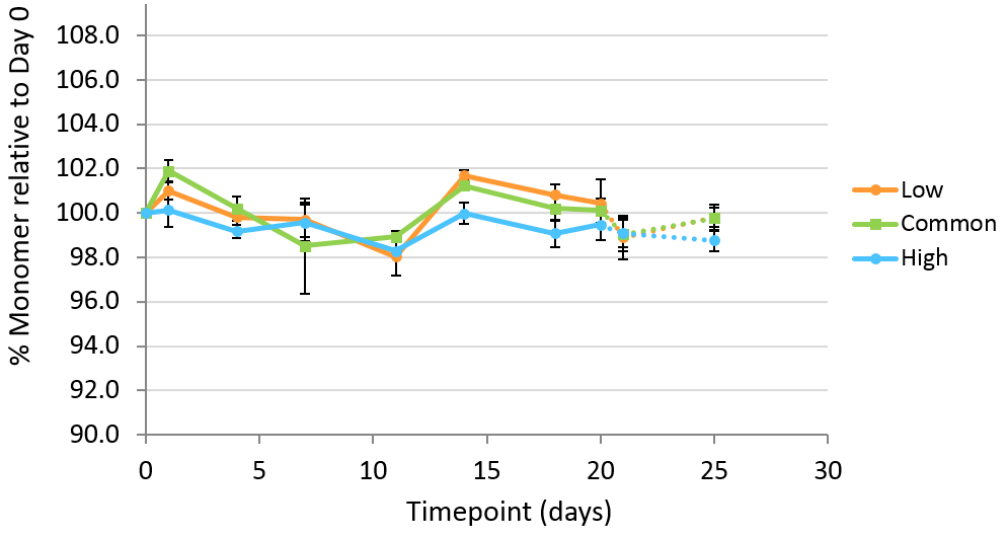

Figure 4.56. SEC analysis of trastuzumab emtansine monomer concentration relative to day 0. No trend is overserved, no change noted is statistically significant. However, the common concentration did reach 102 % relative to day 0 on day 1 and the low concentration reach 98 % relative to day 0 on day 11.

4.6.11 Nano-tracking analysis of nano-particles

The mean particle count of sub-visible particles below 1 µm (50-950 nm) was measured by nanoparticle tracking analysis throughout the study period following method 2.2.5. (**Figures 4.57 – 4.59**) show the mean particle count per unit volume (in millions) measured for the low, common and high concentration of trastuzumab emtansine solutions respectively.

Overall the particle count remains steady over the study across all bags, no sample is statistically significantly different from day 0 ($p < 0.05$, one-way ANOVA, post hoc Bonferroni). In all concentrations, the highest mean particle count is observed after storage at 25 °C for either 24h (high) or 120h (low and common). This is in-line with the SEC results, where we see a slight decrease in the monomer concentration during storage at 25 °C. Overall, there is no significant trend or change in nanoparticle concentration detected during the study.

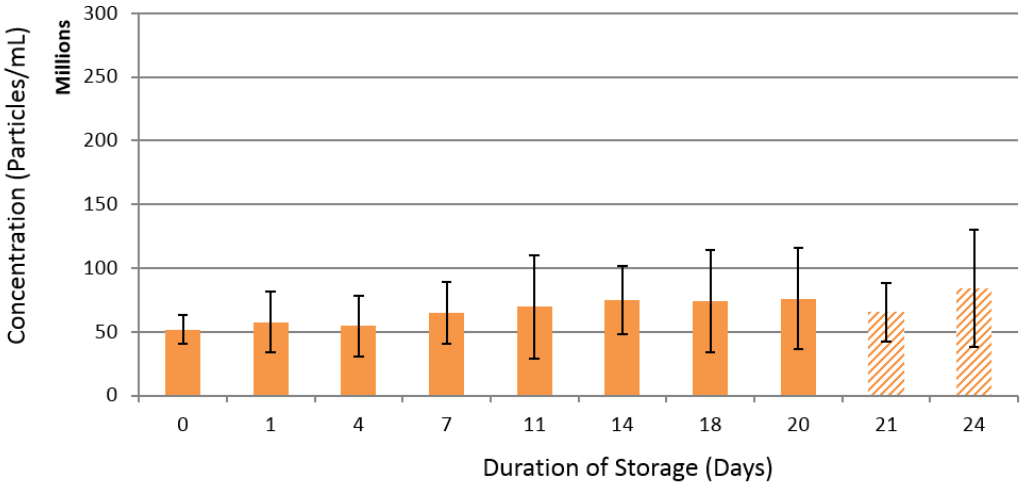

Figure 4.57. NTA analysis of nanoparticle concentration for the low concentration of trastuzumab emtansine. No statistically significant change is observed and no trend of particle concentration increase or decrease is noted.

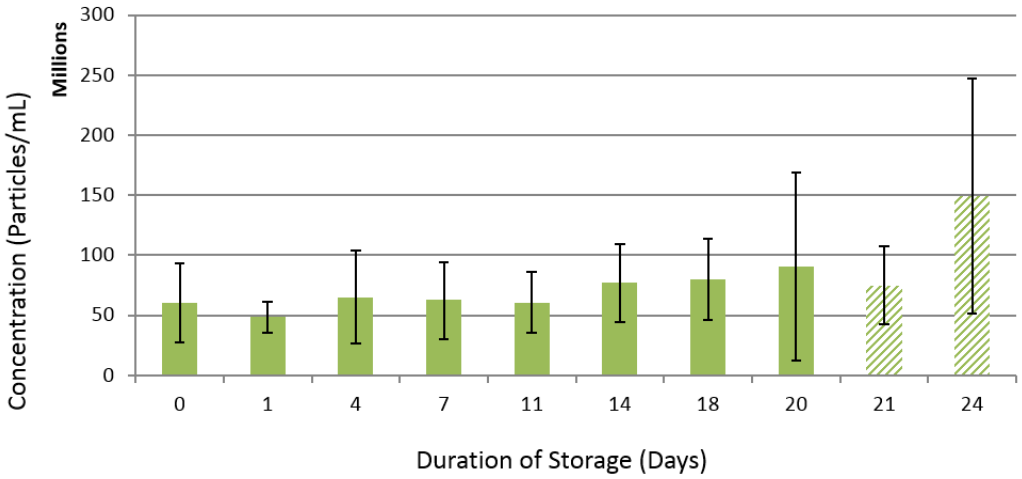

Figure 4.58. NTA analysis of nanoparticle concentration for the common concentration of trastuzumab emtansine. No statistically significant change is observed and a slight trend in particle concentration is seen but this is not statistically significant.

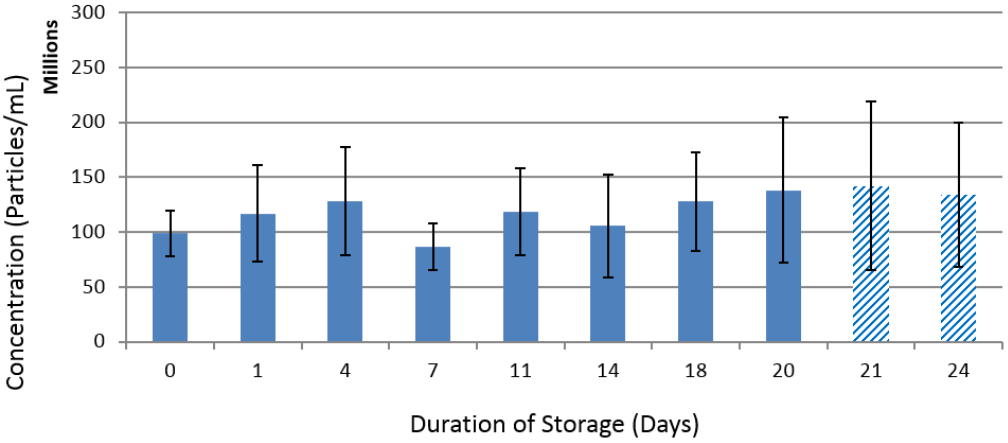

Figure 4.59. NTA analysis of nanoparticle concentration for the high concentration of trastuzumab emtansine. No statistically significant change is observed and no trend of particle concentration increase or decrease is noted.

4.6.12 UV analysis of extractables and leachables

Freeflex infusion bags, used as the containers for this study, are marketed as "plasticizer free" by the manufacturer, as the bags do not contain DEHP. [202] Regardless to maintain compliance with the NHS stability guidance for biopharmaceuticals, [102] the UV absorbance spectra of trastuzumab emtansine was recorded, according to method 2.2.10, to monitor for the accumulation of any leachable and/or extractable substances throughout the study period. The results are shown in (**Figure 4.60**) where trastuzumab emtansine exhibits a delta max at 280 nm. No changes to the delta max or absorption values are apparent from the spectra, indicating that no chromogenic substances are

accumulating in the solutions, to any measurable extent, when stored in Freeflex bags for periods of up to 20 days at 2-8 °C followed by 4 days at 25 °C. This seems like an issue that should be debated with the NHS, as this was unnecessary research that revealed plasticizer free bags don't leach plasticisers.

The absorbance at 280 nm was also recorded and plotted over time as a quick measurement of total protein concentration during the study (**Figure 4.61**). No decrease in protein concentration is observed compared to the measurement recorded on day 1 (SPC limit). This measurement was of interest, as small monomer decreases detected via SEC, combined with no increase in detectable oligomers could be due to aggregates with a diameter greater than 5 µm being trapped on the SEC column. If the detection at 280 nm via the UV assay remained high, while the detection of monomer at 280 nm via SEC declined, it could suggest aggregates larger than 5 µm were forming.

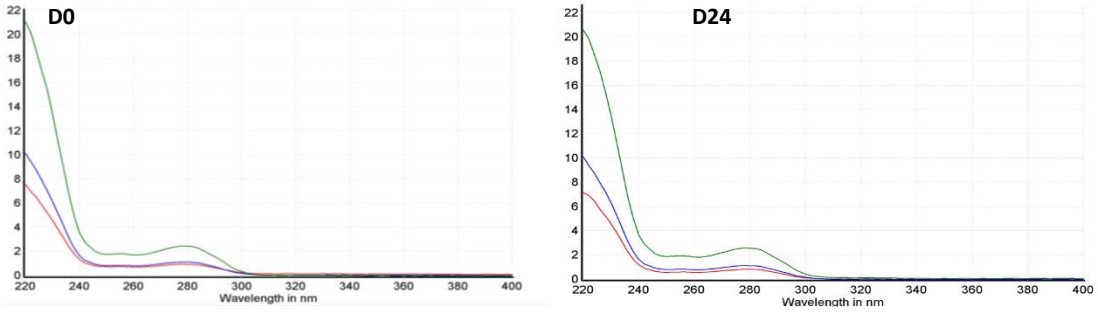

Figure 4.60. UV profile between 220 nm and 400 nm for trastuzumab emtansine, at day 0 and day 24. Delta max was unchanged, no change was noted.

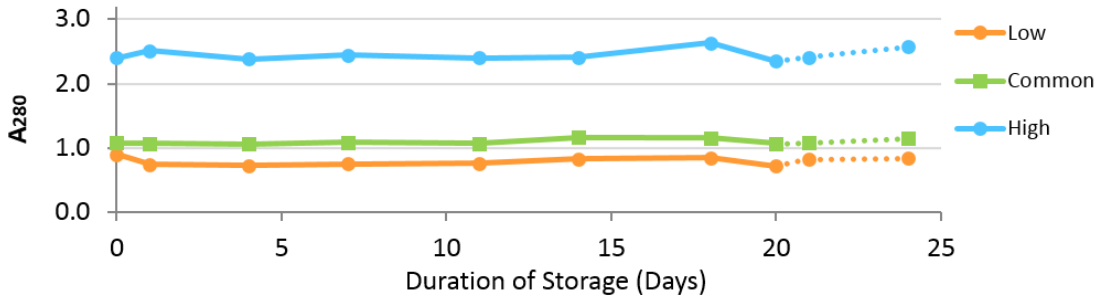

Figure 4.61. UV absorbance at 280 nm for each study concentration. Dashed lines represent 25 °C storage. The absorbance remains constant throughout the study, no trend of loss is apparent, no changes from day 0 were statistically significant.

4.6.13 LC-MS – Chemical degradation

LC-MS data gathered following methods 2.2.12-2.2.14, shows no evidence of chemical degradation occurring to the light or heavy chain fragments of the antibody throughout the course of the study, see (**Figure 4.62 A, B, C & D**), as a demonstration that the trastuzumab glycoprotein molecule remains structurally stable for up to 20 days when stored at 2-8 °C or following storage at 25 °C for up to 120 hours after this 20 day period.

4.6.14 LC-MS – Payload binding

Additional data processing, following method 2.2.23, of LC-MS data was also used to confirm that the cytotoxic DM1 and MCC-DM1 payloads remained covalently attached to the trastuzumab protein throughout the course of the study. The results are expressed as the payload (P) to light chain (LC) or heavy chain (HC) ratio, as shown in (**Figures 4.63 – 4.65).** A trend which indicated an increase in P:LC = 0 or P:HC = 0 throughout the course of the study, accompanied by a decrease in P:LC = 1 or 2 and P:LC = 1 or 2 would suggest that cytotoxic payloads are becoming detached from the trastuzumab protein upon extended storage; however this is not observed throughout the study.

The results indicate that the cytotoxic DM1 containing payloads remain conjugated to the antibody throughout the study period, and that no premature release of the cytotoxic agents occur upon extended storage due to of linker instability or hydrolysis.

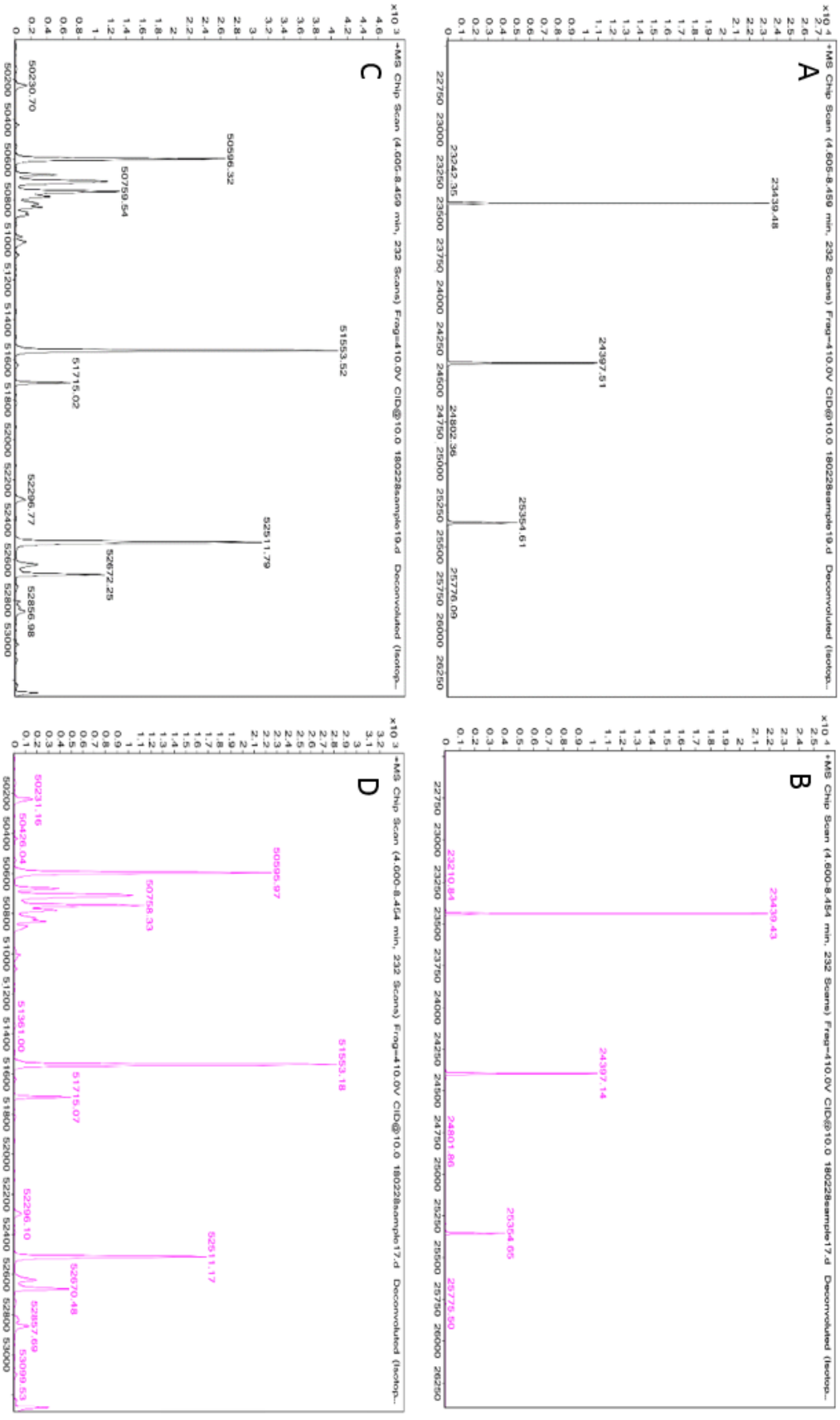

Figure 4.62. Reduced LC-MS analysis of the common concentration of trastuzumab emtansine. Light chain day 0 (**A**), Light chain day 24 (**B**), Heavy chain day 0 (**C**) & Heavy chain day 24 (**D**). Y-axis = TIC, X-axis = Mass (Daltons). No change in the glycosylation pattern or peak intensity was noted between D0 and D24.

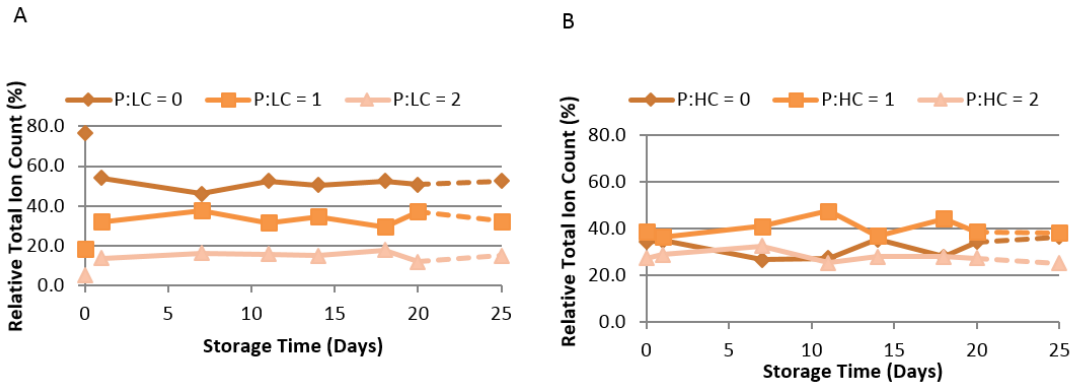

Figure 4.63. LC-MS analysis of low concentration trastuzumab emtansine showing the observed change over time in relative total ion count of light chains (**A**) and heavy chains (**B**) with zero, one or two payloads bound. No trend of loss is observable for any of the light or heavy chain species.

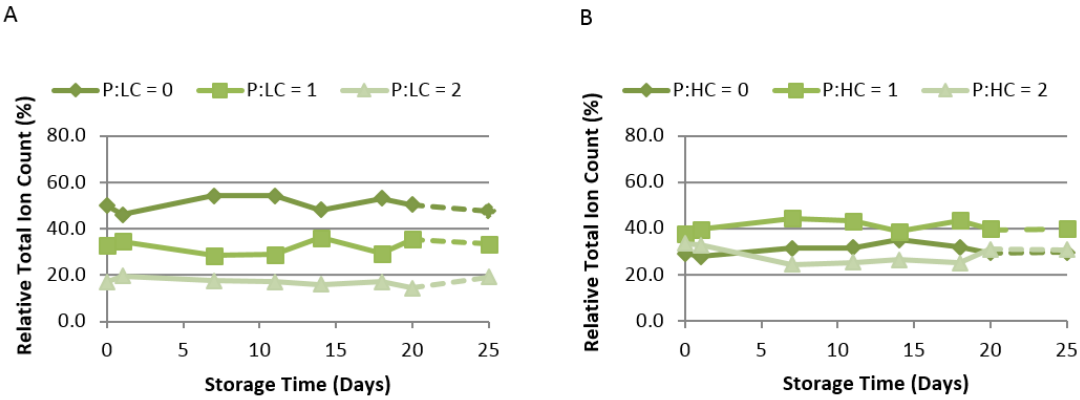

Figure 4.64. LC-MS analysis of common concentration trastuzumab emtansine showing the observed change over time in relative total ion count of light chains (**A**) and heavy chains (**B**) with zero, one or two payloads bound. No trend of loss is observable for any of the light or heavy chain species.

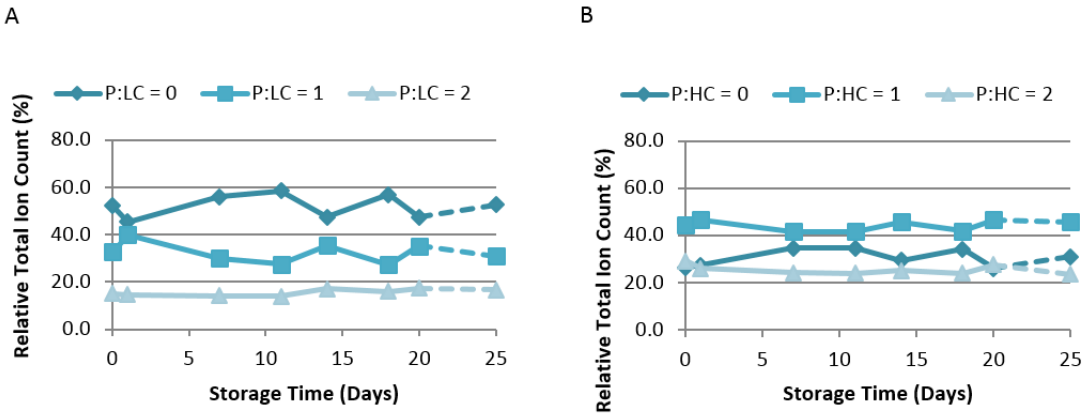

Figure 4.65. LC-MS analysis of high concentration trastuzumab emtansine showing the observed change over time in relative total ion count of light chains (**A**) and heavy chains (**B**) with zero, one or two payloads bound. No trend of loss is observable for any of the light or heavy chain species.

4.6.15 Cellular Assay – On target activity

Plate set up was performed according to method 2.4.2 and the plate was read according to method 2.2.11. Trastuzumab emtansine was assessed by measuring its ability to inhibit the growth of BT474 cells which express the HER-2 receptor via an MTT assay to measure cellular metabolism. This assay models the mechanism of action of the drug in the patients. Efficient inhibition of the growth of this cell line is dependent upon the integrity of the ADC. To control for intra assay variability the performance of the stability samples was indexed against that of a trastuzumab emtansine reference sample stored as concentrate in the glass vial. Throughout the study the performance of the stability study samples matched that of the reference sample (**Figure 4.67**). The performance of samples B.3 and B.4 was low on Day 20 (**Figure 4.67 B**), although this can be explained by the poor growth of the control samples on the assay plate these two samples were tested on. In agreement with this, subsequent tests on these samples saw the results return to normal. These data demonstrate that there was no statistically significant loss of on target activity over the course of the study ($p<0.05$, one-way analysis of variance with post hoc Bonferroni).

4.6.16 Cellular Assay – Off target activity and hepatocyte toxicity

Plate set up was performed according to method 2.4.2 and the plate was read according to method 2.2.11. Trastuzumab emtansine was assessed by measuring its ability to inhibit the growth of human keratinocyte cell line 'HaCaT' and the hepatic carcinoma cell line 'HepG2' which do not express the HER-2 receptor. To control for intra assay variability the performance of the stability samples was indexed against that of a trastuzumab emtansine reference sample stored as concentrate in the glass vial. Throughout the study the performance of the stability study samples matched that of the reference sample (**Figure 4.68**). The performance of samples A.3, A.4 and C3 were low on Day 7 (**Figure 4.68 A**), although this could be explained by a dilution error on the assay plate these two samples were tested on. In agreement with this, subsequent tests on these samples saw the results return to normal. To test more specifically for any

changes in liver toxicity of the study samples the HepG2 was used (**Figure 4.69**). The performance of the stored samples matched that of the reference sample in these tests. These data sets demonstrate that there was no measurable change in functional activity of the stored trastuzumab emtansine samples over the course of the study.

4.6.17 Trastuzumab emtansine stability study conclusion

The results of this stability study described in section 4.6 indicate that trastuzumab emtansine remains physico-chemically and functionally stable for up to 20 days when diluted between a clinically low and high concentration with sodium chloride 0.9% solution for infusion and stored at 2-8 °C in a Fresenius Kabi Freeflex infusion bag. The study also indicates that further storage at 25 °C for up to 96 hours has no detrimental effect on the physicochemical or functional stability of trastuzumab emtansine. A major outcome for this study is the application of a 21-day extended shelf life for Kadcyla brand trastuzumab emtansine.

A 2016 study found that on average, £1312 of Kadcyla is wasted per dose. [278] As Kadcyla is administered every three weeks, according to the median overall survival found in the EMILIA and THER3SA trials, a patient should receive 40 cycles of treatment. [103, 104] This amounts to £52,480 of wasted drug per patient. The 21-day shelf life allows Bath ASU to minimise this wastage by manufacturing multiple doses for either the same or different patients simultaneously, and they can be easily transported to different hospitals around the UK ready for the patients up to three weeks in advance. These savings can be passed onto UK hospitals, reducing the cost burden of Kadcyla as well as providing a unique product, the first ready to use extended stability ADC product in the world, as far as the author is aware of, circa 2018.

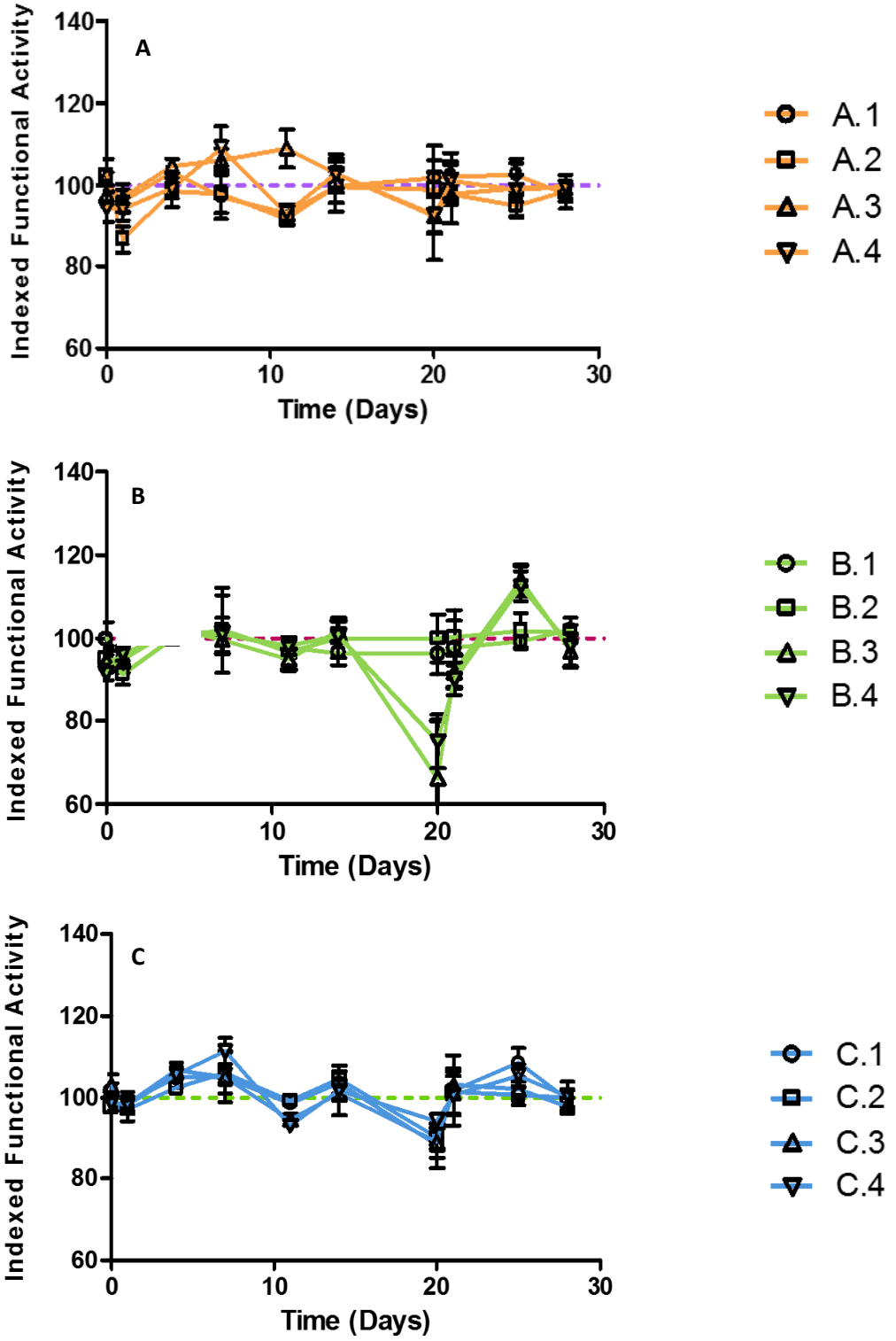

Figure 4.67. On target functional activity of trastuzumab emtansine samples stored diluted at low (**A**), common (**B**), and high (**C**) concentrations. The performance of the stability study samples was indexed against that of a trastuzumab emtansine reference sample. Data shown are means with SD of quintuplicate replicate measurements for each of four bags per concentration. No statistically significant change was observed for any of the concentrations tested.

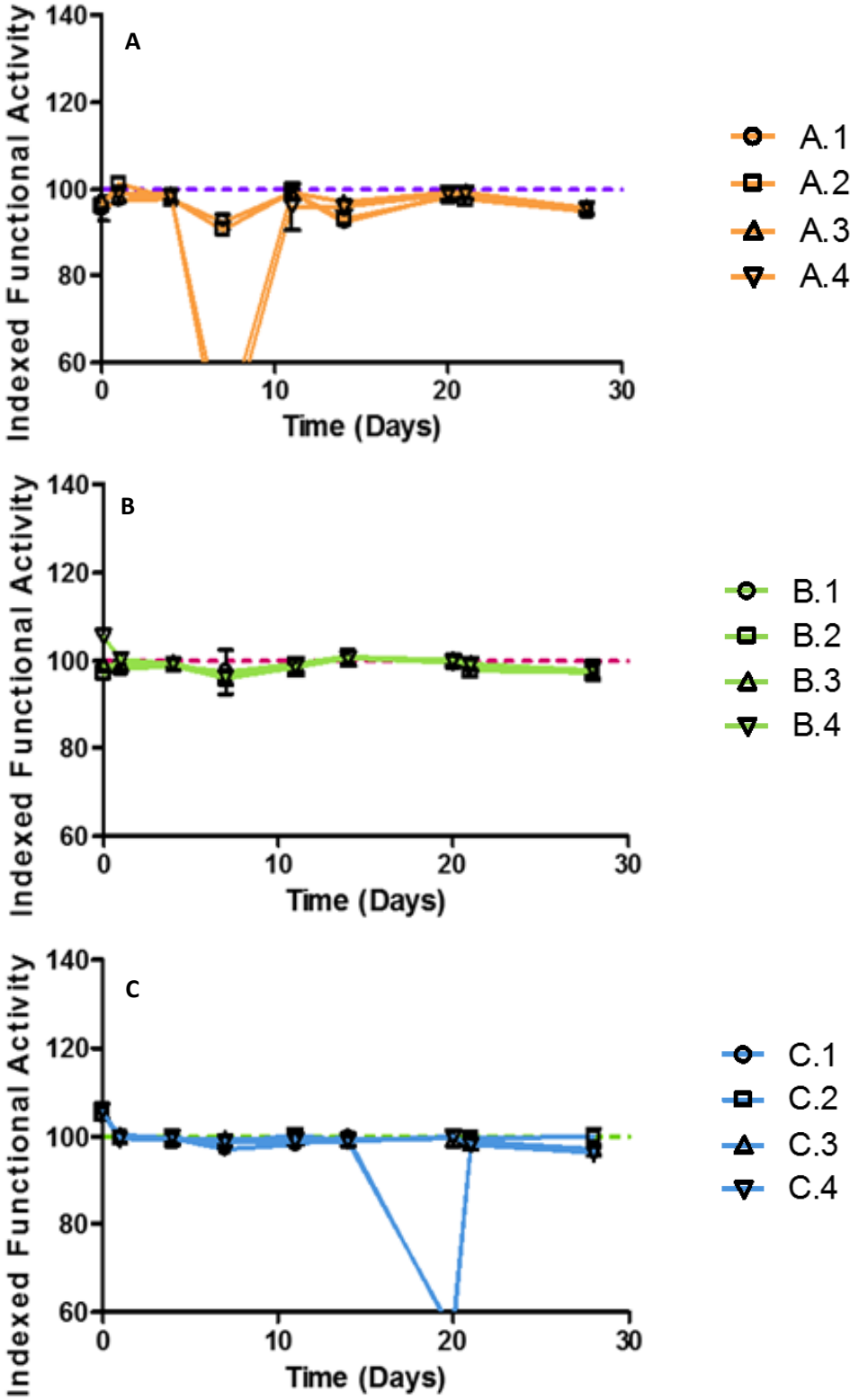

Figure 4.68. HaCaT assessed, off target toxicity of trastuzumab emtansine samples stored diluted at low (**A**), common (**B**), and high (**C**) concentrations. The performance of the stability study samples was indexed against that of a trastuzumab emtansine reference sample. Data shown are means with SD of quintuplicate replicate measurements for each of four bags per concentration. No statistically significant change was observed for any of the concentrations tested. Some data points are off the scale due to dilution errors. The subsequent measurements return to no change, helping identify them as erroneous.

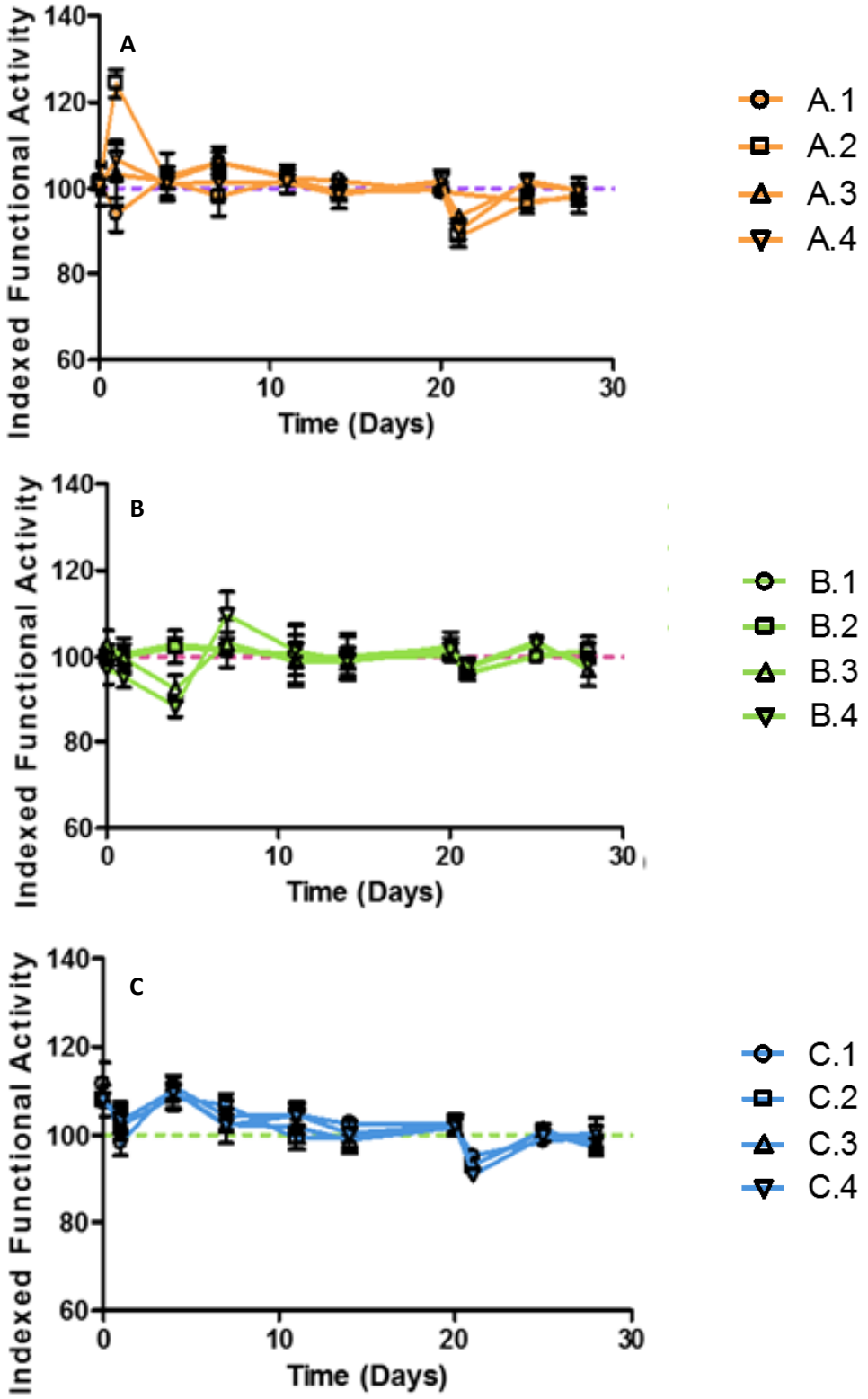

Figure 4.69. HepG2 assessed, off target toxicity of trastuzumab emtansine samples stored diluted at low (**A**), common (**B**), and high (**C**) concentrations. The performance of the stability study samples was indexed against that of a trastuzumab emtansine reference sample. Data shown are means with SD of quintuplicate replicate measurements for each of four bags per concentration. No statistically significant trend was observed.

Chapter 5. Polyolefin infusion bag comparison study

5.1 Introduction

An outcome of the Remsima infliximab study was hundreds of UK hospitals using that data to apply a seven-day shelf life to their Remsima products. However, some hospitals phoned and asked if they could compound Remsima using a different brand of polyolefin infusion bag and still apply the 7-day shelf life. It is well established that the chemical composition of storage devices such as intravenous (IV) infusion bags, can have a significant impact on the stability and quality of pharmaceutical products, especially when storage in the device is over extended periods of time. [126,203-205] Currently there are four main types of plastics used in the manufacture of IV infusion bags, those being polyethylene (PE), polypropylene (PP), poly ethylene vinyl acetate (EVA) and polyvinyl chloride (PVC). Combined with this, there are also a number of processes used for the manufacture of infusion bags, such as co-extrusion and co-polymerisation, while the plastic can also be either a high density or low-density polymer. Finally, IV infusion bags may be comprised of a single plastic layer, or multiple layers, in which case not all of the component plastics will be in contact with the drug. In terms of the specific drug quality aspects affected by the chemical composition of infusion bags, the majority of studies have evaluated their impact on small molecule drugs. Here, the leaching of plasticisers such as di-2-ethylhexyl-phthalate (DEHP) from PVC bags, permeability of oxygen, differing degrees of drug adsorption to the plastic, and differences in aggregation, are found to be the predominant factors influencing drug quality [126,127,203-205]

While primary drug manufacturers must demonstrate the compatibility of drugs with both diluents and storage devices during the 'within-use' period, the requirements for set out in the NHS yellow cover documents for extended stability studies and the application of the stability studies, circa 2015, only stated:

"Extrapolation of data between different containers and infuser devices may be permissible provided the drug degradation pathway and physical properties of the container are well understood. Critical physical properties of a container include oxygen permeability, water permeability (water loss), light permeability, material constitution and possible extractives and adsorbent potential. Any extrapolation must be evaluated and justified. Non-PVC containers (polyolefin) should routinely be the first-choice container. The choice of flexible versus semi-rigid containers is product and/or study specific but it may not always be possible to extrapolate between the two due to fundamental differences in certain properties, which include the material and quantity of residual air" [101].

This allows stability data collected for a drug in one container type to be applied to products made in another container type, often hospitals will request a product in a specific brand of container, this can help reduce administration errors, as the overage in different brands of infusion bags can vary from 70 mL to 95 mL in a 250mL Fresenius Kabi infusion bag compared to a Baxter infusion bag. What this difference in overage volume means is that specific doses will need to be made in different bag sizes and at different concentrations which can cause confusion when changing bag brand or type between hospital inhouse compounding units and external aseptic compounding units. Ideally all compounders could use the same infusion bag but even NHS hospitals will use different bags depending on which regional contract tender they have to abide by. This means that it is not possible to perform a stability study in a single bag type that will suit all hospitals, hence hospitals will request that products be made in the bag types they prefer and explains why the NHS stability guidance document will allow stability data gathered in one bag to be applied to different bag types.

5.2 Study design

This study was designed to investigate what difference infusion containers had on biopharmaceutical stability, and if stability data generated in one container can be safely applied to a different container. As such, this is not a stability study, but a bag

comparison study to investigate the characteristics of biopharmaceutical products most likely to be affected by a change in container material. Therefore, this study will assess monomer concentration, reversible soluble aggregates (dimers, trimers), nanoparticle formation, microparticle formation, visible changes, moisture loss, as well as utilizing scanning electron microscopy to evaluate the morphology of the bag surfaces in detail.

The stability of three different types of licensed biopharmaceutical were investigated: a chimeric antibody, a humanized antibody and a fusion protein, when stored in three different brands of PO infusion containers Viaflo, Freeflex and Macoflex (**Figure 5.1**). All three are described as 'polyolefin' infusion bags, however their plastics are formed using a variety of chemical monomers and each bag is then manufactured using different processes. Viaflo infusion bags are comprised of polyamide, polyethylene and polypropylene polymers and manufactured using a co-extrusion process. Freeflex bags are manufactured using a multi-layer process, where the inner layer in contact with the drug is composed of polypropylene. Macoflex-N bags are manufactured using a co-polymerisation process where the plastic is formed from a mixture containing both ethylene and propylene monomer units.

To improve data comparability the surface area of each bag was calculated, following method 2.5.1, (**Table 5.1**) and a modified final volume was created by withdrawing all saline from the bags before adding a known volume of saline back into the bag, followed by a volume of drug. Four replicate bags were made for each combination of drug and bag, resulting in 36 samples, which were stored at 25 °C. To manage this work, manufacture of the samples was staggered allowing all work on a single day to be confined to a single drug.

Brand	Width (mm)	Length (mm)	Surface Area (cm^2)	Study Fill Volume (mL)	Surface Area : Volume
Baxter	85	123	209	21.3	9.8
Fresenius Kabi	85	115	196	20.0	9.8
Maco Pharma	71	117	166	16.8	9.9

Table 5.1. The dimensions, calculated surface area, study fill volume and surface area to volume ratio of the three brands of polyolefin infusion bags used in this study.

Figure 5.1. A photograph of the three brands of infusion bags investigated during this comparison study. Baxter Viaflo, Fresenius Kabi Freeflex and Maco Pharma Macoflex.

5.3 Results

5.3.1 Visual inspection

Following method 2.2.2, all infusion bags remained clear for the duration of the study with no visible precipitates or particulate matter detected with the naked eye. No change in colour or turbidity was observed over the study period for any drug in any of the three bag types.

5.3.2 Size exclusion chromatography analysis of monomer concentration

Following method 2.2.16, all HPLC chromatograms of the drugs were characterised by a single major peak. Results from HPLC analysis are presented as the percentage change relative to Day 0 samples for each drug across the three types of

infusion bag tested (**Figure 5.2**). Each mean percentage presented for a given drug in a particular type of bag is derived from the average abundance of drug (measured in triplicate) across four independent storage devices. As such, each mean percentage represents an average calculated from twelve independent chromatograms. Both Trastuzumab (**Figure 5.2 A**) and Abatacept (**Figure 5.2 C**) showed no obvious change in drug concentration in any of the devices tested throughout the study period. Rituximab abundance increased over the study (**Figure 5.2 B**), which was considered likely to be due to incomplete mixing of the Day 0 sample.

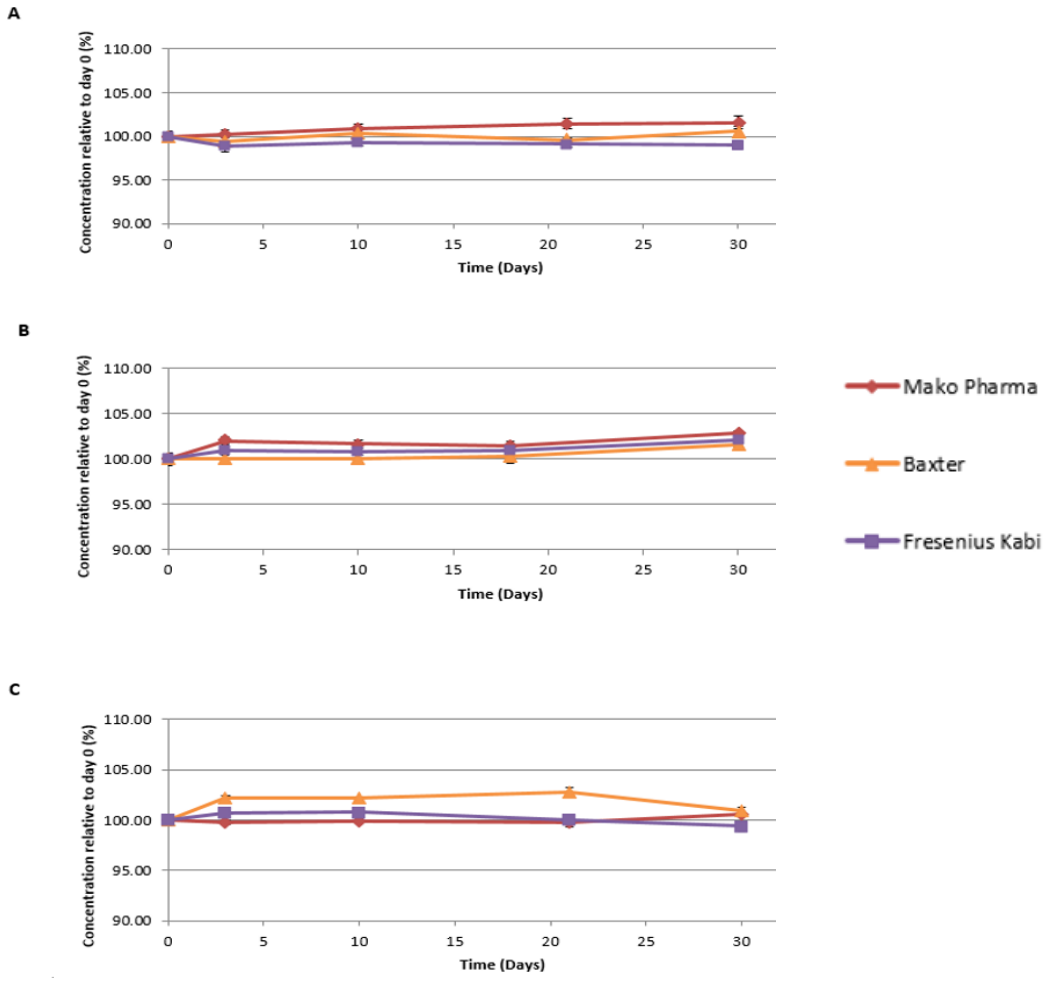

Figure 5.2. SEC analysis of monomer concentration relative to day 0 for (**A**) Trastuzumab, (**B**) Rituximab and (**C**) Abatacept, when stored in three brands of polyolefin infusion bag. Rituximab showed a trend of increase, and Mako Pharma bags showed a statistically significant but temporary increase in abatacept concentration before returning to 100 % relative to day 0.

5.3.3 Dynamic light scattering analysis of sub-visible particles

Dynamic light scattering results collected according to method 2.2.4, are expressed both as the mean diameter and percentage abundance of detected drug particles within the test solution (**Figure 5.3**). A significantly larger mean diameter could suggest the formation of aggregates which have a greater spherical volume, while a decrease in percentage abundance of drug monomer could be attributed to larger aggregate formation. The measured drug diameters were found to be similar for all bags throughout the study (**Table 5.2**), ranging from 9.63 – 13.60 nm immediately after preparation on day 0, to 9.88 – 12.92 nm on day 30. The small differences seen in (**Figure 5.3 A**) could be due to monomer/dimers further aggregating into microscale particles, which appears to occur more readily in Mako Pharma bags, though the differences between the bags was statistically insignificant.

Drug	Bag Brand		Day 0	Day 3	Day 10	Day 21	Day 30
Trastuzumab	Baxter	Mean	12.0	12.5	14.6	13.5	11.9
		±SD	1.3	1.0	1.8	1.4	1.9
	Fresenius Kabi	Mean	12.6	11.6	14.1	12.1	11.9
		±SD	1.5	1.3	1.3	0.7	0.9
	Mako Pharma	Mean	13.6	13.3	14.7	12.7	12.9
		±SD	1.4	2.5	1.4	1.7	1.2
Rituximab	Baxter	Mean	11.9	13.8	13.1	10.9	10.6
		±SD	1.7	1.7	1.7	1.7	1.7
	Fresenius Kabi	Mean	12.6	11.9	12.5	11.2	11.5
		±SD	2.0	1.7	1.7	1.7	1.7
	Mako Pharma	Mean	13.6	13.3	14.7	12.7	12.9
		±SD	1.4	2.5	1.4	1.7	1.2
Abatacept	Baxter	Mean	9.7	9.6	9.5	9.6	9.9
		±SD	0.4	0.4	0.2	0.2	0.2
	Fresenius Kabi	Mean	9.6	9.8	9.6	9.6	9.9
		±SD	0.3	0.4	0.2	0.2	0.2
	Mako Pharma	Mean	9.6	9.6	9.4	0.4	9.8
		±SD	0.3	0.2	0.2	0.2	0.1

Table 5.2. Monomer/Dimer mean diameter (nm) for all drug and bag combinations during the bag comparison study (n=4). No statistically significant changes were observed.

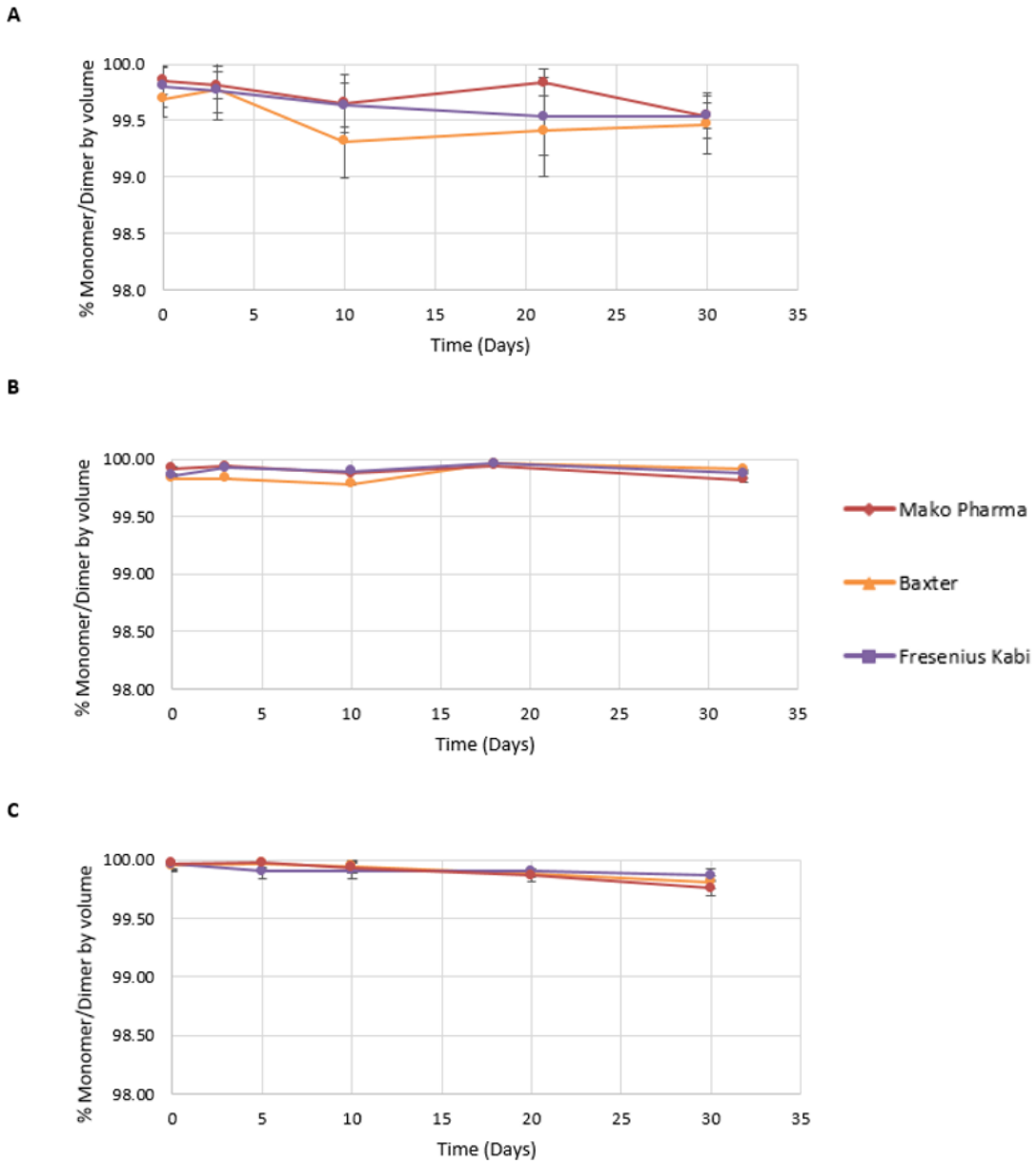

Figure 5.3. Change in % monomer/dimer by volume for (**A**) Trastuzumab, (**B**) Rituximab and (**C**) Abatacept, stored in three brands of polyolefin infusion bag. There were no significant differences between bag brands for any of the drugs tested, however there was a statistically insignificant difference noted for trastuzumab between all bag types on day 21, and on most days between Mako Pharma and other brands.

5.3.4 Microflow imaging analysis of micro-particles

Microflow imaging results, gathered according to method 2.2.6, revealed a dramatic difference in the change in concentration of particles greater than 10 µm and greater than 25 µm between the different bag types (**Figure 5.4 & 5.5**). These particle sizes, are of particular interest as hard particles over 10 µm can occlude blood vessels. [206] Furthermore, the United States of America, British and European pharmacopeia all

place concentration limits on the number of particles present with mean diameters above 10 µm and 25 µm. [110,206] Sub-visible particles are a cause of concern due to their ability to cause vein irritation, anaphylactic shock, phlebitis, pulmonary emboli, pulmonary granulomas, immune system dysfunction, pulmonary dysfunction, infarction, and death. [109] And aggregated drug is a problem as it can raise an immune response in patients, leading to inflammation, anti-drug antibodies, as well as faster rates of drug clearance. [109] Furthermore, aggregated drugs can have reduced binding strength and impaired pharmacokinetics. The aggregation profiles for particles with diameters above 10 µm and 25 µm generally follow the same trends, (**Figure 5.4 & 5.5**).

Regarding particles greater than 10 µm, the chimeric antibody rituximab aggregates the least overall and, in the Fresenius Kabi and Maco Pharma bags actually demonstrates a decrease from levels of particulates on day 0, while in a Baxter bag becomes significantly different by day 32 (**Figure 5.4 B**) ($p<0.05$, one-way analysis of variance with post hoc Bonferroni). Furthermore, rituximab on day 0 has a significantly higher concentration of particles over 10 µm in a Maco Pharma and Fresenius Kabi bag, compared to the Baxter bag (**Figure 5.4 B**).

Trastuzumab in a Fresenius Kabi bag is significantly different by day 10, while in a Baxter bag it is not significantly different until day 30 (**Figure 5.4 A**). At no measured point was trastuzumab different in a Maco Pharma bag (**Figure 5.4 A**). At each timepoint the bag type with the highest and lowest amount of particles over 10 µm remained the same. The concentration of particles over 10 µm in a Maco Pharma bag throughout the study, never exceeded the concentration of 10 µm in a Fresenius Kabi bag, and the concentration of particles over 10 µm in a Baxter bag only exceeded it by Day 30 (**Figure 5.4 A**).

Abatacept was the most aggregation prone drug, reaching almost 40 thousand particles > 10 µm per mL by day 31 in the Baxter bags (**Figure 5.4 C**). Abatacept in Maco Pharma bags was not significantly different until day 31, while it was deemed significantly different by day 10 for FK bags and day 5 for Baxter bags ($p<0.05$, one-way

analysis of variance with post hoc Bonferroni). The trends in the particles greater than 25 micrometres matches the trends observed in the particles greater than 10 micrometres. While particles greater than 10 µm in all bags were similar on Day 0, the particles concentrations rose much faster for Fresenius Kabi and especially Baxter bags, which on Day 0 had the lowest concentration of particles for Abatacept. By Day 20 the particle levels in Baxter bags had eclipsed those in Fresenius Kabi bags (**Figure 5.4 C**).

Regarding particles over 25 µm, the trends are very similar to the trends seen with the particles over 10 µm. However, the absolute numbers are almost ten-fold lower for all combinations of bag and drug. The Fresenius Kabi bag had the highest level of particulates for trastuzumab on Day 0 and demonstrated the greatest increase in particle levels by Day 30, while the Maco Pharma bag had the lowest level of aggregates on Day o and the smallest increase by day 30 (**Figure 5.5 A**).

For rituximab, the Baxter bags had the greatest level of increase by day 32, while the Maco Pharma bags had the greatest level of particles on Day 0 and the particle concentration only decreased over the study. Fresenius Kabi bags had the lowest level of particle on day 0 and particle concentrations only decreased over time (**Figure 5.5 B**).

Abatacept was the most aggregation prone for 25 µm particles as well, reaching around 5000 / mL in the Baxter bags. The trends for 10 µm particles were conserved, with Baxter bags having the highest rate of aggregation, and Maco Pharma bags having the lowest rate of aggregation. Baxter bags also had the lowest level of particulates on Day 0, exceeding Maco Bags by day 10 and Fresenius Kabi bags by day 31 (**Figure 5.5 C**).

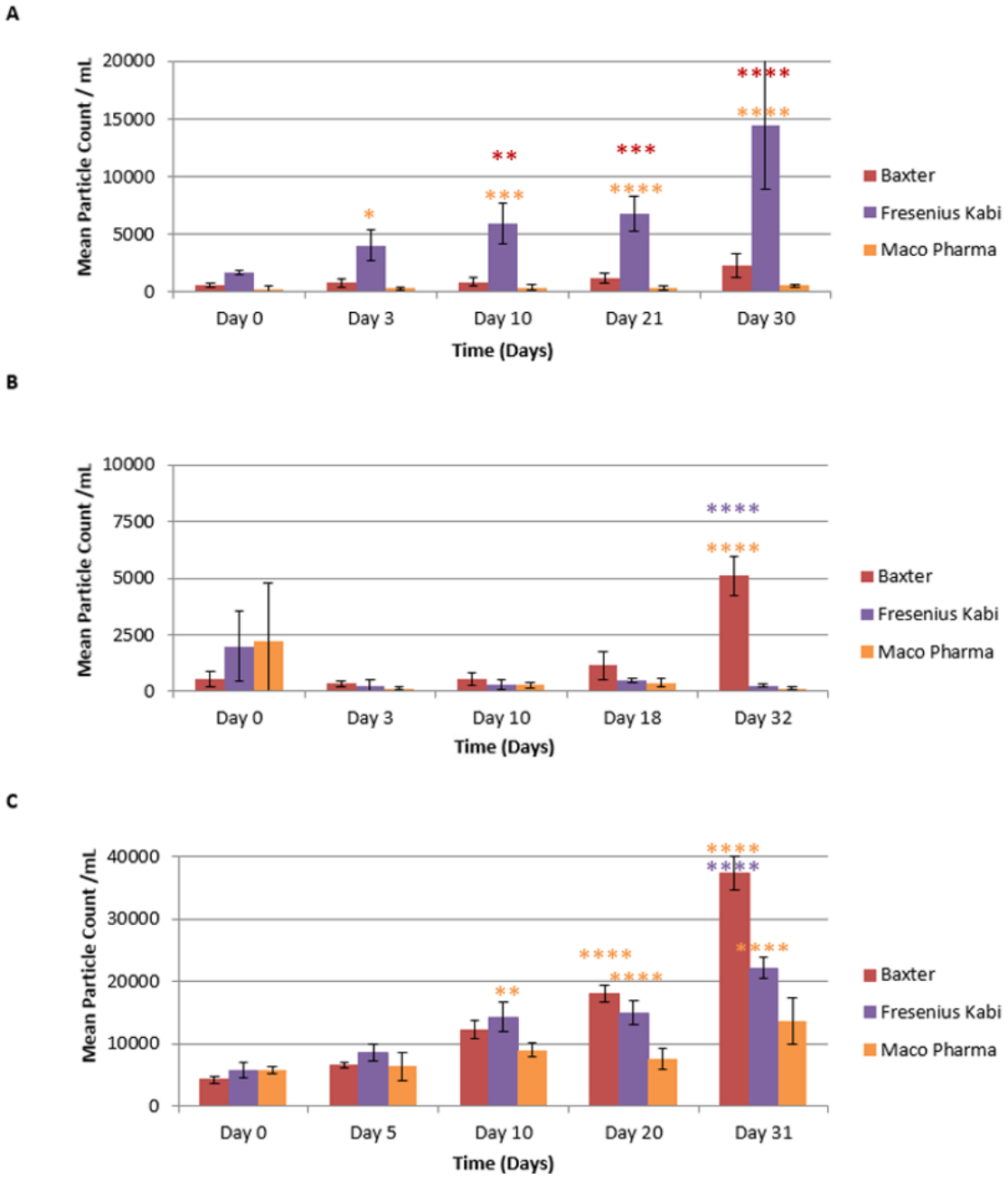

Figure 5.4. Change in concentration of microparticles > 10 µm for (**A**) Trastuzumab, (**B**) Rituximab and (**C**) Abatacept, stored in three brands of polyolefin infusion bag. Particles for trastuzumab and abatacept increased upon storage, however the rate of increase was greatest for abatacept in Baxter bags and greatest for trastuzumab in Fresenius Kabi bags. The trend of increase was only observed for rituximab stored in Baxter brand bags. *, **, *** & **** indicate a p value < 0.05, 0.01, 0.001 & 0.0001 respectively. The colour of the * indicates to which data set the difference is between.

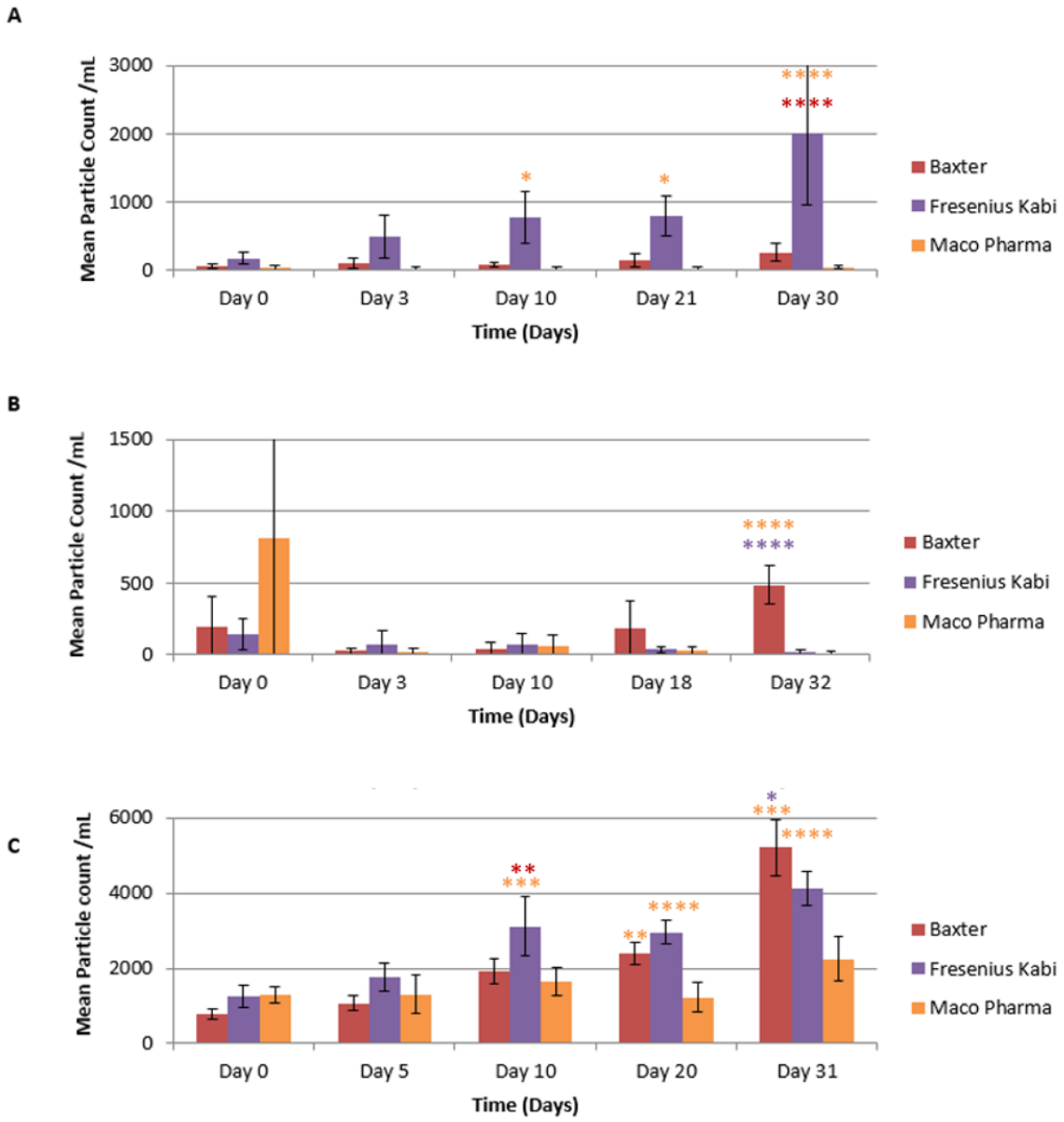

Figure 5.5. Change in concentration of microparticles > 25 µm for (**A**) Trastuzumab, (**B**) Rituximab and (**C**) Abatacept, stored in three brands of polyolefin infusion bag. Particles for trastuzumab and abatacept increased upon storage, however the rate of increase was greatest for abatacept in Baxter bags and greatest for trastuzumab in Fresenius Kabi bags. The trend of increase was only observed for rituximab stored in Baxter brand bags. The trends for particles > 25 match the trends for particles >10 µm. *, **, *** & **** indicate a p value < 0.05, 0.01, 0.001 & 0.0001 respectively. The colour of the * indicates to which data set the difference is between.

5.3.5 Scanning electron microscopy

Scanning electron microscopy was used to image the inner bag surface according to method 2.5.7. This was to investigate if the physical surface was different and could contribute to adhesion and aggregation. This SEM work was performed by Mrs Ursula Potter (University of Bath, Bioimaging Suite). We can see the surface at a x10,000 magnification where the Baxter Viaflow had a rougher surface than either the Maco Pharma or Fresenius Kabi infusion bag (**Figure 5.6**).

We also imaged a Baxter Viaflow and Maco Pharma MacoFlex-N bag after two days storage containing trastuzumab at 25 °C for 48 hours (**Figure 5.7**). This was to measure any differences at the bag surface. It was possible to image a large protein aggregate adhered to the bag surface for both bags, however the particle for the Baxter bag has a larger diameter and is strafed by two other asymmetrical adhered particles (**Figure 5.7 A**). The Maco Pharma bag had a single, more irregular particle, appear to protrude off the bag surface more than the particle on the Baxter bag, this particle has a more three-dimensional structure to it (**Figure 5.7 A**). It is interesting to note the difference in the adhered aggregates shapes, perhaps the smoother Macopharma bag plastic was lass easy to adhere to than the already bound protein, thus a more 3D structure emerges naturally, while in the Baxter bag the protein-surface interaction is as if not more viable than a protein-protein interaction, thus leading to wider, flatter protein deposits. Alternatively it is possible that similar structures to the 3D structure seen on the x10000 magnification may be acting as scaffold to the protein.

The differences in their surface structure must be related to the plastics types and the manufacturing processes used. The Baxter bag appears to have the roughest surface and is the only bag that is made using a co-extrusion of polyamide, polyethylene and polypropylene. Perhaps this process causes the roughness noted. The Maco Pharma and Fresenius Kabi bags have inner surfaces comprised of a single material, of either polypropylene or a polypropylene/polyethylene copolymer, perhaps this explains why their surfaces are generally much smoother than the Baxter bag.

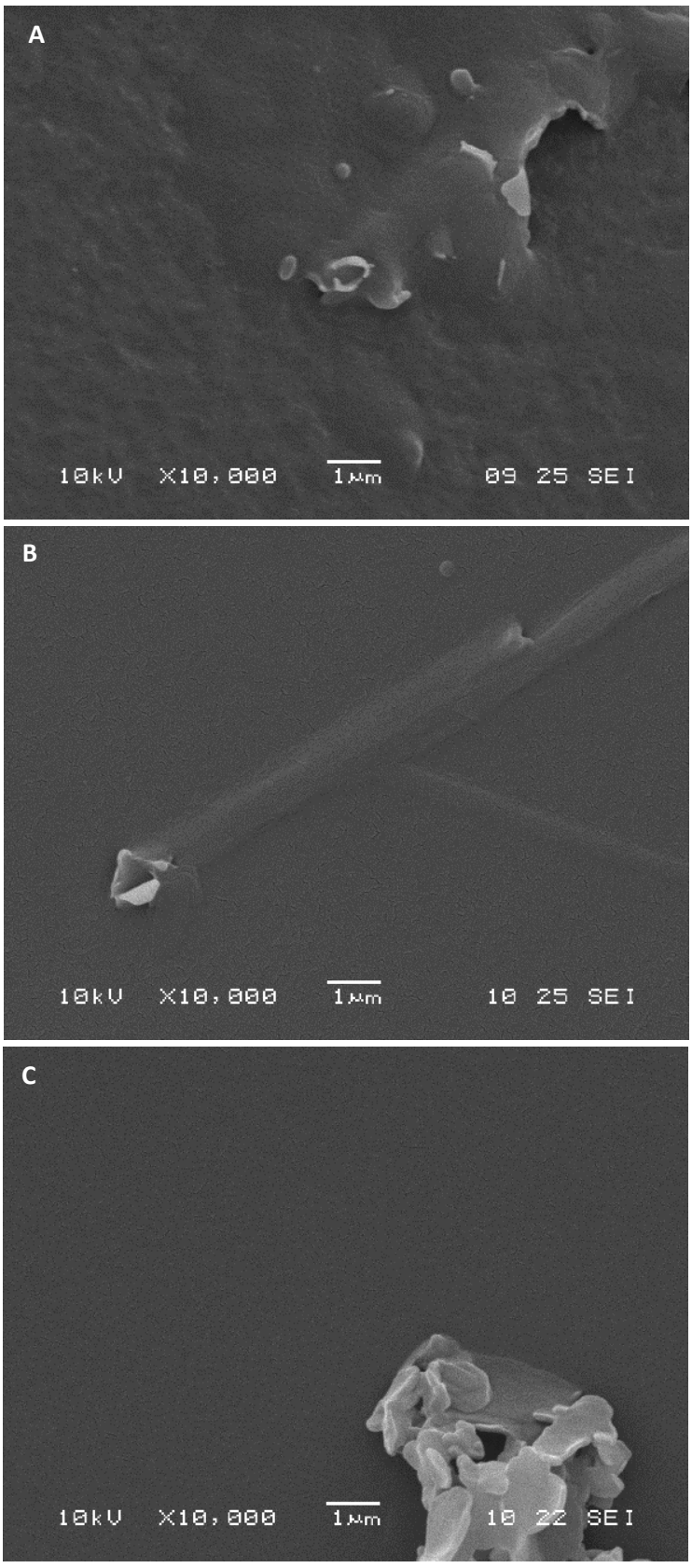

Figure 5.6. SEM images of (**A**) Baxter Viaflo, (**B**) Fresenius Kabi Freeflex, and (**C**) Maco Pharma Macoflex-N polyolefin infusion bags at x10000 magnification. The Baxter Viaflo bag has a rougher surface appearance, the Maco Pharma bag has a large 3D structure sticking out.

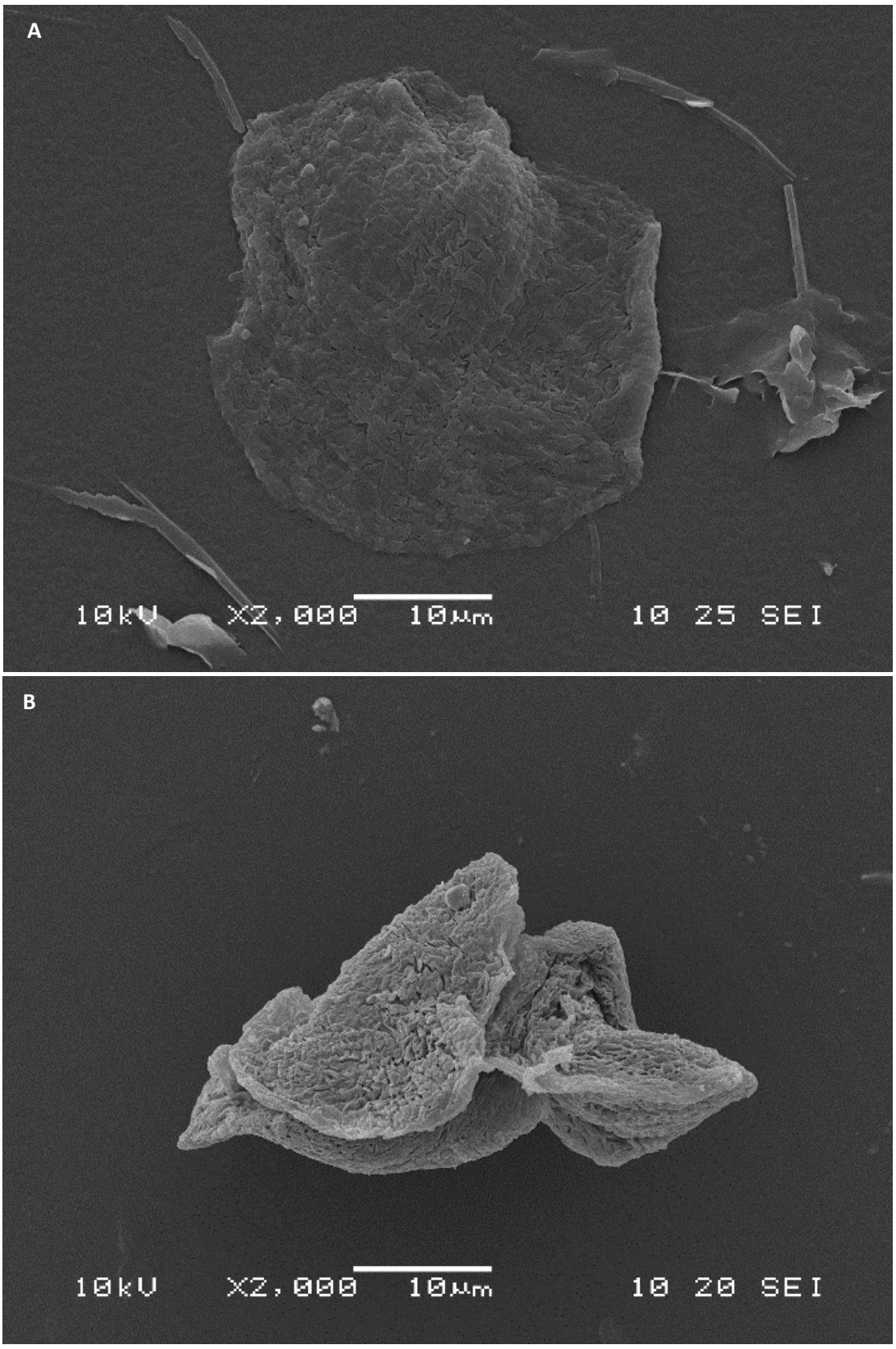

Figure 5.7. SEM images of (**A**) Baxter Viaflo and (**B**) Maco Pharma Macoflex-N polyolefin infusion bags at x2000 magnification after 2 days storing trastuzumab at 25 °C. Both show aggregates, with the Baxter bag having a wider flatter aggregate and the Maco Pharma bag having a taller more 3D structure to it.

5.4 Bag comparison study discussion

No significant or conserved differences in the mean monomer/dimer diameter or percentage abundance by volume were found using DLS (**Figure 5.3 & Table 5.2**). SEC also found no significant or clinically relevant loss of monomer or increase in dimer and trimer. (**Figure 5.2**), suggesting that nanoscale particles formation, early oligomerisation and concentration are not significantly difference for trastuzumab, rituximab or abatacept when stored in Baxter Viaflow, Fresenius Kabi Freeflex or Maco Pharma Macoflex-N polyolefin infusion bags at 25 °C.

However, results from the MFI (**Figure 5.4 & 5.5**) clearly indicate a dramatic and statistically significant difference occurs during storage with regards to microscale particulates above 10 and 25 micrometres, between most bags containing for all drugs tested. Protein aggregation differences due to the container brand, are most likely due to differences in the inner surface of the infusion bags. Protein interactions at solid interfaces are a known issue, which is why non-ionic surfactants such as polysorbate 20 and 80 are added to biopharmaceutical formulations. [237] Proteins will mainly adhere to surfaces via *van der Waals* forces, electrostatic interaction of the surface charge and charge of the protein, also known as the zeta potential and hydrophobic interactions. [238] The inner surfaces were PP, PP & PP co-polymer and a PP, PE & polyamide copolymer. I propose the zeta potential of these surfaces is different, based on research that measured the zeta potential of multiple polymeric plastics including PP. [239] The same paper also identified that at different pHs the plastic polymers zeta potential also changed but at different rates in a non-linear trend. [239] It is possible that as the different drug solutions are at different pHs, ranging from pH 6 to pH 7.5, the zeta potential of each bag plastics could be different for each drug. This could certainly impact the protein surface interaction, which would affect adhesion, which affects conformation, which affects aggregation. It is possible that the Fresenius Kabi bags have a stronger Zeta potential than the Baxter or Maco Pharma bags when filled with the trastuzumab solution. Rituximab also uses polysorbate 80 as its non-ionic surfactant while trastuzumab uses polysorbate 20 and abatacept uses poloxamer 188 as stated in their

summary of product characteristics, however the SPCs do not state the concentration. Studies have shown that at the same concentrations, polysorbate 20 is better at preventing protein adsorption to plastic than polysorbate 80. [240] At a high concentrations poloxamer 188 outperforms polysorbates as a surfactant. [240] However the degree of microparticle aggregation seen between the drugs does not correlate with these facts. One explanation could be, due to the dilution of the drugs, the concentration of the surfactants is too low to work effectively as surfactants. However, as the concentration of the surfactants is not stated in the SPCs of any drugs it is purely speculation.

The SEM results (**Figure 5.6**) demonstrate the surface for polyolefins bags can be different at a subvisible level, leading to different types of aggregation forming at the bag surface (**Figure 5.7**). It is possible that the microarchitecture of the bags, including differences in surface roughness may have in impact on the protein-surface interactions, as a rougher surface as seen in Baxter Viaflo bags increases total internal surface area but also can reduce the size of potential binding patches. This may partially explain why abatacept, which is a fusion protein and thus requires a smaller surface to bind to aggregates so much more in Baxter bags than the Fresenius Kabi and Maco Pharma bags.

It is demonstrable that not all polyolefin infusion bags are equal with regards to the aggregation of biopharmaceuticals. Furthermore, no bag type we investigated can be considered inferior or superior to another for all drugs we investigated, as results (**Figure 5.4 & 5.5**) show at different times and for different drugs each bag could be considered 'best'.

This work was presented to members of the NHS regional quality assurance committee and the NHS yellow cover document was then amended in 2017 with "… care should be taken when extrapolating to a different manufacturer's container, there is some evidence that not all polyolefin bags behave the same with all biologicals." [102]

An important outcome for patient safety, has been the change in stance of Bath ASU, the UKs largest supplier of ready to administer aseptically compounded products to the NHS on stability data. While the NHS does not want to explicitly forbid all stability data extrapolation to different containers, Bath ASU's quality assurance department now does not accept any changes in container material or manufacturing technique from drug stability research.

While this thesis is primarily interested in ADC stability, the cost required to investigate the effect of different storage containers on aggregation was too high to use Kadcyla or Adcetris, thus, cheaper antibodies and fusion proteins were used as model biopharmaceuticals.

Chapter 6. Initial safety considerations for trastuzumab emtansine use in the workplace

6.1 Introduction

Within the secondary care setting, drugs for intravenous infusion or injection can be can be prepared into ready-to-use forms at a wide variety of locations, by a range of staff with varying skill levels. For example, a ward nurse can reconstitute a lyophilized powder in a vial, then transfer a volume of concentrated drug into a device to be administered to a patient on the ward. Alternatively, hospital pharmacy technicians can aseptically compound medicines and have them sent to wards. Lastly, external aseptic compounders, such as Bath ASU, can compound medicinal products according to a doctor's instructions, then the products can be transported to the hospital and then to the ward. This means that many people can be involved in the manipulation and transport of drugs, including highly cytotoxic and mutagenic cancer therapies.

While antibody therapies activate the immune system to induce cell death, they are not themselves directly cytotoxic. As they are proteins, they are digested when swallowed preventing them from functioning. Due to their size mAbs cannot be absorbed through unbroken human skin (unless mAbs are aerosolised and inhaled onto mucosal membranes). While some antibodies have evidence of teratogenicity (ability to affect embryo or foetal development), such as bevacizumab and trastuzumab this is only when administered at therapeutic doses and no evidence from human trials, animal trials or pharmacovigilance suggest subtherapeutic doses are teratogenic, carcinogenic or mutagenic. Because of this, antibodies are handled with less caution than cytotoxic drugs such as vincristine. ADCs, however, combine extremely potent cytotoxic drugs, often too cytotoxic to be administered unconjugated, for example DM-1 or MMAE. When bound to the antibody, the toxic warheads of an ADC cannot exert their cytotoxic action. But when the payloads are detached they are active. Furthermore, at high concentrations even intact trastuzumab emtansine can cause cell death in cell lines that don't express HER2 (**Figure 4.7**). While validating LC-MS methods for assessing

trastuzumab emtansine payload binding, loss of payload was observed at pHs as low as 7 at 40 °C with dramatic loss occurring following exposure to pH 10 at 50 °C (**Figure 4.44 & 4.45**). This indicates payloads may be cleaved from ADCs, exposed to cleaning agents.

Procedures for managing 'spills' of trastuzumab emtansine will vary from hospital to hospital, however a spill could occur at any point during manufacture or transport of a trastuzumab emtansine product at a compounding unit to administration at the ward. The procedures for spills in hospitals tends to be different depending on the area that the spill occurs, and the type of substance spilt. For example, alcohol is the biocide of choice for critical surfaces such as laminar air flow cabinets in aseptic preparation areas according to a study of UK hospitals in 2000 by Murtough *et al* [207]. The NHS Southern Health Trust document 'Infection Prevention and Control policy: Appendix 12 - Version 3' [208] outlines recommended classes of disinfectants, key points about each type and examples of that disinfectant used in Southern Health NHS trust hospitals. This information is summarized in **Table 6.1**.

Disinfectant Class	**Key Points**	**Named Example**
Chlorine based disinfectants	Wide range of bactericidal, virucidal, sporicidal and fungicidal activity	Actichlor (Dichloroisocyanurate) Prochlor (Hypochlorite)
Oxidising Agents	Good bactericidal, virucidal, and fungicidal activity. Superior sporicidal activity.	Tristel (Chlorine dioxide) Clorex (Hydrogen Peroxide)
Alkylating Agents	Not recommended for use	Gigasept Rapid (Peracetic Acid)
70% Ethanol	Indicated for in-patient setting decontamination.	Klercide Spray Blue Clinell Wipes
Chlorhexidine Gluconate	Indicated for ports decontamination on medical devices	Green Clinell Wipes
Quaternary Ammonium Compounds	Good bactericidal, virucidal, and fungicidal activity. Recommended for cleaning and low-level disinfection.	Clinell Sanitising Wipes N10 detergent

Table 6.1. Table of disinfectants used in NHS Southern Health Trust hospitals. [208]

It was noticed the conditions used to de-drug (cause payloads to be removed) trastuzumab emtansine, during the validation of LC-MS methods (**Figure 4.44 & 4.45**),

were not as severe as originally imagined, with evidence of de-drugging even at pH 7. Due to the potent cytotoxicity of the warheads and relative ease of de-drugging, we wanted to investigate the potential for de-drugging while in-use at the workplace and evaluate any potential risk to staff and patients. The most likely scenario to cause de-drugging is during a spill, as any cleaning agents used may be strong enough to degrade the ADC, (**Table 6.1**). Therefore, preliminary work to assess the safety of trastuzumab emtansine in the workplace was carried out.

6.2 Common cleaning agents as payload liberators

We first sought to investigate whether the common cleaning/disinfecting agents used in NHS hospitals and aseptic compounding units were capable of causing de-drugging of Kadcyla under in-use workplace conditions. Following method 2.6.1, trastuzumab emtansine concentrate from the vial was mixed at a ratio of 1:1 with the common disinfectants listed in **Table 6.2** and the effect on the payload binding profiles via the LC-MS method used in the Kadcyla study was assessed, as an indication of payload liberation or de-drugging (**Figure 6.1 – 6.4**). Samples were left for 120 minutes at 20 °C, before being processed for LC-MS analysis via spin filtration (thus removing the disinfectants from the sample and preventing further degradation). Here, it was found that Bleach, Prochlor and Actichlor treatments drastically reduced signal intensity of heavy and light chain peaks, over degrading the ADC (**Figure 6.2 & 6.4**). Klercide (70% ethanol), InSpec N10 detergent and 35% hydrogen peroxide treatments, all cleaved payloads from trastuzumab emtansine. The 70% ethanol was the gentlest condition, while N10 detergent and 35% hydrogen peroxide formed new detectable peaks (**Figure 6.1 C, 6.1 D & 6.3 D**). Hydrogen peroxide is most likely oxidising the heavy and light chains.

Disinfectant Class	Name	pH
Chlorine based disinfectants	Actichlor (Dichloroisocyanurate)	5.87
Chlorine based disinfectants	Prochlor (Calcium Hypochlorite)	3.15
Oxidising Agents	Hydrogen Peroxide 35% (Aqueous)	2.46
Oxidising Agents	Bleach (Sodium Hypochlorite)	12.78
70% Ethanol	Klercide (70% Ethanol)	5.51
Quaternary Ammonium Compound	N10 detergent	12.67

Table 6.2. Table of disinfectants mixed with trastuzumab emtansine vial concentrate.

Compared to the control, which was water, de-drugging was apparent after exposure to a common cleaning agent (**Figure 6.1-6.4**). The control spectras for comparison are (**Figure 6.1 A & 6.2 A**). Exposure to the Klercide 70% ethanol spray, had the smallest effect, but the peak height for the single chain species diminishes while the peak height for the naked chains increase (**Figure 6.1 B & 6.3 B**). Exposure to the N10 detergent almost completely de-drugged the light and heavy chains see (**Figure 6.1 C & 6.3 C**). A new peak was also formed at around 23888 Daltons (**Figure 6.1 C**). Exposure to 35% hydrogen peroxide caused almost complete de-drugging, a loss in overall signal intensity and the appearance of multiple new peaks, most likely oxidised variants of the original heavy and light chains (**Figure 6.1 D & 6.3 D**). Exposure to 1000 parts per million Actichlor caused complete loss of all original mass signals, as well as a 100- fold loss in signal intensity (**Figure 6.2 A & 6.4 A**). Exposure to Prochlor caused another dramatic loss of signal intensity, and complete de-drugging, though as no naked peak chains can be identified it might have caused mass fragmentation (**Figure 6.2 B & 6.4 B**). Exposure to Bleach was similar to exposure to Actichlor and Prochlor, with no masses corresponding to heavy or light chains detectable and a huge loss of signal intensity (**Figure 6.2 C & 6.4 C**). The de-drugging is most likely occurring due to hydrolysis at the amide between the lysine and SMCC linker. This is suggested as there were no species detected which have masses that correlate to a partial payload.

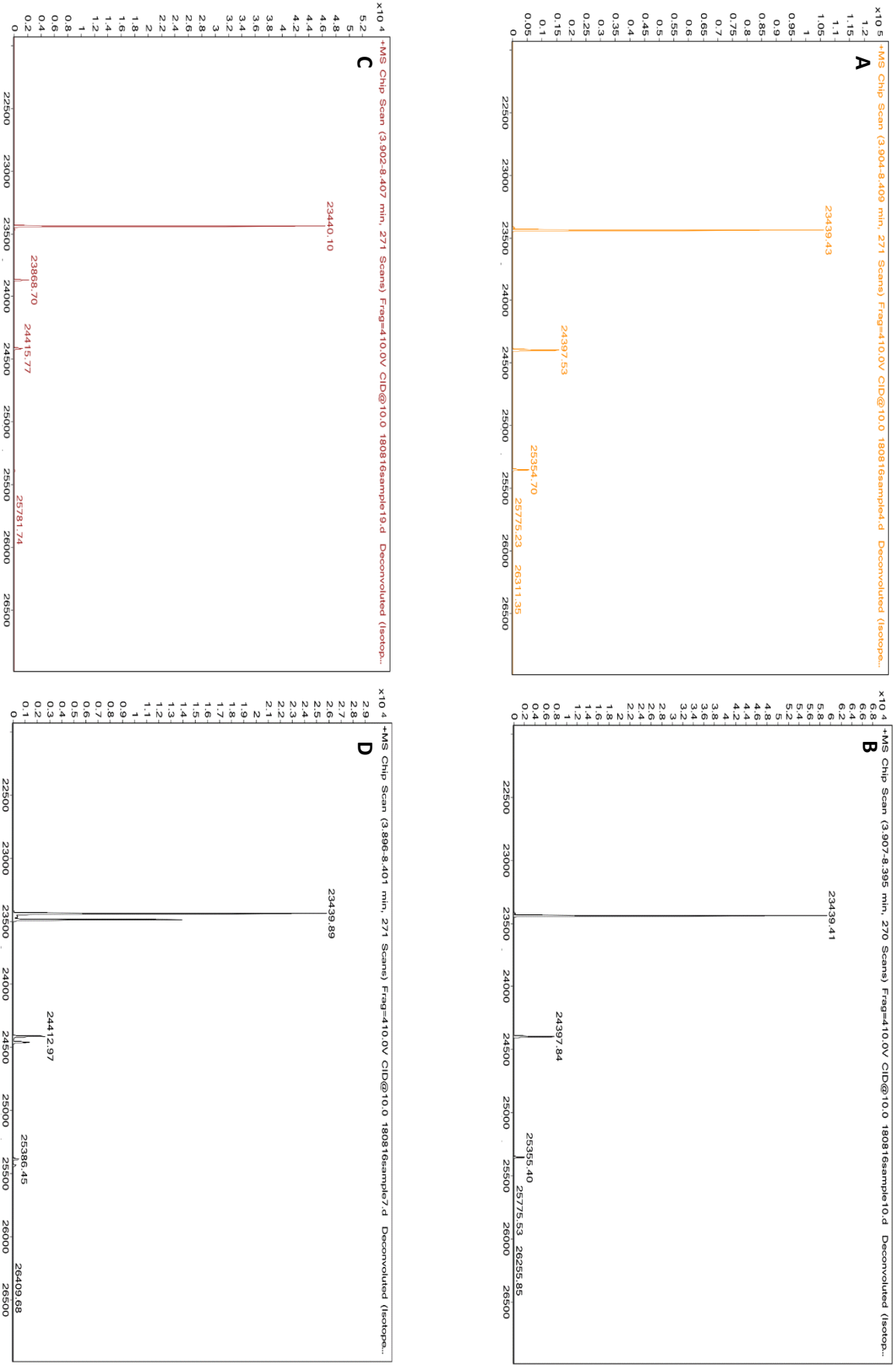

Figure 6.1. LC-MS spectra of trastuzumab emtansine light chain following exposure to (**A**) Water, (**B**) 70% Ethanol, (**C**) N10 Detergent and (**D**) 35% Hydrogen peroxide. Y-axis = TICs, X-axis = Mass (Daltons). The peaks at 24397 and 25354 daltons are diminished in height compared to the water treated sample. Three additional peaks are present in the oxidised sample, all 16 daltons heavier than the water sample peaks.

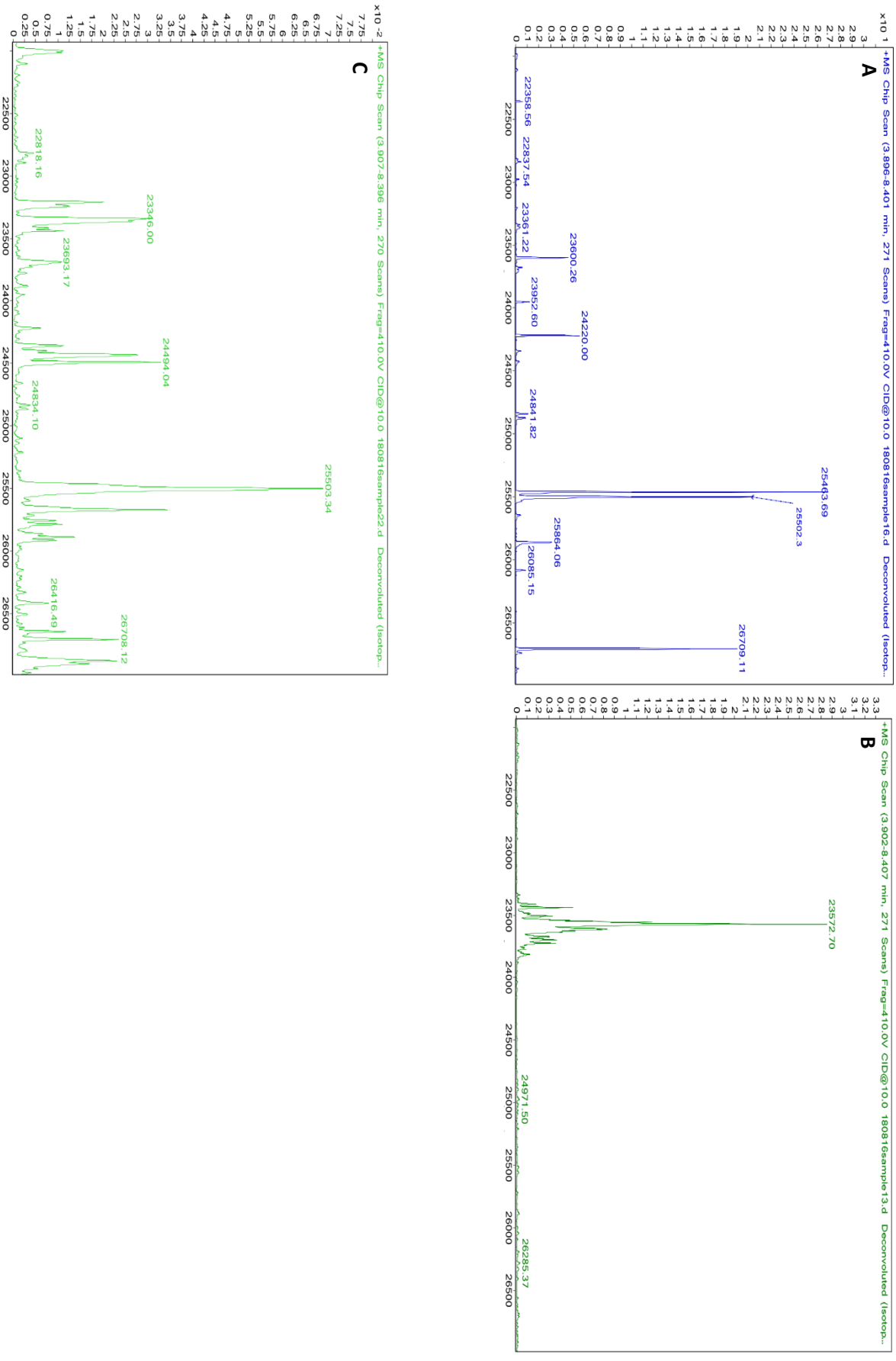

Figure 6.2. LC-MS spectra of trastuzumab emtansine light chain following exposure to (**A**) 1000 ppm Actichlor, (**B**) Prochlor and (**C**) Bleach. Y-axis = TIC, X-axis = Mass (Daltons). None of the peaks observed in these samples match those of the water sample in (**Figure 6.1**). Signal is also massively reduced.

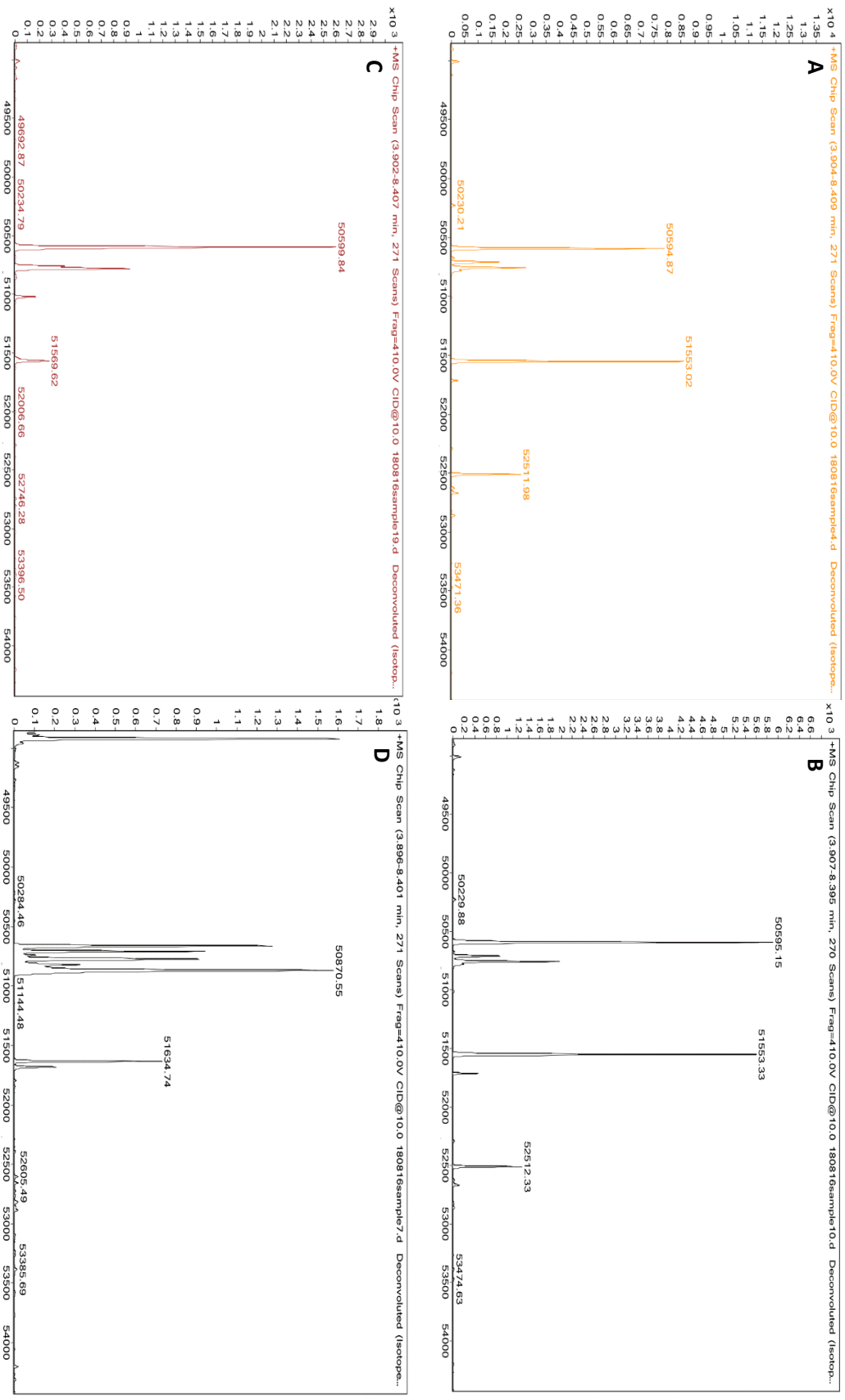

Figure 6.3. LC-MS spectra of trastuzumab emtansine heavy chain following exposure to (**A**) Water, (**B**) 70% Ethanol, (**C**) N10 Detergent and (**D**) 35% Hydrogen peroxide. Y-axis = TICs, X-axis = Mass (Daltons). The peaks at 52553 and 52512 are diminished in the degraded samples compared to the water control. H_2O_2 and N10 treatment eliminated the peak corresponding to double payload species.

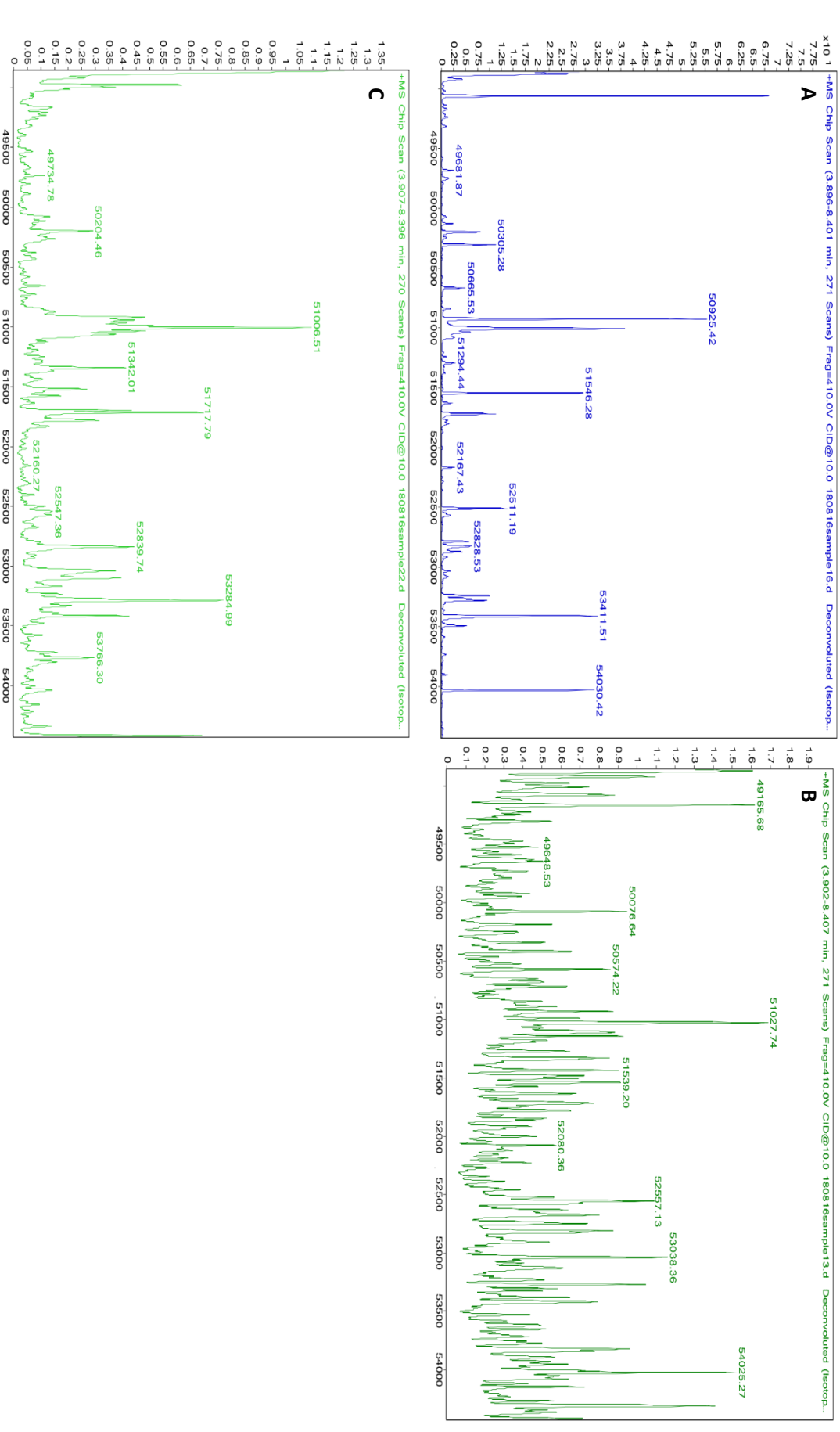

Figure 6.4. LC-MS spectra of trastuzumab emtansine heavy chain following exposure to (**A**) 1000 ppm Actichlor, (**B**) Prochlor and (**C**) Bleach. Y-axis = TICs, X-axis = Mass (Daltons). All peaks are diminished in the degraded samples compared to the water control from (**Figure 6.3**). Signal is also massively reduced.

6.3 The effect of payload liberation to on and off target toxicity

The fact photolytic degradation causes payload liberation in trastuzumab emtansine samples using LC-MS has already been demonstrated (**Figures 4.5 & 4.6**). The same samples were also used in the original assay validation for the trastuzumab emtansine assay using BT-474, HaCaT and HepG2 cells, demonstrating that trastuzumab emtansine did not exhibit increased toxicity towards target on or off target cell lines (**Figure 4.7**) with very small changes to the EC_{50}s for both off target cell lines compared to the change to the EC_{50} on the target cell line, which became over 300% less potent once photolitically degraded.

As LC-MS data suggests that the entire payload is being cleaved, and not just a portion of the DM-1 warhead, it is possible that the liberated payload is unable to enter cells and act as a cytotoxic agent. While DM-1 is extremely potent, the linker prevents it entering cells. This finding can be supported with the results from a 2006 study by Erickson *et al* that found during normal use, trastuzumab emtansine's lysine + payload metabolite is further reduced to S-methyl-DM-1 which is 10^5 fold more toxic inside cells0. [209] Work by Kovtun *et al* 2006, demonstrated that thioether linked ADCs did not exhibit bystander effect cell killing, while reducible bond containing linker ADCs did. [210] To test whether brentuximab vedotin could exhibit bystander killing, brentuximab vedotin degraded photolytically was assessed via an MTT assay following methods 2.6.2 and 2.2.11. The on-target cell line was changed to GCT-27 cells, which express CD30. The results demonstrate that photolytic cleavage of the bond between the ADC and warhead leads to highly potent degradant fragments (**Figure 6.5 & 6.6**).

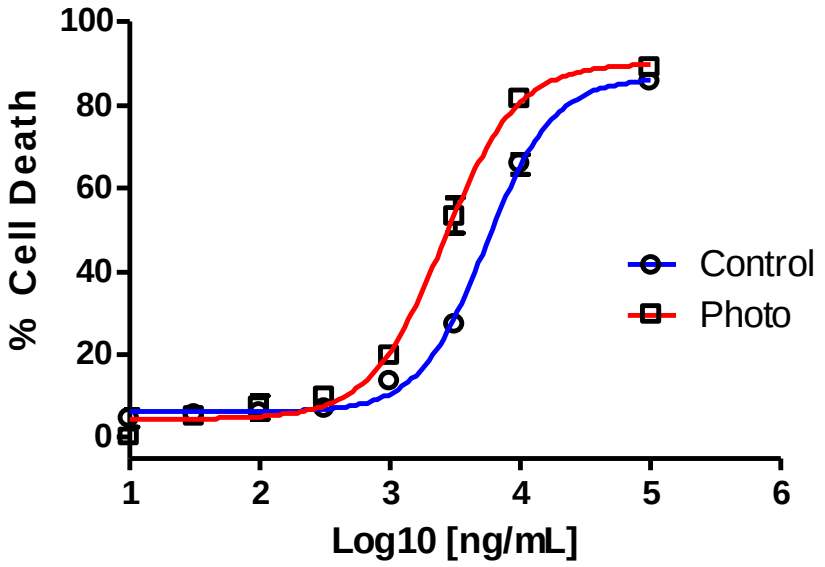

Figure 6.5. Dose response curves of brentuximab vedotin control sample vs photolytically degraded sample with GCT-27 cells. EC_{50} for the control was 5.5 µg /mL and 2.6 µg /mL for the degraded drug. A shift to the left on the X-axis following photolytic degradation is noted, and the EC_{50} more than halving.

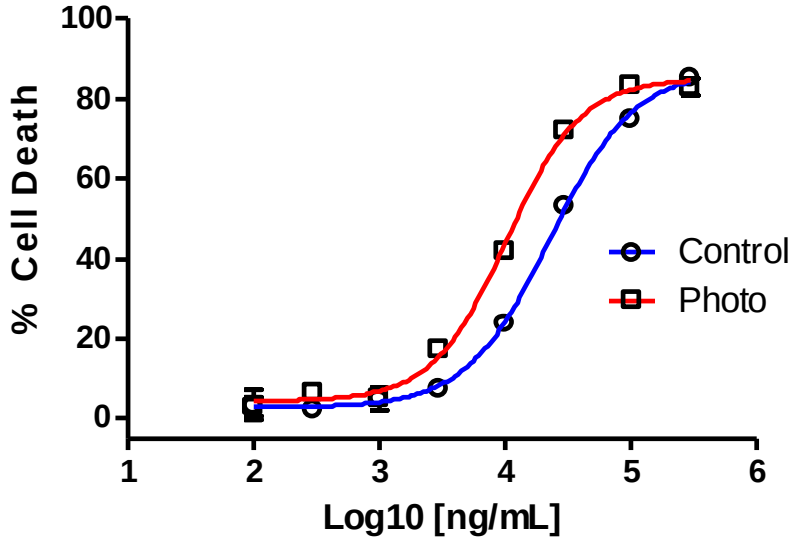

Figure 6.6. Dose response curves of brentuximab vedotin control sample vs photolytically degraded sample with HepG2 cells. EC_{50} for the control was 23.0 µg/mL and 10.4 µg/mL for the degraded drug. A shift to the left on the X-axis is noted, as well as the EC_{50} more than halving following photo-degradation.

6.4 Conclusion regarding ADC in use safety

Trastuzumab emtansine payloads can clearly be cleaved by exposure to common hospital cleaning agents, as demonstrated by the LC-MS spectra (**Figure 6.1 – 6.4**), this is most likely due to hydrolysis of the amide connected to the lysine. However cellular activity assays of trastuzumab emtansine, comparing photodegraded to control samples (**Figure 4.7**), demonstrate that the off-target toxicity is not affected and on target toxicity is reduced when trastuzumab emtansine is de-drugged. Literature supports the idea that catabolites of ADCs with non-reducible thioether linkers such as trastuzumab emtansine are not capable of entering cells and causing apoptosis. However, reducible bond containing ADCs such as brentuximab vedotin, can also be degraded leading to payload release, and these have been demonstrated as increasing off target toxicity and on target toxicity (**Figure 6.5 & 6.6**) where the EC_{50} dropped from 5.5 to 2.6 µg/mL following photolytic degradation against the on-target cell line and against the off-target cell line the EC_{50} dropped from 23.0 to 10.4 µg/mL following photolytic degradation. Treating ADCs with cell permeable degradants, such as brentuximab vedotin, as cytotoxic is appropriate behaviour, considering the potential harm they could cause, where they to become de-drugged. But is unnecessary for ADCs such as trastuzumab emtansine, that have non-cell permeable degradants.

Therefore, although trastuzumab emtansine can be de-drugged by many common cleaning agents used in NHS hospitals and aseptic compounding units, it is not likely to become more dangerous during a clean-up of a 'spill' incident. However, this may not be the case for brentuximab vedotin, though not enough work has been conducted to draw conclusion about brentuximab vedotin's safety in the workplace. To roughly gauge how dangerous completely de-drugged brentuximab vedotin solution would first look at the LD_{50} of MMAE which has been stated as 1 mg/kg in humans. [241] The mass of MMAE is 718 daltons, the mass of brentuximab vedotin is 153 kDa. The mean DAR of brentuximab vedotin is 4, therefore approximately 2 % of brentuximab vedotin is MMAE. As all vials of brentuximab vedotin are 50 mg, this means an entire vial contains 1 mg of MMAE. Therefore, one vial per kilogram of person is around the

LD_{50}. While this may suggest brentuximab vedotin de-drugging is not a big risk to human life, it is worth noting that doses of cytotoxic drugs below their LD_{50} can still have harmful impact. For example, vincristine has an LD_{50} of 1 mg/kg in rats, but at 0.05 mg/kg it causes reproductive and developmental toxicity. [242] Furthermore, 6 doses of 0.02 mg/kg/week caused central nervous system toxicity in dogs. [242] While a single vial may not contain enough MMAE to kill a human it certainly could have enough MMAE to cause harm to humans, especially upon repeated exposure.

Chapter 7. Compatibility of established ADC methods with brentuximab vedotin

7.1 Background

Brentuximab vedotin, marketed as Adcetris by Seattle genetic (Seattle Genetics, Seattle, USA), was the second ADC licensed for use in humans. As described in the introduction it has significant differences in its design compared to trastuzumab emtansine, specifically the attachment of payloads via cysteine instead of lysine residues and the cleavable nature of the linkers, including its self-immolating structure. This means that brentuximab vedotin is far less heterogeneous with regards to DAR and distribution of payload[87] and the degradants include free warhead, which has been demonstrated to have a strong, non-selective cytotoxic activity against human cell lines (**Figure 6.5 & 6.6**).

7.2 Preliminary evaluation of study method compatibility

7.2.1 Introduction

As a preliminarily investigation of method compatibility and to identify any immediate issues arising due to the differences from the structure of brentuximab vedotin compared to trastuzumab emtansine, control samples and a photolytically degraded sample were compared, the samples were prepared according to method 2.7.1. One sample was stored refrigerated for 12 hours, while the other was stored at 25 °C under 20,000 Lux. The intention was to evaluate a control sample (12 hours at 4 °C) to determine if any problems were apparent with a particular study method, and also to evaluate a degraded sample (20,000 Lux at 25 °C) to determine whether each of the methods appeared stability indicating (at least for photolytic degradation).

7.2.2 Visual inspection

To evaluate the visual inspection technique, a control sample of brentuximab vedotin and photolytically degraded sample brentuximab vedotin were compared. The control was clear with no visible colour, particles or turbidity. The photolytically degraded sample had turned cloudy and turbid (**Figure 7.1**). As visual inspection can distinguish a control sample and photolytically degraded sample, this technique appears to be stability indicating. Visual inspection is unaffected by testing brentuximab vedotin as opposed to trastuzumab emtansine or infliximab.

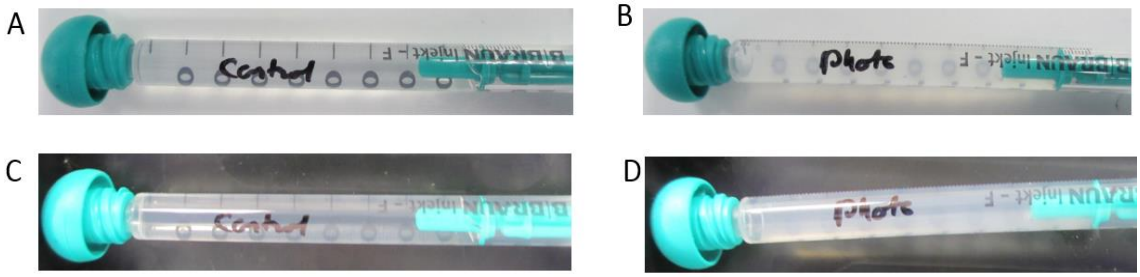

Figure 7.1. Photographs of control (**A & C**) and photolytically degraded (**B & D**) samples. The samples were notably more cloudy and turbid following photolytic degradation compared to the controls.

7.2.3 pH

To evaluate the pH technique (method 2.2.2), a control sample of brentuximab vedotin and photolytically degraded sample brentuximab vedotin were compared. The pH was 6.42 for the control and photolytically degraded sample. While this technique is unaffected by testing brentuximab vedotin as opposed to trastuzumab emtansine or infliximab, it does not appear stability indicating. However according to the ICH Q2 (R1) guidance [105] "pH measurement is a general method and does not require a validation". Therefore, it does not matter that it is not stability indicating for photolytic degradation of brentuximab vedotin.

7.2.4 Nano-tracking analysis of nano-particles

To evaluate nano-tracking analysis of nanoparticles (method 2.2.5), a control sample of brentuximab vedotin and photolytically degraded sample of brentuximab vedotin were compared. The particle count was dramatically different between the control sample and photolytically degraded sample (**Figure 7.2**). The photolytically degraded sample had a concentration of nanoparticles almost two orders of magnitude higher than the control sample. This indicates the method is compatible and likely to be stability indicating. Nano-tracking analysis appears unaffected when testing brentuximab vedotin as opposed to trastuzumab emtansine or infliximab.

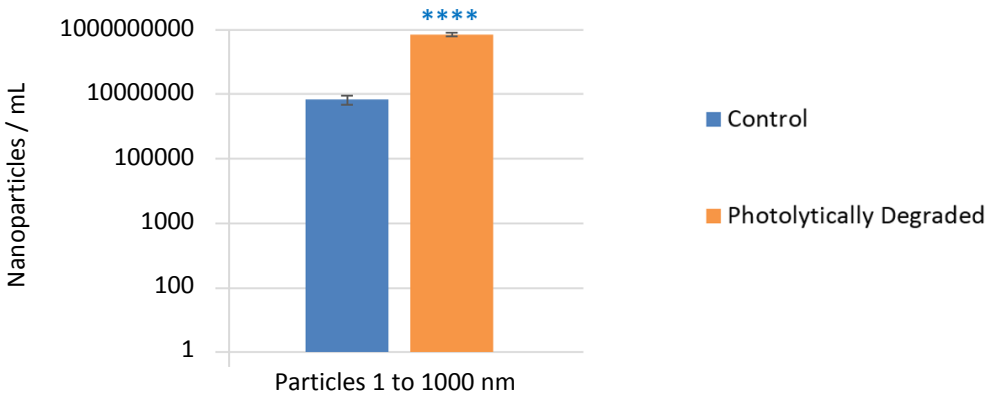

Figure 7.2. Nano-tracking analysis of a control sample and photolytically degraded sample of brentuximab vedotin. Photolytic degradation has caused a statistically significant increase in the number of nanoparticles. **** indicates a p value less than 0.0001.

7.2.5 Microflow imaging analysis of microparticles

To evaluate microflow imaging of microparticles (method 2.2.6), a control sample of brentuximab vedotin and photolytically degraded sample of brentuximab vedotin were compared. The particle counts were dramatically different between the control sample and photolytically degraded sample (**Figure 7.3**). The photolytically degraded sample had a concentration almost two orders of magnitude higher for both particles greater than 10 µm and particles greater than 20 µm micrometres. This indicates the method is stability indicating for brentuximab vedotin. Microflow imaging

is also unaffected when testing brentuximab vedotin as opposed to trastuzumab emtansine or infliximab.

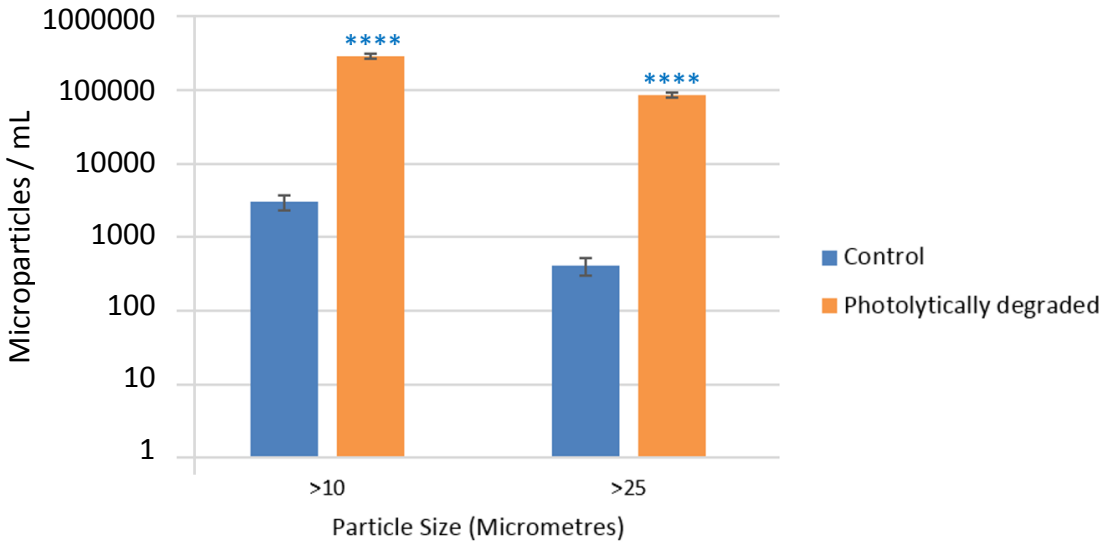

Figure 7.3. Microflow imaging analysis of microparticles greater than 10 µm and 25 µm. Comparison of a control sample and photolytically degraded sample of brentuximab vedotin shows statistically significant increases in microparticle concentration after degradation. **** indicate p values less than 0.0001.

7.2.6 Gel electrophoresis

To evaluate gel electrophoresis analysis of brentuximab vedotin (method 2.2.7), a control sample of and antibody (Obinituzumab), a control sample of brentuximab vedotin and a photolytically degraded sample of brentuximab vedotin were compared (**Figure 7.4**).

Reduced sample analysis appears unaffected. Comparison of photolytically degraded brentuximab vedotin to the control sample shows a feint but detectable band appearing around 75 kDa and a band at above 200 kDa (**Figure 7.4 C1 & E1**). This suggests aggregation and some resistance to the reduction of the interchain disulphide bonds on the brentuximab antibody.

Intact sample analysis for the brentuximab vedotin control appears drastically different to the control sample of obinituzumab (**Figure 7.4 B1 & D1**). There are several new bands appearing which are most likely due to variable dissociation of the heavy and

light chains. The bands are most likely to be due to various combinations of heavy and light chain. Light is approximately 25 kDa, Heavy is approximately 50 kDa, Heavy Light is approximately 75 kDa, Heavy-heavy is about 100 kDa, and Heavy-heavy-light is approximately 125 kDa. When attaching payloads to cysteine residues, the disulphide bonds are reduced to ensure the cysteine residues are available. This means the antibody for any brentuximab vedotin ADC can only have 3 or fewer intact inter-chain disulphide bonds. As part of intact analysis for gel electrophoresis, samples are denatured, causing the proteins to unfold and ensuring that protein mass, and not the three-dimensional shape, controls the distance travelled through the gel. When denatured for analysis via gel electrophoresis, the heavy and light chains likely do not have enough Van der Waals force left to hold them together and dissociate once without a disulphide bond holding them together.

When comparing the intact analysis of the brentuximab vedotin control sample with the photolytically degraded sample can observe differences (**Figure 7.4 D1 & F1**). A strong band above 200 kDa is detectable and the intensity of bands below 150 kDa are much less intense than the band at 150 kDa. The band above 200 kDa suggests a lot of aggregation is present. The loss of band intensity for the 'new' bands below 150 kDa, may suggest that the DAR forms most susceptible to aggregation, may also be the DAR forms most likely to exhibit chain dissociation when denatured. Evidence from the literature can support this claim as the more payloads bound to a cysteine linked ADC the less stable it is, particularly regarding aggregation and fragmentation. [211,212]

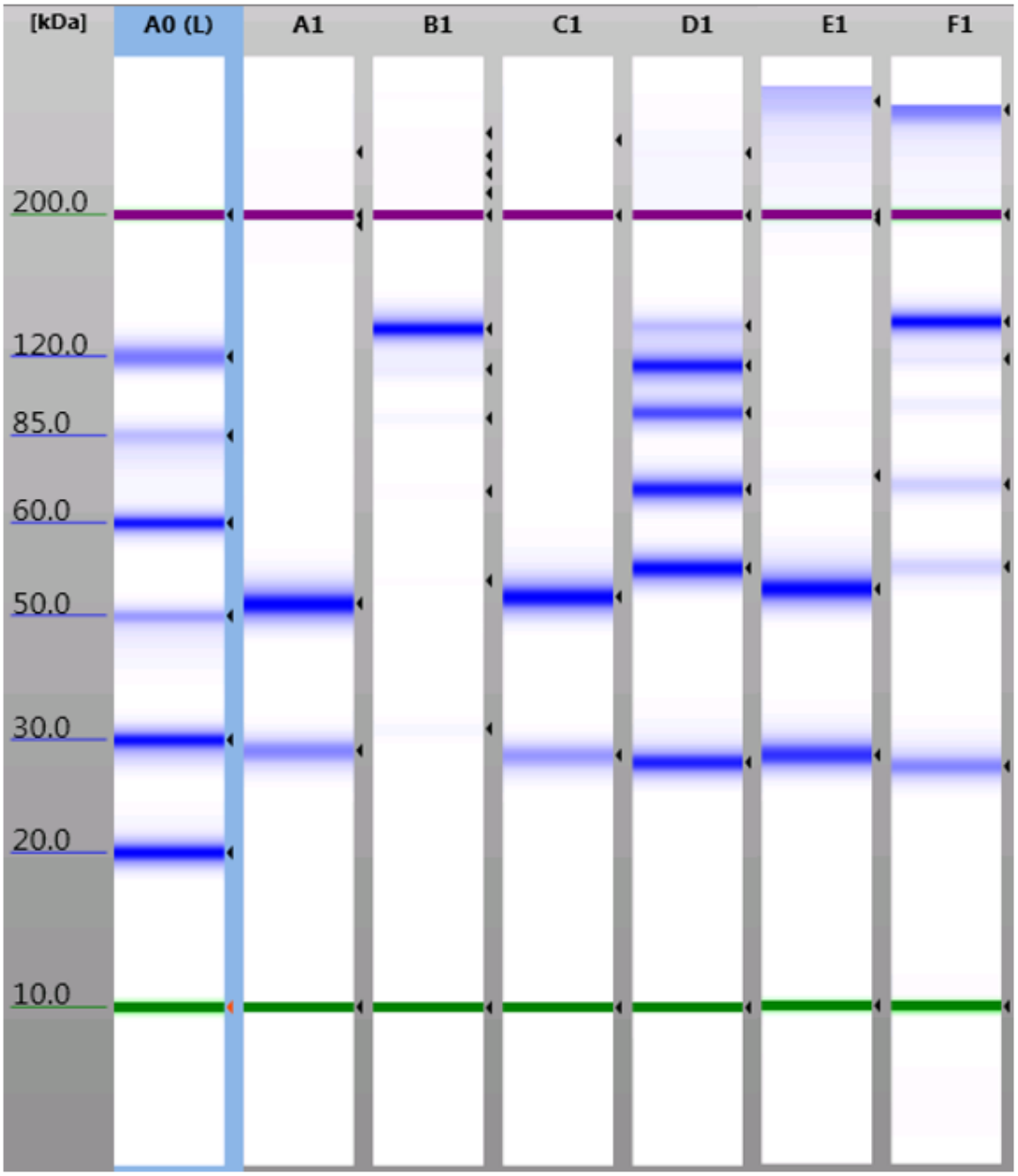

Figure 7.4. Electrophoresis of brentuximab vedotin vs Obinituzumab. The digital ladder (A0), helps to identify band masses. (A1) and (B1) are the reduced and intact analysis of the model antibody obinituzumab. (C1) and (D1) are the reduced and intact analysis of brentuximab vedotin. (E1) and (F1) are the reduced and intact analysis of photolytically degraded brentuximab vedotin.

7.2.7 Cellular MTT assay

The figures for this experiment are in chapter six page 243, and were performed according to method 2.6.2 and 2.2.11 On target activity is antibody specific so using the cell line that works for trastuzumab emtansine or infliximab will not work for

brentuximab vedotin. However, the basic concept of the MTT assay is unaffected when using cells appropriate to brentuximab vedotin, such as GCT-27 cells that express the CD30 protein, (**Figure 6.5**). GCT-27 cells have previously been used by Schönberger *et al* to test brentuximab vedotin's functional activity. [213] Furthermore, off target cellular assays using HepG2 are unaffected and dose response curves are easily generated (**Figure 6.6**). Furthermore, photolytic degradation of brentuximab vedotin causes a shift to the left, for both on target and off target cell lines (**Figure 6.5 & 6.6**). Against the on-target cell line, the EC_{50}s have shifted from 5.5 µg/mL to 2.6 µg/mL once photolytically degraded. Against the off-target cell line, the EC_{50}s have shifted from 23.0 µg/mL to 10.4 µg/mL once photolytically degraded. This data indicates the cellular MTT assay will be stability indicating and is not negatively affected when measuring brentuximab vedotin as opposed to trastuzumab emtansine. These findings also indicate that brentuximab vedotin becomes more cytotoxic towards both target cells and off-target cells, unlike trastuzumab emtansine.

7.2.8 Infrared spectroscopy structure determination

To evaluate infrared spectroscopy structure determination of brentuximab vedotin, a control sample brentuximab vedotin and photolytically degraded sample of brentuximab vedotin were compared using method 2.2.9 (**Figure 7.5**). The photolytically degraded sample has an altered secondary structure, with a 7.9% increase in alpha helix and a 4.7% decrease in beta sheet. As this technique is able to predict a structure for brentuximab vedotin and measure a clear difference compared to the photolytically degraded sample, this preliminary investigation of infrared analysis suggests the method is both compatible and stability indicating in nature brentuximab vedotin. Furthermore, the degree of structural change is significant enough that loss of binding would be expected, however the cellular assay did not demonstrate a loss of function, which may be explained by payload detachment. The technique is unaffected by testing brentuximab vedotin as opposed to trastuzumab emtansine, see (**Figure 7.5**).

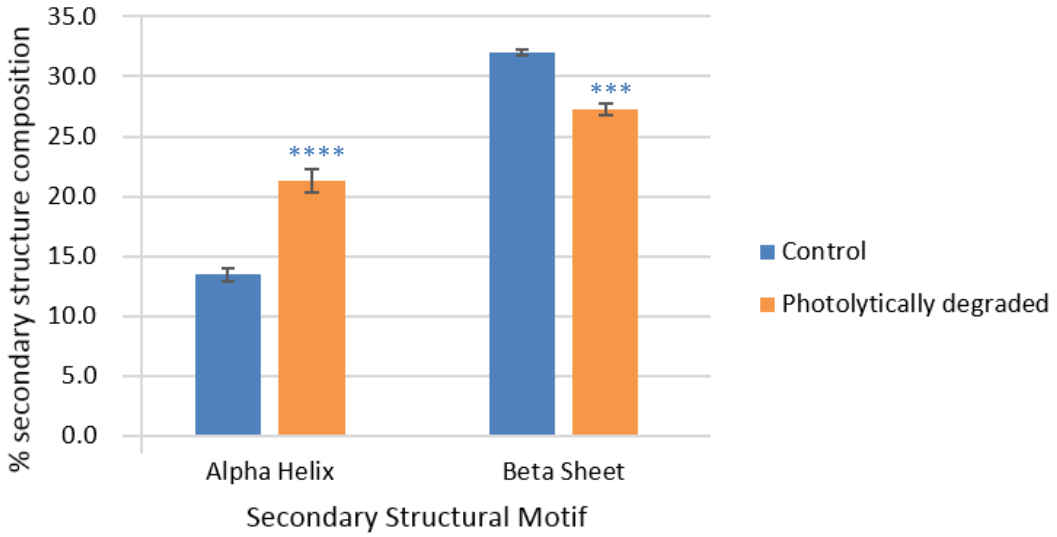

Figure 7.5. Infrared spectroscopy structure determination of brentuximab vedotin's secondary structure. Photolytic degradation has caused statistically significant changes to both alpha helix (7% increase) and beta sheet (5% decrease). *** and **** indicate a P value less than 0.001 and 0.0001 respectively.

7.2.9 LC-MS chemical degradation and payload binding

To evaluate LC-MS analysis of brentuximab vedotin, a control sample brentuximab vedotin and photolytically degraded sample of brentuximab vedotin were compared following methods 2.2.12 – 2.2.14 (**Figure 7.6**). Multiple peaks are detectable in the mass range of the light and heavy chains. While a pure brentuximab antibody was not available to establish the mass of naked chains, a previously published application note demonstrated analysis of reduced brentuximab vedotin on an Agilent 6530 Q-TOF coupled with an ultra-high pressure LC system using a polymeric reverse phase protein column [214], the set-up is touted as having unmatched sensitivity and mass accuracy. They identified the mass of brentuximab light and heavy chains. While the method used here does not use ultra-high-pressure liquid chromatography and is only performed on an Agilent 6420 Q-TOF, it is still possible to identify naked and single payload light and heavy chains (**Figure 7.6**). Naked light and heavy chain have masses around 23726 and 50084 respectively. The mass of a single payload can be calculated as 1316 daltons, which identifies heavy chains with a single, double or triple payload attachment, as well as light chains with a single payload attachment.

Furthermore, light chain with a linker but no warhead is detectable (**Figure 7.6 A**). There are two peaks at 47451 and 48561 daltons (**Figure 7.6 B**) that do not correspond to any expected masses, these will require further investigation.

Comparison of the control sample to the photolytically degraded sample shows a change in the peak heights of heavy chains. Specifically, photolytic degradation reduces the relative TICs of triple payload species, double payload species and single payload species, while increasing the relative TICs for naked heavy chain. This technique appears to be compatible with brentuximab vedotin and as it can distinguish between photolytically degraded and control samples, it is likely to be stability indicating.

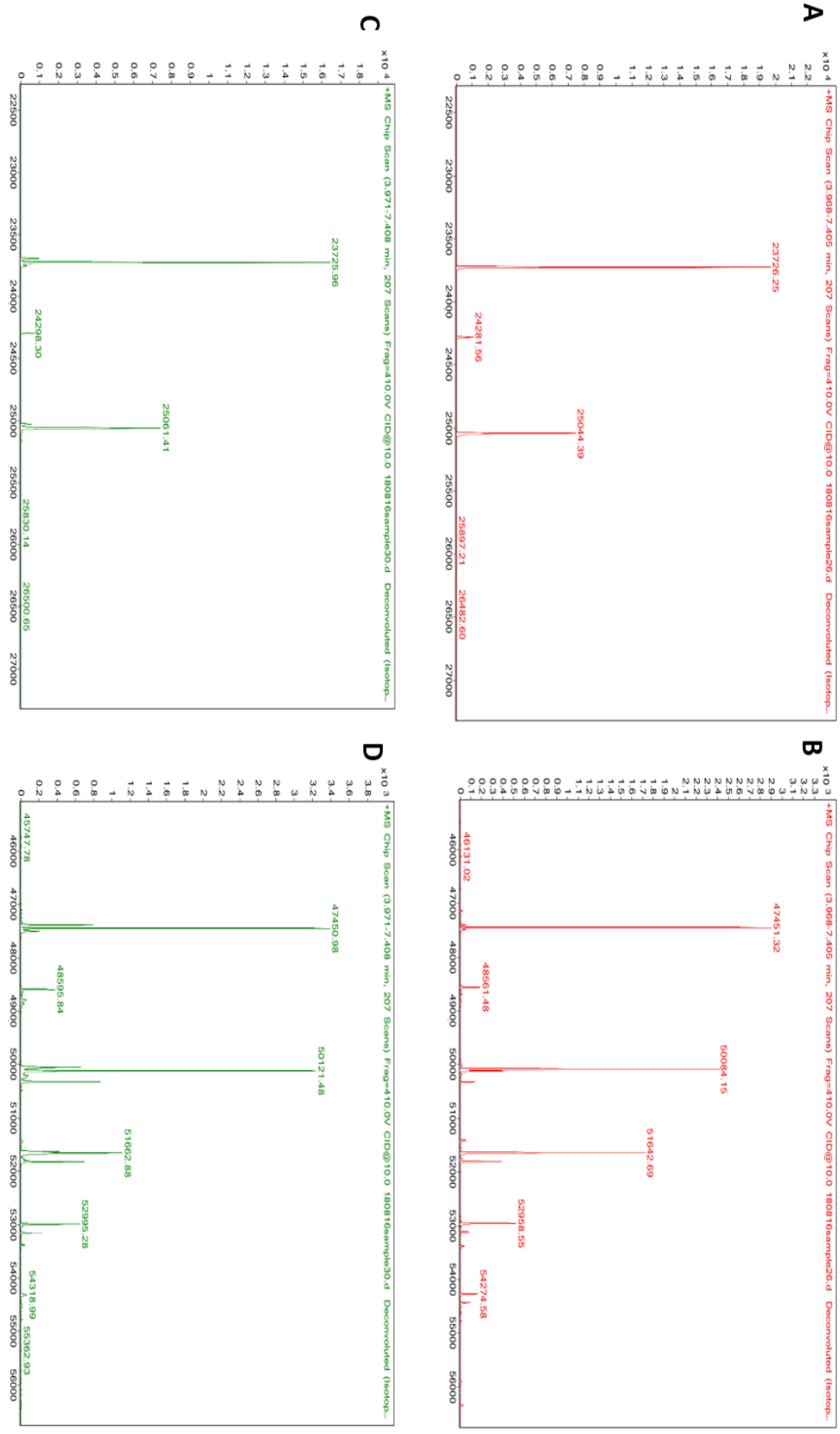

Figure 7.6. LC-MS analysis of (**A & B**) control samples and (**C & D**) photolytically degraded samples of brentuximab vedotin's (**A & C**) light chains and (**B & D**) heavy chains. Y-axis = TICs, X-axis = Mass (Daltons). Signal loss of peaks corresponding to double payload band species is noted.

7.2.10 Size exclusion chromatography

To evaluate size exclusion chromatography analysis of brentuximab vedotin, a control sample brentuximab vedotin and photolytically degraded sample of brentuximab vedotin were compared using method 2.2..17 (**Figure 7.7**). The monomer peak has an asymmetry of 1.26 which is an acceptable level to begin a full validation. Furthermore, the photolytically degraded sample had a drastically reduced absorbance corresponding to the monomer, a 92% loss of absorbance (**Figure 7.7**). The dimer peak has also disappeared, likely due to further aggregation to nano or micro-scale particulates as detected via MFI and NTA analysis. Interestingly, there is a new peak at 8.15 minutes, eluting after the monomer peak. This suggested photolytic degradation has caused fragmentation of the ADC, creating a fragment with a molecular weight between 10 and

0.2 kDa, based on comparison to the BioSep-SEC-s4000 column quality control test report. It is possible that we are observing fragmented payloads, as MMAE, the warhead for brentuximab vedotin has a molecular weight of 718 daltons and the entire payloads has a molecular weight around 1.3. The presence of payload fragments can help explain why no loss of functional activity is noted even after large losses of monomer. This data suggests that size exclusion chromatography method is compatible with brentuximab vedotin and as it can distinguish between the control sample and photolytically degraded sample method is it is likely to be stability indicating too.

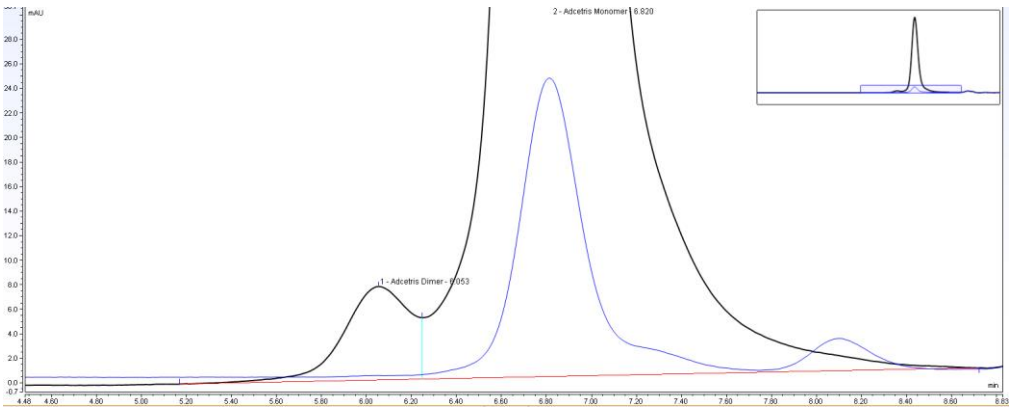

Figure 7.7. Size exclusion chromatography analysis of a brentuximab vedotin control sample (**Black**) vs a photolytically degraded sample (**Blue**). The X-axis is time (minutes). Degradation has caused a large decrease in monomer concentration and the presence of a peak correlating to a fragment.

7.2.11 Hydrophobic interaction chromatography analysis of DAR

This experiment discusses data first presented in chapter 4, collected using method 2.2.15. To evaluate hydrophobic interaction chromatography analysis of brentuximab vedotin's DAR, a control sample brentuximab vedotin was analysed (**Figure 4.32**). It is possible to separate and integrate the peaks corresponding to DAR 0 – 8. This method works for brentuximab vedotin but not for trastuzumab emtansine due to the difference in their site of attachment. Due to the payloads being attached at cysteine residues, the variability of DAR and distribution of payload is greatly reduced. This creates a more restricted hydrophobicity profile, dominated by the DAR instead of the distribution of payload. This allows distinct peaks to be generated when using HIC, providing an alternative method of DAR characterisation to the LC-MS method. HIC results such as (**Figure 4.32**) can be used to calculate the DAR with the following data processing steps.

1) Integrating the peaks corresponding to each DAR
2) Calculating the relative peak area for each DAR peak
3) Multiplying the relative peak areas of each DAR peak by its own DAR value
4) Sum the DAR adjusted relative peak areas
5) Divide the sum of DAR adjusted relative peak areas by 100

Using the above process on the data from **(Figure 4.32**) It was calculated that brentuximab vedotin had a DAR of 4, matching multiple published independent LC-MS and HIC based determinations. [215-219] HIC work was not performed on the degraded samples due to time constraints. However, work by Hamblet *et al* and Wakanker *et al* used HIC to measure the DAR of cysteine linked ADCs. [173, 199] Thus, suggesting that HIC would be a viable method for determining DAR of brentuximab vedotin.

7.3 Conclusion

This preliminary investigation has demonstrated that all methods developed for the stability evaluation of trastuzumab emtansine appear to be compatible for a similar

evaluation of brentuximab vedotin. Furthermore, HIC analysis of DAR, which was incompatible with trastuzumab emtansine, is compatible with brentuximab vedotin.

This work has also highlighted that the chemistry used to attach brentuximab's payloads via cysteine residues destabilises the antibody as disulphide bonds are reduced and therefore the molecular forces holding the antibody component of the ADC together are weaker. Gel electrophoresis shows brentuximab vedotin is unable to remain fully intact when denatured, while trastuzumab emtansine and infliximab were (**Figure 7.4**). Furthermore, brentuximab vedotin was considerably more degraded than trastuzumab emtansine and infliximab when subjected to the same photolytic degradation conditions. Brentuximab vedotin exhibited a greater increase in nanoparticle concentrations, microparticle concentrations, the development of visible turbidity, a greater loss of monomer concentration, as well as loss of payload detectable via LC-MS and maybe as a low molecular weight fragment in SEC analysis.

This preliminary work also demonstrated an increase in potency regarding on and off target activity upon photolytic degradation for brentuximab vedotin (**Figure 6.6)**. The EC_{50}s more than halved against both cell lines suggesting photolytic degradation had more than doubled brentuximab vedotin's cytotoxic potential. This suggests brentuximab vedotin becomes more harmful and cytotoxic following degradation. While trastuzumab emtansine was demonstrated to be degraded by many common cleaning agents used in hospitals and ascetic compounding units, the degradation did not cause an increase in its off-target activity, and only reduced its on-target activity (**Figure 4.7)**. As brentuximab vedotin has been demonstrated as more sensitive to photolytic degradation, most likely due to loss of 1 or more disulphide bonds, it may also be more sensitive to other forms of degradation.

Chapter 8 – Conclusions and Future Work

The overall aim of this project was to develop methods, for the characterisation of the ADC trastuzumab emtansine, compliant with the guidelines set out in the NHS yellow cover documents for stability guidance. The purpose of developing these compliant methods was to enable a valid stability study to be performed to apply an extended shelf-life to Kadcyla. This would enable Bath ASU to offer UK hospitals Kadcyla in a ready to infuse presentation with more than 24 hours of shelf life. To accomplish this aim, much work was required to meet several objectives. During this work many obstacles were encountered, providing ample opportunity to use creative thinking.

An understanding of what is required for a stability study was needed to ensure its results would be appropriate to apply a shelf life extension to the product and it was necessary to identify and understand all critical stability characteristics for a basic antibody and suitable analytical techniques for assessing them. Using the NHS yellow cover stability guidance documents, [101,102] as well multiple ICH guidance documents pertaining to drug stability, biopharmaceuticals and assay validation, [105,158,220-222] what is required of a stability study for its findings to be useable for a shelf life extension of aseptically prepared biopharmaceuticals was learnt. An understanding of the critical characteristics of biopharmaceuticals regarding their stability and safety was gained. Further literature research was required to understand the wealth of techniques that could be used to assess different caveats of the critical characterises, for example, the numerous methods of monitoring particles, [111,5.4,123,126-134] or investigating higher order structure. [135-157] The first major obstacle encountered was when reviewing the vast array of techniques that can be used for assessing the critical characteristics of a biopharmaceutical product. Justification of choosing one technique instead of another was needed. This was made easier by assessing which instruments were accessible at Bath University and Bath ASU. Then it was possible to rule out the techniques that required long periods of time or high levels of expertise, for example x-ray crystallography. Particle assessment has an incredible number of techniques, so the more commonly used methods that used available equipment were chosen.

We wanted to demonstrate that a fully NHS compliant stability study could be designed and executed, using a simple antibody. An issue found when designing the infliximab stability study was the NHS guidance states that study samples will ideally be exact replicates of the ready to use product, however to produce an appropriate number of samples at the required volumes and concentrations would have used a large volume of infliximab costing around £28,000. By scaling down the samples from 250 mL infusion containers, to 50 mL infusion containers we were able to save almost £25,000. This sample scale down approach was later applied to the trastuzumab emtansine study to save approximately £130,000. Another obstacle was the time dependent nature of the proposed antibody stability study. It is required that a full stability characterisation be performed within 24 hrs of compounding, and there are many benefits for doing this at the limit of its SPC shelf life as well. This means all techniques must be run separately on day 0 and 1. It would be impossible for the number of samples required for the stability study to be assessed by a single person during one working day. To that end three measures were employed. Firstly, samples for LC-MS analysis were processed, then frozen and submitted to be run Dr Shaun Reeksting in the Chemical Characterisation and Analysis Facility (CCAF) at Bath University. Secondly, the preparation of different concentrations of samples was staggered, thus reducing the workload on each sampling day. Thirdly, while the techniques and methods were chosen, developed and validated by me, staff at Bath ASU helped collect the data on each time point, with specific tasks assigned to an individual for the duration of the study. A fully NHS compliant stability study was designed and conducted on clinically relevant concentrations of Remsima brand infliximab stored in Fresenius Kabi Freeflex infusion bags. This published study demonstrates infliximab's stability while refrigerated over a seven day period, and allows anyone operating under a Section 10 exemption or a Specials License to be able to also apply a seven day shelf life to Remsima brand infliximab when manufactured according to the methods used in the published study [167]. The publication also demonstrates the ability for a fully NHS compliant study to be performed and proving the study design was practicable, and is cited by the NHS quality assurance committee in the third edition of their biopharmaceutical stability guidance document [102].

Critical characteristics unique to ADCs (as compared to antibodies) needed to be identified. Through literature research regarding antibodies and ADCs, an understanding of ADC structure, stability and safety concerns was gained. [73, 90] For example the difference between: cleavable and non-cleavable linkers, [90] common types of ADC warheads and their mechanisms of action, [91] how potent the warheads of ADCs are when not conjugated, [92] how the site of attachment and linker chemistry controls the ratio of drug payloads to antibody, [88] the importance of DAR [90], and the locational distribution of the payloads across the antibody, what has been referred to a positional -isomers. [90] This knowledge informed me that neither DAR, or off target toxicity were covered by any current guidance document, circa 2016.

By testing control samples and degraded samples of trastuzumab emtansine via each method used during the infliximab study, it was discerned which methods had issues assessing ADCs. For example, circular dichroism spectra to secondary structure software 'Circular Dichroism Neural Network' was found to be incompatible with ADCs.

One of the most significant obstacles encountered was discovering secondary structure analysis via CD, which is commonly used in biopharmaceutical stability studies, was unsuitable for assessing the ADC trastuzumab emtansine. Only minor issues with CD had been found in the literature suggesting some issues with signal magnitude at the near-UV region. Though circular dichroism can still be used to assess conformational stability ADCs using thermal ramps and measuring the melting temperatures, that's not a detailed enough analysis of higher order structure to satisfy the current requirements set out in the NHS yellow cover Part 2 guidance.

However, it did provide an opportunity to explore alternative, and in many ways superior, methods of secondary structure determination, namely infrared spectroscopy analysis. Finding an IR method of determining secondary structure proved a challenge owing to the lack of an IR structure determination method that could work out of the box at clinically low concentrations for antibodies and ADCs. Equipment configurations able to predict structure that were sensitive at clinically high and supra clinical concentrations could were found to be insensitive at clinically low concentrations.

An original quantitative data set was designed, built and validated, which was compatible with infrared spectrometry equipment sensitive enough to detect clinical concentrations of ADCs and antibodies. This allows rapid, precise and accurate measurements of sub-clinical and supra-clinical concentrations of protein structures, including antibodies, fusion proteins, enzymes and antibody drug conjugates. By measuring the amide 1 and 2 bands and comparison to the QDS.

After presenting data collected using this method on multiple antibodies and ADCs, and the validation of the quantitative data set, to members of the NHS pharmaceutical quality assurance committee (2017), infrared spectroscopy was added to their list of recommended techniques suitable for characterising physico-chemical changes.

A mass spectroscopy-based method of assessing DAR was developed and validated, overcoming issues of low sensitivity at clinical constrictions, using the mass spectrometry equipment available at Bath University. This was achieved by using TCEP to reduce the antibody drug conjugate into its heavy and light chain components, which didn't affect the amide or ester bonds of the ADCs. Comparing the relative change in peak ratios corresponding to heavy and light chains with varying numbers of payload bound to them provides sufficient knowledge of the payload binding.

A stability study of trastuzumab emtansine in line with the NHS stability guidance was carried out, having had multiple meetings with members of the NHS quality assurance committee to facilitate regulatory approval of the proposed stability study. A stability study on Kadcyla brand trastuzumab emtansine was designed and performed which was subsequently reviewed by the chair of the NHS pharmaceutical quality assurance committee (2017) and deemed to be compliant with all requirements for a ADC stability study. The study enabled a 21-day shelf life extension to be applied to Kadcyla brand when diluted to clinical concentrations in Fresenius Kabi Freeflex sodium chloride infusion bags and refrigerated at 2-8 °C when protected from light. This is, to the authors knowledge, the world's first shelf life extension of a ready to use ADC

product. This extension has contributed to an 80% increase in batches of Kadcyla manufactured by Bath ASU per annum between 2015 and 2017.

It was also discovered that not all polyolefin infusion bags affect drug stability equally. While it has been known for some time that polyvinylchloride infusion bags generally cause increased adhesion and particle formation, with guidance such as the NHS yellow cover documents and even particular products summaries of product characteristics, stating that polyolefin infusion bags must be used instead of polyvinyl chloride ones. However, it was demonstrated that different methods of bag manufacture and types of polyolefin, affect aggregation and adhesion significantly differently. Furthermore, each bag type was not clearly better or worse for all drugs. This suggests stability study data is only applicable to products manufactured in the same bags type. It also raised the question of whether measurements made of a drug within its SPC shelf life in one bag type can be used as baselines of acceptability for studies in a different bag type, discussion with NHS quality assurance staff made it clear this was not acceptable and based on this research the NHS pharmaceutical quality assurance committee of 2017 amended their own guidance on container choice, adding "Data cannot be extrapolated to other container types and care should be taken when extrapolating to a different manufacturer's container, there is some evidence that not all polyolefin bags behave the same with all biologicals".

Additionally, preliminary investigations to evaluate the in-use safety of trastuzumab emtansine, as well as to the further applicability of methods developed for the study of Kadcyla towards other ADCs such as Adcetris, were conducted. A final challenge that was encountered relates to the preliminary study into the in-use handling of trastuzumab emtansine. There is a lack of publicly accessible information regarding the policies of different NHS hospitals approaches to spills and how to classify spills, based on the substance, concentration, volume and location of spills. Although it was possible to find some information regarding spill procedures and use of different cleaning agents, [207,208] and have conversations with NHS hospitals nurses and pharmacists, it was very hard to obtain good quality and referenceable documents.

Finally, it was also demonstrated that although trastuzumab emtansine can be easily degraded with common cleaning agents used around hospitals and aseptic compounding units, it does not appear to pose any more danger to staff when degraded as the payload fragments are unable to enter cells. However preliminary work on brentuximab vedotin shows this is not the case for all antibodies, suggesting that cleavable linker-based ADCs, like brentuximab vedotin, may become more toxic and less targeted following some types of degradation.

Future Work

In the pursuit of the overarching aim of thesis, there were many interesting findings that were not fully investigated. One area of that would be of interest to return and expand upon would be the bag comparison study. The finding that the choice of different brands of polyolefin infusion bags had a significant impact on drug aggregation was both interesting and useful. A deeper understanding of this would be of value. Ideas include identifying the concentration of non-ionic surfactants used to help to control for that variable. As well as using drugs that have the same surfactants rather than three different ones. Furthermore, measurements of the zeta potential of the plastics inner surface would also be of interest as that was a possible driver of aggregation. Finally, we only tested three brands of bags while there are many bag manufacturers and suppliers on the market. It would be interesting compare the surface roughness and zeta potential of bags that have the same inner surface material and manufacturing process, this could help identify the extent the manufacturing process and surface roughness contribute to the aggregation. As well as zeta potential it may also be of value to measure the hydrophobicity of the materials, by measuring the contact angle of water. Highly hydrophobic materials may interact more strongly with exposed hydrophobic regions of proteins, such as the hinge region and areas exposed during conformational changes.

Another area that was not fully explored was the inability for CDNN to adequately process CD spectra of trastuzumab emtansine to predicted secondary

structures. Further work here could expand upon the differences found by ourselves and Beckley *et al* (2013) that showed the near UV CD spectra of ADCs were affected, with regards to the signal intensity. [233] This is the exact region that CDNN uses to calculate the secondary structure. It would be interesting to make measurements of the other three licensed ADCs to see if they also have the same issues found with trastuzumab emtansine.

There has also been interest in testing methods to determine the tertiary structure of ADCs. While there were issues identified with near UV CD analysis, no issues where found by Beckley regarding the far UV CD spectra, which can be used to characterise the tertiary structure of antibodies. [233] Tertiary structure characterisations can provide useful information regarding protein misfolding, and even predict early aggregation due to exposure of hydrophobic regions upon tertiary conformational changes. [243]

Measurements of payload bound to heavy and light chains were made but it would be interesting to see if these values could be used to calculate a total DAR. This calculated DAR could then be tracked, reducing the number of statistics being presented and increasing the relevance of the data presented.

Ideally, it would be possible able to continue research about the in-use safety concerns of brentuximab vedotin. To do this would require a fully validation of the stability characterisation techniques on brentuximab vedotin. The preliminary research concerning brentuximab vedotin, suggests there should be no problems during validation. Even the unusual appearance during intact gel electrophoresis analysis and the two unidentified peaks identified in heavy chain LC-MS analysis, won't stop an investigation int o the stability upon exposure to common cleaning agents, even if the total amount of MMAE may not be lethal it could certainly still be harmful based on literature of other cytotoxic spindle poisons such as vincristine. [242]

Once that work is done, a stability study on brentuximab vedotin would be possible and has many of the same logistical and financial benefits that a stability study on trastuzumab emtansine does, however it arguably has more of an impact on staff safety than trastuzumab emtansine as brentuximab vedotin has been shown to have more harm potential than trastuzumab emtansine, thus enabling its manufacture to occur in aseptic compounding pharmacies can aid the NHS and private hospitals in their efforts to manage the risk of cytotoxic exposure of their staff and patients.

As preliminary brentuximab vedotin characterisation has already revealed differences to trastuzumab emtansine characterisation it would certainly be of interest to perform an investigation in to either the recently relicensed gemtuzumab ozagamicin or recently licensed inotozumab ozagamicin, as these use a different linker technology and warhead to both previously investigated ADCs.

Furthermore, some techniques used during this project could be improved, for example gel electrophoresis is mainly used as a qualitative test, however the Agilent Tapestation 2200 produces electropherograms, not used in this thesis, which could be exploited to yield a more quantitative characterisation of biopharmauticals.

Concluding Statement

The main purpose of this PhD was to enable a shelf life extension of trastuzumab emtansine. This was achieved, in addition to discovering limitations of existing techniques, developing new methods for ADC characterisation, that are demonstrated to work on multiple types of ADC as well as normal antibodies. Also, novel information pertaining to container construction and material has been discovered which has affected NHS stability guidance. I am proud of the research that I have performed and pleased I was able to achieve all of the original aims and objectives, as well as being able to investigate some interesting off shoots of the main PhD project aim.

Chapter 9. References

1. Rettig, R.A. The war on cancer: An anatomy of failure, a blueprint for the future. *Health Affairs* **25**, 1446-1447 (2006).
2. Fenn, J.E. & Udelsman, R. First Use of Intravenous Chemotherapy Cancer Treatment: Rectifying the Record. *Journal of the American College of Surgeons* **212**, 413-417 (2011).
3. Farber, S., Diamond, L.K., Mercer, R.D., Sylvester, R.F. & Wolff, J.A. Temporary Remissions In Acute Leukemia In Children Produced By Folic Acid Antagonist, 4-Aminopteroyl-Glutamic Acid (Aminopterin). *New England Journal of Medicine* **238**, 787-793 (1948).
4. Evans, A.E., Mariano, P.J., Farber, S. & Brunet, S. Vincristine In Treatment Of Acute Leukemia In Children. *Cancer* **16**, 1302-1309 (1963).
5. Djerassi, I., Farber, S., Abir, E. & Neikirk, W. Continuous Infusion Of Methotrexate In Children With Acute Leukemia. *Cancer* **20**, 233-& (1967).
6. Li, M.C., Hertz, R. & Bergenstal, D.M. Therapy Of Choriocarcinoma And Related Trophoblastic Tumors With Folic Acid And Purine Antagonists. *New England Journal of Medicine* **259**, 66-74 (1958).
7. Wilson, W.L. Chemotherapy Of Human Solid Tumors With 5-Fluorouracil. *Cancer* **13**, 1230-1239 (1960).
8. Wolberg, W.H. & Curreri, A.R. Toxicity Studies Of 5-Fluorouracil Used As An Adjunct To Surgery. *Archives of Surgery* **81**, 244-250 (1960).
9. Ellison, R.R. Collateral Sensitivity To Methotrexate In 6-Mercaptopurine-Responsive Adult Acute Leukemics. *Journal of Clinical Investigation* **36**, 887-887 (1957).
10. Law, L.W. Differences Between Cancers In Terms Of Evolution Of Drug Resistance. *Cancer Research* **16**, 698-716 (1956).
11. Frei, E. Potential for eliminating leukemic cells in childhood acute leukemia. *Proc Amer Assoc Cancer Res* **5**, 20 (1964).
12. Thompson, I., Hall, T.C. & Moloney, W.C. Combination Therapy Of Adult Acute Myelogenous Leukemia - Experience With Simultaneous Use Of Vincristine Amethopterin 6-Mercaptopurine And Prednisone. *New England Journal of Medicine* **273**, 1302-1315 (1965).
13. Luce, J.K. & Gamble, J.F. Combination Chemotherapy (Mopp) In Disseminated Hodgkins Disease (HD). *Cancer Chemotherapy Reports Part 1* **53**, 89-& (1969).
14. Lowenbraun, S., Devita, V.T. & Serpick, A.A. Combination Chemotherapy With Nitrogen Mustard, Vincristine, Procarbazine, And Prednisone In Lymphosarcoma And Reticulum Cell Sarcoma. *Cancer* **25**, 1018-1023 (1970).
15. Sitarz, A.L*., et al.* Induction Of Remission In Childhood Leukemia With Vincristine And 6-Mercaptopurine And Methotrexate - Adminstration In Sequence After Prednisone. *Cancer* **21**, 920-924 (1968).
16. Welch, A.D. Problem Of Drug Resistance In Cancer Chemotherapy. *Cancer Research* **19**, 359-371 (1959).
17. Skipper, H.E., Schabel, F., Trader, M.W. & Thompson, J.R. Experimental evaluation of potential anticancer agents. VI. Anatomical distribution of leukemic cells and failure of chemotherapy. *Cancer Res* **21**, 1154-1164 (1961).
18. Skipper, H.E. Cellular kinetics associated with "curability" of experimental leukemias. *Perspectives in leukemia. Symposium of the Leukemia Society of America. December, 1966*, 187-216 (1968).

19. Skipper, H.E*., et al.* Implications of biochemical, cytokinetic, pharmacologic, and toxicologic relationships in design of optimal therapeutic schedules. *Cancer Chemotherapy Reports Part 1* **54**, 431-439 (1970).
20. Hajdu, S.I. & Vadmal, M. A Note From History: Landmarks in History of Cancer, Part 6. *Cancer* **119**, 4058-4082 (2013).
21. Ward, H.W.C. Antiestrogen therapy for breast-cancer - Trial of tamoxifen at 2 dose levels. *Bmj-British Medical Journal* **1**, 13-14 (1973).
22. Heel, R.C., Brogden, R.N., Speight, T.M. & Avery, G.S. Tamoxifen - review of its pharmacological properties and therapeutic use in treatment of breast-cancer. *Drugs* **16**, 1-24 (1978).
23. Goustin, A.S., Leof, E.B., Shipley, G.D. & Moses, H.L. Growth-factors and cancer. *Cancer Research* **46**, 1015-1029 (1986).
24. Zhou, D.J., Battifora, H., Yokota, J., Yamamoto, T. & Cline, M.J. Association of multiple copies of the c-erbb-2 oncogene with spread of breast-cancer. *Cancer Research* **47**, 6123-6125 (1987).
25. Lin, N.U. & Winer, E.P. Brain metastases: The HER2 paradigm. *Clinical Cancer Research* **13**, 1648-1655 (2007).
26. Achkova, D. & Maher, J. Role of the colony-stimulating factor (CSF)/CSF-1 receptor axis in cancer. *Biochemical Society Transactions* **44**, 333-341 (2016).
27. Druker, B.J*., et al.* Effects of a selective inhibitor of the Abl tyrosine kinase on the growth of Bcr-Abl positive cells. *Nature Medicine* **2**, 561-566 (1996).
28. Lin, N.U. & Winer, E.P. Brain metastases: The HER2 paradigm. in *Clinical Cancer Research*, Vol. 13 (2007) Accessed on 25/07/18
From: http://clincancerres.aacrjournals.org/content/clincanres/13/6/1648/F2.large.jpg?width=800&height=600&carousel=1).
29. Achkova, D. & Maher, J. Role of the colony-stimulating factor (CSF)/CSF-1 receptor axis in cancer. in *Biochemical Society Transactions*, Vol. 44 333-341 (2016) Acessed on 25/07/18.
Image from: https://ai2-s2-public.s3.amazonaws.com/figures/2017-08-08/248076e6ad47a53adef308805fea979bcf6b1ebb/2-Figure1-1.png
30. Prull, C.R. Part of a scientific master plan? - Paul Ehrlich and the origins of his receptor concept. *Medical History* **47**, 332-356 (2003).
31. Strebhardt, K. & µLlrich, A. Paul Ehrlich's magic bullet concept: 100 years of progress. *Nature Reviews Cancer* **8**, 473-480 (2008).
32. Dr Paul Ehrlich and diagrams of his receptor theory. (Accessed on 25/07/18)
Image from: http://tibbs.unc.edu/wp-content/uploads/2015/05/paul-ehrlich.jpg
33. Waxdal, M.J., Konigsberg, W.H. & Edelman, G.M. Structure of a human gamma g immunoglobulin. *Cold Spring Harbor Symposia on Quantitative Biology* **32**, 53-+ (1967).
34. Edelman, G.M*., et al.* Covalent structure of an entire gammag immunoglobulin molecule. *Proceedings of the National Academy of Sciences of the United States of America* **63**, 78-83 (1969).
35. Cohen, S. & Porter, R.R. Structure and biological activity of immunoglobulins. *Advances in Immunology* **4**, 287-349 (1964).
36. Simple diagram of an antibody. (Accessed on: 25/07/18
Image from: https://www.progen.com/media/catalog/category/Antibodies_1.png
37. Fab and Fc digram of an antibody. (Accessed on 25/08/18
Image from: https://static.bio-rad-antibodies.com/blog/blue-antibody-fab-blog.png
38. Wu, T.T. & Kabat, E.A. An analysis of sequences of variable regions of bence jones proteins and myeloma light chains and their implications for antibody complementarity. *Journal of Experimental Medicine* **132**, 211-232 (1970).
39. Simple CDR diagram of an antibody. (Accessed on 25/07/18)

Image from: http://escience.ws/b572/L14/images/CDRx.gif).
40. Kohler, G. & Milstein, C. Continuous cultures of fused cells secreting antibody of predefined specificity. *Nature* **256**, 495-497 (1975).
41. Ruigrok, V.J.B., Levisson, M., Eppink, M.H.M., Smidt, H. & van der Oost, J. Alternative affinity tools: more attractive than antibodies? *Biochemical Journal* **436**, 1-13 (2011).
42. Diagram of monoclonal antibody producing hybridoma cells. (Image from: http://www.biochemj.org/content/436/1/1).
43. Sgro, C. Side-effects of a monoclonal antibody, muromonab CD3 orthoclone OKT3: Bibliographic review. *Toxicology* **105**, 23-29 (1995).
44. Morrison, S.L., Johnson, M.J., Herzenberg, L.A. & Oi, V.T. Chimeric human-antibody molecules - mouse antigen-binding domains with human constant region domains. *Proceedings of the National Academy of Sciences of the United States of America-Biological Sciences* **81**, 6851-6855 (1984).
45. Hwang, W.Y.K. & Foote, J. Immunogenicity of engineered antibodies. *Methods* **36**, 3-10 (2005).
46. Riechmann, L., Clark, M., Waldmann, H. & Winter, G. Reshaping human-antibodies for therapy. *Nature* **332**, 323-327 (1988).
47. Simple diagram of antibodies, with murine protein in blue and human protein in orange. (Accessed on: 25/07/18)
Image from: http://modiquestresearch.nl/services/antibody-optimization/).
48. Grillo-Lopez, A.J.*, et al.* Overview of the clinical development of rituximab: First monoclonal antibody approved for the treatment of lymphoma. *Seminars in Oncology* **26**, 66-73 (1999).
49. Falduto, A.*, et al.* How gene polymorphisms can influence clinical response and toxicity following R-CHOP therapy in patients with diffuse large B cell lymphoma. *Blood Reviews* **31**, 235-249 (2017).
50. Rituximab's mechanisms of action. (Accessed on: 25/07/18)
https://www.researchgate.net/profile/Alessandro_Allegra/publication/314107334/figure/fig1/AS:482562498928641@1492063273783/The-mechanism-of-action-of-rituximab-proposed-including-antibody-dependent-cellular.jpg).
51. Nahta, R., Yu, D.H., Hung, M.C., Hortobagyi, G.N. & Esteva, F.J. Mechanisms of disease: understanding resistance to HER2-targeted therapy in human breast cancer. *Nature Clinical Practice Oncology* **3**, 269-280 (2006).
52. Pegram, M.D. & Slamon, D.J. Combination therapy with trastuzumab (Herceptin) and cisplatin for chemoresistant metastatic breast cancer: Evidence for receptor-enhanced chemosensitivity. *Seminars in Oncology* **26**, 89-95 (1999).
53. Burris, H.A. Docetaxel (Taxotere) in HER-2-positive patients and in combination with trastuzumab (Herceptin). *Seminars in Oncology* **27**, 19-23 (2000).
54. Umana, P.*, et al.* Novel 3(rd) generation humanized type IICD20 antibody with glycoengineered fc and modified elbow hinge for enhanced ADCC and superior apoptosis induction. *Blood* **108**, 72A-72A (2006).
55. Umana, P.*, et al.* Novel third generation humanized type IICD20 antibody with superior direct cell death induction and glycoengineered Fc region for enhanced ADCC induction. *Molecular Cancer Therapeutics* **6**, 3353S-3353S (2007).
56. Morschhauser, F.*, et al.* Results of a phase I/II study of ocrelizumab, a fully humanized anti-CD20 mAb, in patients with relapsed/refractory follicular lymphoma. *Annals of Oncology* **21**, 1870-1876 (2010).
57. Lauc, G., Pezer, M., Rudan, I. & Campbell, H. Mechanisms of disease: The human N-glycome. *Biochimica Et Biophysica Acta-General Subjects* **1860**, 1574-1582 (2016).
58. Examples of different Fc region glycosylation chains and their effects. (Accessed on: 25/07/18)

Image from: https://ars.els-cdn.com/content/image/1-s2.0-S0304416515002883-gr2_lrg.jpg
59. Steplewski, Z.*, et al.* Biological-activity of human mouse IGG1, IGG2, IGG3, AND IGG4 chimeric monoclonal-antibodies with antitumor specificity. *Proceedings of the National Academy of Sciences of the United States of America* **85**, 4852-4856 (1988).
60. Jefferis, R. Antibody therapeutics: isotype and glycoform selection. *Expert Opinion on Biological Therapy* **7**, 1401-1413 (2007).
61. Tao, M.H., Canfield, S.M. & Morrison, S.L. The differential ability of human IGG1 and IGG4 to activate complement is determined by the COOH-terminal sequence of the CH2 domain. *Journal of Experimental Medicine* **173**, 1025-1028 (1991).
62. Correia, I.R. Stability of IgG isotypes in serum. *Mabs* **2**, 221-232 (2010).
63. Diagrams of IgG isotypes. (Accessed on: 25/07/18)
Image from: https://teaching.ncl.ac.uk/bms/wiki/images/3/33/Antibody.jpg).
64. Janeway, C. Travers, P. Walport, M. & Schlomchik. *Immunobiology: The Immune System in Health and Disease. 5th Edition*, (Garland Science, New York, 2001).
65. Highly detailed diagram of an IgG1 antibody. (Accessed on: 25/07/18
Image from: https://www.tandfonline.com/doi/pdf/10.4161/mabs.2.3.5.488).
66. Trail, P.A.*, et al.* Cure of xenografted human carcinomas by br96-doxorubicin immunoconjugates. *Science* **261**, 212-215 (1993).
67. Trail, P.A., Willner, D. & Hellstrom, K.E. Site-directed delivery of anthracyclines for treatment of cancer. *Drug Development Research* **34**, 196-209 (1995).
68. Slichenmyer, W.J.*, et al.* Phase I clinical trials with the immunoconjugate BR96-doxorubicin. *Abstracts of Papers of the American Chemical Society* **211**, 32-37 (1996).
69. Trail, P.A., King, H.D. & Dubowchik, G.M. Monoclonal antibody drug immunoconjugates for targeted treatment of cancer. *Cancer Immunology Immunotherapy* **52**, 328-337 (2003).
70. Saleh, M.N.*, et al.* Phase I trial of the anti-Lewis Y drug immunoconjugate BR96-Doxorubicin in patients with Lewis Y-expressing epithelial tumors. *Journal of Clinical Oncology* **18**, 2282-2292 (2000).
71. Tijink, B.M.*, et al.* A phase I dose escalation study with anti-CD44v6 bivatuzumab mertansine in patients with incurable squamous cell carcinoma of the head and neck or esophagus. *Clinical Cancer Research* **12**, 6064-6072 (2006).
72. Becher, O.J. & Holland, E.C. Genetically engineered models have advantages over xenografts for preclinical studies. *Cancer Research* **66**, 3355-3358 (2006).
73. Bouchard, H., Viskov, C. & Garcia-Echeverria, C. Antibody-drug conjugates-A new wave of cancer drugs. *Bioorganic & Medicinal Chemistry Letters* **24**, 5357-5363 (2014).
74. Mechanism of ADC internalisation and drug release. (Image accessed: 25/07/18
Image from: https://ars-els-cdn-com.ezproxy1.bath.ac.uk/content/image/1-s2.0-S0960894X1401066X-gr1.jpg).
75. Petersdorf, S.H.*, et al.* A phase 3 study of gemtuzumab ozogamicin during induction and postconsolidation therapy in younger patients with acute myeloid leukemia. *Blood* **121**, 4854-4860 (2013).
76. Castaigne, S.*, et al.* Effect of gemtuzumab ozogamicin on survival of adult patients with de-novo acute myeloid leukaemia (ALFA-0701): a randomised, open-label, phase 3 study. *Lancet* **379**, 1508-1516 (2012).
77. Sievers, E.L.*, et al.* Efficacy and safety of gemtuzumab ozogamicin in patients with CD33-positive acute myeloid leukemia in first relapse. *Journal of Clinical Oncology* **19**, 3244-3254 (2001).
78. Dinndorf, P.A.*, et al.* Expression of myeloid differentiation antigens in acute nonlymphocytic leukemia - increased concentration of cd33-antigen predicts poor

outcome - A report from the childrens cancer study-group. *Medical and Pediatric Oncology* **20**, 192-200 (1992).
79. Hamblett, K.J*., et al.* SGN-35, an anti-CD30 antibody-drug conjugate, exhibits potent antitumor activity for the treatment of CD30(+) malignancies. *Blood* **106**, 181A-181A (2005).
80. Beljaards, R.C*., et al.* Prognostic-significance of CD30 (KI-1/BER-H2) expression in primary cutaneous large-cell lymphomas of t-cell origin - A clinicopathologic and immunohistochemical study in 20 patients. *American Journal of Pathology* **135**, 1169-5.48 (1989).
81. Niculescu-Duvaz, I. Trastuzumab emtansine, an antibody-drug conjugate for the treatment of HER2+metastatic breast cancer. *Current Opinion in Molecular Therapeutics* **12**, 350-360 (2010).
82. Rosen, D.B*., et al.* AKT Signaling as a Novel Factor Associated with In Vitro Resistance of Human AML to Gemtuzumab Ozogamicin. *Plos One* **8**(2013
Accessed on 25/07/18 Image taken from: https://www.ncbi.nlm.nih.gov/pmc/articles /PMC3539972/figure/pone-0053518-g001/).
83. Eyre, T.A., Khan, D., Hall, G.W. & Collins, G.P. Anaplastic lymphoma kinase-positive anaplastic large cell lymphoma: current and future perspectives in adult and paediatric disease. *European Journal of Haematology* **93**, 455-468 (2014)
Accessed on 25/07/18 Image from: https://onlinelibrary-wiley-com.ezproxy1.bath.ac .uk/doi/epdf/10.1111/ejh.12360).
84. Gogia, A*., et al.* Trastuzumab Emtansine: Antibody-drug Conjugate in Treatment of Human Epidermal Growth Factor Receptor-2-Positive Metastatic Breast Cancer. *Indian Journal of Medical and Paediatric Oncology* **39**, 79-87 (2018) Accessed on 25/08/18 Image from: http://www.ijmpo.org/temp/IndianJMedPaediatrOncol 39179-2682634_ 072706.pdf).
85. Hoffmann, R.M*., et al.* Antibody structure and engineering considerations for the design and function of Antibody Drug Conjugates (ADCs). *Oncoimmunology* **7**(2018).
86. Chari, R.V.J. Targeted cancer therapy: Conferring specificity to cytotoxic drugs. *Accounts of Chemical Research* **41**, 98-107 (2008).
87. Lu, J., Jiang, F., Lu, A.P. & Zhang, G. Linkers Having a Crucial Role in Antibody-Drug Conjugates. *International Journal of Molecular Sciences* **17**(2016).
88. Hollander, I., Kunz, A. & Hamann, P.R. Selection of reaction additives used in the preparation of monomeric antibody-calicheamicin conjugates. *Bioconjugate Chemistry* **19**, 358-361 (2008).
89. Marcoux, J*., et al.* Native mass spectrometry and ion mobility characterization of trastuzumab emtansine, a lysine-linked antibody drug conjugate. *Protein Science* **24**, 1210-1223 (2015).
90. McCombs, J.R. & Owen, S.C. Antibody Drug Conjugates: Design and Selection of Linker, Payload and Conjugation Chemistry. *Aaps Journal* **17**, 339-351 (2015).
91. Jackson, D. & Stover, D. Using the Lessons Learned From the Clinic to Improve the Preclinical Development of Antibody Drug Conjugates. *Pharmaceutical Research* **32**, 3458-3469 (2015).
92. Kupchan, S.M*., et al.* Tumor inhibitors .73. Maytansine, a novel antileukemic ansa macrolide from maytenus-ovatus. *Journal of the American Chemical Society* **94**, 1354-1360 (1972).
93. Annual Reports in Medicinal Chemistry, Vol 50: Platform Technologies in Drug Discovery and Validation. *Annual Reports in Medicinal Chemistry, Vol 50: Platform Technologies in Drug Discovery and Validation* **50**, 1-675 (2017).

94. Lopus, M.*, et al.* Maytansine and Cellular Metabolites of Antibody-Maytansinoid Conjugates Strongly Suppress Microtubule Dynamics by Binding to Microtubules. *Molecular Cancer Therapeutics* **9**, 2689-2699 (2010).
95. Li, F.*, et al.* Intracellular Released Payload Influences Potency and Bystander-Killing Effects of Antibody-Drug Conjugates in Preclinical Models. *Cancer Research* **76**, 2710-2719 (2016).
96. Shah, D.K.*, et al.* A Priori Prediction of Tumor Payload Concentrations: Preclinical Case Study with an Auristatin-Based Anti-5T4 Antibody-Drug Conjugate. *Aaps Journal* **16**, 452-463 (2014).
97. Lambert, J.M. & Berkenblit, A. Antibody-Drug Conjugates for Cancer Treatment. *Annual Review of Medicine, Vol 69* **69**, 191-207 (2018).
98. MHRA. *Inspection Enforcement and Standards Division Medicines and Healthcare products Regulatory Agency (MHRA) London UK Rules and Guidance for Pharmaceutical Manufacturers and Distributors 2017*, (Pharmaceutical Press, a publishing division of the Royal Pharmaceutical Society, 66-68, East Smithfield, London, E1W 1AW, UK, 2017).
99. Breckenridge, A. Report of the working party on the addition of drugs to intravenous infusion fluids. (London : Department of Health and Social Security, 1976).
100. Beaney, A., M. Preparing injectable medicines safely. (Nursing Times 108 (3), 2012).
101. National-Health-Service-Pharmaceutical-Quality-Assurance-Committee. Standard Protocol for Deriving and Assessment of Stability, Part 1: Aseptic Preparations (Small Molecules). (2017).
102. National-Health-Service-Pharmaceutical-Quality-Assurance-Committee. Standard Protocol for Deriving and Assessment of Stability, Part 2: Aseptic Preparations (Biopharmacuticals). (2017).
103. Krop, I.E.*, et al.* Trastuzumab emtansine (T-DM1) versus lapatinib plus capecitabine in patients with HER2-positive metastatic breast cancer and central nervous system metastases: a retrospective, exploratory analysis in EMILIA. *Annals of Oncology* **26**, 113-119 (2015).
104. Krop, I.E.*, et al.* Trastuzumab emtansine versus treatment of physician's choice in patients with previously treated HER2-positive metastatic breast cancer (TH3RESA): final overall survival results from a randomised open-label phase 3 trial. *Lancet Oncology* **18**, 743-754 (2017).
105. ICH. Q2(R1) Validation of Analytical Procedures: Methodology.
106. Khabar, K.S.A., Siddiqui, S. & Armstrong, J.A. WEHI-13VAR - a stable and sensitive variant of WEHI-164 clone-13 fibrosarcoma for tumor-necrosis-factor bioassay. *Immunology Letters* **46**, 107-110 (1995).
107. Austgulen, R., Hammerstrom, J., Espevik, T. & Nissenmeyer, J. Human monocyte cytotoxic factor mediates cytolysis of WEHI 164 cells. *Cellular Immunology* **98**, 211-220 (1986).
108. Song, M.-Y.*, et al.* Characterization of a novel anti-human TNF-alpha murine monoclonal antibody with high binding affinity and neutralizing activity. *Experimental and Molecular Medicine* **40**, 35-42 (2008).
109. Tawede, S., A. Particulate Matter in Injectables: Main cause for Recalls. in *Journal of Pharmacovigilance*, Vol. 3 (2015).
110. BP. British Pharmacopoeia Appendix XIII Addendum 1996 - Particulate contamination. (1996).
111. Sreedhara, A.*, et al.* Stability of IgG1 monoclonal antibodies in intravenous infusion bags under clinical in-use conditions. *Journal of Pharmaceutical Sciences* **101**, 21-30 (2012).

112. Psathas, P.A., Kuzmission, A., Ikeda, K. & Yasuo, S. Stability of Doripenem in Vitro in Representative Infusion Solutions and Infusion Bags. *Clinical Therapeutics* **30**, 2075-2087 (2008).
113. Lebitasy, M., Hecq, J.D., Vanbeckbergen, D., Jamart, J. & Galanti, L. Long-term stability of tramadol hydrochloride and droperidol mixture in 5% dextrose infusion polyolefin bags at 5 +/- 3 degrees C. *Annales Pharmaceutiques Francaises* **67**, 272-277 (2009).
114. Karbownik, A*., et al.* The physical and chemical stability of cisplatin (Teva) in concentrate and diluted in sodium chloride 0.9%. *Wspolczesna Onkologia-Contemporary Oncology* **16**, 435-439 (2012).
115. Nissen, K.B., Jorgensen, L.B., Berg, D.L. & Andersen, G. Stability study of methotrexate in 0.9% sodium chloride injection and 5% dextrose injection with limit tests for impurities. *American Journal of Health-System Pharmacy* **74**, E211-E223 (2017).
116. Spindeldreier, K.C., Thiesen, J. & Kraemer, I. Physicochemical stability of cabazitaxel containing premix solution and diluted infusion solutions. *European Journal of Hospital Pharmacy-Science and Practice* **22**, 260-266 (2015).
5.4. Paul, M., Vieillard, V., Lemos, R.D., Escalup, L. & Astier, A. Long-term physico-chemical stability of diluted trastuzumab. *International Journal of Pharmaceutics* **448**, 101-104 (2013).
118. Lazzarini, R*., et al.* Physicochemical stability of cabazitaxel and docetaxel solutions. *European Journal of Hospital Pharmacy-Science and Practice* **22**, 150-155 (2015).
119. Joshi, V.S., Kumar, V. & Rathore, A.S. Enhanced product understanding in the QbD paradigm: linkage between charge heterogeneity and stability of monoclonal antibody therapeutic products. *Journal of Chemical Technology and Biotechnology* **93**, 2102-2110 (2018).
120. Leblanc, Y., Ramon, C., Bihoreau, N. & Chevreux, G. Charge variants characterization of a monoclonal antibody by ion exchange chromatography coupled on-line to native mass spectrometry: Case study after a long-term storage at+5 degrees C. *Journal of Chromatography B-Analytical Technologies in the Biomedical and Life Sciences* **1048**, 130-139 (2017).
121. Parekh, B.S*., et al.* Correlating charge heterogeneity data generated by agarose gel isoelectric focusing and ion exchange chromatography methods. *Journal of Chromatography B-Analytical Technologies in the Biomedical and Life Sciences* **1073**, 1-9 (2018).
122. Kantner, T. & Watts, A.G. Characterization of Reactions between Water-Soluble Trialkylphosphines and Thiol Alkylating Reagents: Implications for Protein-Conjugation Reactions. *Bioconjugate Chemistry* **27**, 2400-2406 (2016).
123. Paul, M., Vieillard, V., Jaccoulet, E. & Astier, A. Long-term stability of diluted solutions of the monoclonal antibody rituximab. *International Journal of Pharmaceutics* **436**, 282-290 (2012).
124. Glover, Z.W.K*., et al.* Compatibility and stability of pertuzumab and trastuzumab admixtures in i.v. infusion bags for coadministration. *Journal of Pharmaceutical Sciences* **102**, 794-812 (2013).
125. Hernandez-Jimenez, J*., et al.* The Effects of Light-Accelerated Degradation on the Aggregation of Marketed Therapeutic Monoclonal Antibodies Evaluated by Size-Exclusion Chromatography With Diode Array Detection. *Journal of Pharmaceutical Sciences* **105**, 1405-1418 (2016).
126. Kumru, O.S*., et al.* Compatibility, physical stability, and characterization of an IgG4 monoclonal antibody after dilution into different intravenous administration bags. *Journal of Pharmaceutical Sciences* **101**, 3636-3650 (2012).

127. Kalonia, C*., et al.* Calculating the Mass of Subvisible Protein Particles with Improved Accuracy Using Microflow Imaging Data. *Journal of Pharmaceutical Sciences* **104**, 536-547 (2015).
128. Randolph, T.W*., et al.* Do Not Drop: Mechanical Shock in Vials Causes Cavitation, Protein Aggregation, and Particle Formation. *Journal of Pharmaceutical Sciences* **104**, 602-611 (2015).
129. Telikepalli, S*., et al.* Characterization of the Physical Stability of a Lyophilized IgG1 mAb after Accelerated Shipping-Like Stress. *Journal of Pharmaceutical Sciences* **104**, 495-507 (2015).
130. Cordes, A.A., Carpenter, J.F. & Randolph, T.W. Accelerated Stability Studies of Abatacept Formulations: Comparison of Freeze-Thawing- and Agitation-Induced Stresses. *Journal of Pharmaceutical Sciences* **101**, 2307-2315 (2012).
131. Vlieland, N.D*., et al.* The Impact of Inadequate Temperature Storage Conditions on Aggregate and Particle Formation in Drugs Containing Tumor Necrosis Factor-Alpha Inhibitors. *Pharmaceutical Research* **35**(2018).
132. Vasudev, R., Mathew, S. & Afonina, N. Characterization of Submicron (0.1-1 mu m) Particles in Therapeutic Proteins by Nanoparticle Tracking Analysis. *Journal of Pharmaceutical Sciences* **104**, 1622-1631 (2015).
133. Patois, E., Capelle, M.A.H., Palais, C., Gurny, R. & Arvinte, T. Evaluation of nanoparticle tracking analysis (NTA) in the characterization of therapeutic antibodies and seasonal influenza vaccines: pros and cons. *Journal of Drug Delivery Science and Technology* **22**, 427-433 (2012).
134. Tian, X.S*., et al.* A Comprehensive Evaluation of Nanoparticle Tracking Analysis (NanoSight) for Characterization of Proteinaceous Submicron Particles. *Journal of Pharmaceutical Sciences* **105**, 3366-3375 (2016).
135. Castellanos, M.M., Howell, S.C., Gallagher, D.T. & Curtis, J.E. Characterization of the NISTmAb Reference Material using small-angle scattering and molecular simulation. *Analytical and Bioanalytical Chemistry* **410**, 2141-2159 (2018).
136. Davies, A.M., Rispens, T., Ooijevaar-de Heer, P., Aalberse, R.C. & Sutton, B.J. Room temperature structure of human IgG4-Fc from crystals analysed in situ. *Molecular Immunology* **81**, 85-91 (2017).
137. Harris, L.J., Skaletsky, E. & McPherson, A. Crystallographic structure of an intact IgG1 monoclonal antibody. *Journal of Molecular Biology* **275**, 861-872 (1998).
138. Saphire, E.O*., et al.* Contrasting IgG structures reveal extreme asymmetry and flexibility. *Journal of Molecular Biology* **319**, 9-18 (2002).
139. Singh, S.M., Bandi, S., Jones, D.N.M. & Mallela, K.M.G. Effect of Polysorbate 20 and Polysorbate 80 on the Higher-Order Structure of a Monoclonal Antibody and Its Fab and Fc Fragments Probed Using 2D Nuclear Magnetic Resonance Spectroscopy. *Journal of Pharmaceutical Sciences* **106**, 3486-3498 (2017).
140. Kiss, R., Fizil, A. & Szantay, C. What NMR can do in the biopharmaceutical industry. *Journal of Pharmaceutical and Biomedical Analysis* **147**, 367-377 (2018).
141. Brinson, R.G*., et al.* Application of 2D-NMR with room temperature NMR probes for the assessment of the higher order structure of filgrastim. *Journal of Pharmaceutical and Biomedical Analysis* **141**, 229-233 (2017).
142. Frueh, D.P., Goodrich, A.C., Mishra, S.H. & Nichols, S.R. NMR methods for structural studies of large monomeric and multimeric proteins. *Current Opinion in Structural Biology* **23**, 734-739 (2013).
143. Biswas, A., Ranjan, D., Zubair, M. & He, J. A Novel Computational Method for Deriving Protein Secondary Structure Topologies Using Cryo-EM Density Maps and Multiple Secondary Structure Predictions. *Bioinformatics Research and Applications (Isbra 2015)* **9096**, 60-71 (2015).

144. Bokori-Brown, M.*, et al.* Cryo-EM structure of lysenin pore elucidates membrane insertion by an aerolysin family protein. *Nature Communications* **7**(2016).
145. Fibriansah, G.*, et al.* Cryo-EM structure of an antibody that neutralizes dengue virus type 2 by locking E protein dimers. *Science* **349**, 88-91 (2015).
146. Long, F.*, et al.* Cryo-EM structures elucidate neutralizing mechanisms of anti-chikungunya human monoclonal antibodies with therapeutic activity. *Proceedings of the National Academy of Sciences of the United States of America* **112**, 13898-13903 (2015).
147. Wang, R.Y.R.*, et al.* De novo protein structure determination from near-atomic-resolution cryo-EM maps. *Nature Methods* **12**, 335-U384 (2015).
148. Mason, B.I., Schoneich, C. & Kerwin, B.A. Effect of pH and Light on Aggregation and Conformation of an IgG1 mAb. *Molecular Pharmaceutics* **9**, 774-790 (2012).
149. Sousa, F., Sarrnento, B. & Neves-Petersen, M.T. Biophysical study of bevacizumab structure and bioactivity under thermal and pH-stresses. *European Journal of Pharmaceutical Sciences* **105**, 127-136 (2017).
150. Wang, S.J.*, et al.* Stabilizing two IgG1 monoclonal antibodies by surfactants: Balance between aggregation prevention and structure perturbation. *European Journal of Pharmaceutics and Biopharmaceutics* **114**, 263-277 (2017).
151. Lim, J.Y., Kim, N.A., Lim, D.G., Kim, K.H. & Jeong, S.H. Effects of thermal and mechanical stress on the physical stability of human growth hormone and epidermal growth factor. *Archives of Pharmacal Research* **38**, 1488-1498 (2015).
152. Durowoju, I.B., Bhandal, K.S., Hu, J., Carpick, B. & Kirkitadze, M. Differential Scanning Calorimetry - A Method for Assessing the Thermal Stability and Conformation of Protein Antigen. *Jove-Journal of Visualized Experiments* (2017).
153. Kubelka, J., Pancoska, P. & Keiderling, T.A. Novel use of a static modification of two-dimensional correlation analysis. Part II: Hetero-spectral correlations of protein Raman, FT-IR, and circular dichroism spectra. *Applied Spectroscopy* **53**, 666-671 (1999).
154. Buddanavar, A.T. & Nandibewoor, S.T. Multi-spectroscopic characterization of bovine serum albumin upon interaction with atomoxetine. *Journal of Pharmaceutical Analysis* **7**, 148-155 (2017).
155. Rahmelow, K. & Hubner, W. Secondary structure determination of proteins in aqueous solution by infrared spectroscopy: A comparison of multivariate data analysis methods. *Analytical Biochemistry* **241**, 5-13 (1996).
156. Zangooei, M.H. & Jalili, S. Protein secondary structure prediction using DWKF based on SVR-NSGAII. *Neurocomputing* **94**, 87-101 (2012).
157. Zhang, Y. & Sagui, C. Secondary structure assignment for conformationally irregular peptides: Comparison between DSSP, STRIDE and KAKSI. *Journal of Molecular Graphics & Modelling* **55**, 72-84 (2015).
158. ICH. Stability testing of Biotechnological/Biological products Q5C. (Online, 1996).
159. Sadavarte, R.H. & Ghosh, R. A Thermal-Cycling Method for Disaggregating Monoclonal Antibody Oligomers. *Journal of Pharmaceutical Sciences* **103**, 870-878 (2014).
160. Wang, B., Cicerone, M.T., Aso, Y. & Pikal, M.J. The Impact of Thermal Treatment on the Stability of Freeze-Dried Amorphous Pharmaceuticals: II. Aggregation in an IgG1 Fusion Protein. *Journal of Pharmaceutical Sciences* **99**, 683-700 (2010).
161. Coussot, G., Le Postollec, A., Faye, C. & Dobrijevic, M. A gold standard method for the evaluation of antibody-based materials functionality: Approach to forced degradation studies. *Journal of Pharmaceutical and Biomedical Analysis* **152**, 17-24 (2018).
162. Shah, D.D., Zhang, J.M., Maity, H. & Mallela, K.M.G. Effect of photo-degradation on the structure, stability, aggregation, and function of an IgG1 monoclonal antibody. *International Journal of Pharmaceutics* **547**, 438-449 (2018).

163. Singh, S.R.*, et al.* Effect of Polysorbate 80 Quality on Photostability of a Monoclonal Antibody. *Aaps Pharmscitech* **13**, 422-430 (2012).
164. Bane, J.*, et al.* Photo-oxidation of IgG1 and Model Peptides: Detection and Analysis of Triply Oxidized His and Trp Side Chain Cleavage Products. *Pharmaceutical Research* **34**, 229-242 (2017).
165. Zamani, L., Andersson, F.O., Edebrink, P., Yang, Y. & Jacobsson, S.P. Conformational studies of a monoclonal antibody, IgG1, by chemical oxidation: Structural analysis by ultrahigh-pressure LC-electrospray ionization tune-of-flight MS and multivariate data analysis. *Analytical Biochemistry* **380**, 155-163 (2008).
166. Usami, A., Ohtsu, A., Takahama, S. & Fujii, T. Effect of pH, hydrogen peroxide and temperature on the stability of human monoclonal antibody. *Journal of Pharmaceutical and Biomedical Analysis* **14**, 1133-1140 (1996).
167. Young, B.L.*, et al.* Evaluation of the physicochemical and functional stability of diluted REMSIMA upon extended storage-A study compliant with NHS (UK) guidance. in *Int J Pharm* (2015 The Authors. Published by Elsevier B.V, 2015).
168. Cockrell, G.M., Wolfe, M.S., Wolfe, J.L. & Schoneich, C. Photoinduced Aggregation of a Model Antibody-Drug Conjugate. *Molecular Pharmaceutics* **12**, 1784-1797 (2015).
169. Brockhoff, G.*, et al.* Differential impact of Cetuximab, Pertuzumab and Trastuzumab on BT474 and SK-BR-3 breast cancer cell proliferation. *Cell Proliferation* **40**, 488-507 (2007).
170. Sumikawa, T.*, et al.* Dexamethasone interferes with trastuzumab-induced cell growth inhibition through restoration of AKT activity in BT-474 breast cancer cells. *International Journal of Oncology* **32**, 683-688 (2008).
171. Vanslooten, H.J.*, et al.* Outgrowth of bt-474 human breast-cancer cells in immune-deficient mice - a new in-vivo model for hormone-dependent breast-cancer. *British Journal of Cancer* **72**, 22-30 (1995).
172. Lasfargues, E.Y., Coutinho, W.G. & Dion, A.S. Human-breast tumor-cell line (bt-474) that supports mouse mammary-tumor virus-replication. *In Vitro-Journal of the Tissue Culture Association* **15**, 723-729 (1979).
173. Wakankar, A., Chen, Y., Gokarn, Y. & Jacobson, F.S. Analytical methods for physicochemical characterization of antibody drug conjugates. *Mabs* **3**, 161-172 (2011).
174. Goswami, S., Wang, W., Arakawa, T. & Ohtake, S. Developments and Challenges for mAb-Based Therapeutics. *Antibodies* **2**, 452-500 (2013).
175. Klein, M., Rivera, B. & McGinley, M. Analysis of Antibody Drug Conjugates using High Efficiency Gel Filtration Columns (TN 5.45). (Phenomenex, 2015).
176. Pinho, S.P. & Macedo, E.A. Solubility of NaCl, NaBr, and KCI in water, methanol, ethanol, and their mixed solvents. *Journal of Chemical and Engineering Data* **50**, 29-32 (2005).
177. Renn, C.N. & Synovec, R.E. Effect of temperature on separation efficiency for high-speed size exclusion chromatography. *Analytical Chemistry* **64**, 479-484 (1992).
178. Hong, P., Koza, S. & Bouvier, E.S.P. A review size-exclusion chromatography for the analysis of protein biotherapeutics and their aggregates. *Journal of Liquid Chromatography & Related Technologies* **35**, 2923-2950 (2012).
179. Kabsch, W. & Sander, C. Dictionary of protein secondary structure - pattern-recognition of hydrogen-bonded and geometrical features. *Biopolymers* **22**, 2577-2637 (1983).
180. Frishman, D. & Argos, P. Knowledge-based protein secondary structure assignment. *Proteins-Structure Function and Genetics* **23**, 566-579 (1995).
181. Martin, J.*, et al.* Protein secondary structure assignment revisited: a detailed analysis of different assignment methods. *Bmc Structural Biology* **5**(2005).

182. Park, S.Y., Yokoyama, T., Shibayama, N., Shiro, Y. & Tame, J.R.H. 1.25 angstrom resolution crystal structures of human haemoglobin in the oxy, deoxy and carbonmonoxy forms. *Journal of Molecular Biology* **360**, 690-701 (2006).
183. Barends, T.R.M.*, et al.* Direct observation of ultrafast collective motions in CO myoglobin upon ligand dissociation. *Science* **350**, 445-450 (2015).
184. Majorek, K.A.*, et al.* Structural and immunologic characterization of bovine, horse, and rabbit serum albumins. *Molecular Immunology* **52**, 174-182 (2012).
185. Berglund, G.I.*, et al.* The catalytic pathway of horseradish peroxidase at high resolution. *Nature* **417**, 463-468 (2002).
186. Sugahara, M.*, et al.* Hydroxyethyl cellulose matrix applied to serial crystallography. *Scientific Reports* **7**(2017).
187. Maurady, A., Zdanov, A., de Moissac, D., Beaudry, D. & Sygusch, J. A conserved glutamate residue exhibits multifunctional catalytic roles in D-fructose-1,6-bisphosphate aldolases. *Journal of Biological Chemistry* **277**, 9474-9483 (2002).
188. Chruszcz, M., Wlodawer, A. & Minor, W. Determination of protein structures - A series of fortunate events. *Biophysical Journal* **95**, 1-9 (2008).
189. Purwar, N., McGarry, J.M., Kostera, J., Pacheco, A.A. & Schmidt, M. Interaction of Nitric Oxide with Catalase: Structural and Kinetic Analysis. *Biochemistry* **50**, 4491-4503 (2011).
190. Koch, C., Neumann, P., Valerius, O., Feussner, I. & Ficner, R. Crystal Structure of Alcohol Oxidase from Pichia pastoris. *Plos One* **11**(2016).
191. Wohlfahrt, G.*, et al.* 1.8 and 1.9 angstrom resolution structures of the Penicillium amagasakiense and Aspergillus niger glucose oxidases as a basis for modelling substrate complexes. *Acta Crystallographica Section D-Biological Crystallography* **55**, 969-977 (1999).
192. Raj, S.B., Ramaswamy, S. & Plapp, B.V. Yeast Alcohol Dehydrogenase Structure and Catalysis. *Biochemistry* **53**, 5791-5803 (2014).
193. Vergara, A., Caterino, M. & Merlino, A. Raman-markers of X-ray radiation damage of proteins. *International Journal of Biological Macromolecules* **111**, 1194-1205 (2018).
194. Transue, T.R., Krahn, J.M., Gabel, S.A., DeRose, E.F. & London, R.E. X-ray and NMR characterization of covalent complexes of trypsin, borate, and alcohols. *Biochemistry* **43**, 2829-2839 (2004).
195. Parkin, S., Rupp, B. & Hope, H. Atomic resolution structure of concanavalin A at 120 K. *Acta Crystallographica Section D-Biological Crystallography* **52**, 1161-1168 (1996).
196. Bruker-Optik-GMbH. OPUS Spectroscopy software Version 7 User Manual QUANT. (Bruker, 2011).
197. Kim, M.T., Chen, Y., Marhoul, J. & Jacobson, F. Statistical Modeling of the Drug Load Distribution on Trastuzumab Emtansine (Kadcyla), a Lysine-Linked Antibody Drug Conjugate. *Bioconjugate Chemistry* **25**, 1223-1232 (2014).
198. Quiles, S., Raisch, K.P., Sanford, L.L., Bonner, J.A. & Safavy, A. Synthesis and Preliminary Biological Evaluation of High-Drug-Load Paclitaxel-Antibody Conjugates for Tumor-Targeted Chemotherapy. *Journal of Medicinal Chemistry* **53**, 586-594 (2010).
199. Hamblett, K.J.*, et al.* Effects of drug loading on the antitumor activity of a monoclonal antibody drug conjugate. *Clinical Cancer Research* **10**, 7063-7070 (2004).
200. Dieras, V.*, et al.* Trastuzumab emtansine versus capecitabine plus lapatinib in patients with previously treated HER2-positive advanced breast cancer (EMILIA): a descriptive analysis of final overall survival results from a randomised, open-label, phase 3 trial. *Lancet Oncology* **18**, 732-742 (2017).
201. The Lancet. Trastuzumab emtansine and cost-based decision making (vol 389, pg 2, 2017). *Lancet* **389**, E2-E2 (2017).

202. Factsheet: Freeflex: The Innovative IV-Bag. Fresenius Kabi UK, Runcorn, Ches. Available at: http://www.freseniuskabi-productpartnering.com/files /Factsheet_5_Freeflex.pdf
203. McLeod, A.G., Walker, I.R., Zheng, S. & Hayward, C.P.M. Loss of factor VIII activity during storage in PVC containers due to adsorption. *Haemophilia* **6**, 89-92 (2000).
204. Hill, H.R., Oliver, C.K., Lippert, L.E., Greenwalt, T.J. & Hess, J.R. The effects of polyvinyl chloride and polyolefin blood bags on red blood cells stored in a new additive solution. *Vox Sanguinis* **81**, 161-166 (2001).
205. Jin, S.E., Jeon, S., Byon, H.J. & Hwang, S.J. Evaluation of tacrolimus sorption to PVC- and non-PVC-based tubes in administration sets: Pump method vs. drip method. *International Journal of Pharmaceutics* **528**, 172-179 (2017).
206. Langille, S.E. Particulate matter in injectable drug products. *PDA journal of pharmaceutical science and technology* **67**, 186-200 (2013).
207. Murtough, S.H., S. Palmer, M. Russell, A. A survey of disinfectant use in hospital pharmacy aseptic preparation areas. Vol. 264 (Pharmacutical Journal, Pharmacutical Journal, 2000).
208. Hunt, J. Decontamination of Medical Devices, Infection Prevention and Control Policy: Appendix 12 - Version 3. (2017).
209. Erickson, H.K*., et al.* Antibody-maytansinoid conjugates are activated in targeted cancer cells by lysosomal degradation and linker-dependent intracellular processing. *Cancer Research* **66**, 4426-4433 (2006).
210. Kovtun, Y.V*., et al.* Antibody-drug conjugates designed to eradicate tumors with homogeneous and heterogeneous expression of the target antigen. *Cancer Research* **66**, 3214-3221 (2006).
211. Valliere-Douglass, J.F., Lewis, P., Salas-Solano, O. & Jiang, S. Solid-State mAbs and ADCs Subjected to Heat-Stress Stability Conditions can be Covalently Modified with Buffer and Excipient Molecules. *Journal of Pharmaceutical Sciences* **104**, 652-665 (2015).
212. Adem, Y.T*., et al.* Auristatin Antibody Drug Conjugate Physical Instability and the Role of Drug Payload. *Bioconjugate Chemistry* **25**, 656-664 (2014).
213. Schonberger, S*., et al.* Brentuximab vedotin exerts profound antiproliferative and pro-apoptotic efficacy in CD30-positive as well as cocultured CD30-negative germ cell tumour cell lines. *Journal of Cellular and Molecular Medicine* **22**, 568-575 (2018).
214. Zuo, S.B., T. Babu, S. Measuring Drug-to-Antibody Ratio (DAR) for Antibody-Drug Conjugates (ADCs) with UHPLC/Q-TOF. (2016).
215. Li, H., Han, T.H., Hunder, N.N., Jang, G. & Zhao, B.T. Population Pharmacokinetics of Brentuximab Vedotin in Patients With CD30-Expressing Hematologic Malignancies. *Journal of Clinical Pharmacology* **57**, 1148-1158 (2017).
216. Debaene, F*., et al.* Innovative Native MS Methodologies for Antibody Drug Conjugate Characterization: High Resolution Native MS and IM-MS for Average DAR and DAR Distribution Assessment. *Analytical Chemistry* **86**, 10674-10683 (2014).
217. Sochaj, A.M., Swiderska, K.W. & Otlewski, J. Current methods for the synthesis of homogeneous antibody-drug conjugates. *Biotechnology Advances* **33**, 775-784 (2015).
218. Lhospice, F*., et al.* Site-Specific Conjugation of Monomethyl Auristatin E to Anti-CD30 Antibodies Improves Their Pharmacokinetics and Therapeutic Index in Rodent Models. *Molecular Pharmaceutics* **12**, 1863-1871 (2015).
219. Sassoon, I. & Blanc, V. Antibody-Drug Conjugate (ADC) Clinical Pipeline: A Review. *Antibody-Drug Conjugates* **1045**, 1-27 (2013).
220. ICH. Quality of biotechnological products: Stability testing of biotechnological / biological products Q5C (1995).
221. ICH. Specifications: Test Procedures and Acceptance Criteria for New Drug Substances and New Drug Products: Biotechnological/Biological Products Q6B. (Online, 1999).

222. ICH. Stability testing of new drug substances and products Q1A (R2). (Online, 2003).
223. NHS England. Pharmacy Aseptic Services Review: Summary of Key Findings. (Online 2018)
224. Amin, S., *et al*. Protein aggregation, particle formation, characterization & rheology. *Current Opinion in Colloid & Interface Science* **19**, p438-449 (2014).
225. Ahmadi, M., *et al.* Small Amounts of Sub-Visible Aggregates Enhance the Immunogenic Potential of Monoclonal Antibody Therapeutics. *Pharmacuetical Research* **32**, p1383-1394 (2015).
226. Davydova, N., *et al*. The VD1 Neutralizing Antibody to Vascular Endothelial Growth Factor-D: Binding Epitope and Relationship to Receptor Binding. *Journal of Molecular Biology* **407**, p581-593 (2011).
227. Fu, X., *et al*. Hla-Dr-Alpha Chain Residues Located On The Outer Loops Are Involved In Nonpolymorphic And Polymorphic Antibody-Binding Epitopes **39**. p253-260 (1994).
228. Tan, YH., *et al*. A Nanoengineering Approach for Investigation and Regulation of Protein Immobilization. *American Chemical Society Nano* **2**. p2374-2384 (2008).
229. Ikeda, R., *et al*. Stability of Infliximab in polyvinylchloride bags. *American Journal of Health-System Pharmacy* **69**, 1509-1512 (2012).
230. Alley, SC., *et al*. Contribution of Linker Stability to the Activities of Anticancer Immunoconjugates. *Bioconjugate Chemistry* **19**, p759-765 (2008).
231. Li, J., *et al*. Analysis of phthalates via HPLC-UV in environmental water samples after concentration by solid-phase extraction using ionic liquid mixed hemimicelles. *Talanta* **74**, p498–504 (2008).
232. Guo, Z., Wei, D., Wang, M., Wang, S. Determination of Six Phthalic Acid Esters in Orange Juice Packaged by PVC Bottle Using SPE and HPLC–UV. *Journal of Chromatographic Science* **48**, p760-765 (2009).
233. Beckley, NS., *et al*. Investigation into Temperature-Induced Aggregation of an Antibody Drug Conjugate. *Bioconjugate Chemistry* **24**, p1674-1683 (2013).
234. Arakawa, T., *et al*. Biophysical characterization of a model antibody drug conjugate. *Drug Discoveries and Therapeutics* **10**, p211-217 (2016).
235. Ricker, RD., Sandoval, LA., Fast, reproducible size-exclusion chromatography of biological macromolecules. *Journal of Analytical Chromatography* **743**, p43-50 (1996).
236. Napp Pharmaceuticals Limited., Remsima 100 mg powder for concentrate for solution for infusion – SmPC. *Electronic Medicines Compendium.* [Accessed on: 14/03/2019] https://www.medicines.org.uk/emc/product/3709#DOCREVISION.
237. Bee, JS., *et al*, Effects of Surfaces and Leachables on the Stability of Biopharmaceuticals. *Journal of Pharmaceutical Sciences* **100**, p4158-4170 (2011)
238. Oliveira, R., *et al*, Understanding Adhesion: A Means for Preventing Fouling. *Experimental Thermal and Fluidic Science* **14**, p316-322 (1997)
239. Lameiras, F.S., *et al*, Measurement of the zeta potential of planar surfaces with a rotating disk. *Materials Research* **11**, p217-219 (2008)
240. McAuley, A., *et al*, Modulation of Protein Adsorption by Poloxamer 188 in Relation to Polysorbates 80 and 20 at Solid Surfaces. *Journal of Pharmaceutical Sciences* **103**, p1043-1049 (2014)
241. Petrul, H., *et al*. In vitro and in vivo efficacy of the anti-MN immunoconjugate BAY 79-4620, MN-IC, in MN (CAIX) expressing preclinical tumor models. *Experimental and Molecular Therapeutics* **70**, p2577-2577 (2011)

242. Hospira. Vincristine Sulphate Injection Safety Data Sheet. *Pfizer MSDS Archive.* 2016. Accessed from: https://www.pfizer.com/sites/default/files/products/material_safety_data/Vincristine_Sulfate_Injection(Hospira)_13-Sep-2016_0.pdf Accessed on: 20/03/19
243. Vermeer, AWP., *et al*. The thermal stability of immunoglobulin: Unfolding and aggregation of a multi-domain protein. *Biophysical Journal* **78**, p394-404 (2000)
244. Hanahan, D., Weinberg, R.A., Hallmarks of Cancer: The Next Generation. *Cell* **144**, p646-674 (2011)
245. Neubauer, A., Wollmer, E., Side Effects of tumor pharmacotherapy. *Der Internist* **52**, p1429-1446 (2011)
246. van der Kuip, H., *et al*. Mechanisms of clinical resistance to small molecule tyrosine kinase inhibitors targeting oncogenic tyrosine kinases. *American Journal of Pharmacogenomics* **5**, p101-112 (2005)
247. Rosa, D.D., Ismael, G., Lago, L.D., Awada, A., Molecular-targeted therapies: Lessons from years of clinical development. *Cancer Treatment Reviews* **34**, p61-80 (2008)
248. Saijo, N., Present Status and Problems on Molecular Targeted Therapy of Cancer. *Cancer Research and Treatment* **44**, p1-10 (2012)
249. Schroeder, H.W., Cavacini, L., Structure and Function of Immunoglobulins. *Journal of Allergy and Clinical Immunology* **125**, p41-52 (2010)
250. Alberts, B., Johnson, A., Lewis, J., *et al.* Molecular Biology of the Cell. 4th edition. *Garland Science*. (2002)
251. Meyer, S,. *et al*. Regulation of complement and modulation of its activity in monoclonal antibody therapy of cancer. *MABs* **6**, p1133-1144 (2014)
252. Seidel, U.J., *et al*. Natural Killer Cell Mediated Antibody-Dependent Cellular Cytotoxicity in Tumor Immunotherapy with Therapeutic Antibodies. *Frontiers in Immunology* **4**, (2013)
253. Vidarsson, G., *et al*. IgG Subclasses and Allotypes: From Structure to Effector Functions *Frontiers in Immunology* **5**, (2014)
254. Tiezheng, L., *et al*. Modulating IgG effector function by Fc glycan engineering. *Proceedings of the National Academy of Sciences of the United States of America* **114**, p3485-3490 (2017)
255. Hafeez, U., Gan, H.K., Scott, A.M., Monoclonal antibodies as immunomodulatory therapy against cancer and autoimmune diseases. *Current Opinion in Pharmacology* **41**, p114-121 (2018)
256. Trotman, J., *et al*. Prognostic value of end-of-induction PET response after first-line immunochemotherapy for follicular lymphoma (GALLIUM): secondary analysis of a randomised, phase 3 trial. *Lancet Oncology* **19**, p1530-1542 (2018)
257. Joint Formulary Committee. British National Formulary London: Pharmaceutical Press and BMJ Group <http://www.medicinescomplete.com> [Accessed on 26/03/2019]
258. Reslan, L., *et al*, Understanding and circumventing resistance to anticancer monoclonal antibodies. *MAbs* **1**, p222-229 (2009)
259. Rubleski, J., Prescription Drug Prices Will Drive Health Insurance Premium Increases in 2017. *Seidman Business Review* **23**, p9-10 (2017)
260. Romley, J.A., *et al*. Survey Results Show That Adults Are Willing To Pay Higher Insurance Premiums For Generous Coverage Of Specialty Drugs. *Health Affairs* **31**, P683-690 (2012)

261. Mulero, P., *et al*. Ocrelizumab: a new milestone in multiple sclerosis therapy. *Therapeutic Advances in Neurological Disorders* **11**, p1-10 (2018)
262. Salles, G., *et al*, Atezolizumab in Combination with Obinutuzumab and Lenalidomide Demonstrates Favorable Activity and Manageable Toxicity in Patients with Relapsed/Refractory Follicular Lymphoma (FL): An Interim Analysis of a Phase Ib/II Trial. *Blood* **132**, p1603 (2018)
263. Hawe, A., *et al*, Forced Degradation of Therapeutic Proteins. *Journal of Pharmaceutical Sciences* **101**, p895-913 (2012)
234. Wang, W., *et al*. Protein aggregation—Pathways and influencing factors. *International Journal of Pharmaceutics* **390**, p89-99 (2010)
265. Schmid, I., *et al*. Assessment of susceptible chemical modification sites of trastuzumab and endogenous human immunoglobulins at physiological conditions. *Communication Biology* **1**, p1-10 (2018)
266. Yan, Q., *et al*. Structure Based Prediction of Asparagine Deamidation Propensity in Monoclonal Antibodies. *mAbs* **10**, p901-912 (2017)
267. Gerhardt, A., *et al*. Surfactant Effects on Particle Generation in Antibody Formulations in Pre-filled Syringes. *Journal of Pharmaceutical Science* **104**, p4056-4064 (2015)
268. Wang, W., *et al*. Antibody structure, instability, and formulation. *Journal of Pharmaceutical Sciences* **96**, p1-26 (2006)
269. Mesink, M.A., *et al.* How sugars protect proteins in the solid state and during drying (review): Mechanisms of stabilization in relation to stress conditions. *European Journal of Pharmaceutics and Biopharmaceutics* **114**, p288-295 (2017)
270. Wakankar, A.A., *et al*. The effect of cosolutes on the isomerization of aspartic acid residues and conformational stability in a monoclonal antibody. *Journal of Pharmaceutical Sciences* **96**, p1708-1718 (2007)
271. Motomiya, Y., *et al*. An in vitro evaluation of the glycation potential of a natural disaccharide, trehalose. *Journal of Clinical and Experimental Nephrology* **7**, p195-200 (2003)
272. Wei, B., *et al*. Glycation of antibodies: Modification, methods and potential effects on biological functions. *mAbs* **9**, p586-594 (2017)
273. Zheng, K., *et al*. Characterization of Ring-Opening Reaction of Succinimide Linkers in ADCs. *Journal of Pharmaceutical Sciences* **108**, p133-141 (2019)
274. Tsuchikama, K., *et al*. Antibody-drug conjugates: recent advances in conjugation and linker chemistries. *Protein Cell* **9**, p33-46 (2018)
275. Lyon. R.P., *et al*. Self-hydrolyzing maleimides improve the stability and pharmacological properties of antibody-drug conjugates. *Nature Biotechnology* **32**, p1059-1062 (2014)
276. Vijayan, S., *et al*. Establishment of the first at-home natalizumab infusion service for the treatment of relapsing remitting multiple sclerosis. *Journal of Neurology, Neurosurgery and Psychiatry* **88**, (2017)
277. Orange, J.S., Improved clinical outcomes for patients receiving immunoglobulin therapy through speciality pharmacy or home infusion services. *Annals of Allergy, Asthma & Immunology* **115**, p18 (2015)
278. Bach, P.B., *et al*. Overspending driven by oversized single dose vials of cancer drugs. *The Bristish Medical Journal* **352**, (2016)

279. Fuentes, S., *et al*. Why is intravenous chemotherapy cancelled and how often? Could it be prevented? *Acta Oncologica* **54**, p1056-1062 (2015)

Appendices

Appendix I: Abatacept size exclusion chromatography method validation data

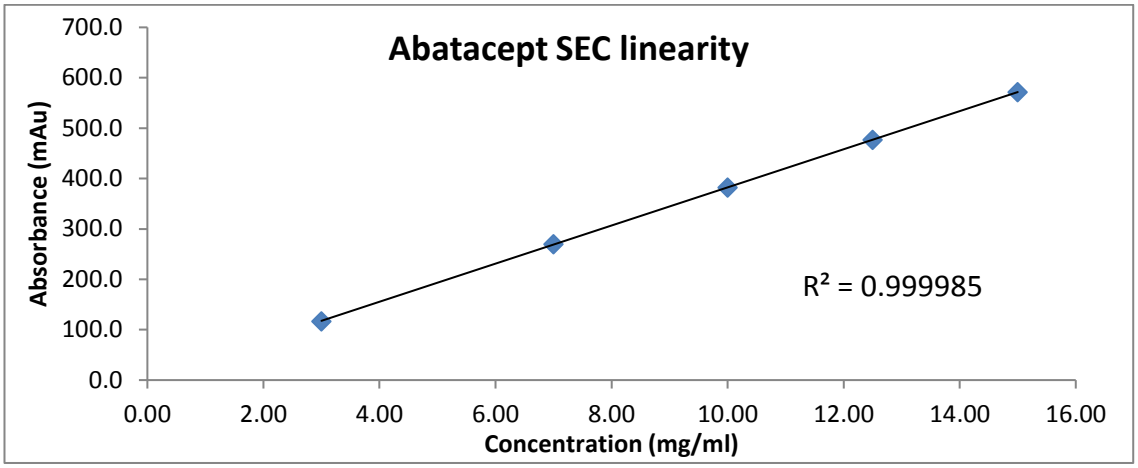

Figure 1A. Size exclusion linearity plot for abatacept.

Injection	Peak Area (mAu.min)	RSD %
1	382.54	**0.27**
2	382.35	
3	383.02	
4	384.69	
5	383.84	
6	381.98	

Table 1A. Repeat injection precision for abatacept.

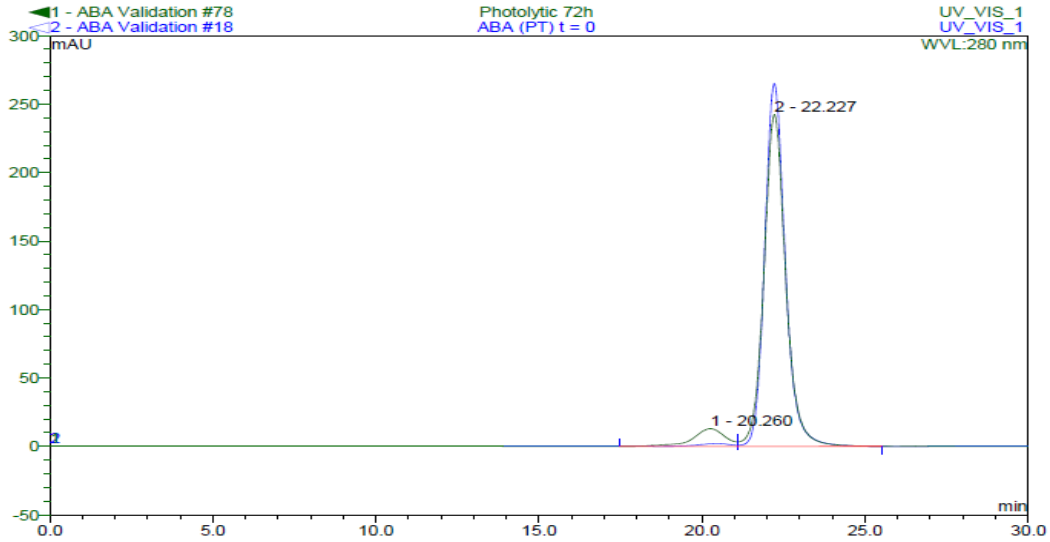

Figure 1B. SEC chromatogram overlay of abatacept control (**Blue**) and Photolytically degraded (**Green**). The X-axis is time (minutes).

Appendix II: Rituximab size exclusion chromatography method validation data

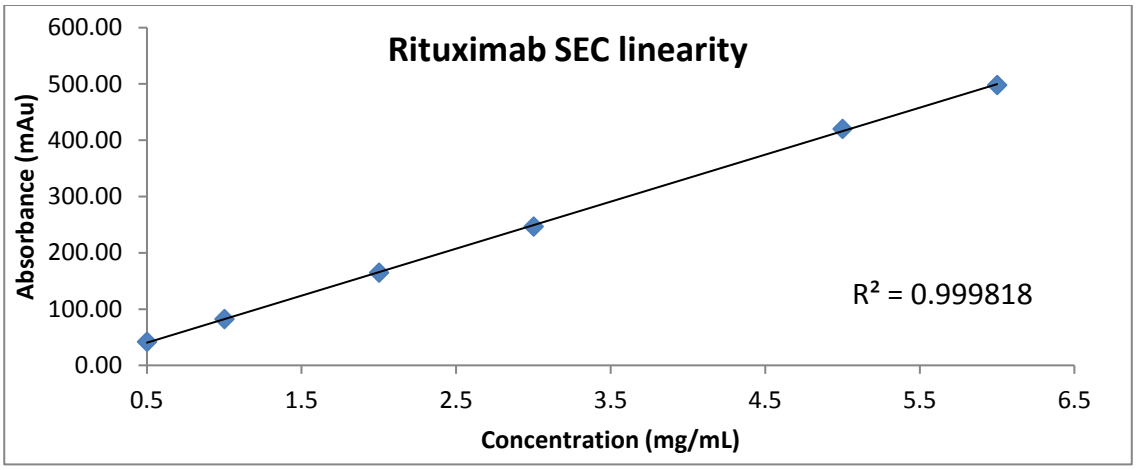

Figure 2A. Size exclusion linearity plot for abatacept.

Injection	Peak Area (mAu.min)	RSD %
1	84.31	**0.33**
2	84.00	
3	83.75	
4	83.46	
5	83.99	
6	83.82	

Table 2A. Repeat injection precision for rituximab.

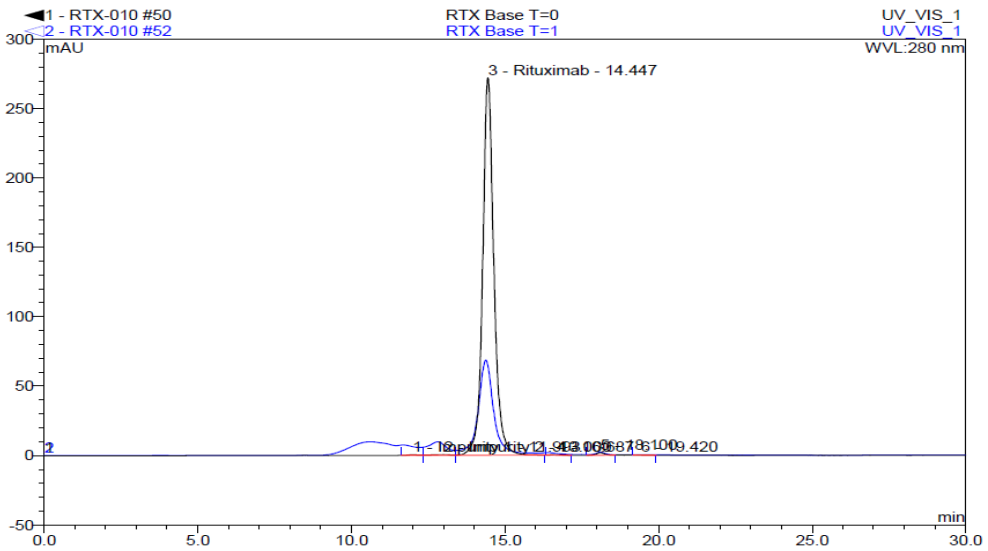

Figure 2B. SEC chromatogram overlay of rituximab control (**Black**) and base hydrolysed (**Blue**). The X-axis is time (minutes).

Appendix III: Trastuzumab size exclusion chromatography method validation data

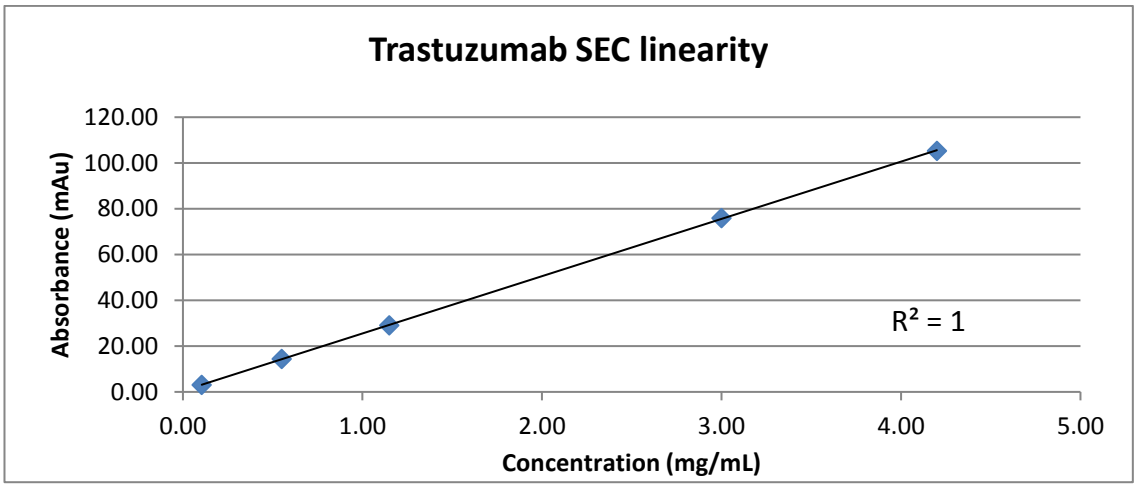

Figure 3A. Size exclusion linearity plot for trastuzumab.

Injection	Peak Area (mAu.min)	RSD %
1	29.03	**0.20**
2	29.01	
3	28.94	
4	29.09	
5	29.08	
6	29.09	

Table 3A. Repeat injection precision for abatacept.

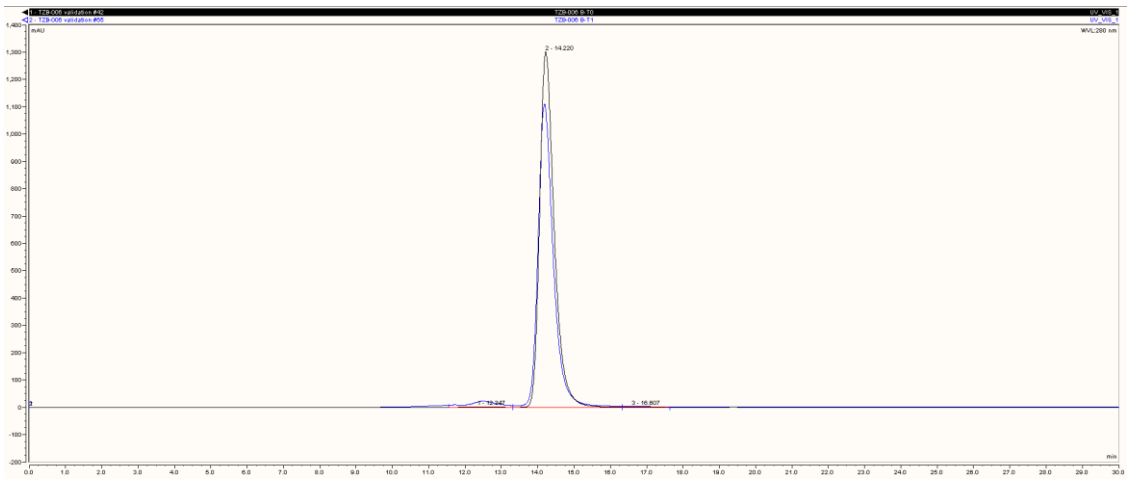

Figure 3B. SEC chromatogram overlay of trastuzmab control (**Black**) and base hydrolysed (**Blue**). The X-axis is time (minutes).

Appendix IV: Infliximab (Remsima) representative sample photographs

Figure 4A. Day 1 sample photographs.

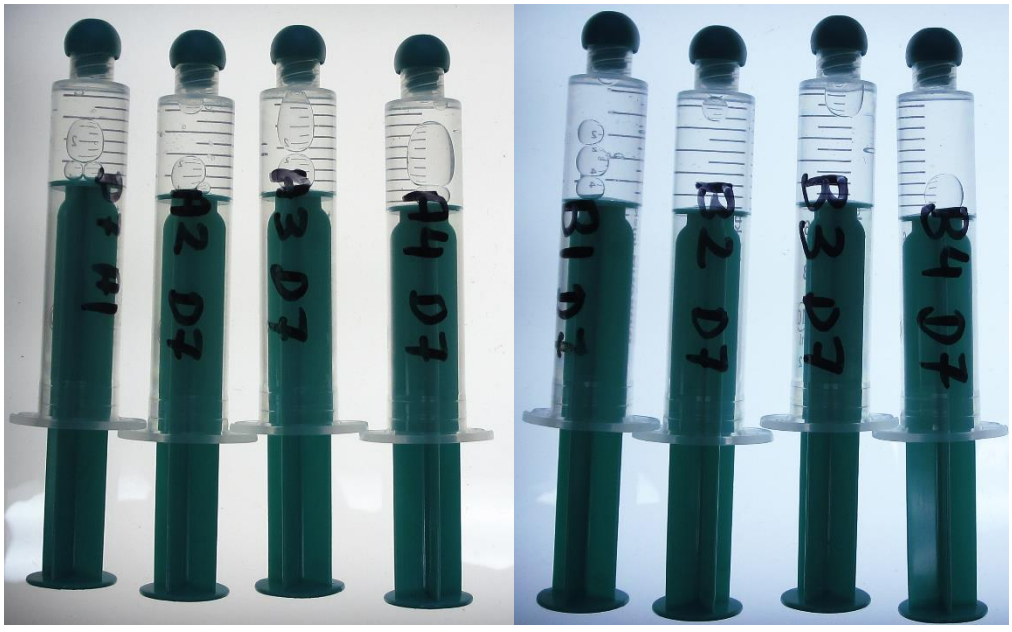

Figure 4B. Day 7 sample photographs.

Appendix V: Trastuzumab emtansine (Kadcyla) representative sample photographs

Figure 5A. Day 1 sample photographs.

Figure 5B. Day 24 sample photographs.